The synthesis and study of novel squaramide-based anion sensors

A thesis submitted to the National University of Ireland in fulfilment of the requirements for the degree of

Master of Science

By

Nan Mao, B.Sc.

Department of Chemistry,

Maynooth University,

Maynooth, Co. Kildare,

Ireland.

October 2018

Research supervisor: Dr. Robert Elmes

Head of Department: Dr. Jennifer McManus

Declaration

I hereby certify that this thesis has not been submitted before, in whole or in part, to this or any university for any degree and is, except where otherwise stated, the original work of the author.

Signed:_____ Date:_____

Maynooth University

Contents

Acknowledgements

First of all, I would like to thank my supervisor Dr. Robert Elmes for accepting me to start this project and imparting his knowledge to me without reservation over the past two years. He always gave me helpful advices and encouragement when I faced trouble with the research. His patience, enthusiasm and wisdom affected me a lot, I was so lucky to have Rob as my supervisor.

I would also like to thank all the members of the Elmes group - Xiang, Anthony, Luke, Lokesh and Michelle. Especially Xiang and Anthony gave me a lot of help when I knew nothing about how to work in the lab at the beginning. In the second year, I also had great time with Luke and Lokesh. Wish them and the new blood of Elmes group this year good luck with their project.

All the academic and technique staff in chemistry department – Ria, Barbara, Walter, Ollie, Noel, Donna and Carol – thank you for your help. I want to say special thank you to Ria for supporting and caring me in the past two years. She was always providing me risk assessments when I used harmful chemicals, helping me get Hydrogen gas from the cylinder and giving us job information. Also, thanks Noel for showing me how to connect my laptop to NMR and the printer.

The whole chemistry department is a big warm family, I want to thank all the other colleagues in the lab- Muhib, Amanda, Harlei, Sam, Mark, Jack, Jessica, Justin, Matthew, Clara and Stephen – for having happy and memorable time with all of you.

Two years life in Ireland away from home in China was supposed to be lonely, however, thanks to Xiang, Rui, Yi, Zhengwei, Anqi, Dongyue, Sheng, Qin, Di, Xiaobo, Ziming, Jie, and Shixin, I was never lonely being with you. I will always remember the time we had hot pot or BBQ party together.

I also want to say thank you to my girlfriend Jing for her understanding and supporting. Eight hours jet lag made everything unreachable, we only had very short time to talk every day. Two years were long for us, but we have made it through.

At the end, the most thank to my parents for their financial and moral support. Although two years away from home, I could always receive care from them. Every time talk to my mum, she always reminded me to have breakfast. Without you, I could not accomplish my research project.

Abstract

This thesis entitled ‘The synthesis and study of novel squaramide-based anion sensors’ is divided into five chapters. Chapter 1 gives a brief introduction of the significance of anions in biology, environment and industry which elicits the history, development and challenge of anion sensing and recognition. The mechanism of H-bonding interaction based anion sensing and recognition are particularly discussed, followed by the introduction of a series examples of anion receptors and sensors containing functional groups with the capability of H-bonding to anions. As the core of this research, squaramide-based anion receptors and sensors are particularly discussed. This chapter ends with the aims and objectives of the research conducted in Chapter 2 and 3.

In Chapter 2, the design and synthesis of novel squaramidoquinoxaline (SQX) moiety based anion sensors are discussed. All desired compounds are synthesized through an efficient two step synthetic protocol and fully characterized. The characterization of their photophysical and anion binding properties reveals the -NO_2 substituted compound to be an interesting candidate . In particular, crystal structure study and F^- test strips study of the -NO_2 substituted compound are also discussed in this chapter.

Chapter 3 discusses the design and synthesis of macrocyclic squaramide (MSQ) moiety based anion sensors. At the beginning, the nitro and dinitro substituted MSQs are synthesized and characterized due to -NO_2 substituted SQX showed great interest in Chapter 2. The preliminary attempts to synthesize fluorescent probe substituted MSQ which is capable of carrying out Förster Resonance Energy Transfer (FRET) are also discussed in this chapter. In addition, the anion binding properties of successfully synthesized MSQs are studied.

Chapter 4 gives an overall conclusion of the entire work carried out in this research and also offers the idea for future work.

In Chapter 5, the instrumentation, reagents, general experimental procedures and characterization of each compound discussed in this thesis are given.

Abbreviations

AIBN	Azobisisobutyronitrile
Br^-	Bromide
CCl_4	Carbon tetrachloride
CH_3COO^-	Acetic acid
Cl^-	Chloride
d	Doublet
DCM	Dichloromethane
dd	Doublet of doublet
DMF	Dimethylformamide
DMSO	Dimethyl sulfoxide
dt	Doublet of triplet
EDG	Electron donating group
eq.	Equivalent
Et_2O	Diethyl ether
Et_3N	Triethylamine
EtOH	Ethanol
EWG	Electron withdrawing group
F^-	Fluoride
FRET	Förster resonance energy transfer
FTIR	Fourier transform infrared
$H_2PO_4^-$	Dihydrogen phosphate
HCl	Hydrogen chloride
HF_2^-	Bifluoride

HOMO	Highest occupied molecular orbital
HRMS	High resolution mass spectroscopy
Hz	Hertz
I^-	Iodide
J	Coupling constant
LUMO	Lowest occupied molecular orbital
m	Multiplet
m/z	Mass charge ratio
MeCN	Acetonitrile
MeOH	Methanol
MSQ	Macrocyclic squaramide
Na_2CO_3	Sodium carbonate
NaOH	Sodium hydroxide
nm	Nanometer
NMR	Nuclear magnetic resonance
NTO	Natural transition orbitals
$Pd(PPh_3)_4$	Tetrakis(triphenylphosphine)palladium(0)
Pd/C	Palladium on carbon
ppm	Parts per million
q	Quartet
s	Singlet
SO_4^{2-}	Sulfate
SQX	Squaramidoquinoxaline
t	Triplet

TD-DFT	Time-dependent density functional theory
THF	Tetrahydrofuran
UV-Vis	Ultraviolet-visible
δ	Chemical shift
ε	Molar extinction coefficient
λ	Wavelength

Chapter 1 Introduction

1.1 Why Are Anions Important

Anions are negatively charged atoms (F^-, Cl^-, Br^-, I^-…) or molecules (CH_3COO^-, NO_2^-, SO_4^{2-}…), which play an important role in biology, environment and industry. Compounds containing fluoride are widely used in oral disease control, organic synthesis and industrial process.[1] For instance, sodium fluoride (NaF) and sodium fluorosilicate ($Na_2[SiF_6]$) are the active ingredients to prevent tooth decay in toothpaste;[2] Fluoride also helps to maintain the health of bones in human body.[3] Tetra-*n*-butylammonium fluoride (TBAF) can be used to remove silyl ether protection group, it's also known as a good phase transfer catalyst and mild base. However, many fluoride-containing compounds are extremely toxic and corrosive, improper treatment of wastes containing fluoride can cause severe pollution to the environment and result in disease to human. Chloride has a close connection to our daily life. Sodium chloride (NaCl) is the most common existential form of chloride, an adult normally needs to intake 2-5g sodium chloride a day, but excess intake of sodium chloride will cause hypertension.[4] Hydrochloric acid is a water solution of hydrochloride (HCl) which is known as a strong monoprotic acid. It's has many industrial applications and it's also the main component of gastric acid. Bromide can be found in urine, serum and saliva of living organisms.[5] Lacking bromide results in hyperthyroidism which inhibits growth, fertility and life expectancy. However, excess of bromide can cause bromism which results in skin eruption.[6] Bromide is also one of the most difficult anions to be sensed due to the large ionic radius, low charge density and low hydrogen bonding ability. Inorganic cyanides are normally known as extremely toxic compounds which can cause severe damage to the environment due to their comprehensive applications in photography, gold mining and petrochemical industry.[7] The prevalence and importance of anions has led to widespread research interest in developing novel anion receptors for monitoring these anions in physiological and environmental samples.

1.2 Anion Recognition and Anion Sensing

The early study of anion receptor chemistry was reported by Shriver and Biallas[8] and by Park and Simmons in the late 1960s.[9] Park and Simmons demonstrated that katapinate ions could encapsulate halides due to the formation of hydrogen bonds within the cavity (Figure 1.1).[9]

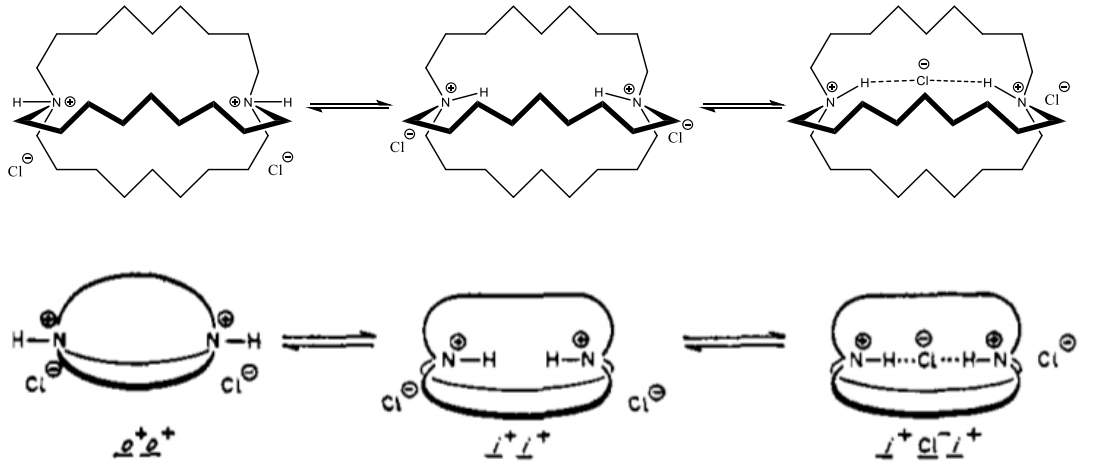

Figure 1.1: Possible binding mode between katapinate ion and Cl^-. Image taken from *J. Am. Chem. Soc.* 1968;90(9):2431-2.

The slow development of research was then followed by Graf and Lehn who reported macrotricyclic ligands as halides receptors in the mid-1970s.[10] However, this field has rapidly blossomed since the 1990s and the research focus has shifted from the development of simple neutral receptors which complex anions in organic solvents to the design of selective anion receptors which can bind and sense anions in aqueous solvent mixture and *in vivo*, transport anions across cell membranes, detect anionic pollutants at very low concentration and extract and transfer specific anionic complex from aqueous to organic solution against Hofmeister bias.[11] Nowadays, this field has become as a fundamental pillar of supramolecular chemistry with applications in many areas.[12]

Chemosensor is a typical example of anion sensors which can produce changes in color or fluorescence properties when reacted with anions. The design of chemosensor has attracted many researchers' interest due to the cheap price and user-friendly analysis method comparing to the classical methodologies.[13] The "binding site-signaling subunit" approach is one of the main approaches used in the design of chemosensor where the binding unit and the signaling subunit of the chemosensor are connected through a

covalent bond.[14] The binding unit react with anions via non-covalent interactions such as hydrogen bonding thus lead to change in absorbance (color) or fluorescence which can be detected by UV/Vis spectrophotometer, fluorescent spectrophotometer or naked eye (Figure 1.2).[6]

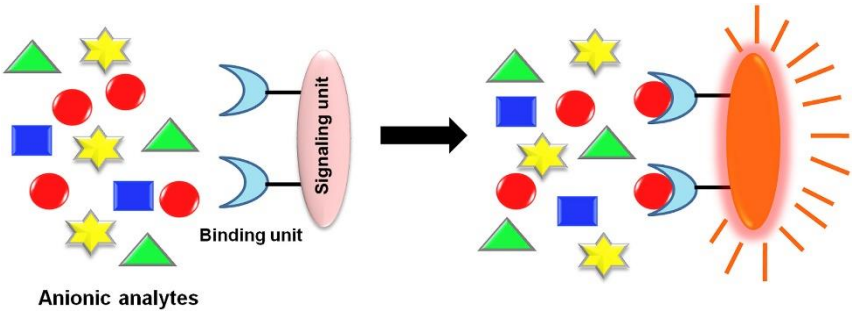

Figure 1.2: General binding and sensing mechanism of "binding site-signaling subunit" type chemosensor. Image taken from *Trends. Analyt. Chem*. 2017;95:86-109.

However, despite the intense research effort, design of selective and sensitive chemosensors are still challenging. The large size of anions leads to low charge to size ratio which inhibits their potential towards electrostatic interactions with the chemosensors. The different shapes of anions and their pH sensitivity also impede the development of chemosensors (Figure 1.3).[15] Moreover, polar solvent like water tend to compete with anions for binding with chemosensors.[11, 15]

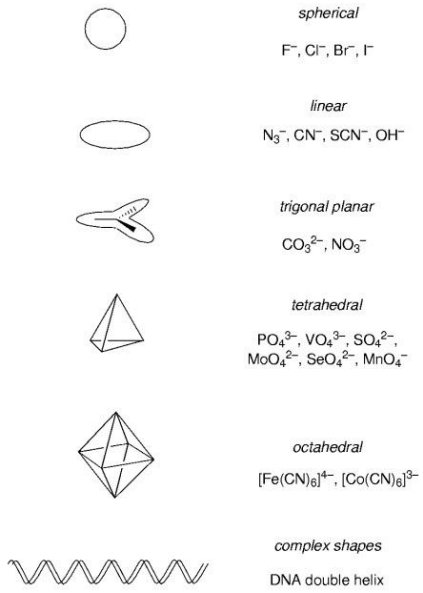

Figure 1.3: The structural variety of anions. Image taken from *Angew. Chem. Int. Ed.* 2001;40(3):486-516.

Cationic chemosensors bind to anions via electrostatic interaction, while neutral chemosensors bind to anions through non-covalent interactions like ion-dipole interactions, π-π^* interactions and H-bonding interactions.[16] Hydrogen bonding is important due to its critical role in enzymatic catalysis, arrangement of molecules in crystals, crystal engineering, proton transfer reaction and life processes.[17] Moreover, design of chemosensor that bind anions through H-bonding interaction is the most common strategy for anion sensing. A hydrogen bond is known as an electrostatic attraction between H and electronegative atom such as N^-, O^- or F^-. The anion receptors normally act as H-bond donor whereas anions are the H-bond acceptor. The directionality of H-bond allows for the possibility of designing preorganized receptors with specific shapes that are capable of selectively binding anions with different geometries or H-bonding requirements in non-polar solvents.[15] Effective design of neutral H-bond donor/receptor species allows the binding of anions in aqueous solutions which can overcome the enthalpic penalty.[11] Several functional groups such as amide, thiosemicarbazide, urea, thiourea, pyrrole and squaramide are found to capable of efficiently forming H-bond to anions (Figure 1.4). All these functional groups contain at least one NH motif which enable them to be a good H-bond donor. Moreover, in case of amide, urea or thiourea, the presence of electron withdrawing carbonyl or thiocarbonyl group further increase the acidity of the NHs thus enables strong complex formation between anions and receptors. Squaramide motif is particularly special due to the existence of two NHs and the two adjacent carbonyls enabling it to become effective H-bond donor and acceptor simultaneously.[18, 19]

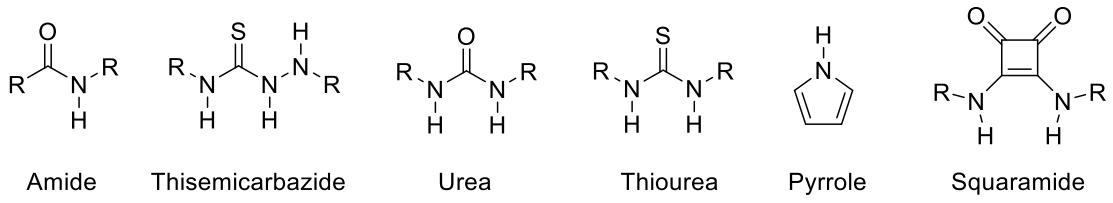

Figure 1.4: Some functional groups capable of H-bonding to anions.

So far from the beginning of the anion receptor chemistry, researchers have been raising enthusiasm for the study of the H-bond based anions receptors. For instance, Gavette *et al.* reported a di-urea based anion-modulated switch which could adapt three different conformation depending on the anion guests.[20] Li *et al.* reported a family of N-*tert*-butyl sulfinyl squaramide receptors which had highest binding affinity for Cl^- in 2017.[21] The

following sections of this chapter will provide an overview of the design and application of amide-, pyrrole-, calixpyrrole-, urea-, thiourea- and squaramide-based anion receptors from published literature.

1.3 Amide Based Anion Receptors

Amide-based anion receptors attract many chemists' attention due to their less pH dependence and better solubility in organic media.[6] More interestingly, employing neutral amide as H-bond acceptor to proteins is the most often way that allows anion binding by proteins.[22] Lining the inside of a macrocyclic or affixing the groups to an acyclic framework in a pendant structure or as part of cleft or other rigid skeleton contribute to the most commonly preorganized anion receptors containing amide binding units.[22] Several receptors using the amide binding site will be discussed in this section.

Deetz *et al.* reported a macrobicyclic receptor **1** containing a dibenzo-18-crown-6 and a bridging 1,3-phenyldicarboxamide scaffolds.[23] The authors demonstrated that in the presence of 1 mol equiv. of K^+ or Na^+, the receptor showed 9- or 8-fold enhancement of binding affinity to Cl^-, respectively. Receptor **1** also capable of selectively binding to DMSO (K_a = 160 M^{-1} at 295 K) comparing to acetonitrile, nitromethane or acetone in chloroform solvent. Latterly, Mahoney and co-workers reported another macrobicyclic receptor **2** with less space between the cation and anion binding sites which may enhance the binding cooperativity.[24] In this case, receptor **2** showed 40-fold enhancement of binding affinity for Cl^- in the presence of K^+ and 5-fold in the presence of Na^+.

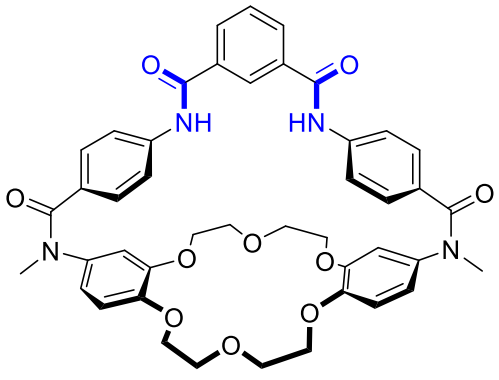

1

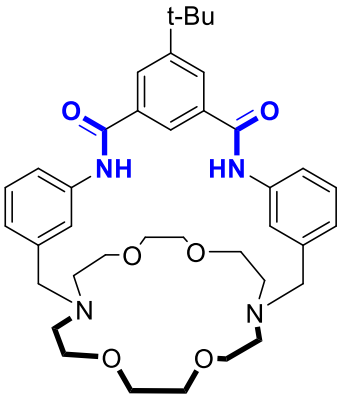

2

In 2002, Piatek *et al.* reported a selective colorimetric anion sensor based on an amide group containing macrocycle.[25] Association constants were calculated from the ^{1}H NMR titrations for complexes of receptor **3** with F^-, AcO^-, $H_2PO_4^-$. HSO_4^-, Br^- and Cl^- in DMSO-d_6 and CD_3CN. Except for F^-, a crucial increase of the association constant was obtained by the change of solvent from DMSO-d_6 to CD_3CN. $H_2PO_4^-$ showed greatest increase with K_a = 142 (DMSO-d_6) and K_a = 4271 (CD_3CN) was attributed to the additional H-bonding interactions between the OH group of $H_2PO_4^-$ and ethereal oxygen atoms of receptor **3**. Dramatic color change from colorless to dark blue was observed upon the addition of F^- towards DMSO solution of the receptor **3**, and yellow color change of receptor **3** was also observed upon the addition of AcO^- and $H_2PO_4^-$ ions, respectively. Moreover, acetonitrile solution of receptor **3** showed selective coloration for these anions from colorless to turquoise (F^-), yellow (AcO^-) and purple ($H_2PO_4^-$) allowed receptor **3** to be an ideal anion sensor (Figure 1.5).

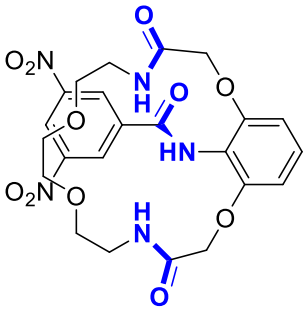

3

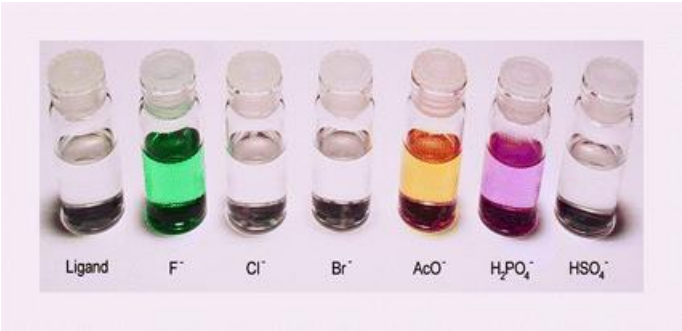

Figure 1.5: Color changes (if any) induced by the addition of anions. From left to right (acetonitrile solutions): **3**; **3** + F^-; **3** + Cl^-; **3** + Br^-; **3** + AcO^-; **3** + $H_2PO_4^-$; **3** + HSO_4^-. Image taken from *Chem. Commun.* 2002;(20):2450-1.

Jana and *et al.* synthesized a group of quinoline-functionalized bis-amide receptors **4 - 6**, where the cooperation of the two amide NH groups symmetrically disposed about the central spacer.[26] The ^{1}H NMR titration revealed the 1:1 complexes formation between

receptors **4 - 6** and the tested anions. Receptors **4** and **5** showed enhanced binding ability to the tested anions comparing to their open-chain counterparts. However, receptor **6** showed relative weaker binding ability comparing to receptors **4** and **5** owing to the far distance between the binding sites of m-xylylene core.

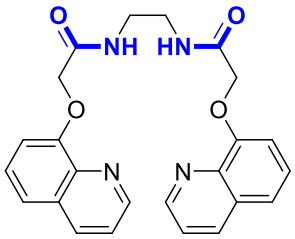

4

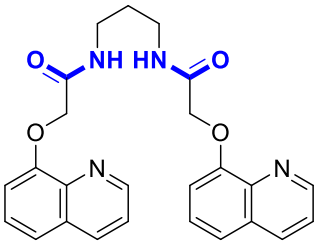

5

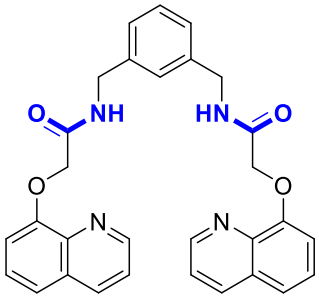

6

Latterly, Fagade *et al.* synthesized an amide-based dipodal Zn^{+} complex which could be used to detect HSO_4^- in a semi-aqueous system.[27] The anion binding ability of receptor **7** was evaluated by the addition tetrabutylammonium salts of various anions (F^-, Cl^-, Br^-, I^-, CH_3COO^-, $H_2PO_4^-$, NO_3^-, CN^- and HSO_4^-) in a DMSO-H_2O (50:50, v/v) solvent system. Interestingly, only the addition of HSO_4^- leaded to a distinct decrease as well as a blue shift in the fluorescence intensity of receptor **7** (Figure. 1.6). After various studies(fluorescence, UV/Vis and DFT calculations), the authors suggested that the quenching of the fluorescence of receptor **7** is resulted from the formation of hydrogen-bonded complex between the amide sites of the receptor and HSO_4^-.

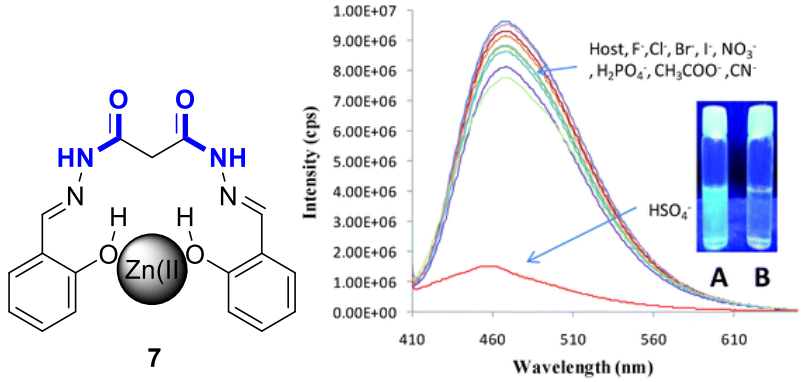

Figure. 1.6: Fluorescence emission spectra of receptor **7** upon addition of a particular anion (F^-, Cl^-, Br^-, I^-, CH_3COO^-, $H_2PO_4^-$, NO_3^-, CN^- and HSO_4^-) of tetrabutylammonium salts in DMSO–H2O (50:50, v/v). The inset represents: (A) a solution of **7** and (B) **7** + HSO_4^-, both solutions were irradiated under UV light. Image taken from *Org. Biomol. Chem.* 2013;11(39):6824-8.

1.4 Pyrrole and Calix[4]pyrrole Based Anion Receptors

Pyrrole- and calix[4]pyrrole-based anion receptors differ from the amide-based anion receptors discussed above. They can only act as H-bond donors owing to lack of H-bond acceptor functional groups. However, calix[4]pyrrole-based receptor with nonplanar, tetrapyrrolic macrocyclic conformation that capable of binding to Lewis basic anions such as halides.[28] Since the first work of introducing calix[4]pyrrole into the design of anion receptors by Sessler *et al.* in the mid-1990s, calix[4]pyrrole-based receptors have been proven to show high affinity and selectivity towards various anions by incorporating straps on one side of calix[4]pyrrole or introducing probe units at the periphery of the mother macrocyclic.[28, 29] This section will discuss some pyrrole- and calix[4]pyrrole-based anion receptors from published literatures.

Anandan and co-workers reported pyrrole-based Schiff bases as colorimetric and fluorescent chemosensors for fluoride and hydroxide anions.[30] Receptors **8** and **9** showed high selectivity towards F^- and OH^-. The solution of receptors **8** and **9** in acetonitrile turned into yellow and permanganate colored upon the addition of F^- and OH^- respectively. Receptor **9** showed predominant color change than receptor **8** due to the presence of NO_2 group. The results indicated that both receptors could become useful candidates for F^- and OH^- sensing.

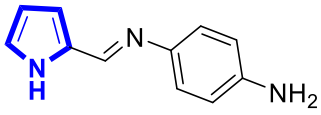

8

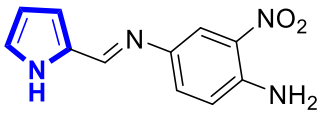

9

Anzenbacher and co-workers synthesized fluorescent sensors **10-14** based on the calix[4]pyrrole structure and its expanded congener calix[2]benzo[4]pyrrole with respective fluorophore moiety attached through conjugated vinyl linker.[31] NMR, UV/Vis, and fluorescence titration experiments were used to investigate the anion binding properties of five sensors, and calculate the corresponding affinity constants for the tested anions. The present fluorescent sensors **10-14** were demonstrated to show cross binding reactivity. Moreover, the parent calix[4]pyrrole-based **10**, **12** and **14** were found to be more efficient sensors for anions, including dicarboxylates. A fluorescence-based microarray device of five fluorescent sensors **10-14** was used to successfully classify 18 different anions and to perform multiple quantitative analyses. The graphical output of the linear discriminant analysis (LDA) showed all the 18 analytes were recognized by an array of five sensors with 100% correct classification in trials (Figure 1.7).

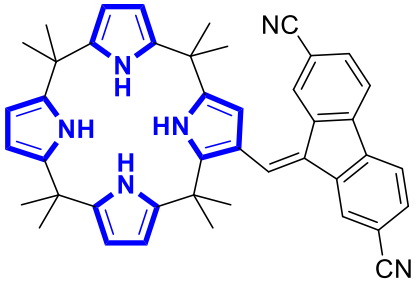

10

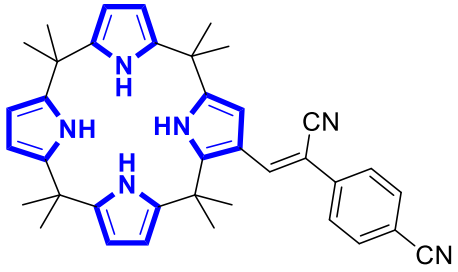

11

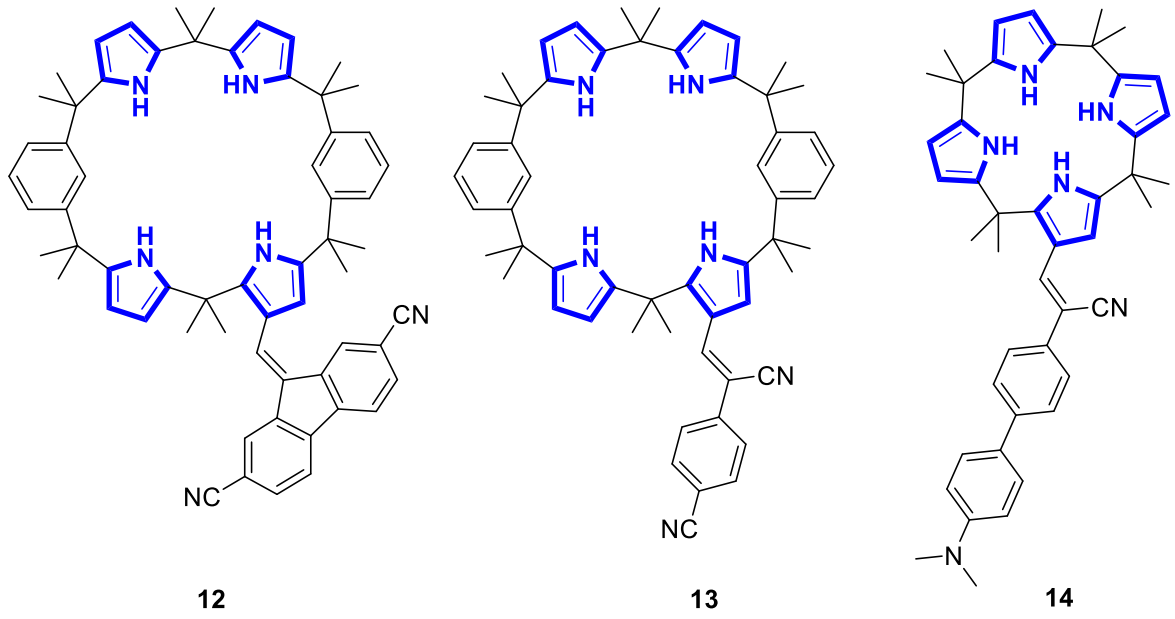

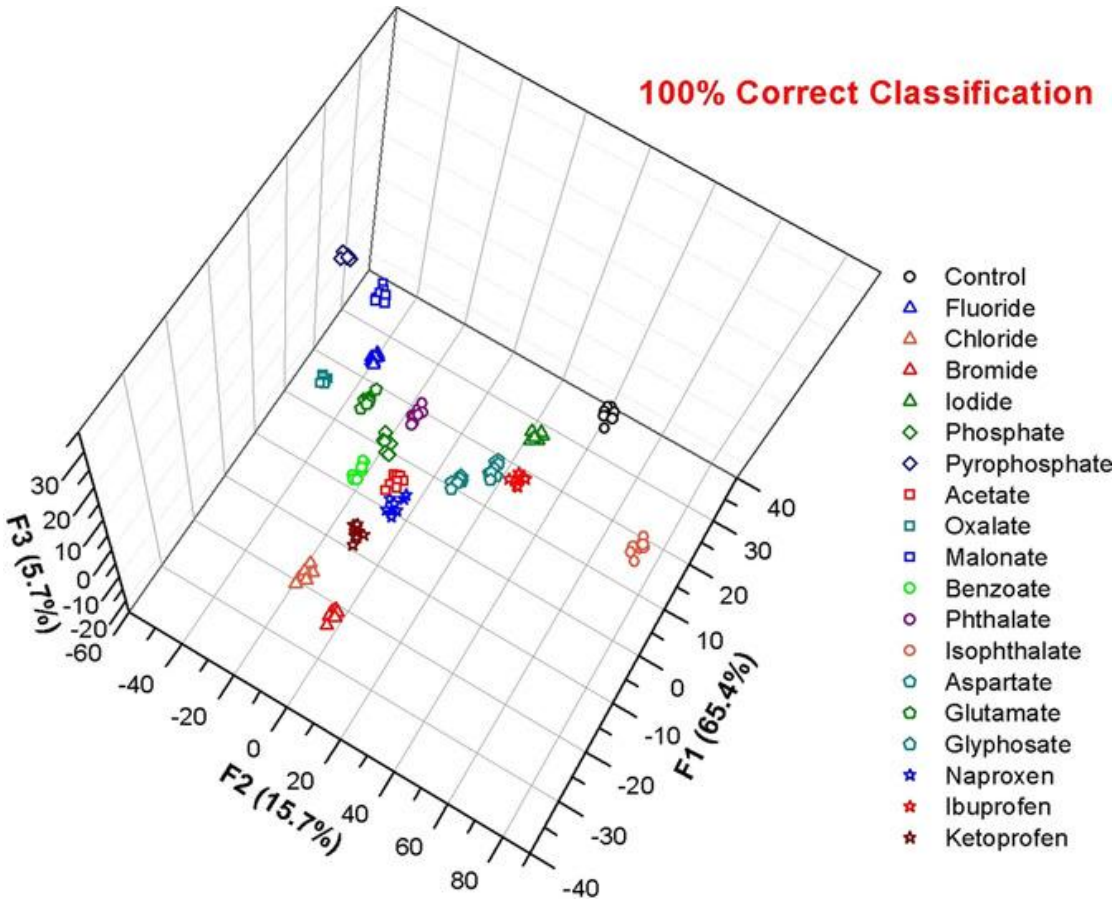

Figure 1.7: Graphical output of the linear discriminant analysis (LDA) showing the response pattern of the sensors **10-14** to 18 individual analytes. Clear clustering of results was observed, allowing 100% correct classification in individual trials. Image taken from *Chem. Eur. J.* 2018;24(19):4879-84.

Taner and *et al.* synthesized a colorimetric receptor **15** based on calix[4]pyrrole binding oxime for selective recognition for F^- ions.[32] UV/VIS, and ^1H NMR titrations study revealed that the receptor exhibits selective recognition towards F^- over other anions which is mainly due to the H-bond interaction between receptor and F^-. Color change from colorless to yellow of **15** in the presence of F^- was observed by naked eye, thus provided a simple and general method for the detection of F^- ions.

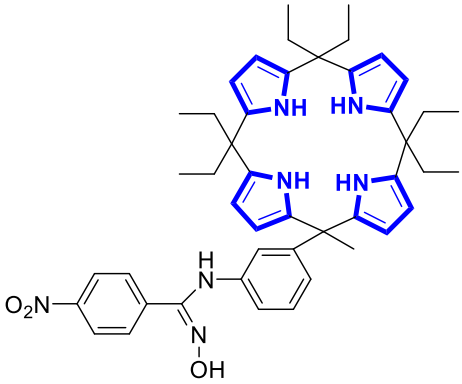

15

Güler's group reported a calix[4]pyrrole derivative containing Bodipy unit as potential fluorometric and colorimetric sensor for F^- ion.[33] The receptor **16** showed colorimetric and 'turn-off' fluorescent response in the presence of high electronegative and small size anions F^- due to the formation of H-bonds between anions and NH proton of receptors (Figure 1.8).

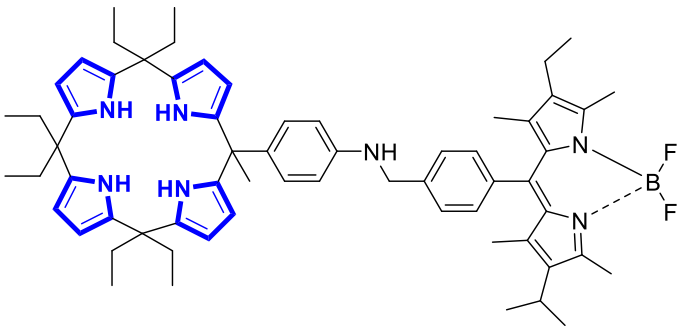

16

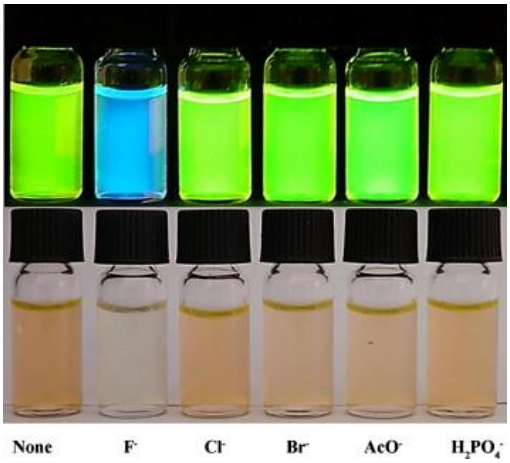

Figure 1.8: The photographs of **16** (1.0×10^{-4} M) solutions in acetonitrile in the presence of various anions (10 equiv.), taken either under day light (down) or in the dark and lightened by 365 nm light from a hand-held UV lamp. Image taken from *Spectrochim. Acta. A. Mol. Biomol. Spectrosc*. 2014;118:903-7.

1.5 Urea and Thiourea Based Anion Receptors

Urea is known as the most classical and one of the first investigated -NH containing receptor as it contains two NHs and on electron withdrawing carbonyl group.[34] Two NHs make it more effective H-bond donor and carbonyl group further promote the anion binding ability of urea. Urea and thiourea moiety are excellent H-bond donors therefore have been used widely in the design of anion receptors, gelators and medicines etc.[35] With the nature of forming parallelly oriented hydrogen bonds, urea and thiourea are found to form eight-membered ring complexation with oxoanions at high affinity. They are also able to form six-membered ring with spherical halides (Figure 1.9).[36] The formation of the ring system allows the strong and stable binding towards anions.

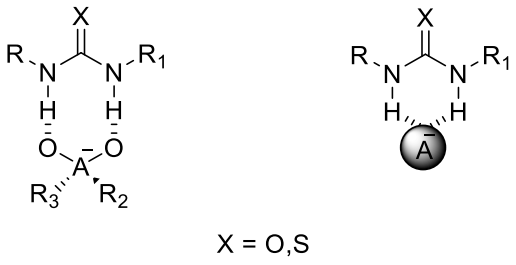

Figure 1.9: H-bond orientation of urea or thiourea receptors in oxoanions and halide complexes.[36]

Gómez *et al.* studied the difference of anion binding ability between urea and thiourea based anion receptors **17** and **18**.[37] The higher acidity of thiourea enables strong complex formation between receptor and anion, but also easily leads to deprotonation of the receptor, where deprotonation of receptor **18** was observed with all the tested anions except with the least basic Cl^-. Moreover, only F^- deprotonated the less acidic urea-based receptor **17**. Interestingly, the strongest binding was achieved with CH_3COO^- due to the geometrically favored bifurcated conformation of H-bond.

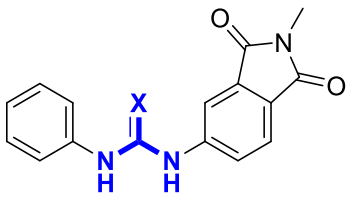

17 X = O
18 X = S

Monzani and co-workers investigated the interactions between 4-nitrophenyl substituted urea-based anion receptor **19** and selected anions.[38] The presence of electron withdrawing subsitituents $-NO_2$ was expected to increase the acidity therefore enhance the H-bond donor properties of the receptor. The optical properties of the chromogenic nitrophenyl may also provide a pathway for monitoring the receptor-anion interaction through optical sensing method. The addition of CH_3COO^- led to a color change of **19** from light yellow to bright yellow. The ^1H NMR titration, UV/Vis and IR study revealed that the color change is due to the formation of H-bond between CH_3COO^- and amide binding site of the receptor (Figure 1.10). However, the addition of other oxoanions such as $H_2PO_4^-$, NO_3^-, NO_2^-, HSO_4^-, and $C_6H_5COO^-$ caused no color change which could be attributed to less basicity of these anions. Interestingly, the addition of F^- ion caused dramatic color change of the receptor from light yellow to orange then to red. The authors demonstrated that this result is due to a two-step deprotonation of the N-Hs of the urea group.

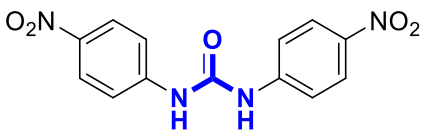

19

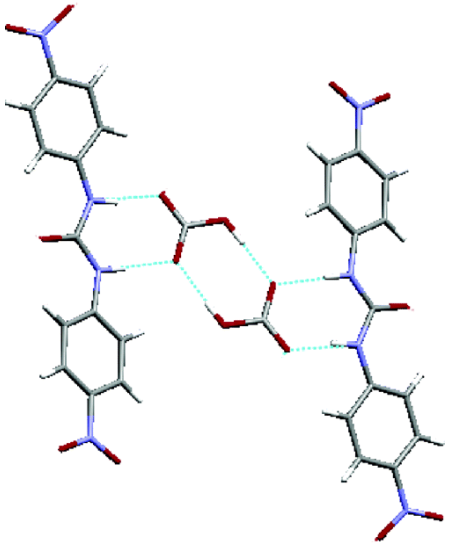

Figure 1.10: H-bond motif in the {[**19**,HCO_3]$^-$}2 dimer. H-bonds have been drawn in light blue. Image taken from *J. Am. Chem. Soc*. 2004;126(50):16507-14.

Recently, Matsumoto *et al.* developed an anthracene-diurea based fluorescence sensor with a new ON^1-OFF-ON^2 switching mechanism using the excited state intermolecular proton transfer (ESIPT) reaction.[39] 9,10BtDSPUA(compound **20**) showed maximum fluorescence in the presence of 0 mM of TBAAc (ON^1). Then the fluorescence was quenched by adding 0.30mM of TBAAc (OFF). However, with the addition of more TBAAc, intrinsic and enhanced fluorescence was observed again in the presence of 11.8 mM of TBAAc (ON^2) (Figure 1.11). The red-shifted fluorescence peak of ON^2 relative to that of ON^1 suggested that different electronic structures were formed in the emission state depending on the absence and presence of TBAAc. This demonstrates that fluorescence quenching and enhancement depend on the concentration of TBAAc. Therefore, the addition of TBAAc to **20** gives rise to an ON^1–OFF–ON^2 switching response.

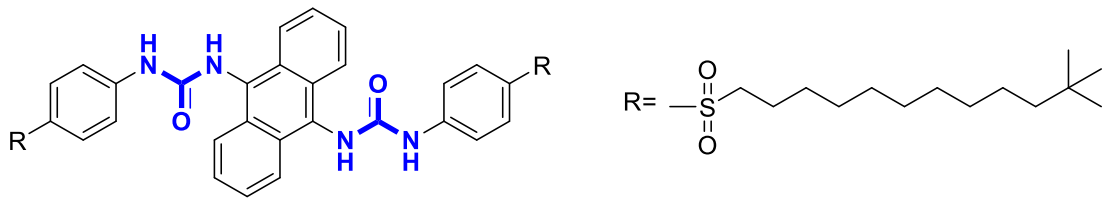

20

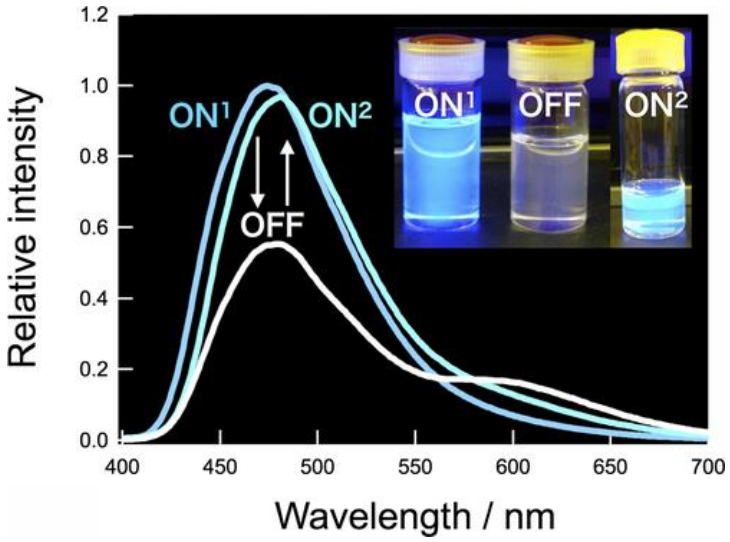

Figure 1.11: Emission spectra of **20** in the presence of 0, 0.30, and 11.8 mM of TBAAc for ON^1, OFF, and ON^2, respectively. Inset: photographs of samples taken in the dark under illumination by UV light. Image taken from *Photochem. Photobiol.* 2017;93(5):1187-92.

Noroozi-Shad *et al.* reported a series of the neutral N-phenylthiourea substituents (p-OC_2H_5, p-CH_3, m-CH_3, H, p-Cl, p-Br, m-Cl, and p-NO_2) as potential sensors for acetate and fluoride anions.[40] A theoretical DFT study (M062X and ωB97XD functionals) was used to investigate the sensing activity of the N-diphenylthiourea derivatives through the hydrogen bond formation between the anions and the N-H fragment of the thiourea functional group. ωB97XD functional showed a more reasonable correlation than M062X. *p*-nitro derivative **21** showed a stronger complex formation than the other derivatives with F^- (complex formation constants $K_f = 3 \times 10^7$). Therefore, *p*-nitro derivative **21** was supposed to be the best candidate for fluoride sensing.

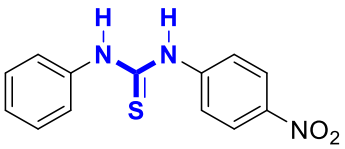

21

Singh *et al.* reported a thiourea based dipodal receptor for Br^- ion in an aqueous medium.[41] Receptor **22** reasonable selectivity to Br^- with detection limit of 3.79 nM. Moreover, receptor **22** showed reasonable stability under various conditions of pH, salt effect and chronoamperometric tests thus declared receptor **22** as potential sensor for Br^- ions.

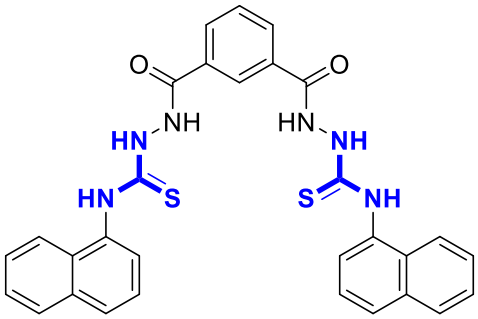

22

In 2015, Pfeffer and co-workers synthesized a series of peptidomimetic norbornene-based anion receptors **23-29** which mimic vancomycin as potential D-alanine hosts.[42] These receptors were found to bind to acetate or D-alanine in 1:1 anion:receptor stoichiometry by formation of H-bonds through urea or thiourea binding site. The amide N-H of receptor 2**9** was also found to assist the binding of anions. However, receptor 2**5** which contained a isopropyl side chain was demonstrated to have no tendency forming desired tridentate binding conformation. Although only modest binding affinity (average Log K_a = 1.9) of these receptors to acetyl-D-alanine was observed, the authors found a promising method for designing highly functionalized fused [*n*]polynorbornene-based vancomycin mimics.

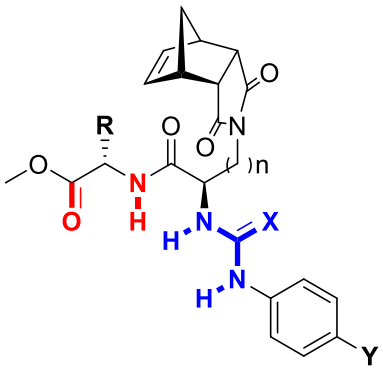

23	**X =** S	**Y=** H	**R=** H	**n=** 1
24	S	F	H	1
25	S	H	*i*-Pr	1
26	S	H	CH_3	1
27	S	H	H	4
28	O	F	*i*-Pr	1
29	O	F	H	1

23-29

Recently, Pfeffer's group reported another group of fused [3]polynorbornanes functionalized terephthalate and isophthalate receptors **30-32** with two flexible ethylenethiourea "arms" and different electron withdrawing groups at the end of each arm.[43] All receptors showed efficient binding towards terephthalate (Log K_a =3.0 to 3.3) in d_6-DMSO. The binding of isophthalate was much higher than that of terephthalate but with low accuracy. The authors undertook the titrations in more competitive solvent 5% H_2O:d_6-DMSO again to ensure the accuracy. The binding strength increased along with

the increasing electron withdrawing power of the aryl substituent (F < CF_3 <NO_2). MMFF94 force field calculations were used to determine the energy minimized binding conformations of receptor **30** with terephthalate and isophthalate in gas phase (Figure 1.12). The predicted structure of **30**:isophthalate complex showed that each N-H of the two thiourea binding site bind to each carboxylate oxygen atom through H-bond. However, in the presence of terephthalate, one thiourea arm formed two H-bonds toward a single oxygen atom which led to the weaker binding affinity. Thus, the large energetic penalty for the binding of guests revealed that these receptors designed with flexible arms are far more selective than intuitively predicted and only tolerate very small changes.

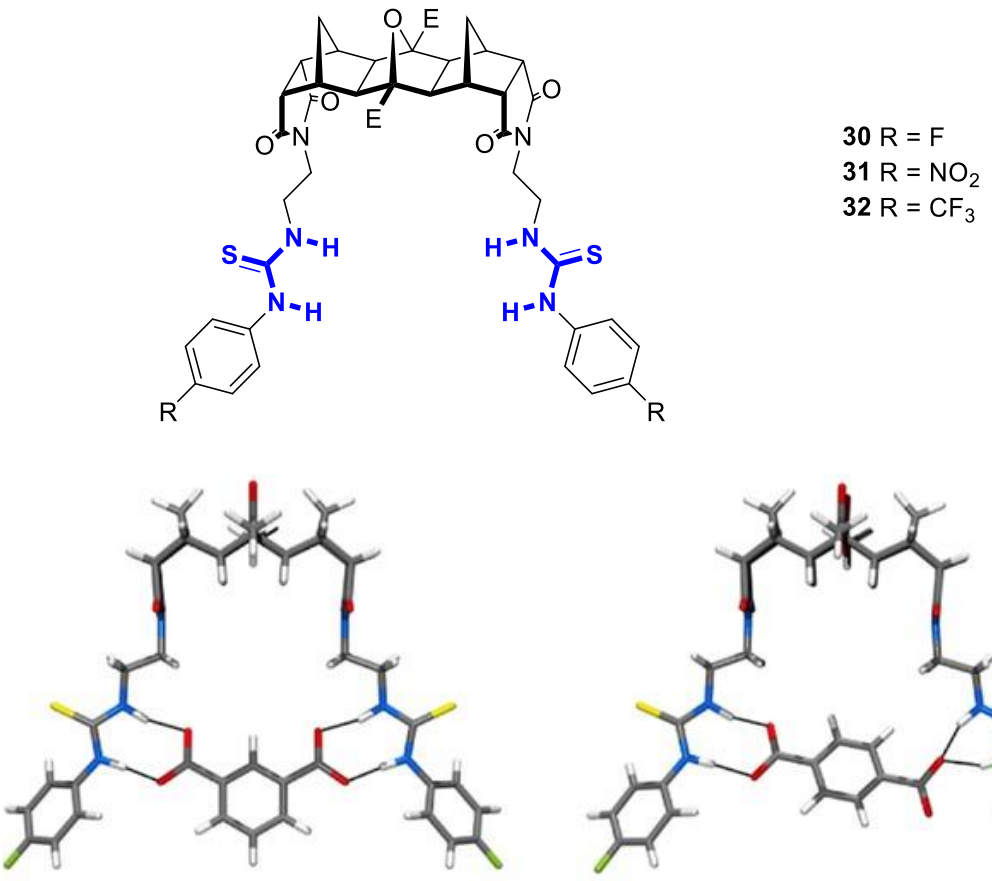

Figure 1.12: Molecular modelling of **30** with isophthalate (left) and terephthalate (right). Image taken from *ChemistrySelect*. 2017;2(17):4605-8.

1.6 Squaramide Based Anion Receptors

Secondary squaramide, as one of the various derivatives of squaric acid, is used widely in the design of effective anion receptors,[44] self-assembly motifs[45] and organocatalysts.[46]

Frontera, Deya and co-workers revealed that the NH groups of squaramide can act as H-bond donors while its carbonyl groups can act as H-bond acceptors thus squaramide was recognized to form H-bond to acceptors, donors and to mixed acceptor-donor groups (Figure 1.13).[18, 47] One of its most striking properties arises from the delocalization of a nitrogen lone pair into the cyclo-butenedione ring system conferring the four membered ring with aromatic character (Hückel's rule:(4n + 2) p electrons, n = 0). It was reported that the predicted aromaticity of delocalized squaramide *via* NICS (Nucleus Independent Chemical Shift) is -8.7 ppm, which is similar to the aromaticity of benzene (NICS = -10.1 ppm).[18] In addition, the capacity of squaramides to form strong hydrogen bonds that simultaneously increase the aromatic character of the four membered ring is highly advantageous where self-assembly and molecular recognition processes can benefit from favourable thermodynamic stability brought about by aromatic gain.[48, 49] This fact, along with other advantages of squaramides such as synthetic versatility, conformational rigidity and relative stability has encouraged an increasing research effort over the past few decades towards exploiting this most useful of scaffolds.

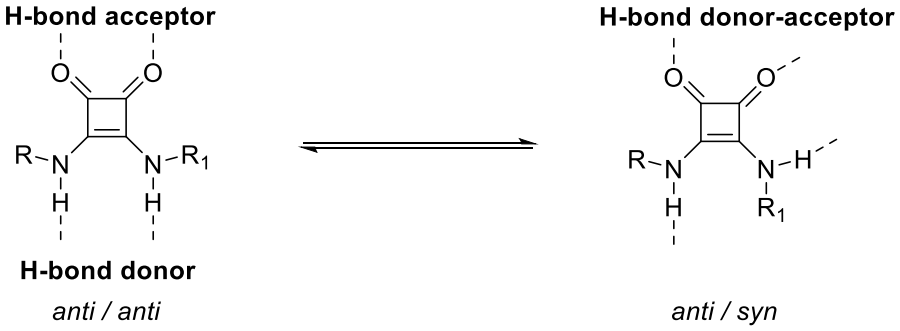

Figure 1.13: Hydrogen bonding donor-acceptor ability of squaramides.[18, 47]

The early pioneering study of squaramide facilitated anion recognition was reported by Costa's group in 1998.[50] The authors investigated the H-bonding ability of squaramide-based receptors **33-41**. Only moderate to good association constants of Neutral compounds **33-35** was obtained. However, the positively charged group containing receptor **36** showed an eight- to ten-fold increase in binding. Molecular modeling study of receptors **37-40** showed significant binding towards dicarboxylates derived from glutaric or glutaconic diacids. Although the association constants of the complexes formed between the TBA glutarate and receptors **37-40** in pure DMSO solution are too large to be measured by NMR, the addition of water lowered the association constants

into a measurable range. Receptor **41**, with an extra squaramide unit, was reported to have higher association constant comparing to receptors **37-40**.

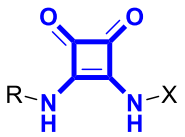

33: R,X = ^{t}Bu
34: R,X = Bu
35: R = Bn, X = $CH_2CH_2NMe_2$

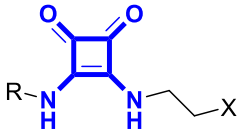

36: R = Bn, X = NMe_3+

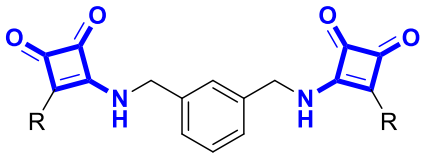

37: R = NHC_6H_{11}
38: R = NHBn
39: R = $NHCH_2CH_2NMe_2$
40: R = $NHCH_2CH_2NMe_3$+

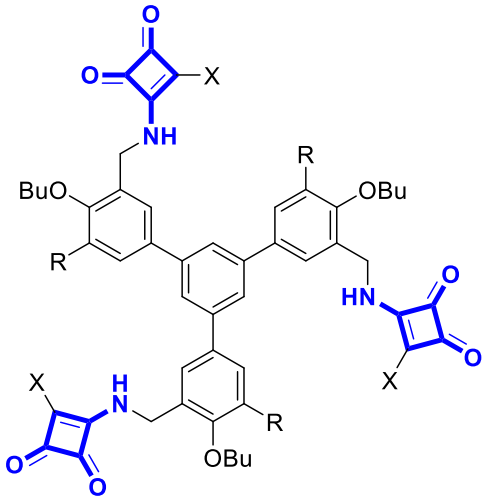

41: R = nPr, X = NHBn

Costa's group also developed a family of positively charged squamide-based receptors **42-47** for sensing SO_4^{2-} and HPO_4^{2-}.[51] In this case, it was the first time to use Cresol Red for signaling the presence of SO_4^{2-} or HPO_4^{2-}. The authors demonstrated that the charged squaramide receptors change the acid-base equilibrium of Cresol Red by complexation with the dianionic form of the indicator.

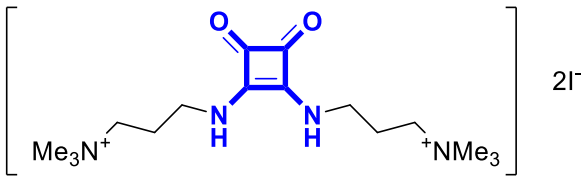

42

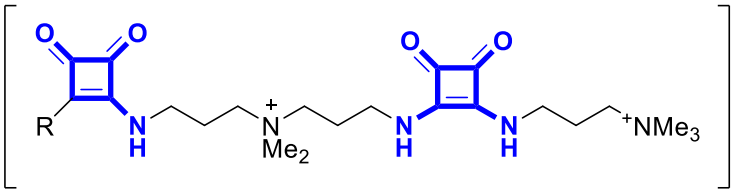

43 R = OEt
44 R = $NH(CH_2)_3NMe_2$

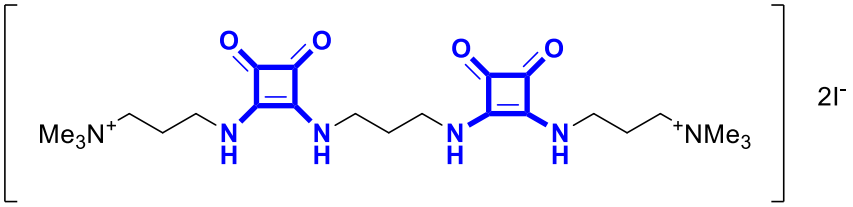

45

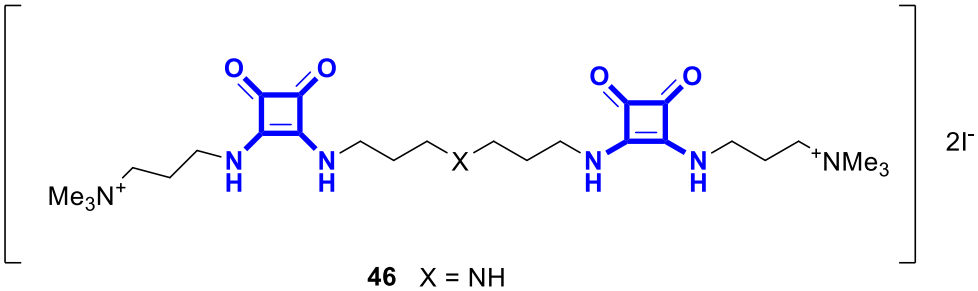

46 X = NH
47 X = CH_2

Fabbrizzi's group latterly undertook a direct comparison of the anion recognition ability between urea-based receptor **48** and squaramide based receptor **49**.[52] A combination of NMR spectroscopy, UV/Vis analysis, X-ray crystal structure analysis and theoretical calculations were used to show that both **48** and **49** were able to form 1:1 receptor : anion complexes with Cl^- *via* hydrogen bonding interactions but with the squaramide derivative **49** exhibiting a higher binding affinity in comparison to urea derivative **48** when measured by spectrophotometric titration ($\log K = 4.55$ for **48** *vs.* $\log K = 6.05$ for **49** when measured in MeCN at 25°C). This group also reported a subsequent study showing another squaramide derivative **51** has superior binding ability when compared to urea **50** and sulfonamide-based receptor **52**.[52] The results of spectrophotometric titrations, isothermal calorimetry (ITC) and ^{1}H NMR spectroscopic titrations in acetonitrile again suggested that squaramide based receptor **51** was capable of forming stable 1:1 receptor:anion complexes with Cl^- and with other oxoanions such as AcO^- and $H_2PO_4^-$.

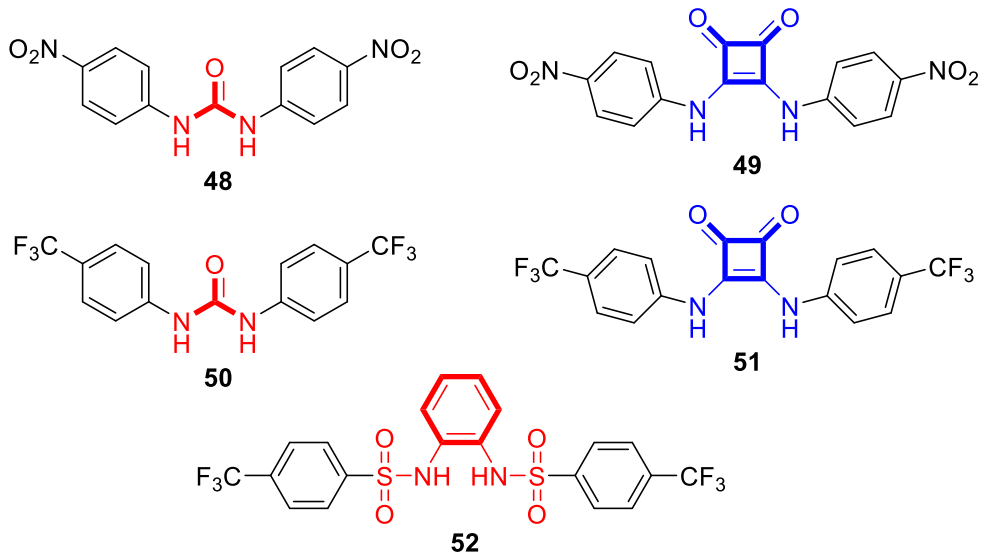

Piatek and co-workers designed ion pair receptors **53** and **54** containing a sodium-selective *N*-acyl aza-18-crown-6 binding domain and two anion-binding domains.[53] Single-crystal X-ray diffraction analysis of squaramide-based receptor **54** showed that the methyl group of the molecular platform brings all three binding domains point in one direction, thus providing an effective binding cavity for ion-pair (Figure 1.14). The authors demonstrated that the strength of sodium complexation was increased by 23 times upon binding of chloride to urea-based anion receptor **53**. Receptor **54** showed similar binding strength but with lower cooperativity. However, the strong binding between this receptor and NaCl (log K_a = 6.52 M^{-1}) revealed receptor **54** to be a more effective ion-pair receptor.

(a)

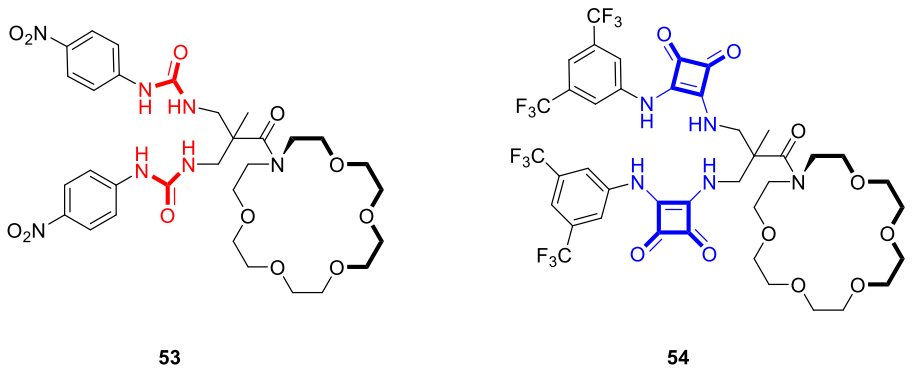

(b)

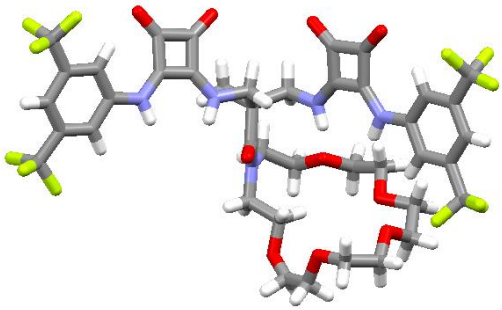

Figure 1.14: (a) The chemical structures of **53** and **54**. (b) X-ray crystal structure of **54** showing the alignment of both squaramide binding domains in one direction. Image taken from *Dalton. Trans*. 2016;45(39):15557-64.

A relative work from Zdanowski *et al*. demonstrated the use of **55** capable of extracting and transporting chloride salts from aqueous to organic phase.[54] UV/Vis and ^{1}H NMR studies showed strong complexation of receptor **55** and tested salts. They also reported that the presence of two anion binding sites are essential for the cooperativity of anion binding. The authors performed the extraction of chloride from aqueous organic solvent, toluidine blue was used to monitor the process (Figure 1.15). However, the transport of Cl^- only took place when soft countercations were used whereas hard countercations resulted in an unsatisfactory performance.

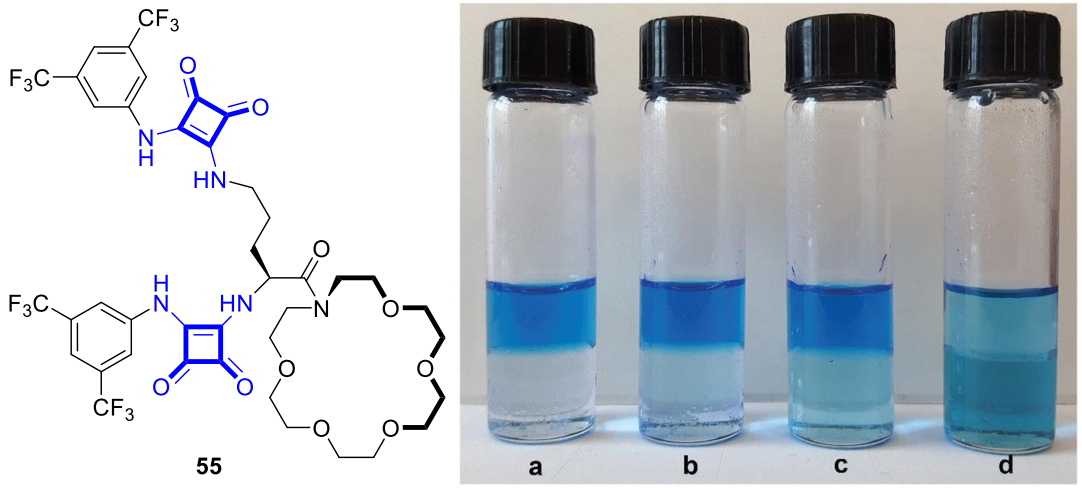

Figure 1.15: The chemical structure of **55** and extraction of aqueous solution of toluidine blue (top layers) with: (a) 20% n-butanol in chloroform, (b) 1 equiv. of receptor **55** in the organic phase, (c) 10 equiv. of receptor **55** in the organic phase, (d) 100 equiv. of receptor **55** in the organic phase (bottom layers). Image taken from *New. J. Chem*. 2016;40(8):7190-6.

Elmes *et al.* have synthesized a small family of amino acid and dipeptide-based anion receptors **56-61** with larger constructs using solid-phase synthetic strategy.[55] It was demonstrated that these anion receptors, particularly those containing squaramides displayed a significantly higher affinity for SO_4^{2-} over various other anions (AcO^-, BzO^-,$H_2PO_4^-$ and Cl^-) where ^1H NMR titrations exhibited large modulations in chemical shift upon titration with SO_4^{2-}. Interestingly, the stereochemistry of the amino acid backbone showed little influence on the binding affinity of the receptors towards their target anions. However, the presence of the backbone amide NH protons was shown to be particularly important to the receptor : anion interaction where dipeptide receptors **58-61** displayed significantly higher binding affinities for SO_4^{2-} when compared with their single amino acid analogues **56** and **57**.

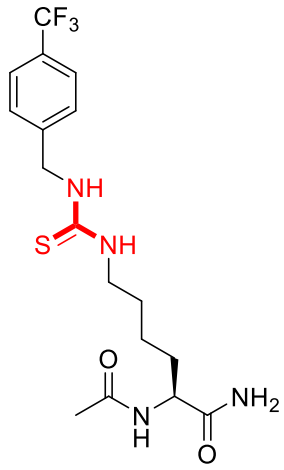

56

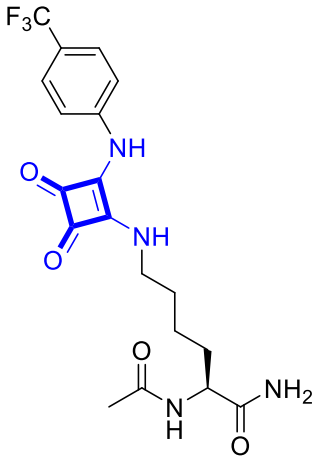

57

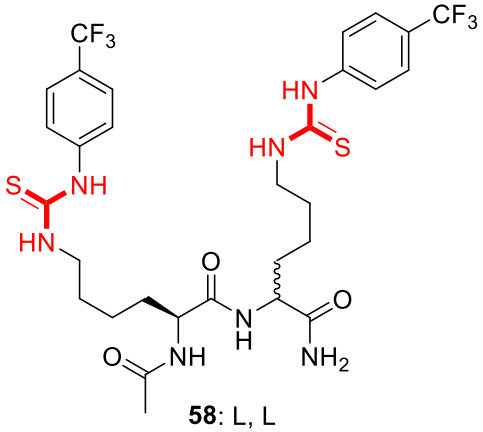

58: L, L
59: D, L

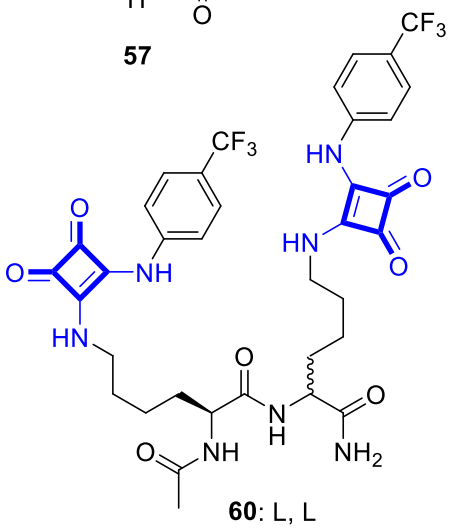

60: L, L
61: D, L

A subsequent article from Elmes *et al.* investigated the anion binding ability of *L*-lysine-based squaramide anion receptors **62-69** by using ^{1}H NMR spectroscopic titrations.[56] All these receptors again demonstrated the selective binding ability towards SO_4^{2-} over other anions such as Cl^-, AcO^- and BzO^- in aqueous DMSO solution. The also demonstrated that fine-tuning of the lipophilicity of the receptors at the C- and N- termini had no influence on their anion-binding capabilities.

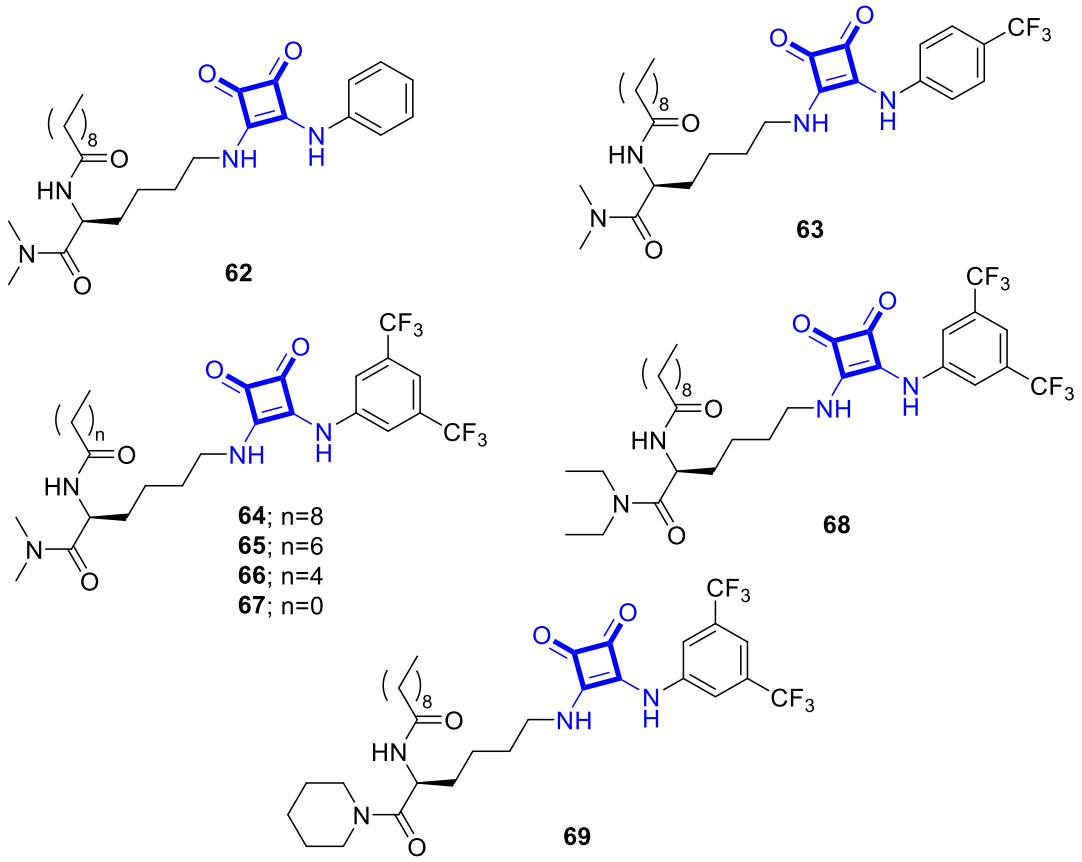

Recently, Qin *et al.* reported a family of macrocyclic squaramides **70-75** containing either two or three squaramide units.[57] ^{1}H NMR titration studies revealed that the macrocyclic squaramide (MSC) receptors **70**, **71**, **74** and **75** displayed very high selectivity for SO_4^{2-} in aqueous DMSO-d_6 solution. Upon complexation to SO_4^{2-}, The ^{1}H NMR spectrum of **70** showed large chemical shift and the signal for methylene protons was split into two distinct signals. The authors suggested that upon complexation to SO_4^{2-}, the receptor fixed in a single conformation instead of adopting several conformations in solutions at room temperature. Indeed, X-ray crystal structure analysis showed that **70** preferred to form a bowl-like conformation with SO_4^{2-} in 1:1 receptor/anion complex instead of forming the chair-like conformation found for free macrocycle(Figure 1.16). Additionally, receptor

71 and **75** containing three squaramide units were found to better match the size and shape of the SO_4^{2-} ion than smaller compounds **70** and **74** and demonstrated high affinity and selectivity for SO_4^{2-} even in mixtures of anions stimulating the composition of nuclear waste or blood plasma.

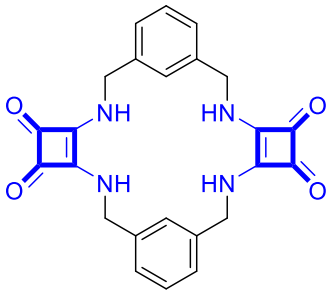

70

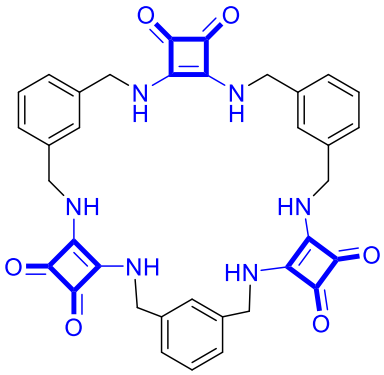

71

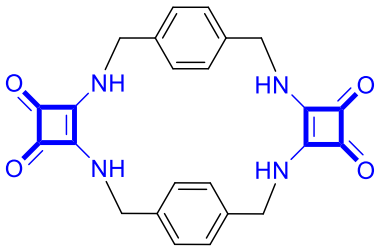

72

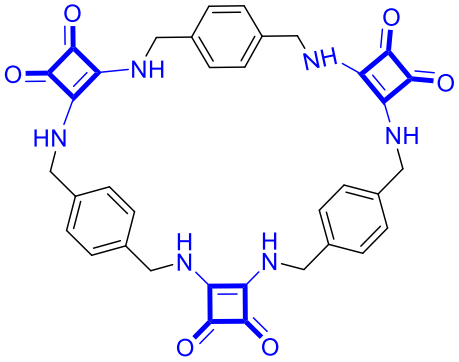

73

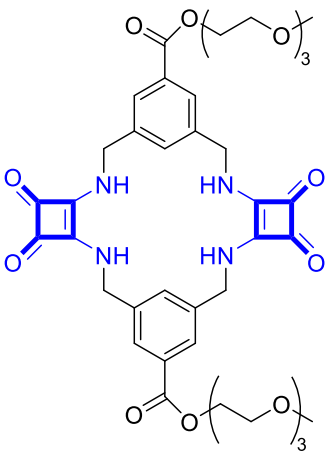

74

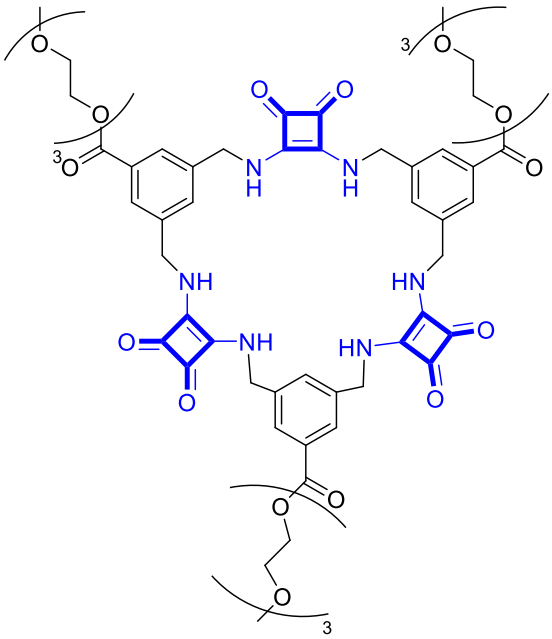

75

(A) (B)

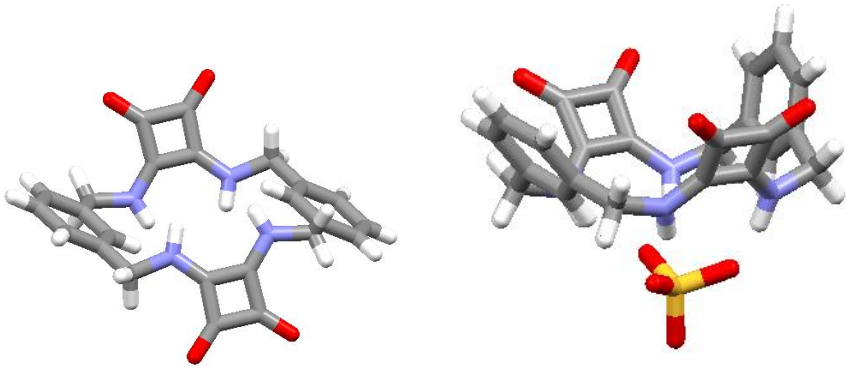

Figure 1.16: Single crystal X-ray diffraction structures of (A) **70** and (B) the complex formed between **70** and SO_4^{2-} clearly showing the interaction of SO_4^{2-} with the squaramide NH protons inside the macrocyclic cavity. Image taken from *Chem. Sci*. 2016;7(7):4563-72.

Elmes *et al.* synthesized a group of squaramide-based colorimetric and luminescent anion sensors **76-79** by introducing an anthracene moiety to the squaramide scaffold.[58] Little interaction of the sensors with non-basic anions such as Br^-, I^- and NO_2^- was reported, however, upon addition of Cl^- to **76** and **77**, their absorption spectra underwent hyperchromic shifts at 393 nm, with a hypochromic shift at 355 nm. A naked eye color change from colorless to yellow was also observed (Figure 1.17).

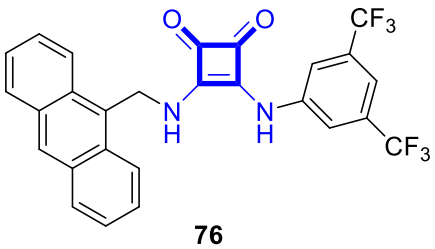

76

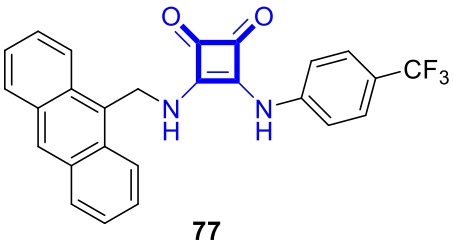

77

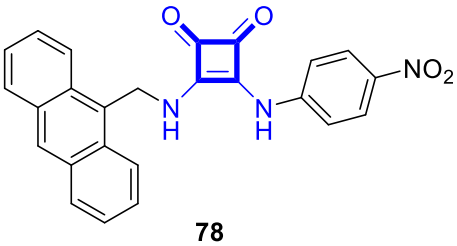

78

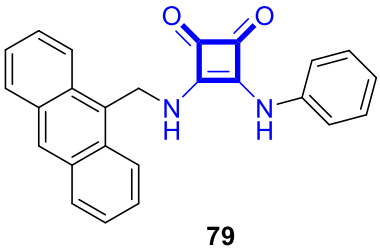

79

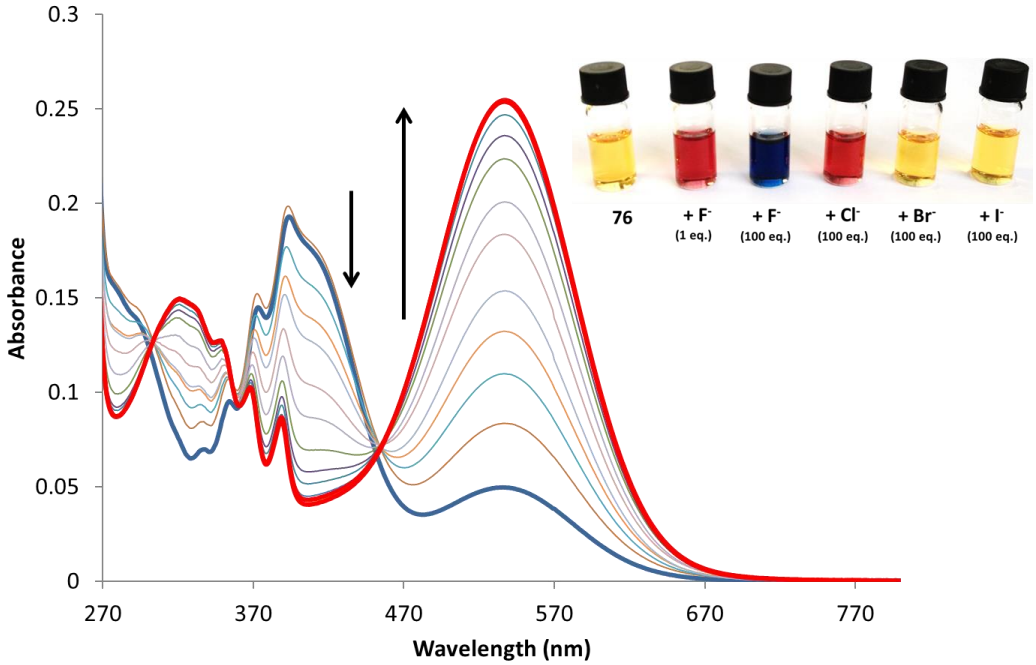

Figure 1.17: Changes observed in the absorption spectrum of **78** upon addition of TBACl in DMSO. (Inset): The corresponding changes seen by the naked eye with various halide anions. Image taken from *Org. Lett.* 2013;15(22):5638-41.

This chapter has given a detailed discussion of the crucial role anions play in biology and the environment and has tried to highlight some examples of anion recognition motifs based on H-bonding scaffolds. Particular emphasis has been placed on squaramide based receptors where can selectively bind to anions *via* H-bonding with high affinity. Several anion receptors which can selectively bind to anions *via* H-bonding were also introduced in this chapter. Below we will outline the aims and objectives set out in this thesis.

1.7 Aims and Objectives

Squaramide, as an emerging binding motif, has been reported to show superiority binding affinity compared to similar structure such as urea/thiourea motifs owing to the stronger formation of H-bond.[53, 55, 59] These advantages have attracted increasing research interest over the past number of years. Inspired by recent research within the Elmes group, the aim of this project is to synthesize two families of squaramide-based anion receptors. The first family of compounds that will be discussed is based on the squaramidoquinoxaline

scaffold where compound **80-85** will be synthesized to investigate the effect of various functional group substitution on the SQX structure and its effect on anion recognition.

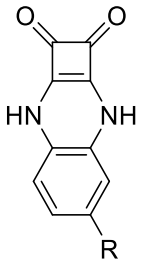

80 = H
81 = NO_2
82 = OMe
83 = COOH
84 = CN
85 = Br

We envisaged that the incorporation of electron withdrawing or donating group on the SQX motif will modulate the binding/recognition ability of the receptors which should influence anion selectivity and sensitivity.

The second aim will be the synthesis of another family of macrocyclic squaramide (MSQ) based macrocyclic compounds **70** and **86-90** (Figure 1.18). It has previously been shown that **70** is capable of strong and selective sulfate recognition where X-ray crystal structure analysis has revealed that the anion is bound in the macrocyclic cavity. X-ray analysis also revealed that sulfate recognition stimulates a conformational change in the molecule from a chair- to a bowl-like conformation.[57] We proposed that this effect may be exploited to develop fluorescent anion sensors based on a FRET mechanism. Compound **70** and **86-90** are proposed as target compounds and Chapter 3 will outline in detail for this choice of structures proposed as novel fluorescent sulfate sensors.

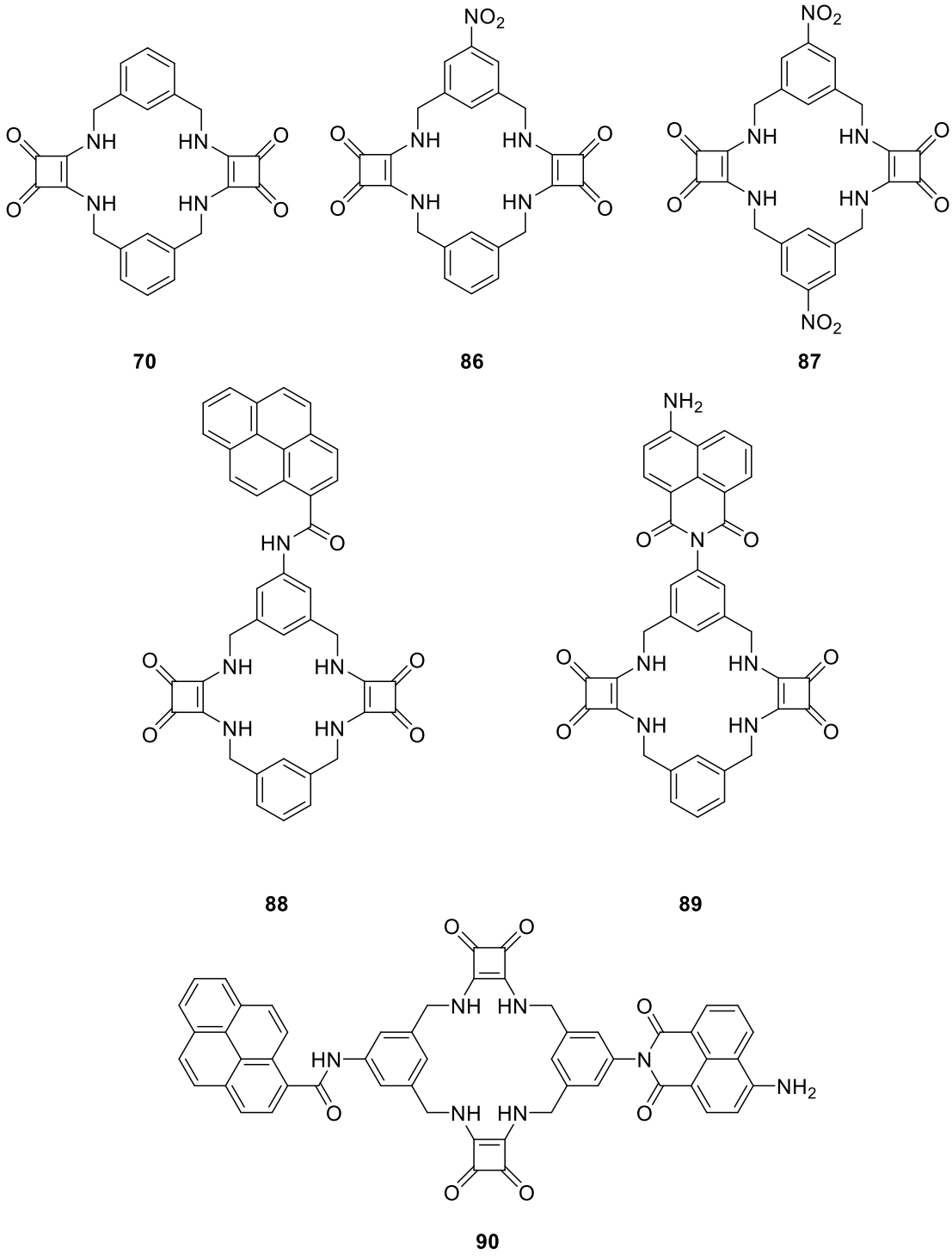

Figure 1.18: Structure of compound **70** and **86-90**.

Chapter 2 Squaramidoquinoxaline (SQX) Moiety Based Chemosensors

2.1 Introduction

Squaramides with their inherent rigidity and strong hydrogen bond donor ability have garnered great research interest in the design of anion receptors,[44, 51, 60-62] self-complementary molecular recognition motifs,[63] and many organocatalysts.[46] Elmes group and others have focused on the development of a characteristically different family of receptors based around the squaramide motif.[57, 58, 64-69] For instance, as discussed in chapter 1, Elmes *et al.* reported a group of squaramide-based colorimetric and luminescent anion sensors **76-79** with an anthracene moiety connected to the squaramide scaffold (Figure 2.1).[58] Upon the addition of basic anion Cl^- towards the receptors, the absorption spectra change of **76** and **77** together with a naked eye color change from colorless to yellow revealed that these compounds to be good anion sensors.

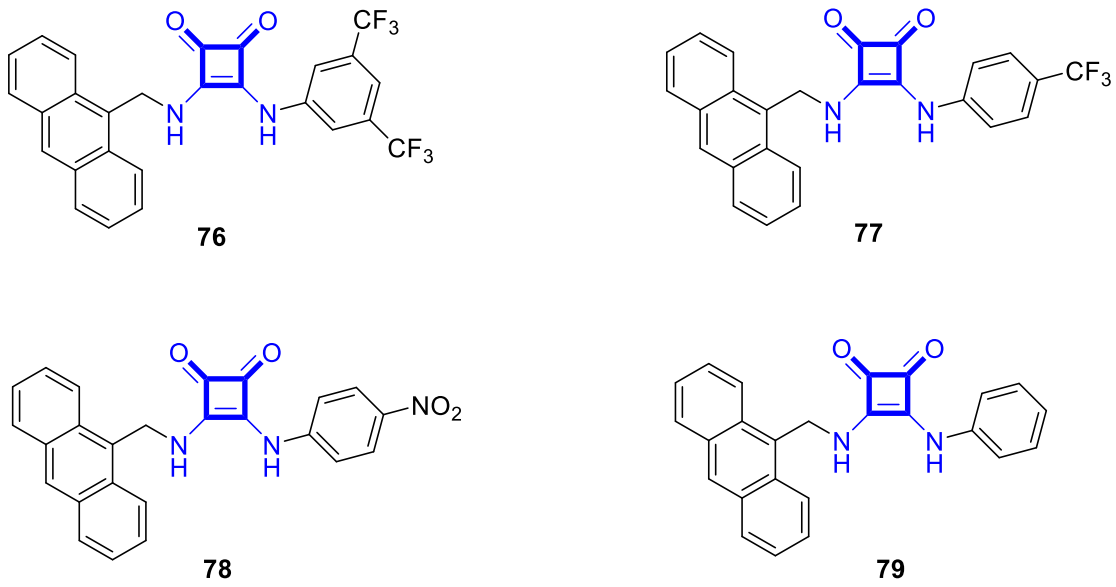

Figure 2.1: Structure of squaramide-based anion sensors **76-79.**

Encouraged by the previous work, we wished to develop a novel squaramide motif cyclobuta[b]quinoxaline-1,2(3H,8H)-dione or 'squaramidoquinoxaline' which has two amines connected to one aryl ring with various functional groups (Figure 2.2).

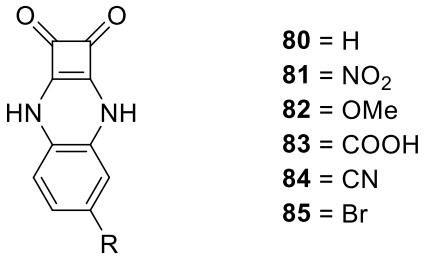

Figure 2.2: Structure of squaramidoquinoxaline-based anion sensors **76-79.**

We expected that by modification of a parent squaramidoquinoxaline scaffold with either electron withdrawing or electron donating groups we could modulate the acidities of the NHs of the squaramide thereby provide a level of control over the selectivity of any anion binding that may occur. The electron withdrawing group (EWG) which connected to the benzene of the squaramidoquinoxaline scaffold is supposed to pull the electron density of the NHs all the way back thereby making the increasing of the acidity of NHs. Conversely, electron donating group (EDG) is supposed to cause the reduction of acidity of the NHs (Figure 2.3).

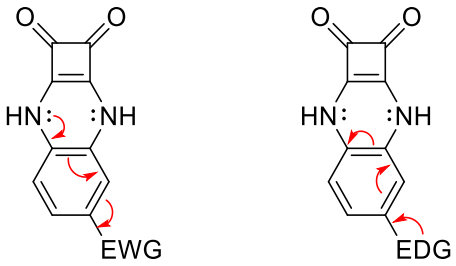

Figure 2.3 Charge transfer within the molecule when binds to EWG and EDG.

The aim of this chapter is to synthesis and characterise a group of compounds **80-85** based on the squaramide motif and identify their potential as possible anion sensors using a range of physical and theoretical techniques such as UV/Vis titration, NMR titration, computational study and test strip study.

2.2 Synthesis of Compounds 80-85

The Retrosynthetic analysis of the target molecules showed that by breaking the C-N bonds which connect the secondary amine and the cyclobutene ring resulted in diethyl squarate and respective phenylenediamine (Scheme 2.1). The diethyl squarate could be

easily synthesized from squaric acid and all the functionalized phenylenediamines were commercially available compounds.

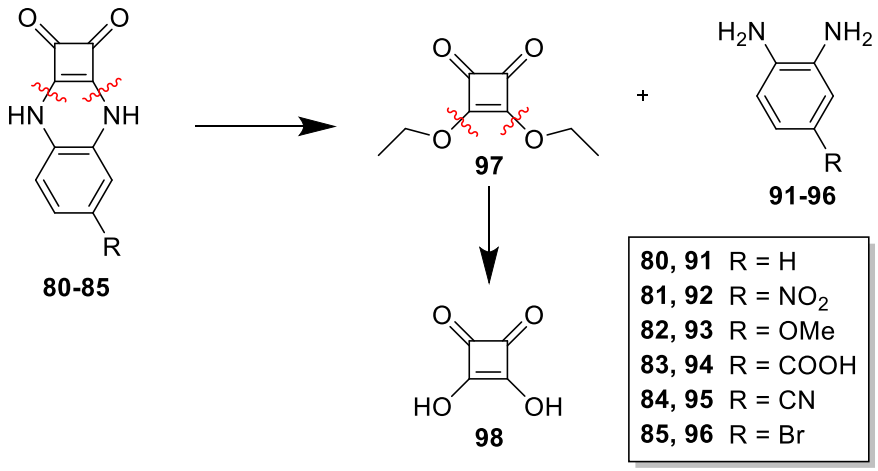

Scheme 2.1: Retrosynthetic analysis of the target molecules.

Thus, novel anion sensors could be synthesized by two simple steps with mild conditions. For instance, the synthesis of compound **80** was achieved by the condensation of diethyl squarate **97** and *o*-phenylenediamine **91**. Diethyl squarate **97** was synthesized as outlined in scheme 2.2, by refluxing the solution of commercially available squaric acid **98** (3,4-dihydroxycyclobut-3-ene-1,2-dione) and triethyl orthoformate in EtOH. Removal of solvent followed by purification using silica gel column chromatography yielded yellow oily product **97** in 95% yield.

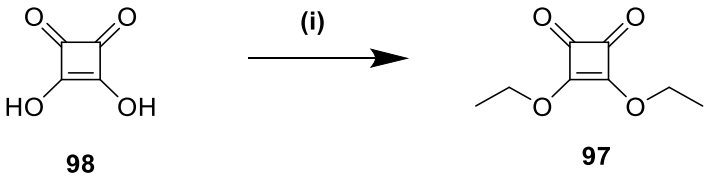

Scheme 2.2: Synthetic pathway of compound **97. (i)** Triethyl orthoformate, EtOH, reflux, 95%.

Compound **80** was synthesized *via* nucleophilic substitution by stirring the solution of diethyl squarate **97** with *o*-phenylenediamine **91** and zinc triflate in EtOH at room temperature (scheme 2.3). Removal of solvent by filtration yielded the orange solid target molecule **80** in 64% yield.

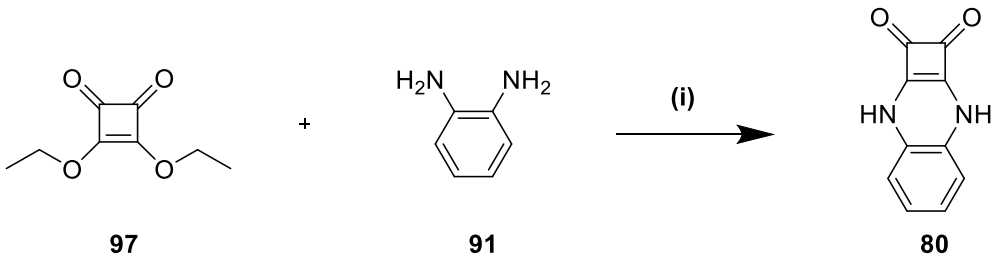

Scheme 2.3: Synthetic pathway of compound **80. (i)** Zinc triflate, EtOH, rt, 64%.

Same method was applied in the synthesis of compound **81-85** using diaminobenzene **91-97**, respectively. The products yielded as purple, brown, orange, orange and orange solids respectively in 73%, 97%, 77%, 87% and 84% yield. Compounds **81-85** were fully characterized by ^{1}H NMR, ^{13}C NMR, HRMS and FTIR spectroscopy. As a representative example the ^{1}H NMR of compound **80** is presented in Figure 2.4. The singlet at 10.0 ppm is attributed to the two NH protons. The doublets at 6.66 and 6.36 ppm assigned to the aromatic protons of the aryl ring. Successful formation of compound **80** was also supported by accurate mass spectrometry, where **80** displayed a peak at 186.0429 corresponding to the [M + H] ion. The ^{1}H NMR and ^{13}C NMR spectra of compounds **80-85** are shown in the Appendix section. All other compounds were similarly characterized as outlined before.

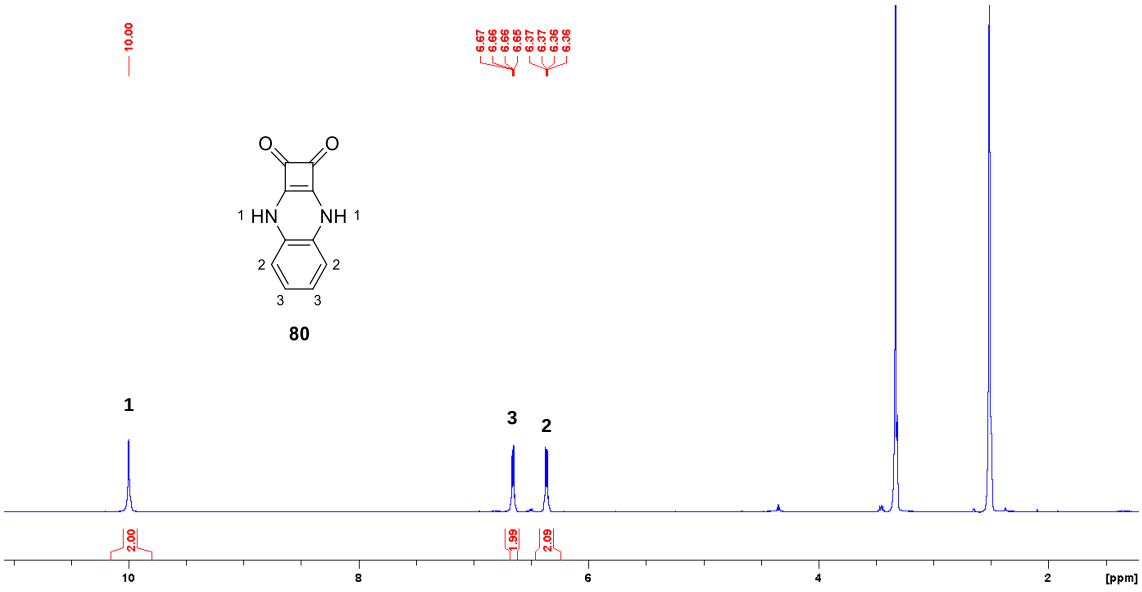

Figure 2.4: The ^{1}H NMR spectrum of compound **80** (500.13 MHz, DMSO-d_6).

In figure 2.5, the broad signal at 10.45 ppm assigned to two NH protons. The doublet of doublet at 7.5t ppm assigned to aromatic proton H4, the doublet signal at 7.01 ppm

assigned to aromatic proton H5 and the doublet at 6.41 ppm assigned to aromatic proton H3. Comparing the ^{1}H NMR spectrum of compound **81** to **80,** a distinct split of the NH signal peak and three peaks of aromatic protons were observed which were attributed to the asymmetric structure of compound **81**. Moreover, due to the existence of strong electron withdrawing -NO_2 group, all the signal peaks showed a downfield shift in comparison to the ^{1}H NMR spectrum of **80**.

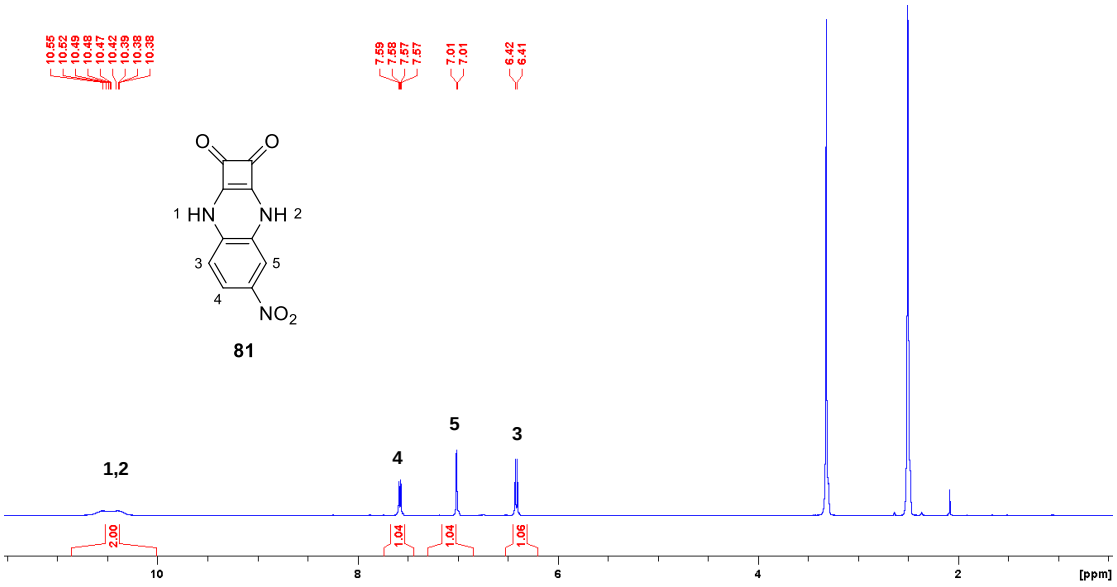

Figure 2.5: The ^{1}H NMR spectrum of compound **81** (500.13 MHz, DMSO-d_6).

While not completely pure, compound **82** was sufficiently pure for further evaluation. As shown in the ^{1}H NMR spectrum of another asymmetric compound **82** (Figure 2.6), the split signal peak at 10.0 ppm assigned to the two NH protons peak was observed again, the doublet at 6.34 ppm assigned to aromatic proton H5, the doublet of doublet at 6.24 ppm assigned to aromatic proton H4 and the doublet at 6.02 ppm assigned to aromatic proton H3. The peak centred at 3.63 ppm assigned to protons H6. A distinct upfield shift of the aromatic proton signals were observed in comparison to **80** which was ascribed to the electron donating ability of the -OCH_3 group. To provide a more visualized view of how the functional groups prompted the signal shifts of compound **80-82**, an overlap of their ^{1}H NMR spectrum is shown in Figure 2.7.

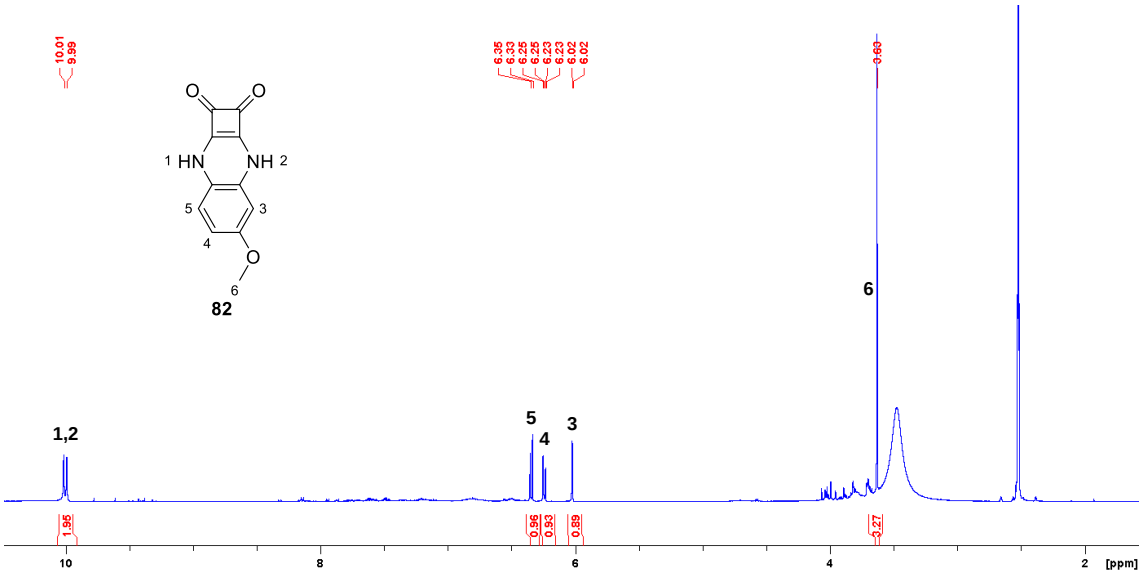

Figure 2.6: The ^{1}H NMR spectrum of compound **82** (500.13 MHz, DMSO-d_6).

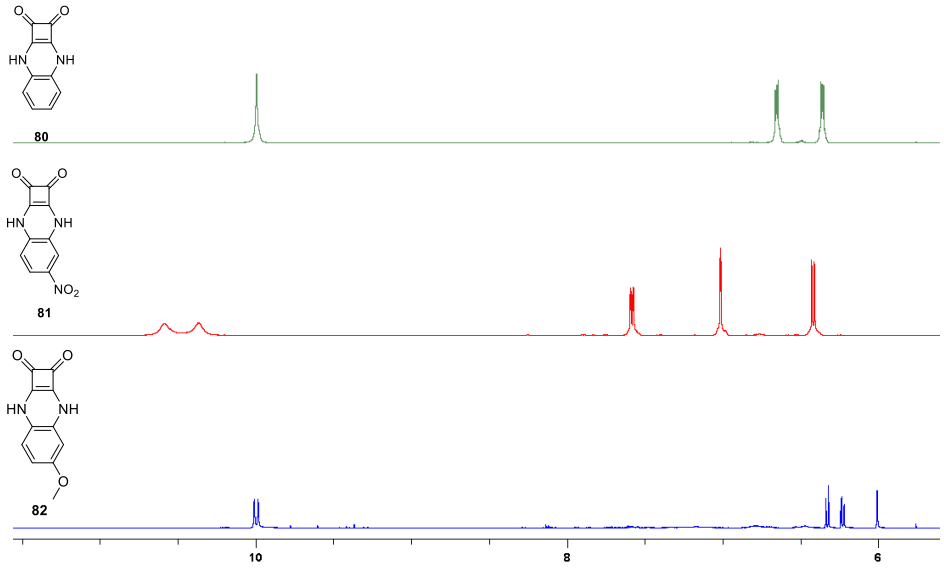

Figure 2.7: The multiple display ^{1}H NMR spectrum of compound **80-82** (500.13 MHz, DMSO-d_6).

2.3 UV/Vis Absorption Properties

Photophysical properties of compound **80-85** were characterised using UV/Vis absorption spectrometer with the aim to better understand the photophysical behaviour of receptors upon interaction with anions.

As a representative example, the UV/Vis absorption spectrum of compound **80** is shown in Figure 2.8. Absorbance values at 306 and 337nm were plotted as a function of concentration, the slope was obtained as the extinction coefficient with values of 3821 and 4490 $M^{-1}cm^{-1}$, respectively.

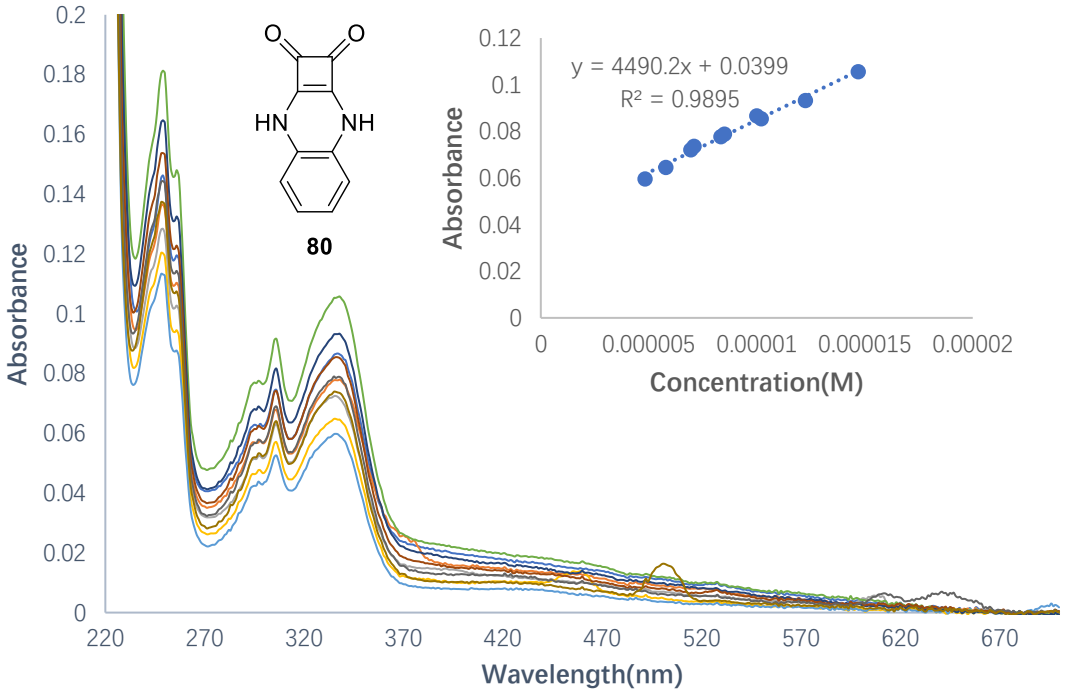

Figure 2.8: Changes in UV/Vis spectrum upon increasing concentration of **80** in PBS buffer solution. **Inset:** Plots of absorbance at 337 nm as a function of increasing concentration of **80**.

All the other compounds were similarly tested as outlined above and the spectra are shown in Appendix section. The extinction coefficient of **80-85** at is shown in Table 2.1 below.

Compound	λmax (nm)	ε ($M^{-1}cm^{-1}$)	λmax (nm)	ε ($M^{-1}cm^{-1}$)
80	337	4490	306	3821
81	374	11036	307	27047
82	349	10519	312	11373
83	347	16678	309	17101
84	351	20388	297	20517
85	345	14573	309	11531

Table 2.1: The extinction coefficient of **80-85**. For each compound, two λmax values and their corresponding extinction coefficient are shown in this table.

In 0.5% H_2O in DMSO solution the absorption spectrum of **81** showed strong π – π* absorption bands at 310 nm and 390 nm respectively with an additional broad shoulder centered at 532 nm ascribed to a charge transfer within the molecule owing to the presence of the electron withdrawing nitro group.[52] An additional long wavelength shoulder at 715 nm was also observed. However, for compounds **80** and **82-85** only broad bands (312 nm and 347 nm for **80**, 320 nm and 354 nm for **82**, 305 nm and 344 nm for **83**, 338 nm and 388 nm for **84**) owing to to π – π* transitions were observed from their UV spectra whereas only one significant peak was observed at 339 nm for **85**. Inspired by the specific UV/Vis absorption property of **81**, we assumed that the electron withdrawing nitro group causes the poor electron density of the NHs of **81,** thus may induce the reactivity of the NHs towards acids or bases. The acid/base test was undertaken by adding 1% acetic acid or triethylamine to a dilute solution of **81** (10μM) in 0.5% H_2O in DMSO. The addition of acetic acid caused the disappearance of the absorption band at 715 nm and an increase in absorbance of the bands at 310 nm, 390 nm and 532 nm but did not result in any observable colour change. Interestingly, addition of 1% triethylamine caused an increase in the absorbance of the bands at 715 nm and 450 nm and was concomitant with a dramatic colour change from pink to green clearly visible to the naked eye (Figure 2.9).

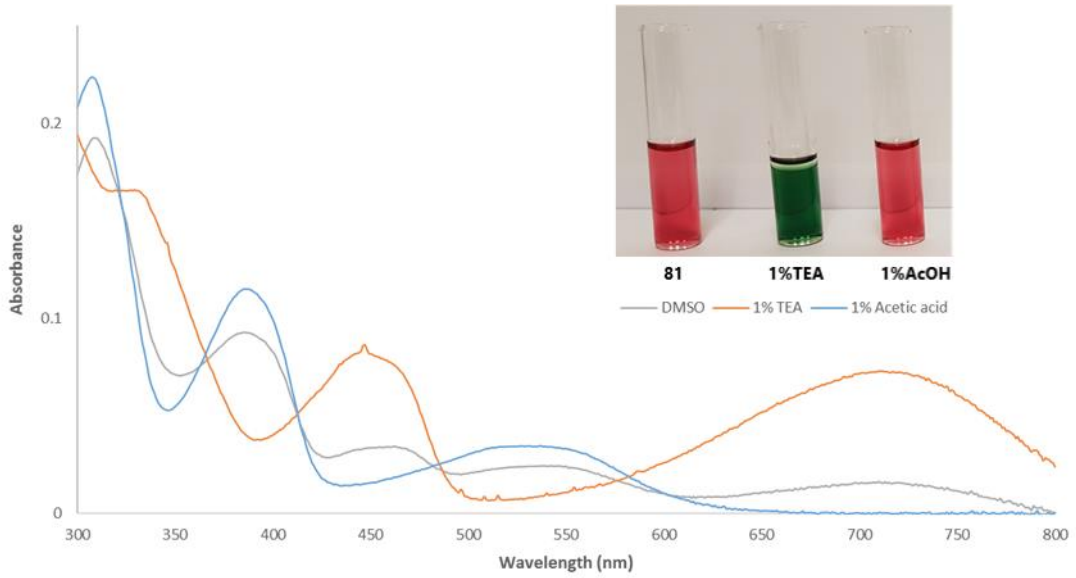

Figure 2.9: The absorption spectra of **81** (0.5 x 10^{-5} M) in DMSO (grey), 1% Et_3N in DMSO (orange) and 1% acetic acid in DMSO (blue). **Inset**: The appearance of the corresponding solutions to the naked eye.

In order to investigate the observed UV spectral changes, a computational study was conducted in collaboration with Dr.Tobias Krämer at Maynooth University. TD-DFT calculations at the SMD-PCM/B3LYP/6-311G+(2p,d) level of theory was used to investigate the observed UV/Vis spectral changes. The calculated absorption spectrum of **81** is in coincident with experiment, with three peaks predicted at 301 nm, 382 nm and 549 nm. The π-π* type character of these transitions is revealed by analysis of the associated Natural Transition Orbitals (NTO). In contrast to analysis of excitation amplitudes in the canonical molecular orbital basis, NTOs provide an easy means to interpret the character of electronic transitions. The low-energy peak at 549 nm corresponds to the HOMO-LUMO transition, which is dominated by an intramolecular charge-transfer process between the squaramide ring system and the nitro group (Figure 2.10). The nature of the other two transitions can be readily identified from the NTO plots. Single deprotonation of **81** causes a red-shift of the peak at 549 nm, irrespective of which tautomeric form of **[81-H]**$^-$ is considered (see Appendix section). Calculated peaks at 653 and 730 nm for tautomer N1 and N2, respectively, are consistent with a reduced HOMO-LUMO gap for these anionic species. Likewise, the peak at 382 nm in **81** is shifted to around 420 nm in both tautomers. In summary, the calculations further indicate that the

characteristic red-shift in the presence of base is due to single deprotonation of **81**. It should be noted that a linear energy scale for comparison between experimental and theoretical excitation energies is more convenient, and in the present case the deviation is 0.03-0.20 eV. Since these values fall into the common error range for TD–DFT,[70] it is not possible to discriminate between the two tautomeric forms of **[81-H]**$^-$ based on their calculated UV/Vis spectra.

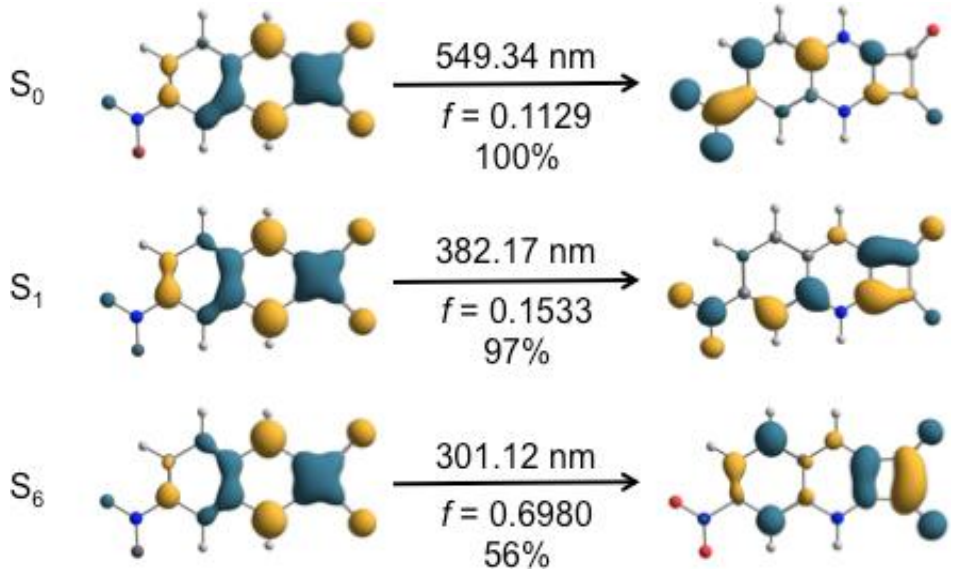

Figure 2.10: Plots of NTOs (isovalue = 0.05) for key electronic transitions in **81**. Excitation energies are given along with oscillator strengths and weights of NTO pairs.

Combined, the above results suggest that in solution a proportion of **81** may exist in its mono-deprotonated form (Scheme 3.4) even in the absence of base. This effect has previously been reported by Taylor and co-workers for squaramide systems containing strongly electron withdrawing aryl substituents and is thought to be favoured due to the possibility of delocalisation of the formal negative charge in to the cyclobutenedione ring.[44] A pH-spectrophotometric titration in a mixture of acetonitrile/water (9/1 v/v; in the presence of 0.1 M $TBAPF_6$) was undertaken to further investigate the observed UV/Vis spectral and colour changes as reported by Elmes *et al*.[65, 67] The significant shift of the UV/Vis absorption spectrum, where a hypochromism centered at 375 nm and 500 nm and a concomitant hyperchromism at 415 nm and 615 nm between pH ≈ 6 – 9.5 revealed that **81** undergo two distinct deprotonation events. This was followed by a second spectral change between pH ≈ 10.3 - 12 in which hypochromism across the entire

spectrum was observed. The colour changes to the naked eye from pink to green to yellow was observed simultaneously with the spectral change. We also found that the pink – green colour change (1st deprotonation step) is reversible by addition a protic solvent, while the green – yellow (2nd deprotonation step) cannot be reversed and it appears that the di-deprotonated derivative undergoes a time dependent fragmentation. The pKa titration profile is shown in Figure 2.11. The obtained pKa value for the first deprotonation was determined as 8.25 ± 0.03 (this value was determined by the four parameter sigmoid curve fit with the point of inflexion corresponding to the pKa value), however a pKa value for the di-deprotonated derivative could not be determined due to its instability at pH values below 12 evidenced by further time dependent spectral changes occurring at high pH values.

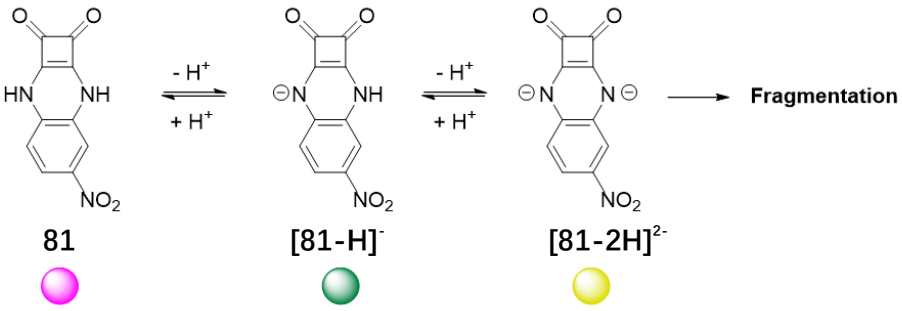

Scheme 3.4: Proposed acid-base behaviour and corresponding colorimetric response of **81.**

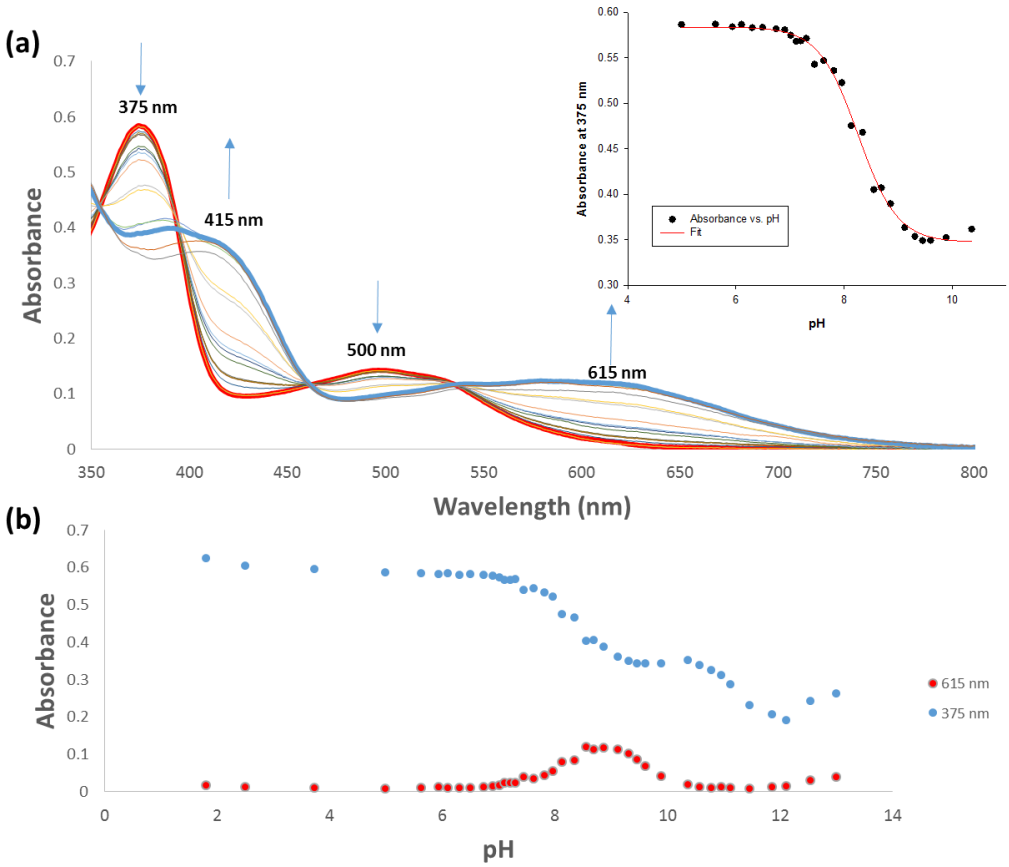

Figure 2.11: (a) Absorption spectra taken over the course of the pH-spectrophotometric titration of **81** (1×10^{-5} M) from pH ≈ 6 – 9 in an acetonitrile–water mixture (9/1 v/v; in presence of 0.1 M $TBAPF_6$). (Inset): Four parameter sigmoid curve fit with the point of inflexion corresponding to the pKa value (b) Plots of absorbance vs. pH at 375 nm and 615 nm showing two distinct deprotonation events from pH 2 – pH 13.

2.4 Anion Binding Study

2.4.1 UV/Vis Absorption Anion Titrations

It has been observed that compound **81** underwent a distinct colour changes in the presence of base. We next wished to investigate its potential as a colorimetric anion sensor where, with the enhanced acidity afforded by the nitro group. We expected that this compound may give rise to a selective sensor for F^- as the most basic of the halides. The halide sensing ability of **80-85** were tested in 0.5% H_2O in DMSO solution (1×10^{-5} M of each compound) by titration of F^- in the form of tetrabutylammonium salt (TBA^+), observing any changes in their ground state properties (See Appendix). As expected, the most dramatic colour change of the solution of **81** from pink to green was observed upon

addition of F^- (similar to that observed upon addition of Et_3N), while other compounds showed no significant colour change towards the addition of F^-. The UV/Vis sprectrum of **81** showed that the absorption at 310 nm underwent a red shift to 324 nm and, along with the bands at 390 nm and 532 nm, experienced a strong hypochromic effect. However, the formation of a new band centred at 450 nm and a strong increase in the shoulder at 715 nm were also observed at the same time (Figure 2.12). Formation of four isosbestic points at 364 nm, 416 nm, 484 nm and 597 nm were also clearly observed suggesting that only two species coexist at this equilibrium. However, further addition of F^- resulted in the intensity of the bands centred at 324 nm, 540 nm and 715 nm to rapidly decrease, which suggested that the interaction of F^- with **81** underwent two well-defined steps. Given these results, we assumed that upon addition of low concentrations of F^-, a distinct redshift of the charge-transfer bands results from the first deprotonation of **81** [**81** – H]$^-$, however, subsequent addition of excess F^- leads to a second deprotonation of the squaramide NH proton [**81** – 2H]$^{2-}$ and a second colour change from green to yellow was observed at the same time. Such behaviour has previously been observed with urea[38] and squaramide derivatives containing electron-withdrawing substituents.[44, 58] Moreover, the results obtained in the pH-spectrophotometric titration above clearly support these observations. Treatment of **81** (1×10^{-5} M in 0.5% H_2O in DMSO solution) with Cl^-, Br^- and I^- resulted in comparatively minor changes, however, the addition of each of these anions did result in absorbance increases at 715 nm and 450 nm suggesting that the presence of Cl^-, Br^- and I^- may promote the mono-deprotonation of **81** in DMSO solution (Figure 2.13). Interestingly, the addition of these anions did not result in any observable colour change of the solution. Addition of more basic oxoanions ($H_2PO_4^-$, SO_4^{2-}, CH_3COO^-) gave similar results to that of F^- where a colour change from pink to green was observed further confirming the propensity of basic anions to deprotonate sensor **81** (Figure 2.14). From the observed changes in the UV−vis absorption studies, the association constants of **81** with the different halides were estimated using global curve fitting analysis (BindFit software).[71, 72] Curves were fitted to the absorption data at 715 nm, 532 nm, 450 nm and 390 nm in each case according to a 1:1 binding model. From these titrations we estimated association constants for **81** to be 23262 M^{-1} (error = 3.67%), 5835 M^{-1} (error = 3.67%), 4323 M^{-1} (error = 12%), and 2257 M^{-1} (error = 4.86%) for F^-, Br^-, I^- and Cl^-, respectively (See Appendix).

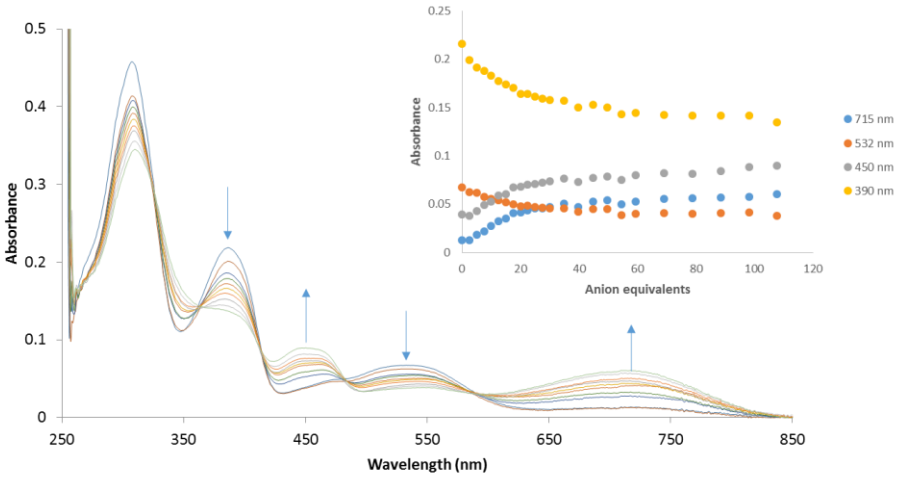

Figure 2.12: Changes observed in the absorption spectrum of **81** (1 x 10^{-5} M) upon addition of TBAF (0 – 0.07 mM) in 0.5% H_2O in DMSO solution. (Inset): Absorbance changes observed at 715 nm, 532 nm, 450 nm and 390 nm.

(a)

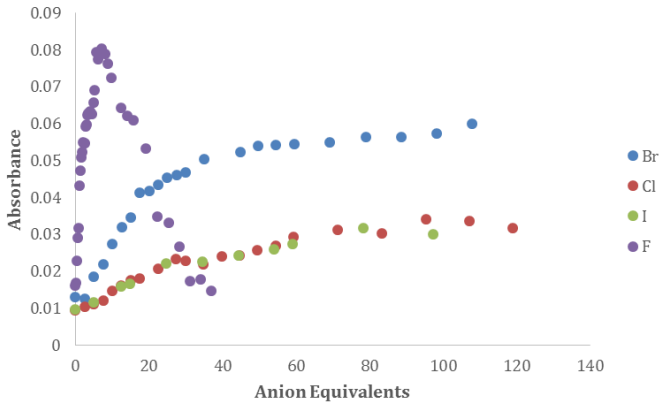

(b)

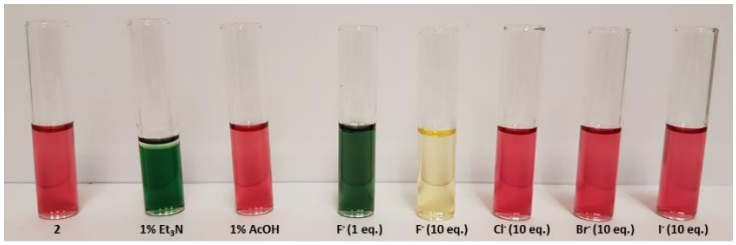

Figure 2.13: (a) Comparison of the absorbance changes observed at 715 nm upon addition of TBAF (0 – 0.37 mM), TBAI (0 – 1.1 mM), TBACl (0 – 1.2 mM) and TBABr (0 – 1.1 mM) to a solution of **81** (1 x 10^{-5} M) in 0.5% H_2O in DMSO solution. **(b)** Colourimetric changes observed for **81** (1 x 10^{-3} M) under acidic conditions, basic conditions and in the presence of various halides in DMSO at 25 °C.

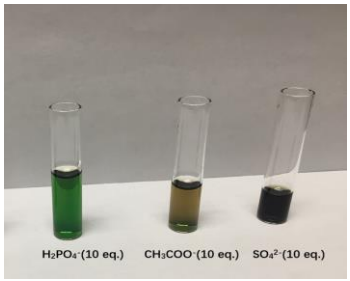

Figure 2.14: Colourimetric changes observed for **81** (1 x 10^{-3} M) upon addition of $H_2PO_4^-$(10 eq.), CH_3OCO^-(10 eq.), SO_4^{2-}(10 eq.) in DMSO at 25 °C.

When these measurements were repeated using **82**, the changes in the absorption spectrum were comparably minor upon addition of F^-, Cl^-, Br^- and I^- (see appendix). As a representative example, the addition of F^- towards compound **82** did give rise to an additional absorption centred at 387 nm which upon subsequent additions disappeared (Figure 2.15). This culminated in a change in colour of the solution from a pale orange to a slightly darker orange. Compound **83-84** also showed the disappearance of absorption centre upon the addition of F^- and concomitant minor colour change (see Appendix). Similarly, **80** showed comparatively minor changes in colour upon addition of F-, going from yellow to a darker shade of yellow. Given that the spectroscopic behaviour of **80** has recently been studied by Niu *et. al.* we did not pursue this line of experiments.[73] However, the bromo-substituted compound **85** did not show significant change in its absorption spectrum (see Appendix).

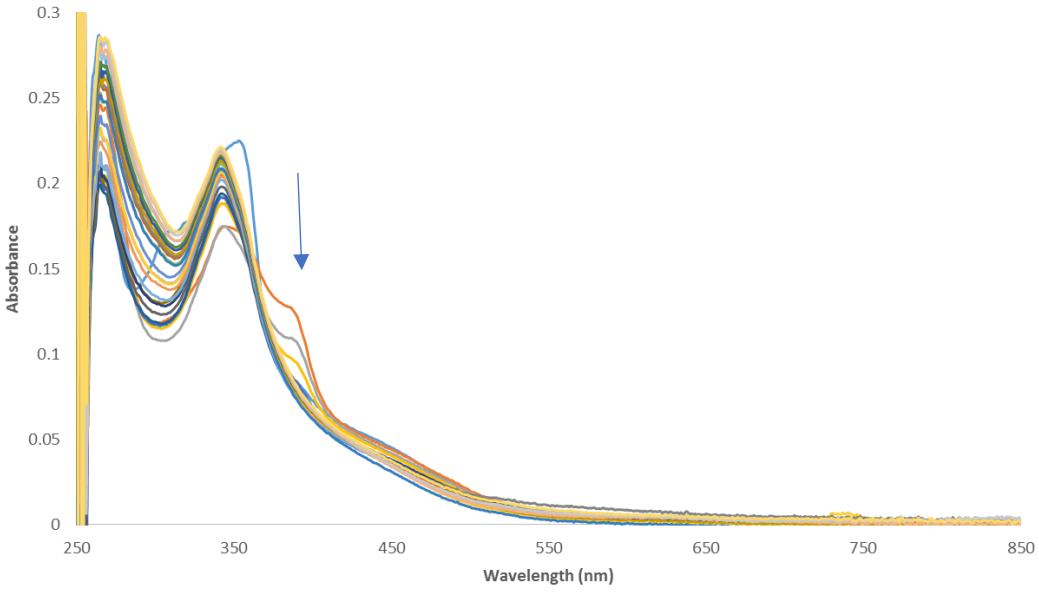

Figure 2.15: Changes observed in the absorption spectrum of **82** (1 x 10^{-5} M) upon addition of TBAF (0 – 1 mM) in 0.5% H_2O in DMSO solution.

2.4.2 ^{1}H NMR Anion Titrations

^{1}H NMR anion titration study was another useful tool we used to further support our observations in the UV/Vis titrations. 2.5 x 10^{-3} M of compound **81** in 0.5% H_2O in DMSO-*d6* solution was tested with increasing equivalent of different halide anions in their tetrabutylammonium salt (TBA^+) from 0 eq. to 2.0 eq. (0.2 eq. was added each time). Interestingly, no obvious changes were observed in the presence of Cl^-, Br^- and I^- suggesting that little interaction of these anions is occurring with **81** and that the observed UV/Vis spectroscopic changes must be related to a small increase in the propensity of **81** to become mono-deprotonated. It was expected that the acidity of the squaramide NH protons may have yielded a strong hydrogen bond donating group to interact with the halides, in particular with Cl^- which is known to bind to the conventional squaramide moiety containing electron withdrawing aryl substituents.[58] However, in this case, only a very minor downfield shift of the NH signal, coupled with some peak broadening was observed, suggesting that Cl^-, Br^- and I^- are not binding to **81** to any meaningful extent. In the presence of F^- a considerably more complicated behaviour was observed whereby initial additions of F^- (0 – 0.6 eq.) resulted in a large degree of peak broadening observed for the NH signals and a significant upfield shift of all three aromatic signals. Combined with results obtained in the previous section we ascribe this initial behaviour to acid–base interactions with F^-. Subsequent additions of F^- again resulted in a second distinct process occurring where three new peaks evolved at 8.3 ppm, 8.5 ppm and 8.9 ppm at the same time as the original aromatic peaks disappeared. Again, this process was concomitant with an original colour change from pink to green followed by a second change from green to yellow. We suggest again that this behaviour can be explained by the occurrence of a second deprotonation event being triggered by the presence of excess F^-. The representative spectra for titration of **81** with F^- is shown in Figure 2.16, illustrating the significant broadening of the squaramide proton signals and the subsequent spectral changes upon addition of increasing F^-.

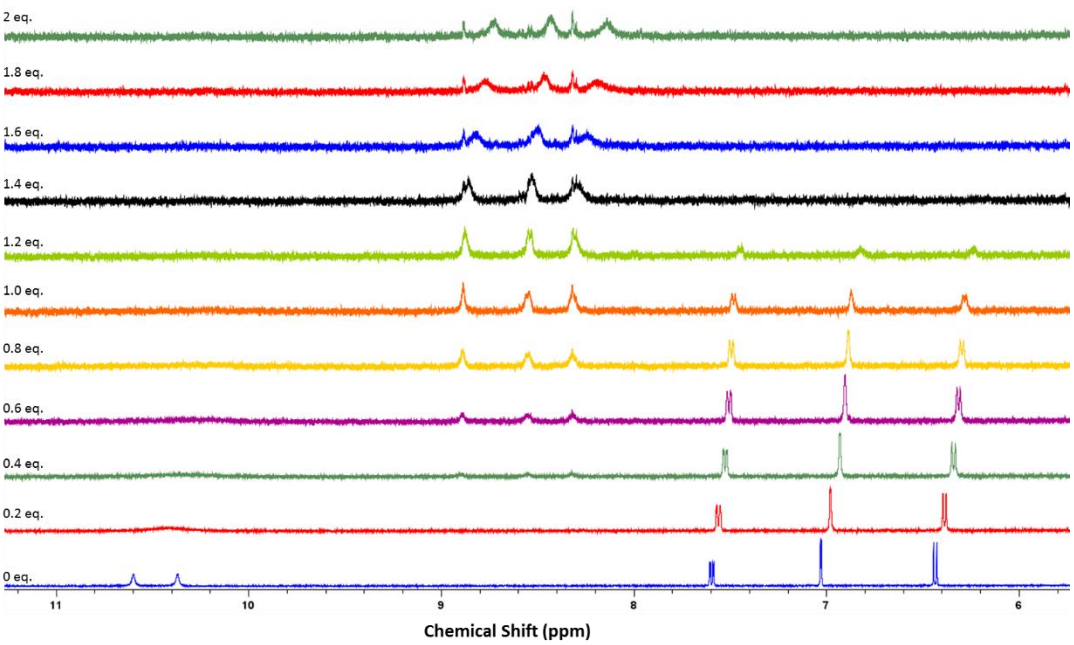

Figure 2.16: Stack plot of ^{1} H NMR spectra of **81** (2.5 x 10^{-3} M) upon addition of TBAF (0 - 2 equiv.) in DMSO-d_6 at 25 °C.

Furthermore, upon the addition of 5 equivalents of TBAF to a solution of **81** in DMSO-d_6, the formation of a triplet at 16.2 ppm in the ^{1}H spectrum was also clearly observed confirming the formation of HF_2^-; a product of the acid/base reaction between **81** and TBAF (Figure 2.17).[74]

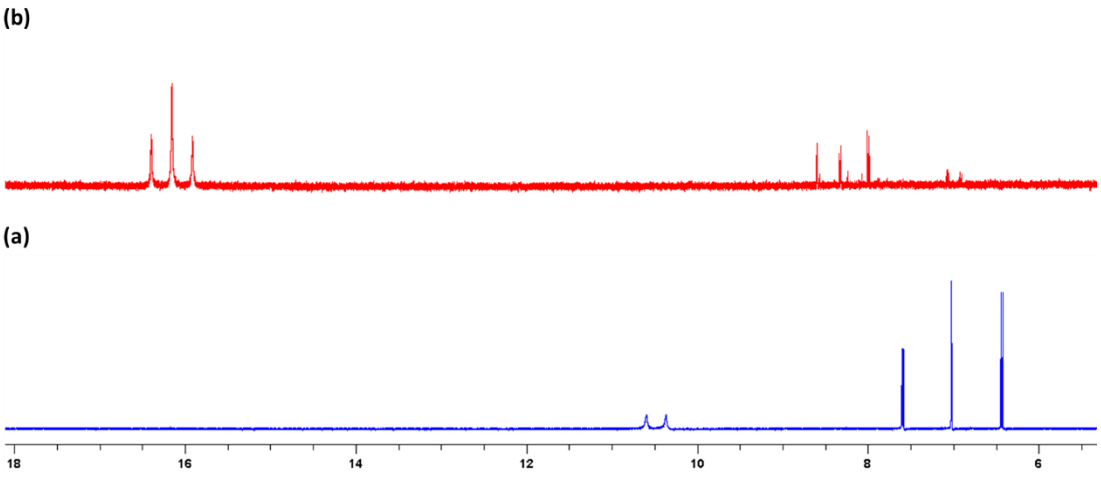

Figure 2.17: ^{1}H NMR stackplot of **81** (a) before and (b) after addition of TBAF (5 eq.) in DMSO-d_6 clearly showing the disappearance of the squaramide NH peaks and the appearance of a characteristic triplet at ≈ 16.2 ppm.

2.5 Crystal Structure Study

Additionally, in collaboration with Dr. Jonathan Kitchen at Southampton University, we investigated the crystal structure of compound **81** in DMSO solution. Small red block-like crystals of **81**·DMSO were grown by slow evaporation of a DMSO solution and the low temperature (100 K) molecular structure determined (Figure 2.18). **81**·DMSO crystallised in the triclinic space group *P*-1 and contained two crystallographically independent molecules of **81** in the asymmetric unit as well as two interstitial DMSO molecules (Figure 2.18) that form strong hydrogen bonds to one of the NH groups of each independent molecule [N2···O100 = 2.742(4) Å and <(NH···O) = 171°; N21···O200 = 2.728(4) Å and <(NH···O) = 176°].

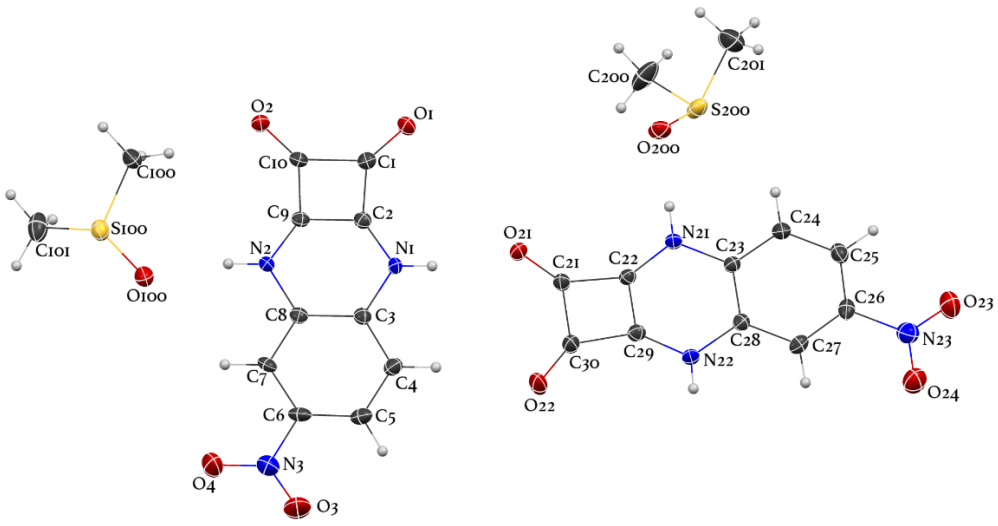

Figure 2.18: Molecular structure of **81**·DMSO with thermal elipsoids set at 50%.

The structure exhibits some interesting packing interactions that involve classic hydrogen bonding, weaker non-classical CH-based hydrogen bonding and π···π stacking. NH and CH-based hydrogen bonding between neighbouring molecules of **81** results in a hydrogen bonded zig-zag chain (Figure 2.19) where the squaramide oxygen atoms form H-bonding interactions to the NH and CH groups on a neighbouring molecule [N1···O21 = 2.783(4) Å and <(NH···O) = 170°; C4···O22 = 3.248(5) Å and <(CH···O) = 171°; N22···O2 = 2.806 Å and <(NH···O) = 161°; C27···O1 = 3.240(5) Å and <(CH···O) = 173°] (Figure 2.199). This propagates throughout the structure to give the overall H-bonded zig-zag chain. These chains are further linked into sheets *via* weaker CH-based hydrogen bonds

between the oxygen atoms of the nitro group and neighbouring CH group [C25···O3 = 3.360(5) Å and < (CH···O) = 165°] (Figure 2.20). The sheets of **81** are finally arranged into layers through π···π stacking interactions [inter centroid distances ~3.5 Å] between adjacent aromatic groups to give an overall layered topology (Figure 2.20).

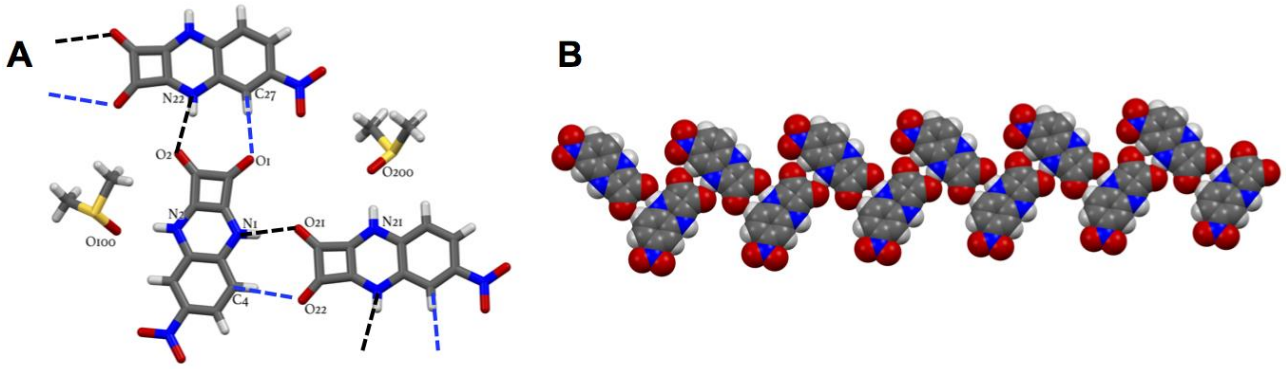

Figure 2.19: Hydrogen bonding interactions in **81**·DMSO that result in the formation of the zig-zag chain (A) – [N1···O21 = 2.783(4) Å and <(NH···O) = 170°; C4···O22 = 3.248(5) Å and <(CH···O) = 171°; N22···O2 = 2.806 Å and <(NH···O) = 161°; C27···O1 = 3.240(5) Å and <(CH···O) = 173°]; and space filling representation showing the long range ordering of the zig-zag H-bonded chain (B)

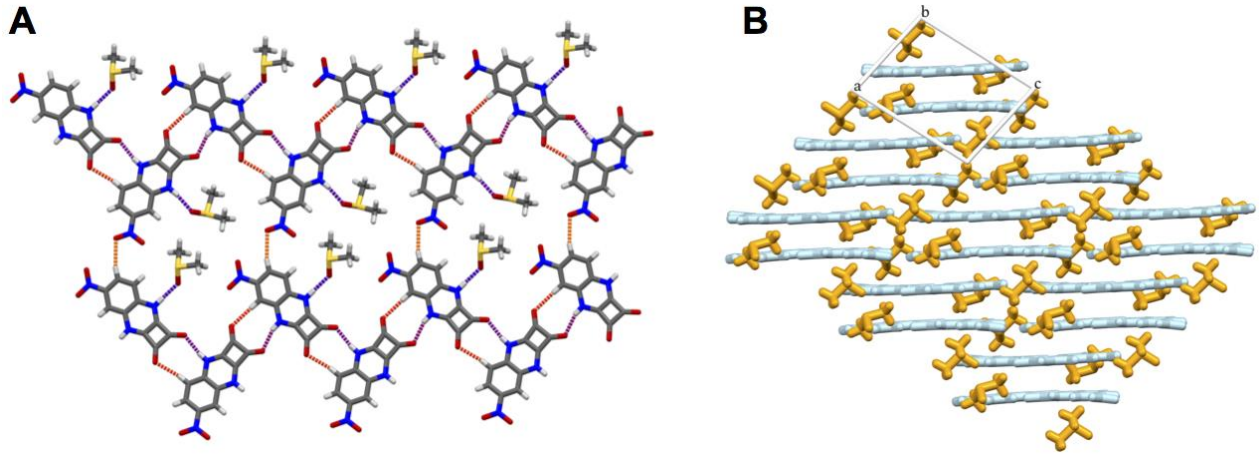

Figure 2.20: All H-bonding interactions present in the formation of the 2D sheets of **81** (A) - purple dashed lines are NH-based H-bonds and orange dashed lines are CH-based H-bonds. View of the π-stacked layers formed between the 2D sheets (B) of **81** (in blue) and the dispersion of interstitial DMSO molecules (in orange) throughout the layered structure.

2.6 Application of Compound 81 towards F^- Test Strips

Since the anion sensing mechanism of compound **81** has been studied, we next wished to evaluate its potential as a sensor for F^- with real life application. Test strips of **81** were prepared by immersing filter papers into a DMSO solution of **81** (40.7 mM) before allowing the strips to dry fully in an oven (60°C for 12 hrs). The test strips containing **81** were then used to demonstrate the applicability of this molecule towards halide sensing. Figure 2.23 shows photographs of the test strips after additions of 2 µL of DMSO solutions of TBAF, TBACl, TBABr and TBAI (0.445 M). Upon addition of TBAF the colour was observed to change instantly from pink to green while the areas of the filter paper treated with the other halides were shown to remain unchanged (Figure 2.21(a)). Additionally, when an aqueous solution of TBAF (0.445 M) was also added, followed by gentle heating, the colour was again observed to change instantly from pink to green clearly demonstrating the practical use of this very simple sensor molecule to the analysis of aqueous solutions containing F^- (Figure 2.21(b)). Compound **81** was also tested to show capability of sensing the presence of F at different pH values ranging from pH 5 to pH 8 (Figure 2.22).

(a) (b)

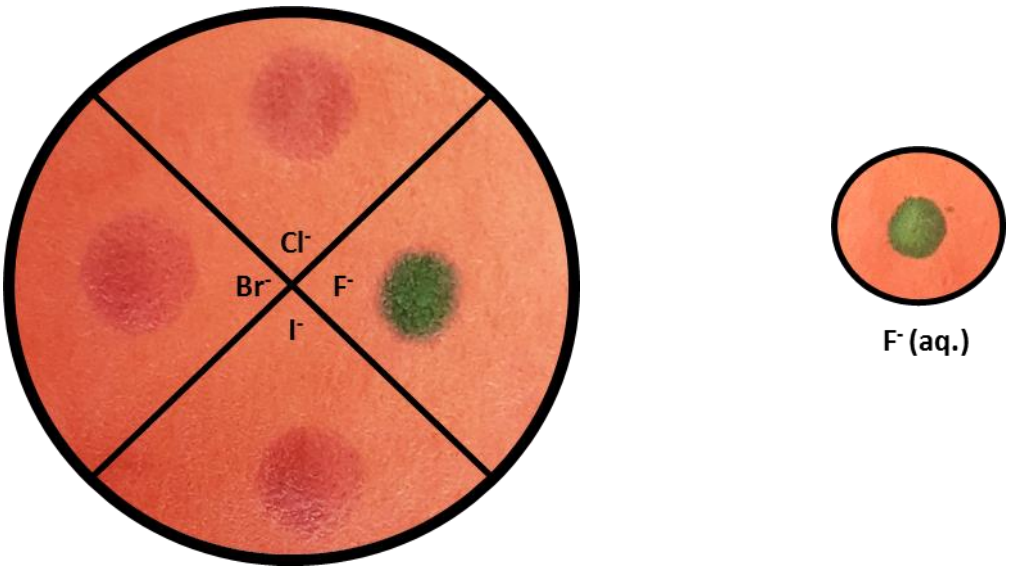

Figure 2.21: Photograph of filter paper impregrated with **81** (40.7 mM) and the colorimetric response observed upon addition of 2 µL of (a) TBAF, TBACl, TBABr and TBAI (0.445 M) in DMSO and (**b**) TBAF (0.445 M) in H_2O after gentle drying.

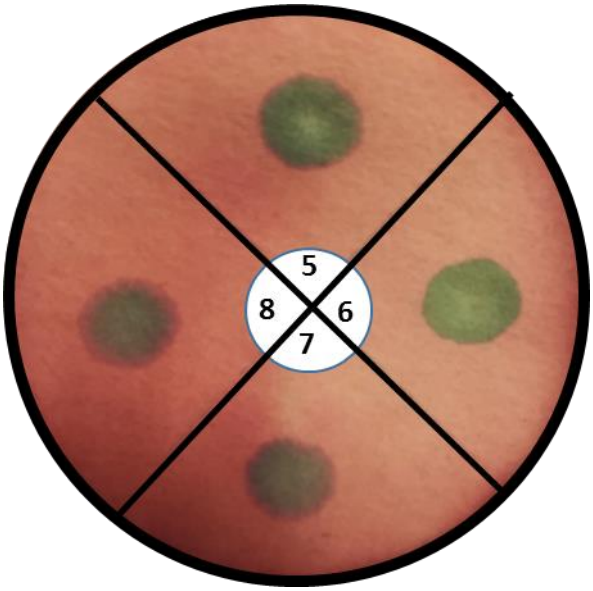

Figure 2.22: Photograph of filter paper impregrated with **81** (41 mM) and the colorimetric response observed upon addition of 2 µL of TBAF (0.45 M) at various pH values as indicated.

2.7 Conclusion

In conclusion, we have successfully synthesized a family of compounds **80-85** based on the 'squaramidoquinoxaline' moiety where the new structures have been characterized by a combination of NMR spectroscopy, mass spectrometry and FT-IR spectroscopy. Moreover, we also got the X-ray crystallography for compound **81**. UV/Vis absorption properties of compound **81** was shown to display a characteristic long wavelength absorption at 715 nm. The halide recognition abilities of the receptors were also investigated where **81** was shown to undergo drastic colorimetric changes from pink to green upon titration with F^- which culminated in a large increase in absorption at 715 nm suggesting the existence of a deprotonation event. Further addition of F^- led to a second colour change from green to yellow and a concomitant reduction of all absorption bands in the UV/Vis absorption spectrum. The NO_2 derivative **81** was also found to be a selective colourimetric sensor for F^- where no such changes were observed in the presence of the other halides Cl^-, Br^- or I^-. Using UV/Vis, NMR and TD-DFT analysis we conclude that the observed colour changes are likely to be due to a two-step process involving two NH deprotonation steps. Colour changes of the other compounds **80** and **82-85** were not as apparent in the presence of F^- owing to the reduced acidity of the NH functionality of the squaramidoquinoxaline and the apparent lack of a relative strong

electron withdrawing group that allows for charge transfer within the molecule. We also demonstrated application of F^- sensing using a test strip method of **81** where addition of TBAF caused the colour of a filter paper impregnated with **81** to change instantly from pink to green while areas treated with the other halides were shown to remain unchanged. The results of this study again demonstrate the use of squaramide derivatives as valuable building blocks in the field of anion recognition and sensing and demonstrate that the electron withdrawing aryl substituent is directly related to the sensing ability/acidity of the squaramide protons and can be used to tune their anion recognition behavior. Moreover, we envisaged that squaramidoquinoxalines might be useful building blocks for anion-responsive supramolecular self-assembly formations according to the interesting packing interactions observed in the crystal structure of **81** that involve classic hydrogen bonding, weaker non-classical CH-based hydrogen bonding and π- π stacking interactions.

Chapter 3 Macrocyclic Squaramide (MSQ) Moiety Based Anion Sensors

3.1 Introduction

The higher degree of preorganization in size, shape, orientation and rigidity of their binding sites enable macrocycles to have superior binding capacity in comparison to their acyclic counterparts.[6] For instance, Calix[4]pyrrole as expanded pyrrole-containing macrocycles that lack conjugation between the pyrrole units are particularly effective for anion binding and sensing.[75] Calix[4]pyrroles also show good anion-binding capability both in the solution phase and in the solid phase.[76, 77] The macrocyclic squaramide **70** which has been outlined in Chapter 1.6 is another molecule of interest. It was reported that **70** showed excellent binding affinity towards SO_4^{2-} in which the SO_4^{2-} was bound to the macrocyclic cavity of **70** *via* hydrogen bonding.[57] Furthermore, this work also revealed that the binding of **70** toward sulfate anion in the macrocyclic cavity allowed the crystal structure to transform from chair- to bowl-like conformation which forced the two benzenes to get closer to each other in space (Figure 3.1).

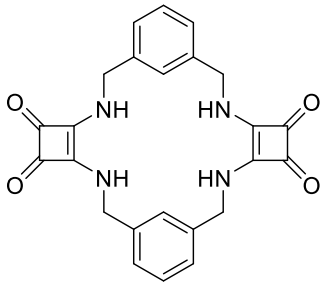

70

(a) (b)

Figure 3.1: Single crystal X-ray diffraction structures of (a) **70** and (b) the complex formed between **70** and SO_4^{2-} clearly showing the interaction of SO_4^{2-} with the squaramide NH protons inside the macrocyclic cavity. Image taken from *Chem. Sci*. 2016;7(7):4563-72.

Based on this fact, we envisaged that incorporation of fluorophores on the periphery of aryl ring may result in FRET (Förster Resonance Energy Transfer) within the macrocycle system when bound to anions due to the bowl-like conformation having a closer distance between the fluorophores. To understand the proposed concept, below will detail a short section describing FRET.

FRET is an energy transfer process occurs from an excited donor (D) fluorophore to a suitable acceptor (A) protein or fluorophore *via* long-range dipole–dipole coupling mechanism.[78] The donor absorbs energy at shorter wavelength whereas the acceptor has energy absorption at longer wavelength. FRET is collision-free, but distance-dependent photophysical process. Collision between donor and acceptor would prevail at distance below 1 nm, whereas photon emission by donor would be dominant at distances higher than 10 nm. Thus, FRET occurs only when two fluorophores are in the distance within 1-10 nm. FRET can take place not only between two spectroscopically different fluorophores which is termed heteroFRET, but also between spectroscopically identical fluorophores with small excitation-emission separation of the spectral peaks. Energy transfer between like fluorophores is known as homoFRET. The sensitivity of FRET towards molecular distance enables various applications in the determination of dynamic molecular events such as conformational change in macromolecules, cis- or trans-association/or assembly in macromolecules *etc.* The Jablonski diagram gives the simplest explanation of how FRET occurs in terms of donor/acceptor excitation and emission (Figure 3.2).[78]

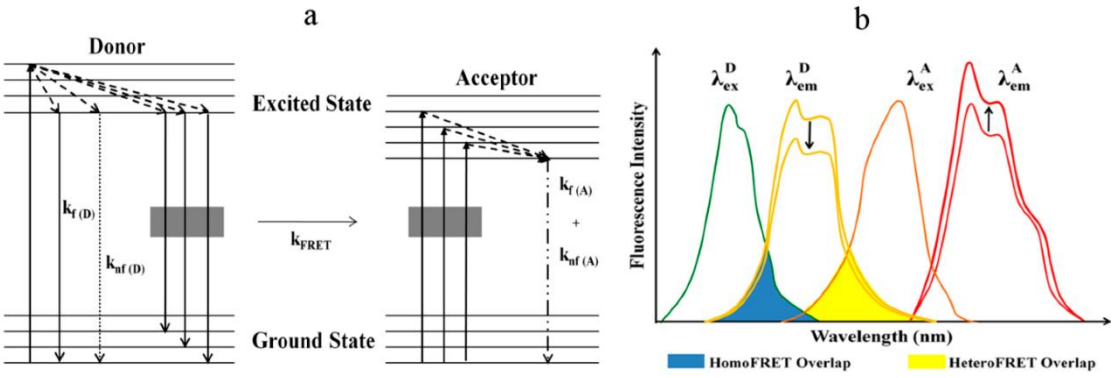

Figure 3.2: (**a**) The figure shows the Jablonski diagram demonstrating mechanism of Förster Resonance Energy Transfer (FRET). On absorption of energy, electrons in both donor and acceptor are excited from the ground state to an excited state, and they lose energy as fluorescence with rate constant k_f(D) for donor or k_f(A) for acceptor and non-fluorescence mechanisms with rate constant k_{nf}(D) for donor or k_{nf}(A) for acceptor. On

the occurrence of FRET, excited energy of the donor is also lost *via* FRET to an acceptor with rate constant k_{FRET}; and (**b**) Spectral overlap: The absolute requirement of FRET is illustrated in this figure. The symbols "λ_{ex}^{D} " and "λ_{em}^{D} " or "λ_{ex}^{A} " and "λ_{em}^{A} " indicate excitation (λex) and emission spectra (λem) of donor and acceptor fluorophores respectively with upper index letters denoting fluorophores. Essential spectral overlap in the case of heteroFRET (yellow) and homoFRET (blue) is also highlighted in the figure. Image taken from *Int. J. Mol. Sci*. 2015;16(4):6718-56.

In our hypothesis, the pyrene fluorophore absorbs energy at shorter wavelength and could act as a FRET donor whereas the 4-nitro-1,8-naphthalimide probe absorbs energy at higher wavelength could act as FRET acceptor. Thus, compound **90** with FRET donor and acceptor on the opposite sides could undergo FRET upon binding with anions due to the bowl-like conformation allowing the two fluorescent probes to get closer within the range of 1-10 nm. As a result, FRET process of compound **90** provides a pathway to detect anions by fluorogenic methods. A diagram below gives a more concise explanation of how FRET might take place within **90** upon the binding with SO_4^{2-} anion (Figure 3.3).

(a)

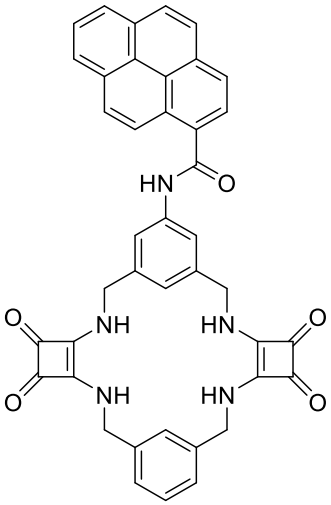

88

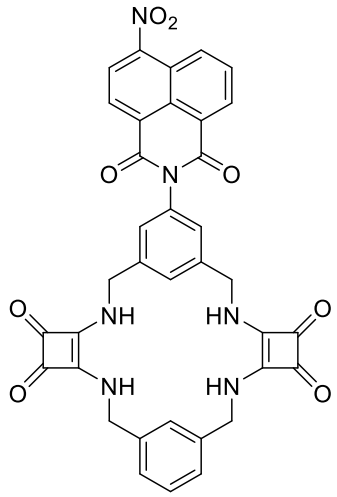

89

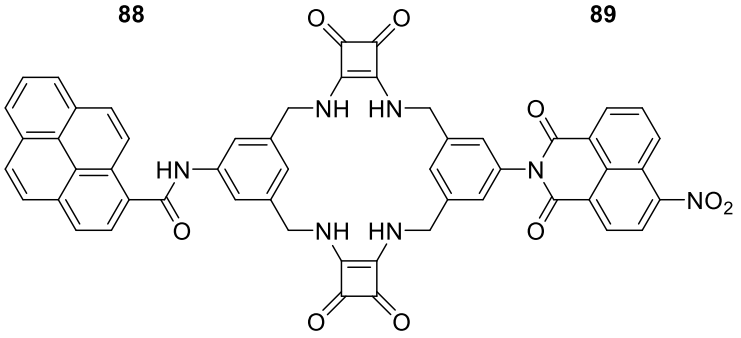

90

(b)

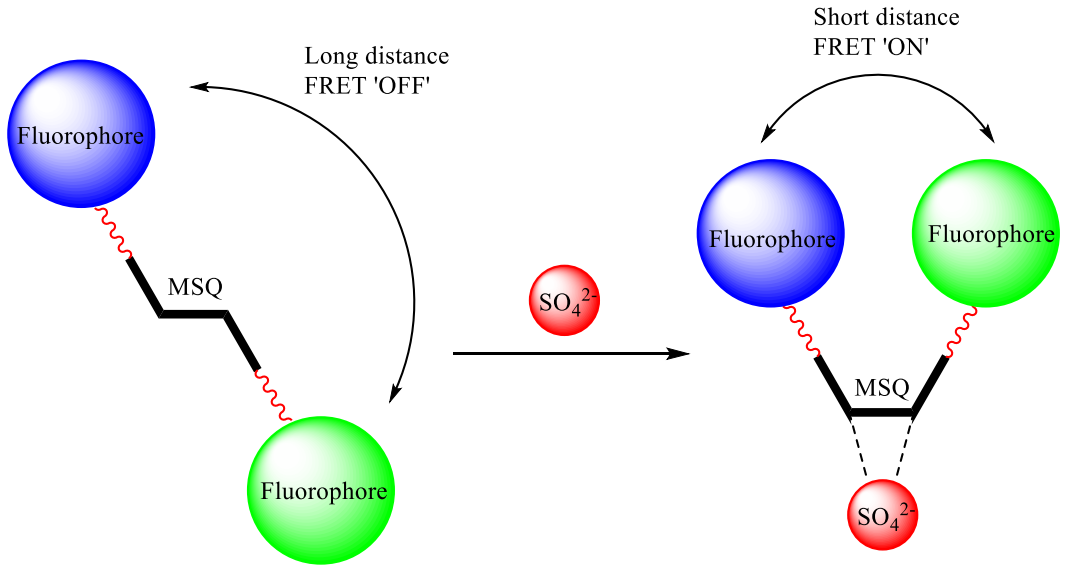

Figure 3.3: (a) Structure of target molecule **88-90**. **(b)** FRET 'switched on' due to conformational change from chair- to bowl-like of the MSQ upon binding with SO_4^{2-}.

3.2 Synthesis of Model Compounds

Initially we resynthesized compound **70** in order to compare with model compounds (Scheme 3.1).[57] The intermediate compound **99** was achieved by stirring the solution of diethyl squarate with *m*-xylylenediamine and triethylamine in EtOH at room temperature. Removal of solvent by filtration yielded the light-yellow solid intermediate **99** in 12% yield. Then the macrocycle squaramide **70** was achieved by refluxing the very diluted solution of **99** and triethylamine with slow addition of *m*-xylylenediamine in EtOH at 90 °C. Removal of solvent by filtration yielded the light-yellow target molecule **70** in 67% yield.

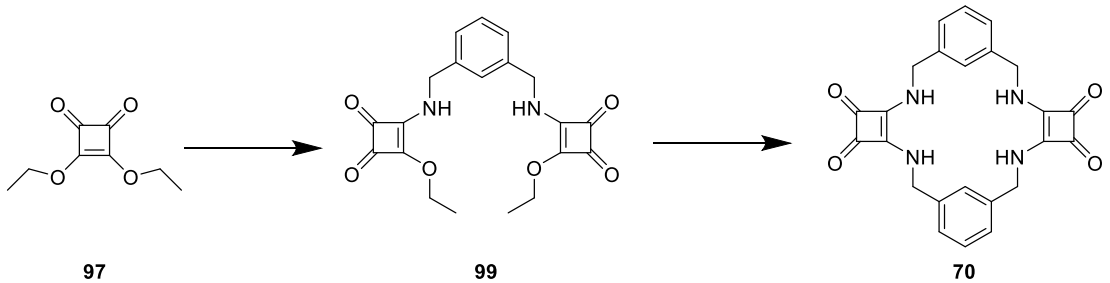

Scheme 3.1: Synthetic pathway of compound **70**. **(i)** *m*-xylylenediamine, triethylamine and EtOH, rt, 12%. **(ii)** *m*-xylylenediamine, triethylamine and EtOH, 90 °C, 67%.

We also wished to synthesize **86** and **87** to verify that functionalisation of the MSQ did not affect SO_4^{2-} binding. The key point to synthesize compound **86** and **87** is getting the -NO_2 substituted *m*-xylylenediamine **104** as shown in scheme 3.2. The amine group could be synthesized from bromine using Gabriel Synthesis while the bromine could be easily converted from alcohol using phosphorus tribromide. The alcohol substituted intermediate **101** can be achieved by reduction of commercially available 5-nitroisophthalic acid **100.**

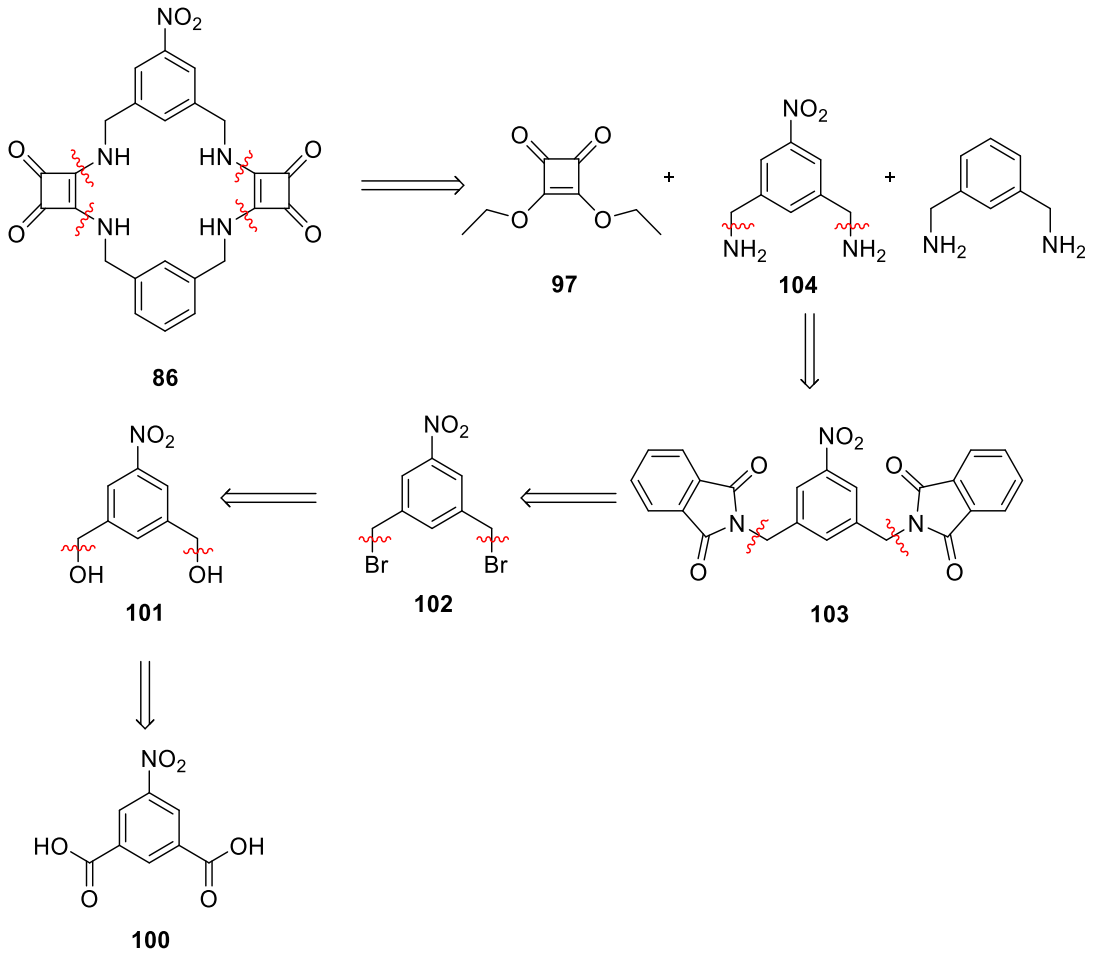

Scheme 3.2: Retrosynthetic analysis of the target molecule **86**.

As shown in Scheme 3.3, compound **101** was achieved by stirring the solution of 5-nitroisophthalic acid **100** and borane dimethyl sulphide complex in DCM at 0 ℃ for 1 hour, the at room temperature for 48 hours. Work up with MeOH and washed with $NaHCO_3$ and Brine to yield a beige solid **101** in 41% yield. Then the reaction of compound **101** with phosphorus tribromide in DCM yielded intermediate **102** as off-

white solid in 78% yield. In the next step, compound **103** was achieved by refluxing of compound **102** with phthalimide potassium salt in EtOH, refluxing of **103** with hydrazine in EtOH then removal of solvent and followed by dissolving in water, adjusting pH to 13, extracting with DCM and removal of solvent again yielded compound **104** as brown solid in 58% yield.

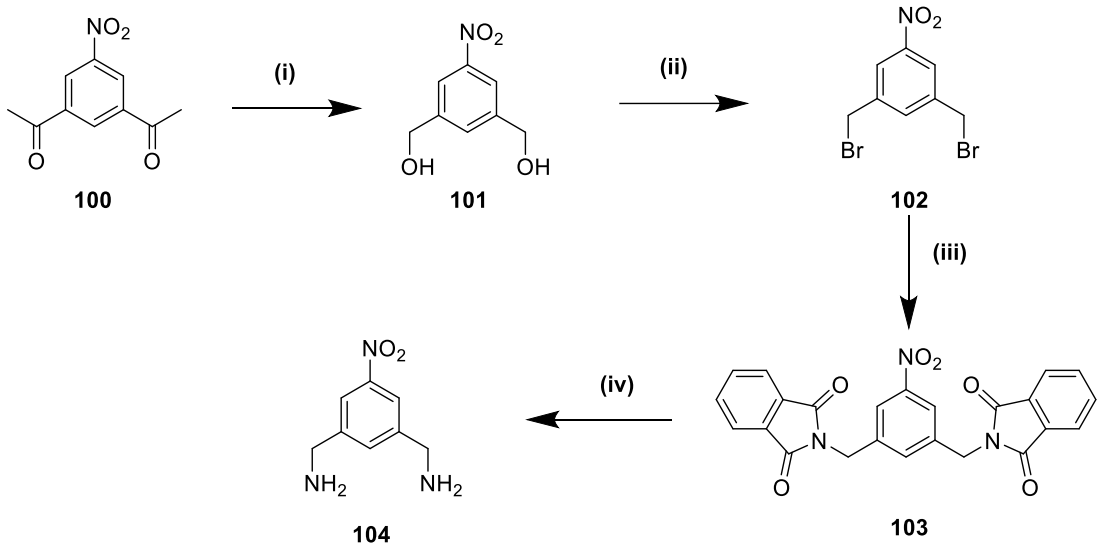

Scheme 3.3: synthetic pathway of the compound **104**. **(i)** BH_3, DCM, 0 ℃ to rt, 41%. **(ii)** PBr_3, DCM, rt, 78%. **(iii)** Potassium phthalimide, EtOH, reflux, 97%. **(iv)** Hydrazine, EtOH, reflux, 58%.

At this stage, all the reaction intermediates **101-104** were successfully synthesized and characterized by ^{1}H NMR, ^{13}C NMR, HRMS and IR-ATR spectroscopy. The ^{1}H NMR of compound **101** showed that the signal peak at 8.06 ppm assigns to two aromatic protons H1, the peak at 7.72 ppm assigns to the aromatic proton H2, the triplet at 5.53 ppm are two -OH protons and doublet with chemical shift at 4.63 ppm assigns to four aliphatic protons H3 (Figure 3.4).

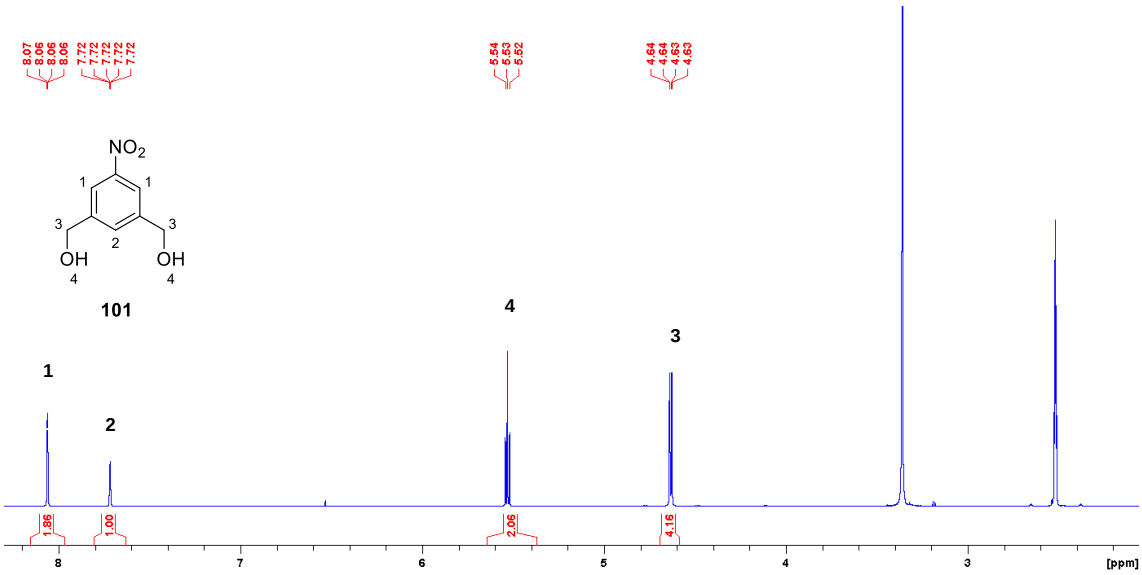

Figure 3.4: The ^{1}H NMR spectrum of compound **101** (500.13 MHz, DMSO-d_6).

^{1}H NMR spectrum of intermediate compound **102** and **103** is shown in Appendix section. Comparing the ^{1}H NMR spectrum of compound **104** to **101**, the signal of aromatic protons have similar chemical shifts. However, the aliphatic protons H3 moved upfield ($\Delta\delta$= 0.8 ppm) due to the more shielded H3 affected by the electron donating -NH_2 group (Figure3.5).

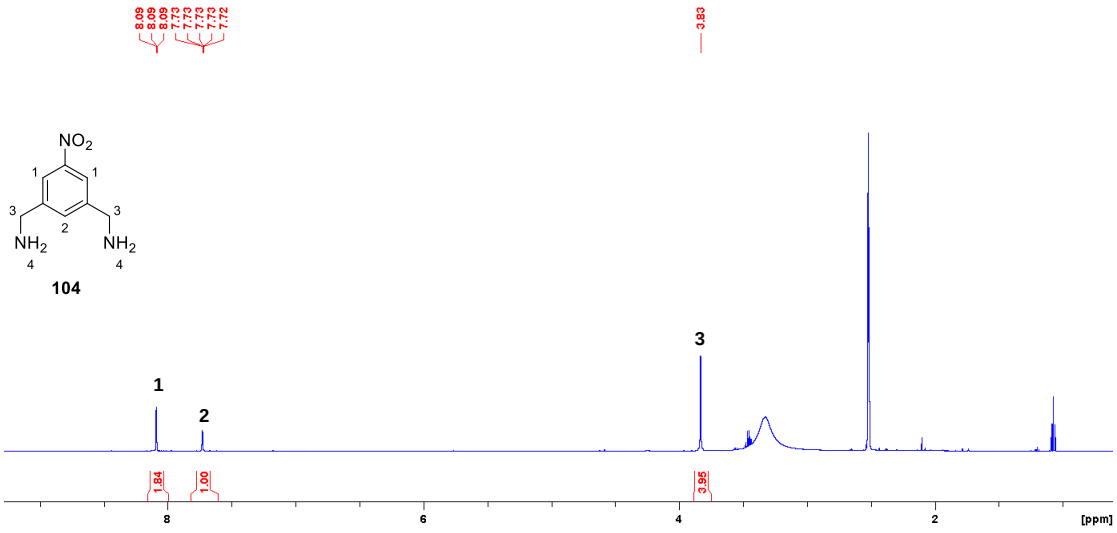

Figure 3.5: The ^{1}H NMR spectrum of compound **104** (500.13 MHz, DMSO-d_6).

The plotted ^{1}H NMR spectrum of compound **101** and **104** below gives a more visualized view of how the functional groups prompted the signal shifts of from **101** to **104** (Figure 3.6).

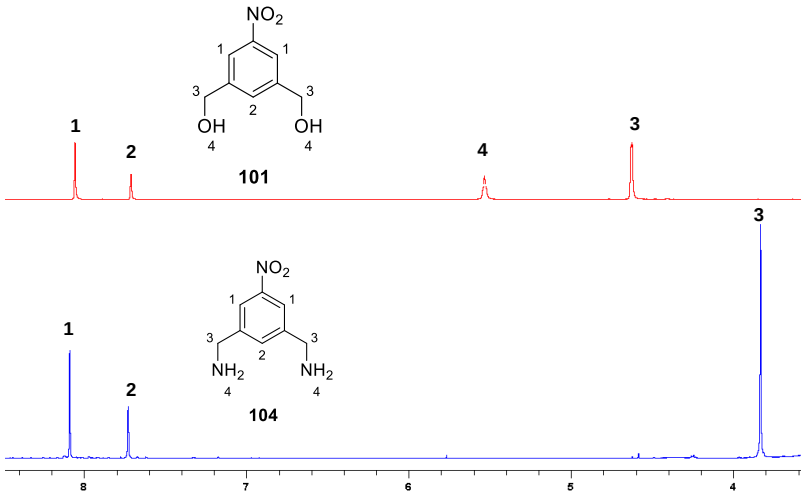

Figure 3.6: The multiple display ^{1}H NMR spectrum of compound **101** and **104** (500.13 MHz, DMSO-d_6).

Since the successful synthesis of (5-nitro-1,3-phenylene)dimethanamine **104**, compound **105** could be achieved using the same method as the synthesis of compound **99** (scheme 3.4). Compound **105** was isolated as an orange solid in 63% yield. Then, the reaction of **105** with *m*-xylylenediamine or **104** resulted in macrocycle **86** and **87**, respectively.

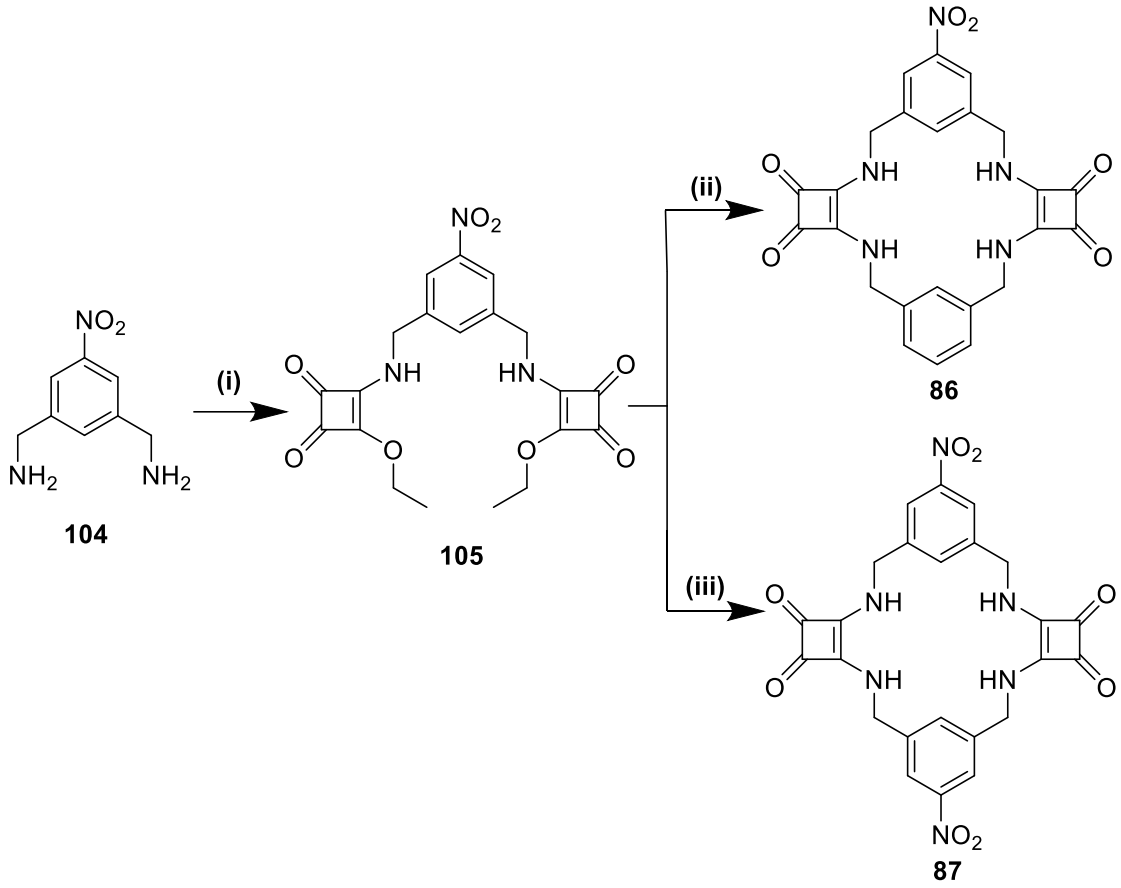

Scheme 3.4: synthetic pathway of the compound **86** and **87**. **(i)** diethyl squarate, EtOH, rt, 63%. **(ii)** *m*-xylylenediamine, EtOH, 90 ℃, 88%. **(iii) 104**, EtOH, 90 ℃, 71%.

The ^{1}H NMR spectrum of compound **105** is shown in Figure 3.7, all protons were labelled by numbers. The two singlets were observed at 9.33 and 9.13 ppm for two NH protons, the singlets at 8.13 and 7.68 ppm were attributed to aromatic protons H2 and H3. Peaks from 4.61-4.82 ppm were observed for eight CH_2 protons H4 and H5, a pair of triplets was observed 1.37 ppm for six CH_3 protons H6, this may suggest some degree of aggregation or conformational exchange in this molecule.

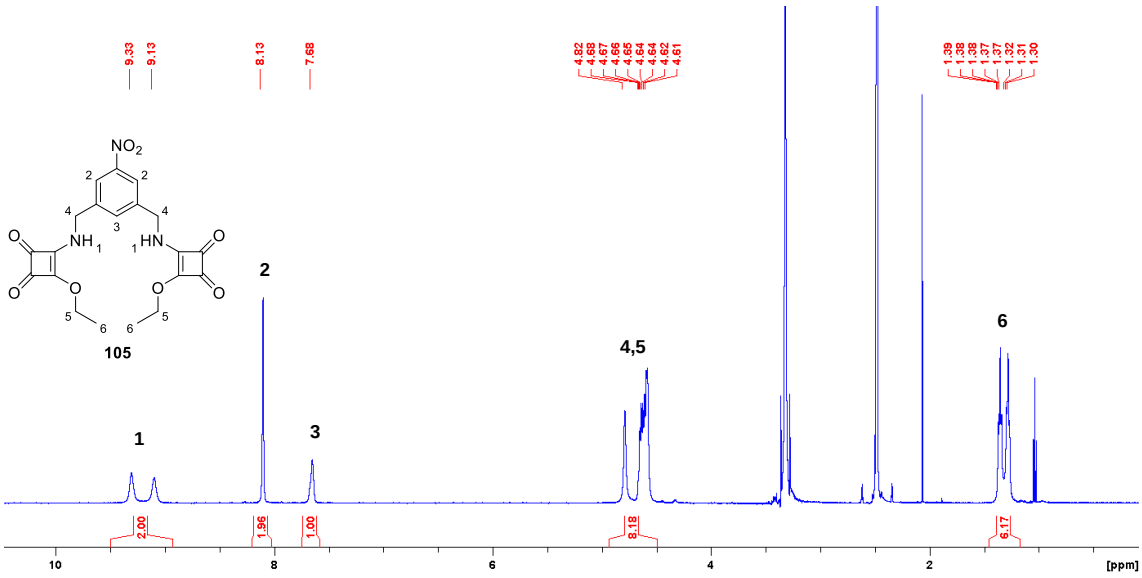

Figure 3.7: The ^{1}H NMR spectrum of compound **105** (500.13 MHz, DMSO-d_6).

Compounds **86** and **87** were fully characterized by ^{1}H NMR, ^{13}C NMR, HRMS and FTIR spectroscopy. The ^{1}H NMR spectrum of compound **86** and **87** could not be accurately characterized due to significant peak broading. However, addition of $TBASO_4$ into the NMR samples of **86** and **87** resulted in better resolution. This phenomenon is possibly ascribed to the flexible structure conformations of compound **86** and **87**, binding of compound **86** or **87** towards SO_4^- anions stabilized the conformational changes. The ^{1}H NMR spectrum of compound **86** is shown in Figure 3.8, the broad peak at 9.21 ppm was observed for four NH protons H1 and H2. Peaks from 7.10 to 8.25 ppm assigned to seven aromatic protons H3-H7. HRMS of [**86**+Na]$^+$ was observed at 496.1219 m/z (PPM:-1.8).

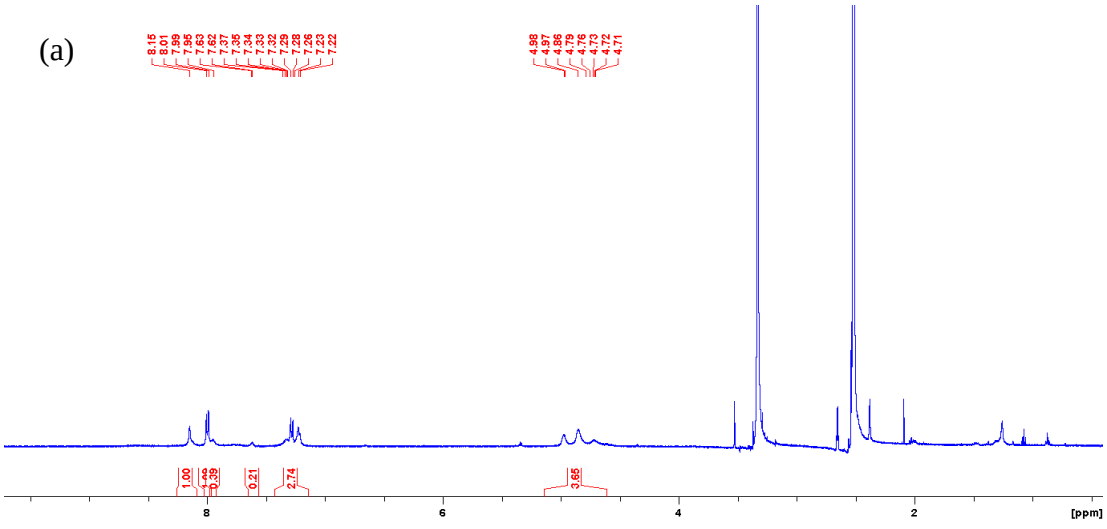

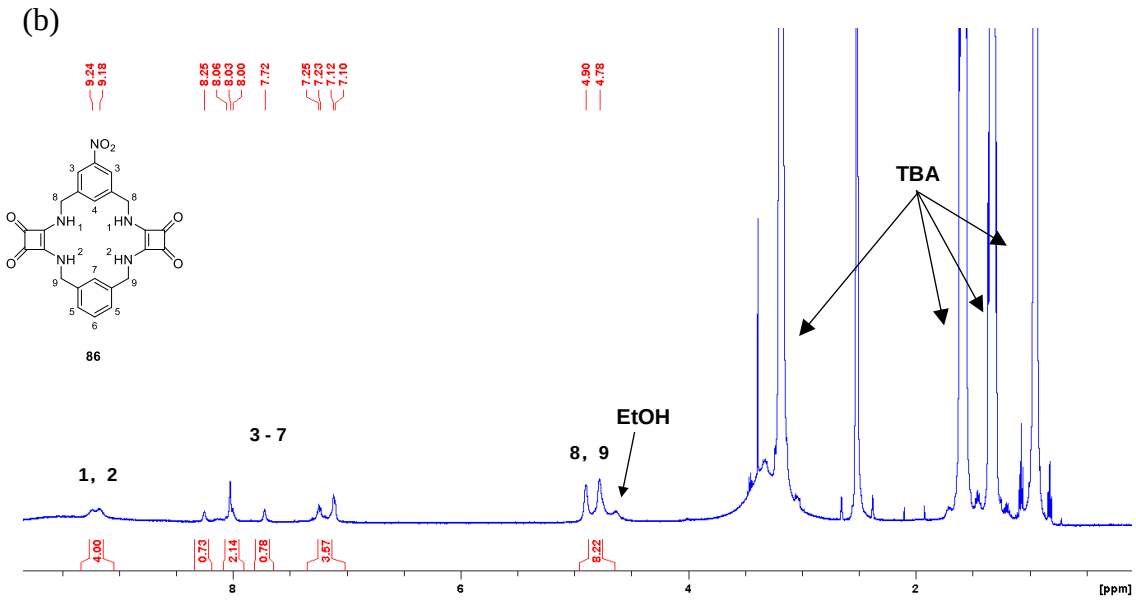

Figure 3.8: The ^{1}H NMR spectrum of compound **86** (500.13 MHz, DMSO-d_6). (a) Absence of SO_4^{2-}. (b) Presence of SO_4^{2-}.

As is shown in Figure 3.9, the ^{1}H NMR spectrum of compound **87** with $TBASO_4$ also showed better resolution comparing to the spectrum without $TBASO_4$. The singlet at 9.74 ppm was observed for four NH protons H1. Singlets at 7.99 and 8.41 ppm assigned to aromatic protons H2 and H3, respectively. The peak at 4.89 ppm was observed for eight CH_2 protons H4. HRMS of [**87**+Na]$^{+}$ was observed at 541.1081 m/z (PPM: 0.5).

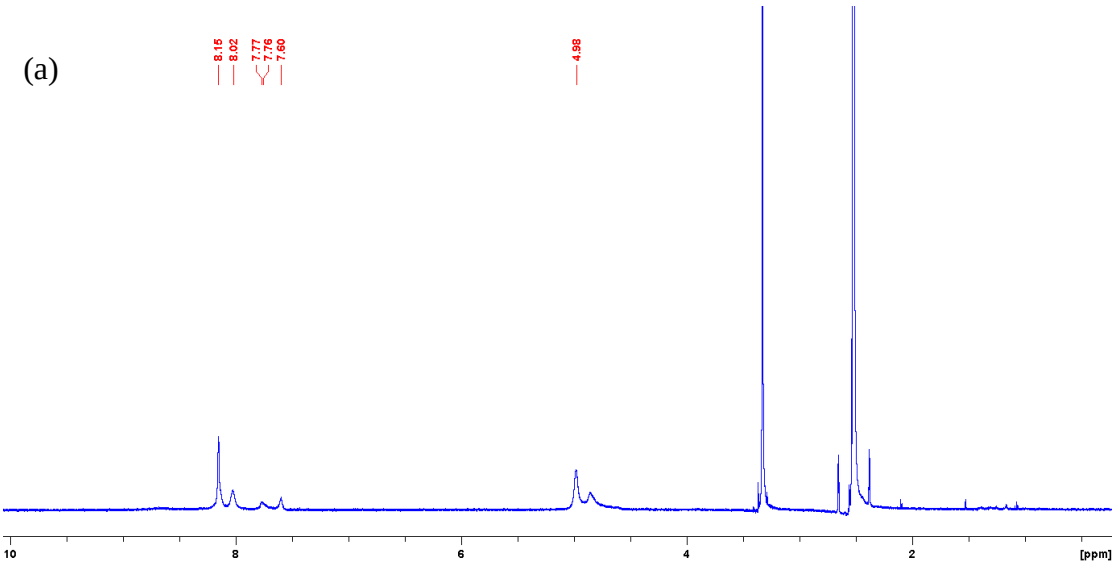

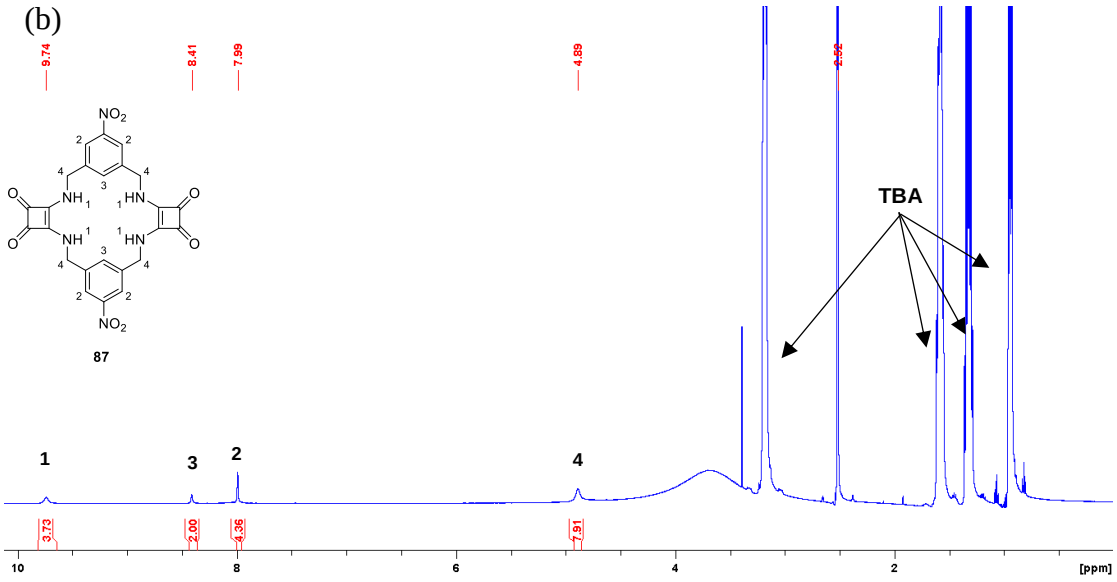

Figure 3.9: The ^{1}H NMR spectrum of compound **87** (500.13 MHz, DMSO-d_6). (a) Absence of SO_4^{2-}. (b) Presence of SO_4^{2-}.

This observation of changes and simplification of the ^{1}H NMR spectra gave us an early indication of SO_4^{2-} binding and suggested that substitution at the periphery of the benzene can yield receptors capable of binding anions. With this important observation we next set out to synthesize compound **88** where a fluorophore was conjugated at this position.

In order to introduce pyrene group into the macrocyclic squaramide, the initial strategy was using amide as a linkage between pyrene and the periphery of the benzene of **70**. As shown in the retrosynthetic analysis of compound **88** (Scheme 3.5), two -NH_2 groups could be achieved using Gabriel Synthesis as described previously. The amide linkage could be achieved by condensation of compound **106** and commercially available 1-pyrenecarboxylic acid **107**. Compound **106** could be achieved by reduction of compound **103** which was successfully obtained in the synthetic process of compound **86** and **87.**

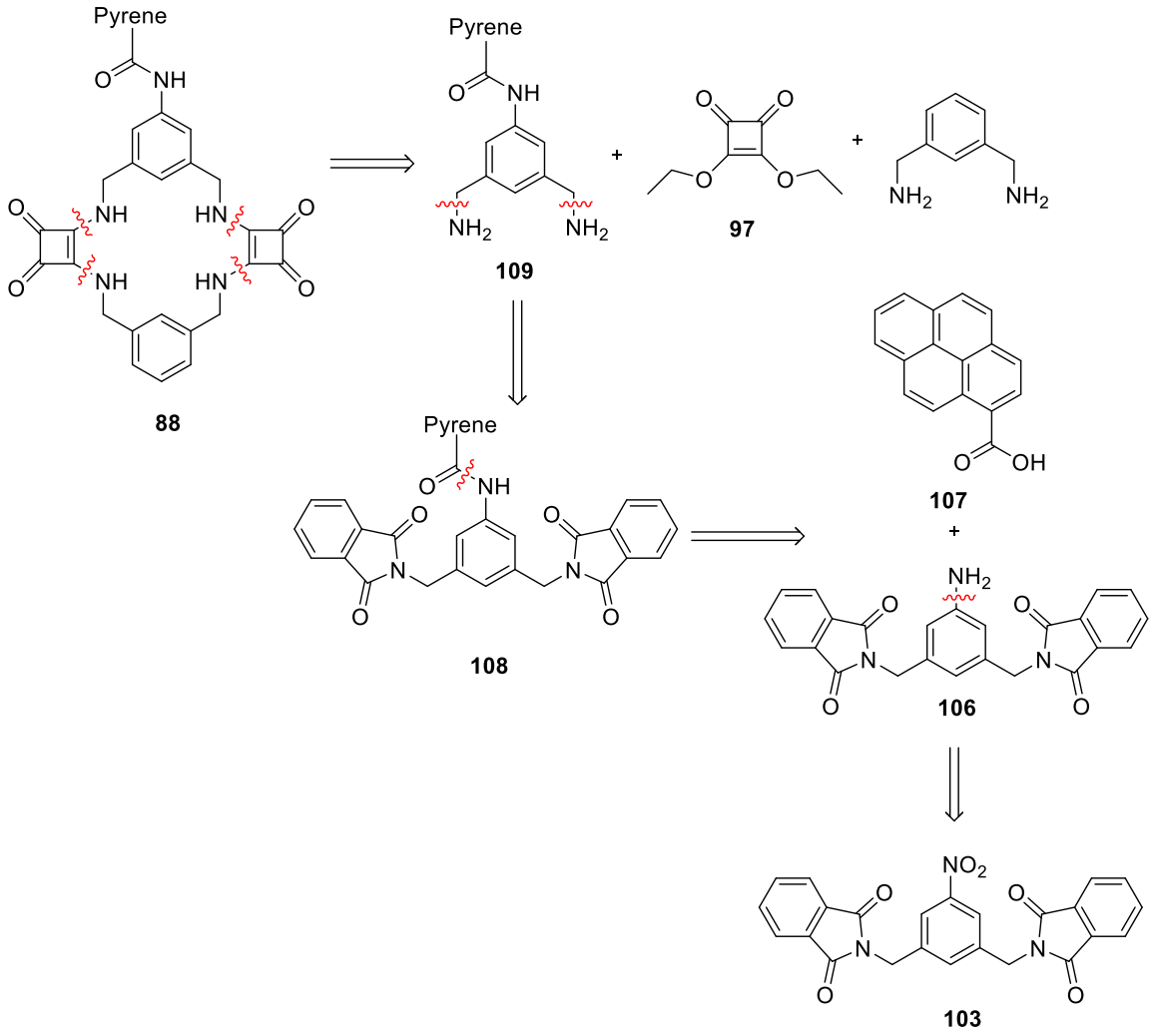

Scheme 3.5: Retrosynthetic analysis of the compound **88**.

Compound **103** was synthesized as outlined in Scheme 3.3, then reduction of **103** under H_2 gas atmosphere using Pd/C as catalyst in DMF resulted in compound **106** as a beige solid in 72% yield (Scheme 3.6). Compound **108** was synthesized by stirring the solution of **106** and 1-pyrenecarboxylic acid in DMF with 4-methylmorpholine as base and PyBOP as coupling reagent at room temperature. Removal of solvent by filtration yielded an off-white solid in 19% yield.

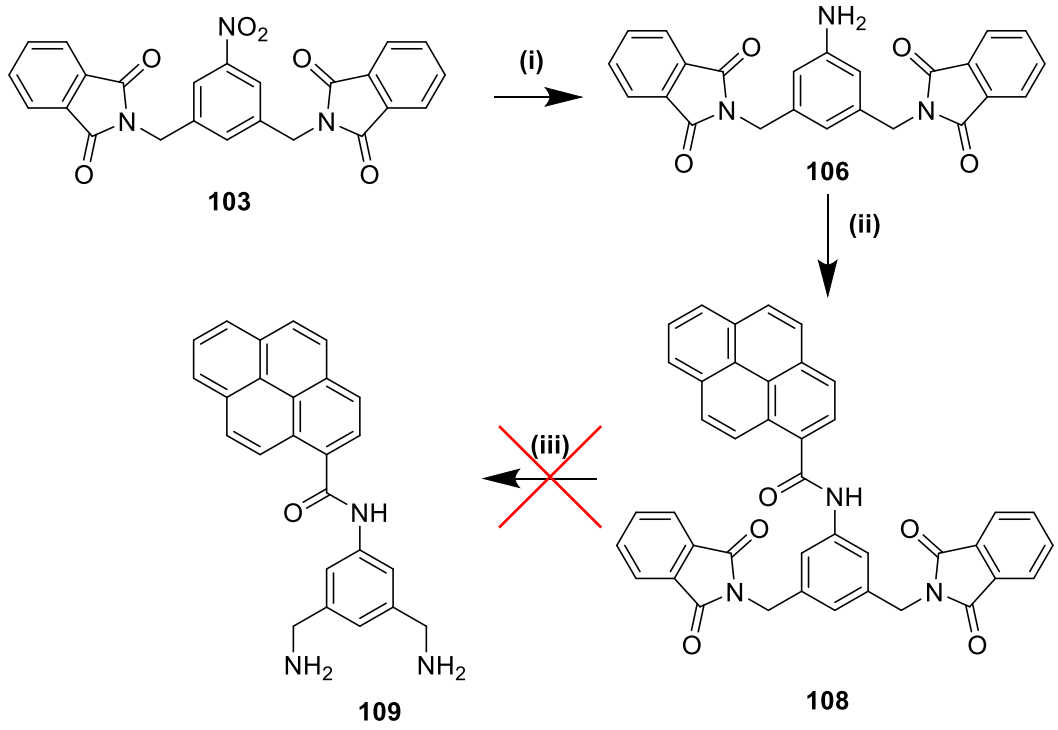

Scheme 3.6: Synthetic pathway of compound **109**. **(i)** H_2, Pd/C, DMF, rt, 72%. **(ii)** 1-Pyrenecarboxylic acid, 4-methylmorpholine, PyBOP, DMF, rt, 19%. **(iii)** Hydrazine, DMF, reflux.

At this stage, intermediate compound **106** and **108** were successfully synthesized and characterized by ^{1}H NMR, ^{13}C NMR, HRMS and IR-ATR spectroscopy. The ^{1}H NMR spectrum of compound **106** is shown in Figure 3.10, a multiplet signal was observed with chemical shift at 7.88 ppm for the aromatic protons H1 and H2 of the phthalimide group, whereas the peaks at 6.39 and 6.33 ppm was observed for the aromatic protons H3 and H4. The broad peak at 5.15 ppm assigned to two NH protons H5 and peak at 4.59 ppm assigned to the protons H6 of CH_2 group.

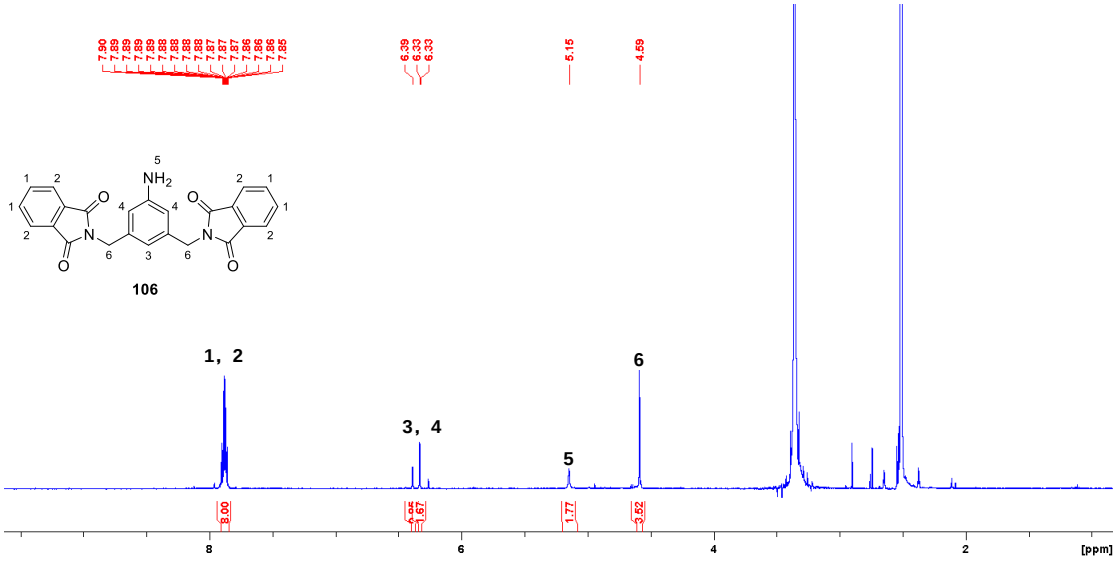

Figure 3.10: The ^{1}H NMR spectrum of compound **106** (500.13 MHz, DMSO-d_6).

In comparison to compound **106**, the ^{1}H NMR spectrum of compound **108** showed downfield shift of NH signal from 5.15 to 10.72 ppm due to the formation of amide and extra peaks were observed from 8.12 to 8.41 ppm for the aromatic protons of pyrene group (Figure 3.11). Downfield shifts of aromatic protons H3, H4 and CH_2 protons H6 were also observed ($\Delta\delta_{H3} = 0.71$ ppm, $\Delta\delta_{H4} = 1.41$ ppm, $\Delta\delta_{H6} = 0.22$ ppm).

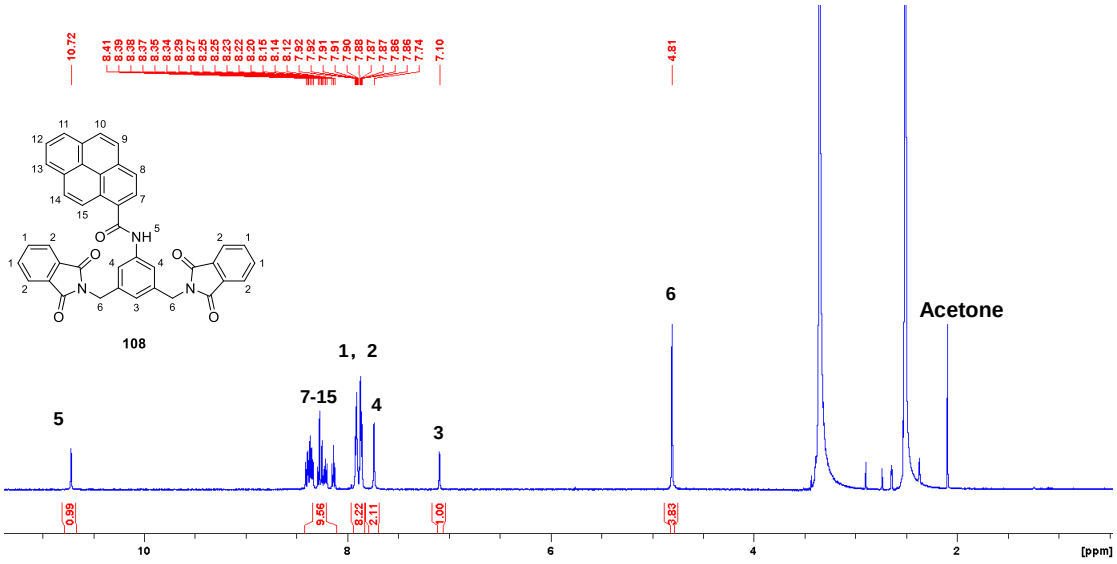

Figure 3.11: The ^{1}H NMR spectrum of compound **108** (500.13 MHz, DMSO-d_6).

An attempt was made to deprotect compound **108** by refluxing with hydrazine in DMF overnight. Removal of solvent under reduced pressure and re-dissolved in DCM resulted in precipitate which was then washed with sat. $NaHCO_3$ and 1M HCl. The precipitate was

filtered and washed with small amount of water. However, the ^{1}H NMR spectrum of the precipitate showed that although there was no signal peak of aromatic protons of phthalimide groups, the integration of aromatic region was much higher than expected which suggested that compound **108** might underwent a hydrolysis reaction of the amide linkage (Figure 3.12). In addition, in order to verify the phthalimide deprotection, an attempt was made to reprotect the free amines with Boc_2O. This reaction failed thus supporting the conclusion that target compound **109** was not successfully formed.

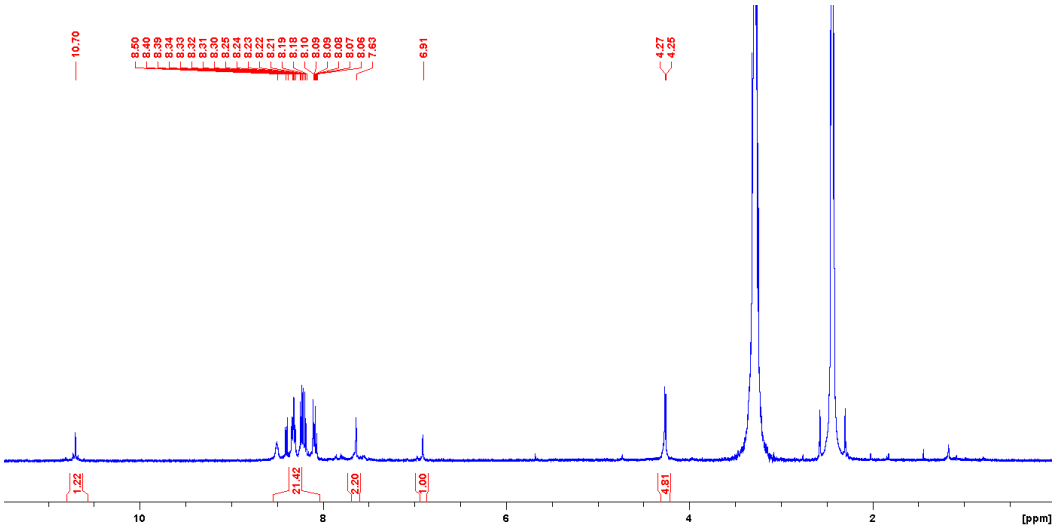

Figure 3.12: The ^{1}H NMR spectrum of potential product **109** (500.13 MHz, DMSO-d_6).

Moreover, in LCMS spectrum of the precipitate, no signal of the target molecule ($[M+H]^+$ = 380.5, $[M+Na]^+$ = 402.5) was observed further revealed that this deprotection was not successful (Figure 3.13). After several attempts to identify the product that had been formed using NMR and MS techniques the structure of the reaction product remains unknown.

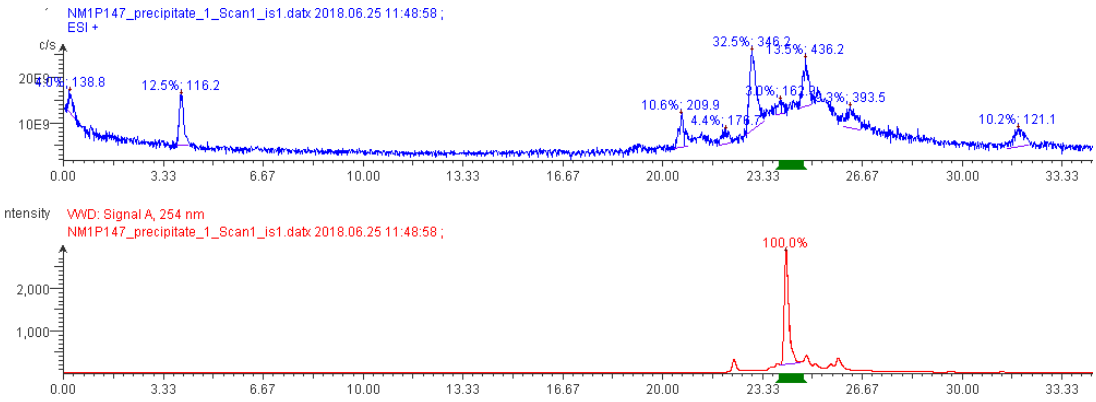

Figure 3.13: LCMS spectrum of potential product **109.**

Based on the failed attempt to deprotect **108** and to avoid the hydrolysis of the amide linkage, a C-C single bond which could be formed using Suzuki coupling reaction was considered to connect the pyrene probe and the macrocyclic squaramide. In this case, the coupling partners were pyrene-1-boronic acid **113** and bromo substituted compound **112** (Scheme 3.7)**.** Compound **112** could be synthesized from 1-bromo-3,5-bis(bromomethyl)benzene **111** using Gabriel synthesis as described in Scheme 3.3. Compound **111** could be synthesized from commercially available 1-Bromo-3,5-dimethylbenzene **110** using Wohl–Ziegler reaction.[79] Wohl–Ziegler reaction is known as a radical reaction which enables the bromination of allylic or benzylic hydrocarbon using N-bomosuccinimide and a radical initiator.

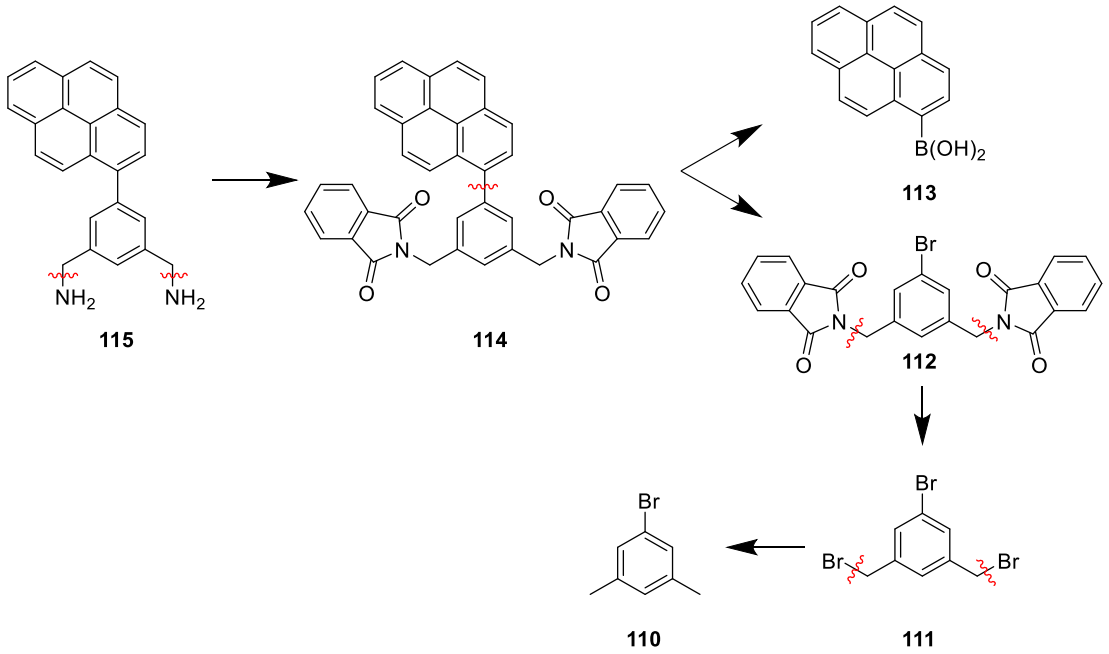

Scheme 3.7: Retrosynthetic analysis of the compound **114**.

The synthetic procedure of compound **115** is shown in Scheme 3.8, compound **111** was obtained by refluxing the solution of 1-Bromo-3,5-dimethylbenzene **110** and N-bromosuccinimide in MeCN using AIBN as radical initiator under argon yielded a white crystalline product in 5.4% yield. The low yield of this radical bromination reaction brought difficulty to the subsequent synthesis steps. However, after several attempts to increase the yield including modification of solvent, temperature and reaction duration, the mono-brominated product was always found to be dominant in this reaction.

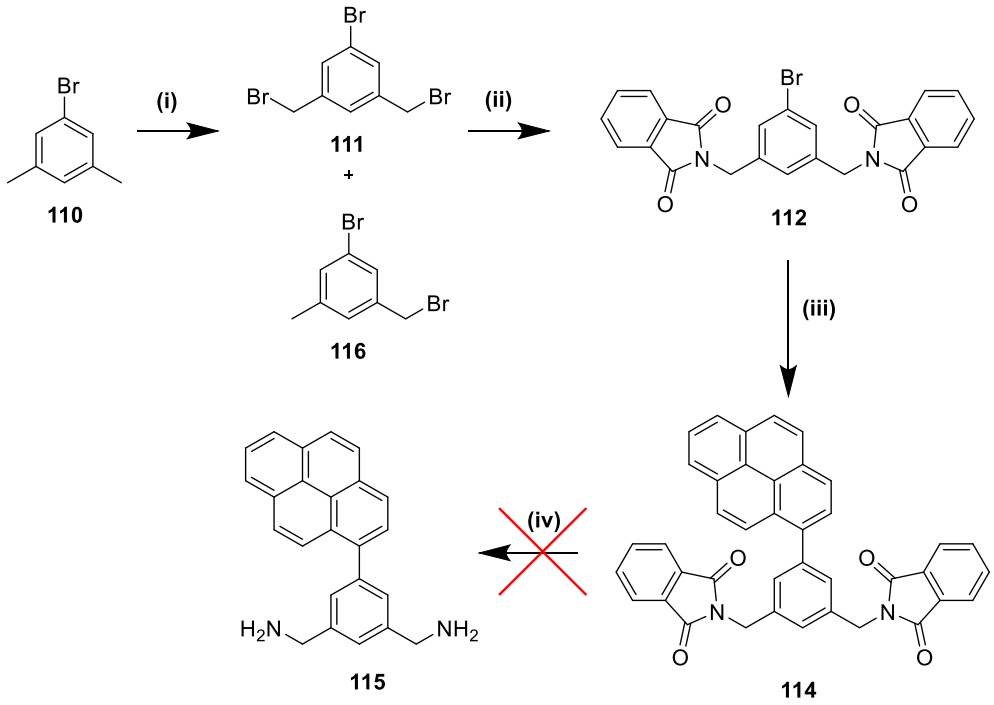

Scheme 3.8: Synthetic pathway of compound **115**. **(i)** N-bromosuccinimide, AIBN, MeCN, reflux under Ar, 5.4%. **(ii)** Potassium phthalimide, EtOH, reflux, 92%. **(iii)** Pyrene-1-boronic acid, $Pd(PPh_3)_4$, Na_2CO_3, THF/H_2O, reflux under N_2, 8%. **(iv)** Hydrazine, DMF, reflux.

As shown in the ^{1}H NMR spectrum of compound **111** (Figure 3.14), peaks at 7.34 and 7.47 ppm were observed for the aromatic protons H1 and H2, the peak at 4.41 ppm was observed for the CH_2 proton H3.

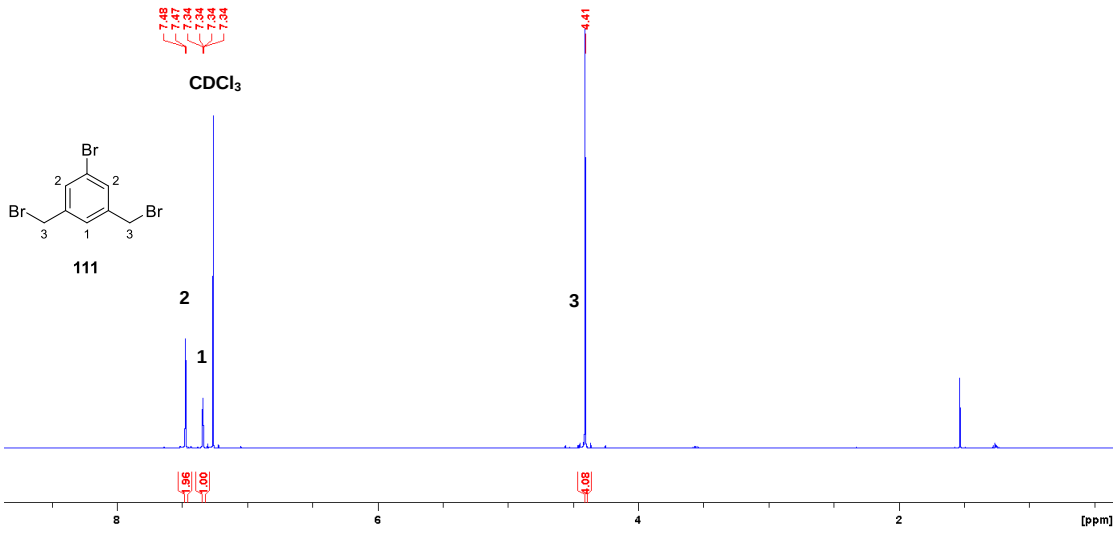

Figure 3.14: The ^{1}H NMR spectrum of compound **111** (500.13 MHz, $CDCl_3$).

Compound **112** was achieved as white solid in 92% yield by refluxing of compound **111** with phthalimide potassium salt in EtOH.

The signal peak of aromatic protons H1,2 and CH_2 protons H3 were also observed with chemical shift at 7.24, 7.44 and 4.75 ppm, respectively (Figure 3.15). Comparing to the ^{1}H NMR spectrum of compound **111**, an extra multipet was observed at 7.87 ppm for eight aromatic protons H4 and H5 of two phthalimide groups.

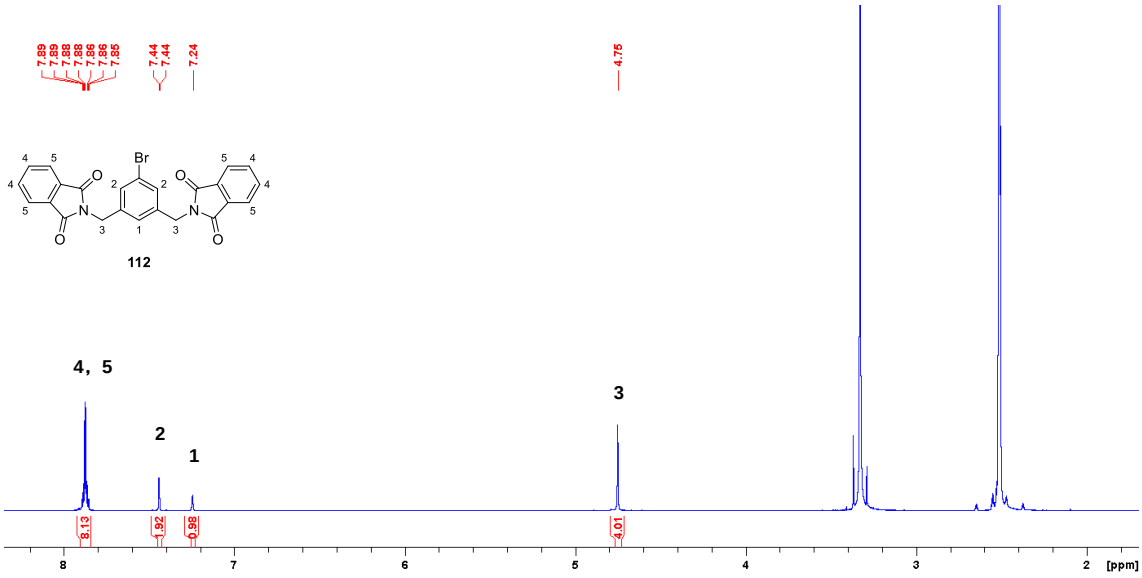

Figure 3.15: The ^{1}H NMR spectrum of compound **112** (500.13 MHz, DMSO-d_6).

Subsequent Suzuki coupling was undertaken for the synthesis of compound **114** by refluxing the solution of **112** and pyrene-1-boronic acid **113** with Na_2CO_3 in THF/H_2O mixture using $Pd(PPh_3)_4$ under N_2 atmosphere to yield the product as a brown solid in 8% yield. The low yield of this Suzuki reaction brought difficulty to the subsequent deprotection step again, although this Suzuki reaction was previously reported in some literature with 80% yield.[80]

The ^{1}H NMR spectrum of compound **114** is shown in Figure 3.16, peaks from 7.97 to 8.22 ppm were observed for aromatic protons H6-14 of pyrene group, multiplet at 7.86 ppm was observed for aromatic protons H4 and H5 of phthalimide groups.

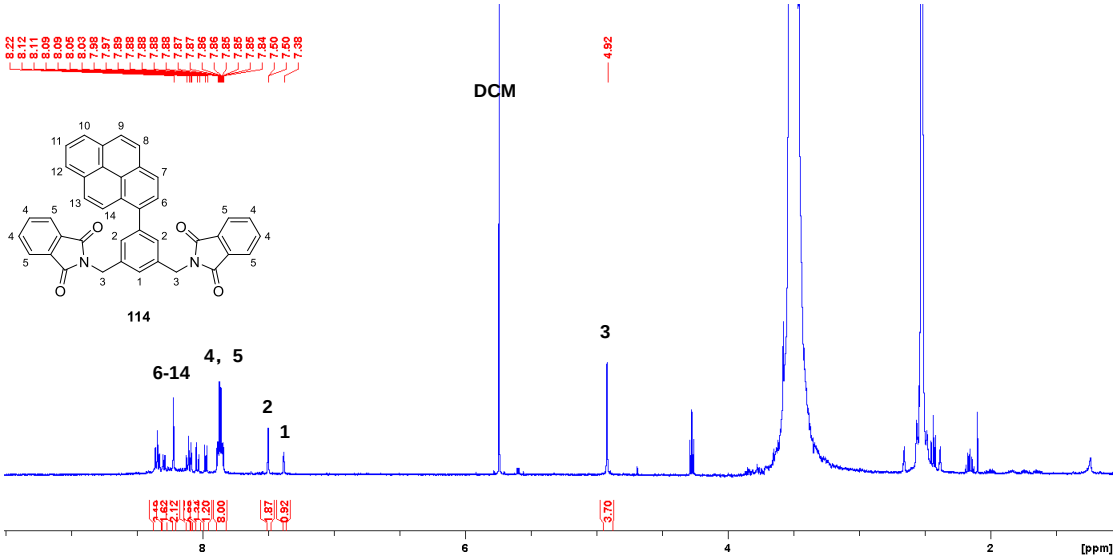

Figure 3.16: The ^{1}H NMR spectrum of compound **114** (500.13 MHz, DMSO-d_6).

Another attempt to deprotect compound **114** by refluxing with hydrazine in DMF overnight was carried out. Solvent was removed under reduced pressure and the residue was re-dissolved in water. The water solution was then adjusted to alkaline using 1 M NaOH and extracted by DCM to yielded yellow residue which was characterized by ^{1}H NMR spectroscopy. However, only the signal peak of phthalimide was observed in the aromatic region. Then water solution was adjusted to acidic using 1M HCl and extracted by DCM, no signal peak of the target molecule was observed form the ^{1}H NMR spectra (Figure 3.17).

(a)

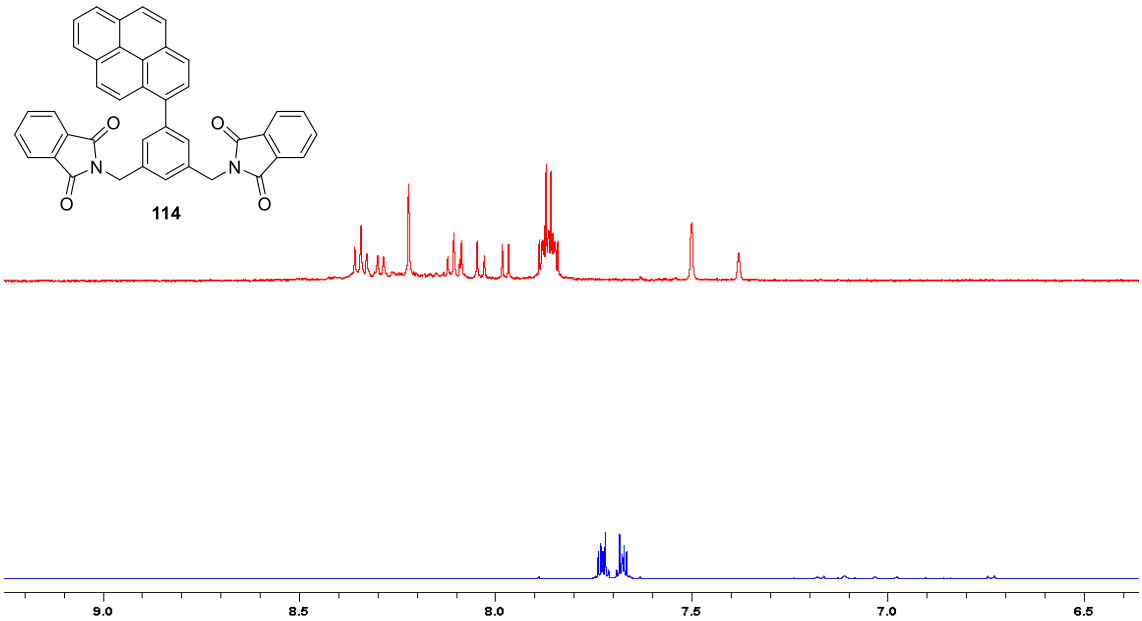

(b)

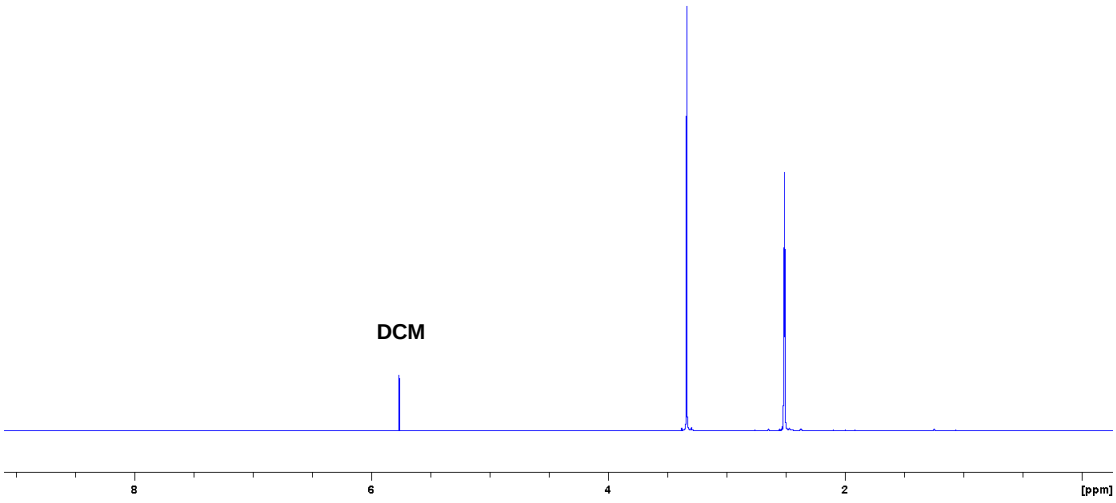

Figure 3.17: (a) Multiple display of partial ^{1}H NMR spectrum of **114** and the residue after base wash. **(b)** ^{1}H NMR spectrum of the residue after acid wash.

The extraction of phthalimide from base washed reaction mixture revealed that the deprotection might happen. However, due to the low yield of intermediate **111** and **114**, only 20mg **114** was used for the deprotection which brought difficulty to the purification of the reaction mixture. Although we failed to introduce the pyrene group into the MSQ, the successful synthesis of MSQ **86** and **87** enabled to investigate the effect of substitution on the periphery of MSQ in SO_4^{2-} binding.

3.3 ^{1}H NMR Titration Study of Compound 86 and 87

Considering the difficulty in obtaining the proposed compounds we wished to further explore the SO_4^{2-} binding ability of compounds **86** and **87** in order to fully understand the effect of substitution on the periphery of the macrocycle. The successful synthesis and characterization of compound **86** and **87** enabled us to investigate their anion binding ability in comparison to non -NO_2 substituted macrocycle **70**. In this ^{1}H NMR titration study, 2.5 x 10^{-3} M of compound **86** and **87** in 0.5% H_2O in DMSO-*d6* solution was tested with increasing equivalent of SO_4^{2-} anions in its tetrabutylammonium salt (TBA^{+}) from 0 eq. to 12.0 eq., respectively. As shown in Figure 3.18, addition of SO_4^{2-} resulted in

significant downfield shift of NH proton signals from 7.95 to 10.08 ppm (Δδ= 2.13 ppm). Downfield shift of aromatic proton C-H_a was observed from 7.62 to 8.64 ppm (Δδ= 1.02 ppm) whereas upfield shift of aromatic proton C-H_b was observed from 8.15 to 7.96 ppm (Δδ= 0.19 ppm).

(a)

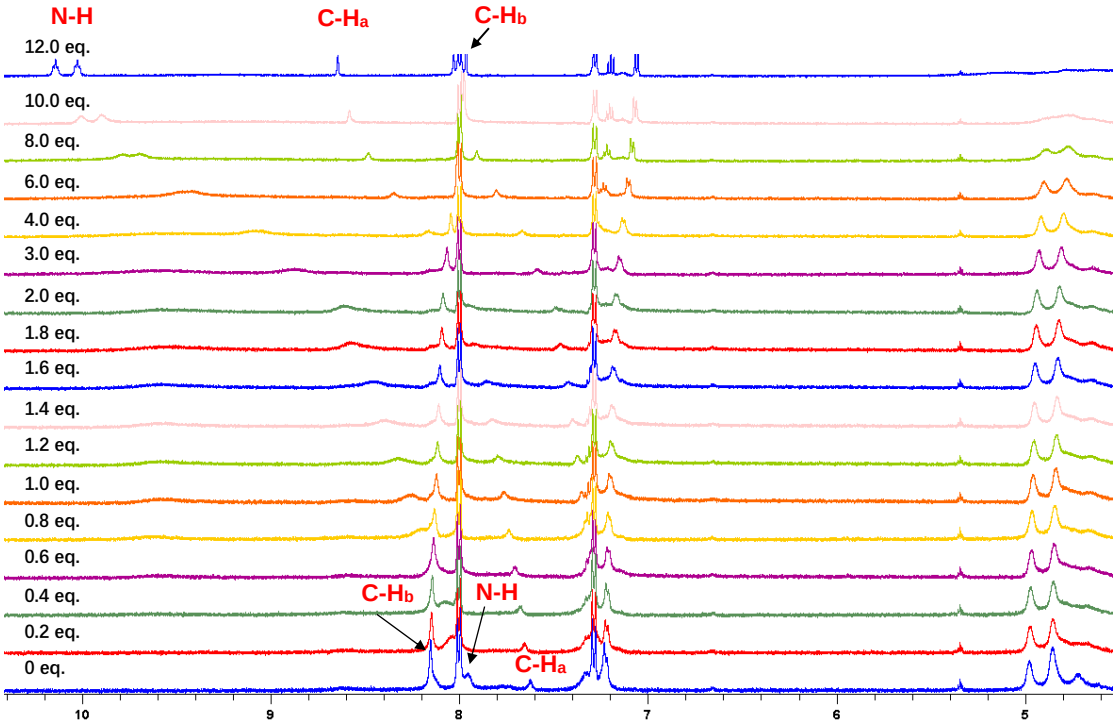

(b)

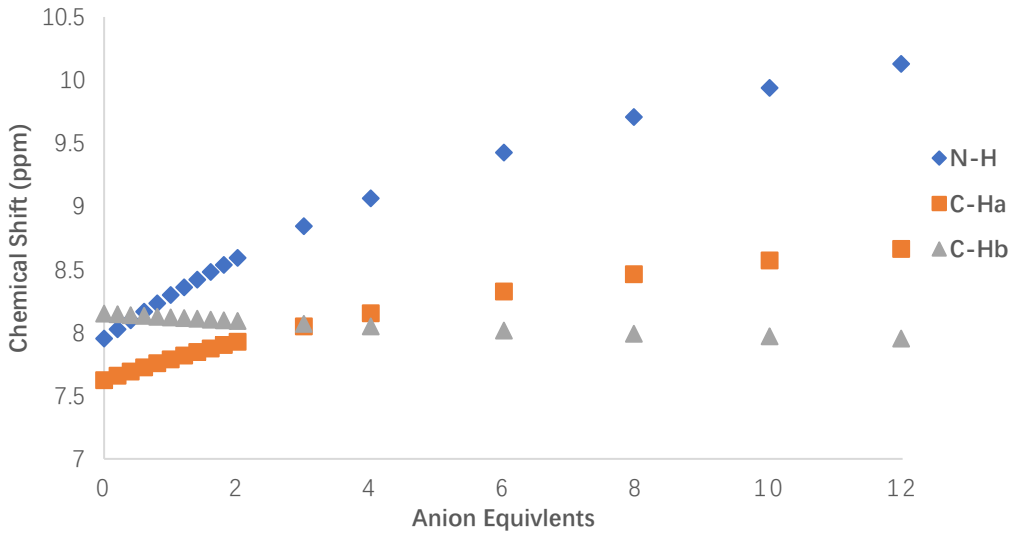

(c)

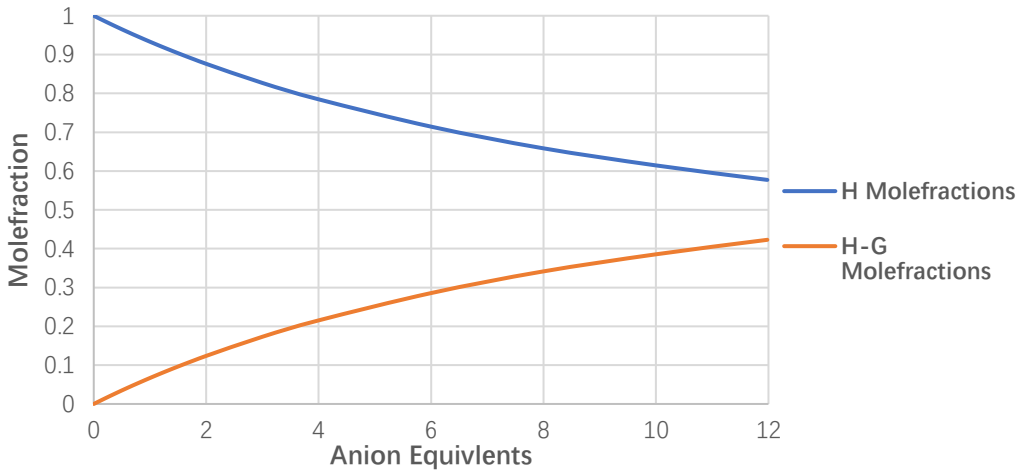

Figure 3.18: (a) Stack plot of ^{1}H NMR spectra of **86** (2.5 x 10^{-3} M) upon addition of $(TBA)_2SO_4$ (0 - 12 equiv.) in DMSO-d_6 at 25 °C. **(b)** Comparison isotherms of squaramide NH, aromatic protons (Ar-H_a, H_b) for **86** in the presence of increasing concentrations of SO_4^{2-}. **(c)** Comparison of host (H) and host-guest (H-G) molefractions in the presence of increasing concentrations of SO_4^{2-}.

As shown in Figure 3.19, addition of SO_4^{2-} resulted in significant downfield shift of NH proton signals from 8.03 to 9.82 ppm ($\Delta\delta$= 1.79 ppm). Downfield shift of aromatic proton C-H_a was observed from 7.60 to 8.43 ppm ($\Delta\delta$= 0.83 ppm) whereas upfield shift of aromatic proton C-H_b was observed from 8.15 to 8.0 ppm ($\Delta\delta$= 0.15 ppm).

(a)

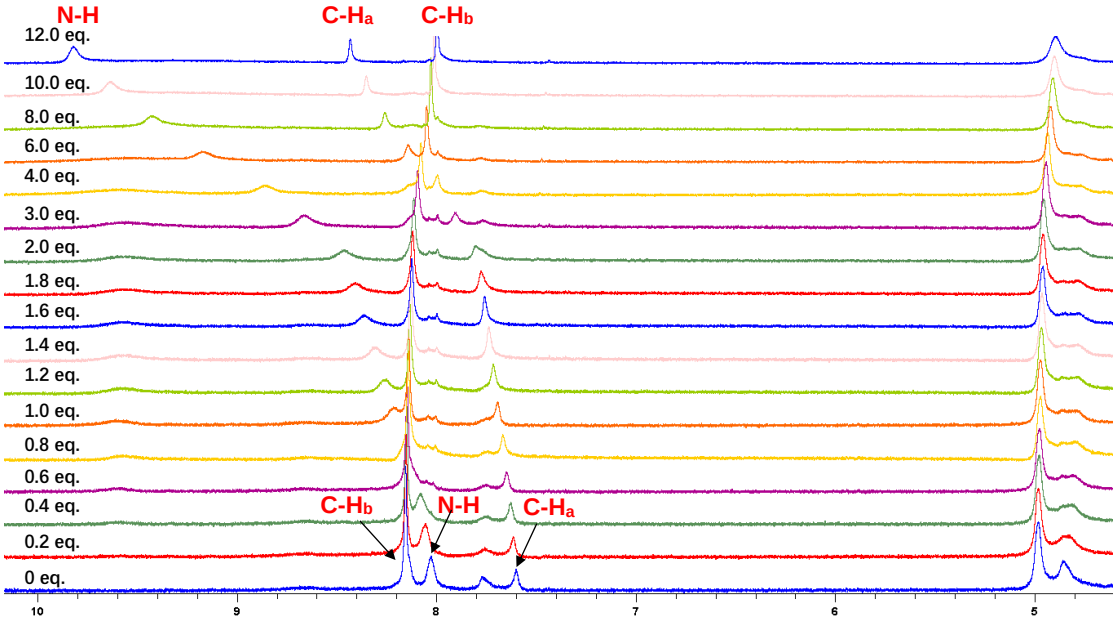

(b)

(c)

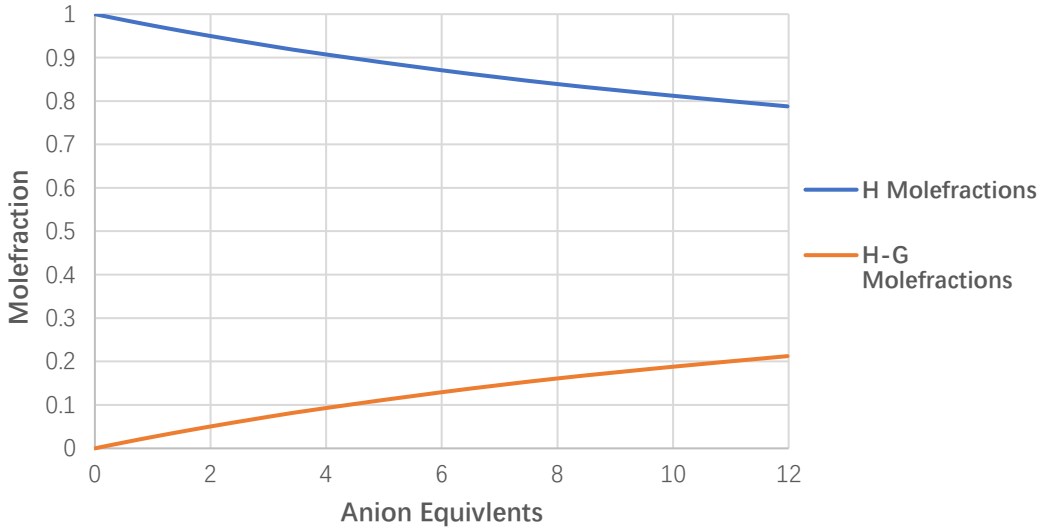

Figure 3.19: (a) Stack plot of ^{1}H NMR spectra of **87** (2.5 x 10^{-3} M) upon addition of $(TBA)_2SO_4$ (0 - 12 equiv.) in DMSO-d_6 at 25 °C. **(b)** Comparison isotherms of squaramide NH, aromatic protons (Ar-H_a, H_b) for **87** in the presence of increasing concentrations of SO_4^{2-}. **(c)** Comparison of host (H) and host-guest (H-G) mole fractions in the presence of increasing concentrations of SO_4^{2-}.

The ^{1}H NMR titration data of two MSQs **86** and **87** in the presence of increasing concentrations of SO_4^{2-} fitted to a 1:1 binding mode using BindFit.[81] The apparent stability constant (K_a) as summarized in Table 3.2 (K_a = 31.38 M^{-1} and 11.34 M^{-1} for **86**

and **87**, respectively (error < 2%)). In comparison to non-NO_2 substituted MSQ **70** of which $K_a > 10^4\ M^{-1}$, MSQs **86** and **87** showed relatively low binding affinity towards SO_4^{2-} anion.

MSQ	Ka (M^{-1})
70	**$>10^4$**
86	**31.38**
87	**11.34**

Table 3.1: Apparent stability constant (K_a) of the binding of MSQ **70**, **86** and **87** towards SO_4^{2-} anion.

3.4 Conclusion

In conclusion, we have successfully synthesized nitro substituted macrocyclic squaramide (MSQ) **86** and **87**, both MSQs have been characterized by a combination of NMR spectroscopy, mass spectrometry and FT-IR spectroscopy. The ^1H NMR spectra of compound **86** and **87** were poorly resolved until addition $(TBA)_2SO_4$ revealed clear binding interactions with SO_4^{2-}. The ^1H NMR titration study of **86** and **87** were performed by addition of SO_4^{2-} with the resulting data fit to a 1:1 binding mode using BindFit. However, compound **86** and **87** showed quite low apparent stability constant ($K_{a\ 86}$ = 31.38 M^{-1}, $K_{a\ 87}$ = 11.34 M^{-1}) comparing to non-nitro substituted compound **70** ($K_a > 10^4\ M^{-1}$).

The synthesis of pyrene-substituted MSQ **88** was also discussed in this chapter. In our initial work, the pyrene probe was planned to be introduced into the MSQ using an amide linkage. Unfortunately, in the deprotection step of compound **108**, the amide linkage appeared to be hydrolyzed in the presence of hydrazine. To avoid this, the C-C bond was considered to connect pyrene probe and the MSQ using Suzuki coupling. However, the deprotection step of compound **114** again did not result in the target molecule **115**. Thus, although the Gabriel synthesis showed good result in the synthesis of compound **86** and **87**, however, it was not suitable in the synthesis of compound **115**. The low yield of intermediate **108**, **111** and **114** (19%, 5.4% and 8%, respectively) also brought difficulty to the repeating attempt to synthesize the target molecule.

Chapter 4 Overall Conclusion and Future Work

In this thesis, we aimed to prepare and study two families of novel squaramide-based anion sensors. The design, synthesis, characterization as well as anion binding study of novel squaramidoquinoxaline (SQX) based anion sensors **80-85** were discussed in Chapter 2. The design, synthesis, characterization as well as SO_4^{2-} binding test of macrocyclic squaramide (MSQ) **86, 87** and the attempt to synthesize pyrene functionalized MSQ **88** were discussed in Chapter 3.

In Chapter 2, compound **81** showed a characteristic long wavelength absorption at 715 nm in its UV/Vis absorption spectrum. The investigation of halide recognition abilities of the receptors revealed that **81** underwent drastic colorimetric changes from pink to green along with a large increase in absorption at 715 nm upon titration with F^- suggesting the existence of a deprotonation event. Further addition of F^- led to a second colour change from green to yellow and a concomitant reduction of all absorption bands in the UV/Vis absorption spectrum. The NO_2 derivative **81** was also found to be a selective colourimetric sensor for F^- among the tested halides. Using UV/Vis, NMR and TD-DFT analysis we conclude that the observed colour changes are likely to be due to a two-step process involving two NH deprotonation steps. Colour changes of the other compounds **80** and **82-85** were not as apparent in the presence of F^- owing to the lack of a strong electron withdrawing group that allows for charge transfer within the molecule. Test strips study of compound **81** showed that this compound is capable of instant recognition of F^- even under different pH conditions. The study of this chapter demonstrated the use of squaramide-based molecules as useful building blocks in the field of anion recognition and sensing. It also demonstrated that the electron withdrawing aryl substituent is directly related to the sensing ability/acidity of the squaramide protons. Moreover, the crystal structure of **81** showed the packing interactions including hydrogen bonding, weaker non-classical CH-based hydrogen bonding and π- π stacking interactions which could enable **81** to be useful building blocks for anion-responsive supramolecular self-assembly formations.

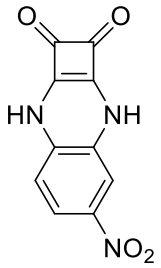

81

Figure 4.1: Chemical structure of compound **81.**

In Chapter 3, we have successfully synthesized and characterized the asymmetrically -NO_2 substituted MSQ **86** and symmetrically -NO_2 substituted MSQ **87**. We also outlined our attempts to synthesize pyrene-substituted MSQs. Two strategies were carried out to synthesize the target molecule, one strategy was using an amide linkage to connect the pyrene group and the MSQ, another strategy was using C-C single bond to connect two moieties. However, the attempt to synthesize the pyrene-substituted MSQ was unsuccessful. The deprotection of the phthalimide group failed for both strategies and suggested that the Gabriel synthesis was not suitable here although useful in the synthesis of compound **86** and **87**. The ^{1}H NMR titration study of **86** and **87** were demonstrated by addition of SO_4^{2-} with the resulting data fit to a 1:1 binding mode using BindFit. However, compound **86** and **87** showed relatively low apparent stability constant ($K_{a\ 86}$ = 31.38 M^{-1}, $K_{a\ 87}$ = 11.34 M^{-1}) comparing to their parent compound **70** ($K_a > 10^4\ M^{-1}$). This result suggests that substitution of the macrocycle in its periphery may be detrimental to anion recognition.

We failed at the last step to introduce the pyrene group into the macrocyclic squaramide. However, we provided a preliminary idea of using FRET (Förster Resonance Energy Transfer) to monitor the anion binding process of fluorescent probe substituted MSQ and this work will continue in the Elmes lab.

The future work to continue this project should look to improve the synthesis and increase the yield of some relevant steps as described in section 3.3, as many synthetic steps suffered from low reaction yields. An alternative method to obtain the key diaminomethyl-substituted intermediate could use azide chemistry as outlined below (Scheme 4.1). This reaction was originally avoided due to the safety issues of azide

chemistry and should be considered carefully as the diazide substituted intermediate may be an explosive risk due to its high N atom ratio.

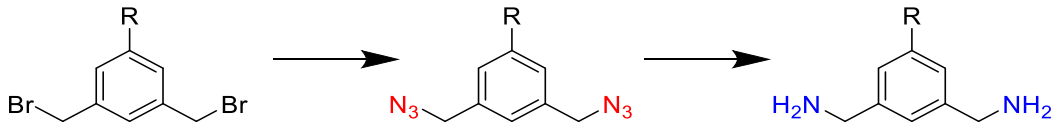

Scheme 4.1: synthesis of amine using azide chemistry.

Once synthesized FRET based MSQs may yield an entirely new class of anion sensors and we expected will have broad applicability to rea world applications.

Chapter 5 Experimental

5.1 Instrumentation and Reagents

Commercial materials were supplied by Sigma Aldrich or TCI Europe and were used without further purification. HPLC grade solvents were used as received. ^{1}H NMR spectra were recorded using a Bruker Avance III 500 spectrometer at a frequency of 500.13 MHz as parts per million (ppm) and calibrated to the residual protio-solvent preak in DMSO-d_6 (δ = 2.50 ppm) or $CDCl_3$ (δ = 7.26 ppm). Stack plots were made using TopSpin 3.5. The data are reported as chemical shifts (δ), multiplicity (br = broad, s = singlet, d = doublet, t = triplet, m = multiplet, dd = doublet of doublets, dt = doublet of triplets), coupling constant (*J*, Hz) and relative integral. ^{13}C NMR were recorded using a a Bruker Avance III 500 spectrometer at a frequency of 125.76 MHz as parts per million (ppm) and calibrated to the residual protio-solvent peak in DMSO-d_6 (δ = 39.5 ppm) or $CDCl_3$ (δ = 77.1 ppm). High resolution ESI sprctra were recorded on an Agilent 63010 LCMS TOF. Analytical TLC was performed using pre-coated silica gel plates (Merck Kieselgel 60 F254). Infrared absorption spectra were recorded on a Perkin Elmer Spectrum 100 FT-IR/ATR spectrometer and reported in wavenumbers (cm^{-1}).

5.2 Photophysical Characterizations

Photophysical characterizations were performed by diluting the PBS buffer solution of each receptor. The stock solution of the receptor in DMSO was used to make two PBS buffer solutions with concentration of 1×10^{-5} M and 2×10^{-5} M, respectively. For each sample, it was diluted by taking out 0.5 mL solution then adding 0.5 mL PBS buffer for four times. UV/Vis spectrum was recorded using a Varian Cary 50 UV/Vis spectrophotometer after each operation and plotted into one chart. Extinction coefficient of the receptor was obtained as the slope of the absorption spectrum in the unit M^{-1}.

5.3 Spectroscopic Binding Studies

Spectroscopic titrations were performed by additions of aliquots of the putative anionic guest as the tetrabutylammonium (TBA) salt, in a solution of the receptor (1×10^{-5} M) in

DMSO to a 1×10^{-5} M solution of the receptor in DMSO. Typically, 0 up to 0.12 M of the anions were added to the solution. Both salt and receptor were dried under high vacuum prior to use. UV/Vis data was recorded using a Varian Cary 50 UV/Vis Spectrophotometer. The absorbance was recorded from 250 nm to 850 nm. To determine association constants for the receptor-anion complexes, global analysis of the absorbance data was carried out using the open access BindFit software program.[71, 82]

5.4 ^{1}H NMR Binding Studies of Novel Receptors

NMR titrations of novel receptors **81** were performed by additions of aliquots of the putative anionic guest as the tetrabutylammonium (TBA) salt (0.15 – 0.2 M), in a solution of the receptor (2.5×10^{-3} M) in DMSO-d_6 to a 2.5×10^{-3} M solution of the receptor in DMSO-d_6. Typically, up to 2 equivalents of the anion were added to the solution. NMR titrations of receptors **86** and **87** were performed by additions of SO_4^- as the tetrabutylammonium (TBA) salt (0.125 M), in a solution of the receptor (2.5×10^{-3} M) in DMSO- d_6. Typically, up to 12 equivalents of the anion were added to the solution. Both salt and receptor were dried under high vacuum prior to use. ^{1}H NMR spectra were recorded on a Bruker Avance III 500 spectrometer at a frequency of 500.13 MHz and calibrated to the residual protio solvent peak in DMSO-d_6 (δ = 2.50 ppm). Stack plots were made using TopSpin 3.2.

5.5 Experimental Procedure and Characterizations

(80) cyclobuta[b]quinoxaline-1,2(3H,8H)-dione

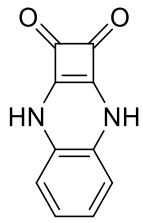

A solution of 3,4-diethoxycyclobut-3-ene-1,2-dione (1 g, 5.88 mmol, 1 eq) and Zinc trifluoromethanesulfonate (0.427 g, 1.16 mmol, 0.2 eq) in EtOH (10 mL) was added slowly into the solution of benzene-1,2-diamine (0.76 g; 7.07 mmol, 1.2 eq) in EtOH (5 mL). The reaction was left to stir at room temperature for 48 hours. The precipitate was collected by suction filtration and washed with EtOH and Et_2O to yield the product as a beige solid. (0.708 g, 64%), m.p.≥300 °C. **^{1}H NMR** (500 MHz, DMSO-d_6) δ 10.0 (s, 2H, NH), 6.66 (dd, 2 H, J = 5.6/3.4 Hz, Ar), 6.36 (dd, 2 H, J = 5.6/3.6 Hz, Ar); **^{13}C NMR** (125 MHz, DMSO-d_6): 178.7, 174.9, 132.2, 125.4, 116.9; **HRMS** (ESI): Calculated for $C_{10}H_6O_2N_2$ $[M+H]^+$, expected: 187.0428, observed: 187.0501, PPM:-0.64; **νmax (film)/cm^{-1}:** 3123 (N-H stretch, secondary amines), 2955, 2017, 1913, 1805, 1790, 1657 (C=O stretch, ketones), 1614, 1558, 1478, 1458, 1358, 1304, 1245, 1213, 1180, 1129, 1075, 1041, 930, 900, 806, 777, 743, 666.

(81) 5-nitrocyclobuta[b]quinoxaline-1,2(3H,8H)-dione

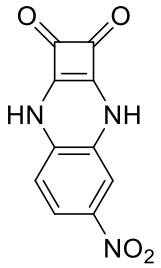

A solution of 3,4-diethoxycyclobut-3-ene-1,2-dione (1 g, 5.88 mmol, 1 eq) and Zinc trifluoromethanesulfonate (0.427 g, 1.16 mmol, 0.2 eq) in EtOH (10 mL) was added slowly into the solution of 4-nitrobenzene-1,2-diamine (1.08 g; 7.05 mmol, 1.2 eq) in EtOH (5 mL). The reaction was left to stir at room temperature for 48 hours. The precipitate was collected by suction filtration and washed with EtOH and Et_2O to yield

the product as a purple solid. (1.004 g, 74%), m.p.≥300 °C. **^{1}H NMR** (500 MHz, DMSO-d_6) δ 10.55 (s, 1,H, NH), 10.39 (s, 1H, NH), 7.58 (dd, 1 H, *J* =8.6/2.5 Hz, Ar), 7.01 (d, 1H, *J* = 2.5 Hz, Ar), 6.41 (d, 1 H, *J* = 8.6 Hz, Ar); **^{13}C NMR** (125 MHz, DMSO-d_6): 179.6, 178.5, 175.7, 174.8, 144.0, 139.8, 133.9, 122.7, 115.9, 110.4; **HRMS** (ESI): Calculated for $C_{10}H_5O_4N_3$ $[M+H]^+$, expected: 232.0282, observed: 232.0354, PPM:0.71; **νmax (film)/cm-1:** 3572, 3141 (N-H stretch, secondary amines), 2974, 2020, 1870, 1794, 1665 (C=O stretch, ketones), 1632, 1583 (N-O stretch, aromatic nitro), 1529, 1487, 1419, 1322 (N-O stretch, aromatic nitro), 1267, 1247, 1218, 1202, 1092, 1073, 945, 883, 861, 837, 803, 788, 745, 670, 646.

(82) 5-methoxycyclobuta[b]quinoxaline-1,2(3H,8H)-dione

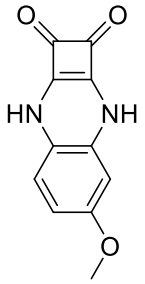

A solution of 3,4-diethoxycyclobut-3-ene-1,2-dione (0.51 g, 3 mmol, 1 eq) and Zinc trifluoromethanesulfonate (0.218 g, 0.6 mmol, 0.2 eq) in EtOH (8 mL) was added slowly into the solution of 4-methoxybenzene-1,2-diamine (0.76 g; 3.6 mmol, 1.2 eq) in EtOH (2 mL). The reaction was left to stir at room temperature for 48 hours. The precipitate was collected by suction filtration and washed with EtOH and Et_2O to yield the productas a brown solid. (0.646 g, 97%), m.p.≥300 °C. **^{1}H NMR** (500 MHz, DMSO-d_6) δ 10.01 (s, 1H, NH), 9.99 (s, 1H, NH), 6.34 (d, 1 H, *J* = 8.6 Hz, Ar), 6.24 (dd , 1 H, *J* = 8.6/2.7 Hz, Ar), 6.02 (d, 1 H, *J* = 2.7 Hz, Ar), 3.63 (s, 3H, CH_3); **^{13}C NMR** (125 MHz, DMSO-d_6): 179.1, 178.2, 174.6, 173.7, 157.2, 133.1, 125.1, 117.2, 107.5, 104.9, 56.0. **HRMS** (ESI): Calculated for $C_{11}H_8O_3N_2$ $[M+H]^+$, expected: 217.0535, observed: 217.0620, PPM:5.55; **νmax (film)/cm^{-1}:** 3123 (N-H stretch, secondary amines), 2944, 1797, 1660 (C=O stretch, ketones), 1351, 1315, 1279, 1217 (C-O stretch, aromatic ether) , 1160, 1123, 1084, 1067, 1032, 941, 854, 788, 718, 672.

(83) 5-Carboxylcyclobuta[b]quinoxaline-1,2(3H,8H)-dione

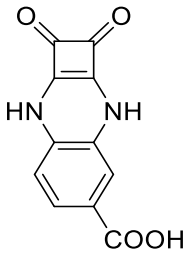

A solution of 3,4-diethoxycyclobut-3-ene-1,2-dione (1 g, 5.88 mmol, 1 eq) and Zinc trifluoromethanesulfonate (0.427 g, 1.16 mmol, 0.2 eq) in EtOH (10 mL) was added slowly into the solution of 4-nitrobenzene-1,2-diamine (1.07 g; 7.05 mmol, 1.2 eq) in EtOH (5 mL). The reaction was left to stir at room temperature for 48 hours. The precipitate was collected by suction filtration and washed with EtOH and Et_2O to yield the product as an orange solid. (1.046 g, 77%), m.p.≥300 °C. **^{1}H NMR** (500 MHz, DMSO-*d_6*) δ 10.29 (s, 1H, NH), 10.15 (s, 1H, NH), 7.26 (dd, 1 H, *J* = 8.0/1.7 Hz, Ar), 6.86 (d , 1 H, *J* = 1.7 Hz, Ar), 6.40 (d, 1 H, *J* = 8.0 Hz, Ar); **^{13}C NMR** (125 MHz, DMSO-*d_6*): 179.2, 178.4, 175.4, 174.7, 166.4, 136.7, 132.5, 127.8, 127.2, 116.8, 116.2. **HRMS** (ESI): Calculated for $C_{11}H_6O_4N_2$ $[M+H]^+$, expected: 231.0328, observed: 231.0401, PPM:0.32; **νmax (film)/cm^{-1}:** 3135 (N-H stretch, secondary amines), 2971 (O-H stretch, carboxylic acid), 1799, 1655 (C=O stretch, ketones and carboxylic acid), 1604, 1485, 1408 (O-H bend, carboxylic acid), 1288 (C–O stretch, carboxylic acid), 1268, 1190, 1138, 1102, 1028, 898 (O-H bend, carboxylic acid), 848, 763, 669.

(84) 5-Carbonitrilecyclobuta[b]quinoxaline-1,2(3H,8H)-dione

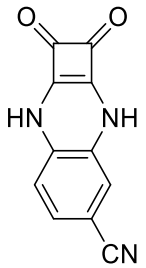

A solution of 3,4-diethoxycyclobut-3-ene-1,2-dione (0.5 g, 2.94 mmol, 1 eq) and Zinc trifluoromethanesulfonate (0.214 g, 0.588 mmol, 0.2 eq) in EtOH (10 mL) was added slowly into the solution of 4-nitrobenzene-1,2-diamine (0.47 g; 3.53 mmol, 1.2 eq) in EtOH (2 mL). The reaction was left to stir at room temperature for 48 hours. The

precipitate was collected by suction filtration and washed with EtOH and Et_2O to yield the product as an orange solid. (0.543 g, 87%), m.p.≥300 °C. **^{1}H NMR** (500 MHz, DMSO-*d_6*) δ 10.37 (s, 1H, NH), 10.26 (s, 1H, NH), 7.12 (dd, 1 H, *J* = 8.1/1.7 Hz, Ar), 6.51 (d, 1 H, *J* = 1.7 Hz, Ar), 6.38 (d, 1 H, *J* = 8.1 Hz, Ar); **^{13}C NMR** (125 MHz, DMSO-*d_6*): 179.2, 178.6, 175.6, 174.8, 137.6, 133.8, 131.1, 118.6, 116.7, 106.7. **HRMS** (ESI): Calculated for $C_{11}H_5O_2N_3$ $[M+H]^+$, expected: 221.0382, observed: 212.0462, PPM:3.35; **νmax (film)/cm^{-1}:** 3136 (N-H stretch, secondary amines), 2936, 2227 (C≡N stretch, nitrile), 1797, 1657 (C=O stretch, ketones), 1601, 1569, 1468, 1407, 1329, 1254, 1213, 1155, 1125, 1078, 945, 878, 836, 725, 669.

(85) 5-Bromocyclobuta[b]quinoxaline-1,2(3H,8H)-dione

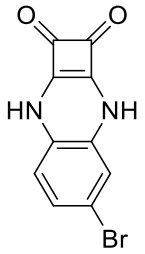

A solution of 3,4-diethoxycyclobut-3-ene-1,2-dione (1 g, 5.88 mmol, 1 eq) and Zinc trifluoromethanesulfonate (0.427 g, 1.16 mmol, 0.2 eq) in EtOH (10 mL) was added slowly into the solution of 4-nitrobenzene-1,2-diamine (1.318 g; 7.05 mmol, 1.2 eq) in EtOH (5 mL). The reaction was left to stir at room temperature for 48 hours. The precipitate was collected by suction filtration and washed with EtOH and Et_2O to yield the product as an orange solid. (1.323 g, 84%), m.p.≥300 °C. **^{1}H NMR** (500 MHz, DMSO-*d_6*) δ 10.08 (s, 2H, 2 x NH), 6.81 (dd, 1H, *J* = 8.3/2.2 Hz, Ar), 6.41 (d, 1H, *J* = 2.2 Hz, Ar), 6.24 (d, 1H, *J* = 8.3 Hz, Ar); **^{13}C NMR** (125 MHz, DMSO-*d_6*): 178.8, 178.5, 175.0, 174.7, 134.1, 131.9, 127.5, 119.0, 118.0,116.4. **HRMS** (ESI): Calculated for $C_{10}H_5O_2N_2Br$ $[2M+Na]^+$, expected: 552.9534, observed: 552.8965, PPM:8.17; **νmax (film)/cm^{-1}:** 3165 (N-H stretch, secondary amines), 2939, 1793, 1665 (C=O stretch, ketones), 1605, 1531, 1472, 1395, 1335, 1290, 1267, 1242, 1209, 1188, 1128, 1082, 1031, 924, 909, 864, 812, 781, 714, 666.

(99) 4,4'-((1,3-phenylenebis(methylene))bis(azanediyl))bis(3-ethoxycyclobut-3-ene-1,2-dione)

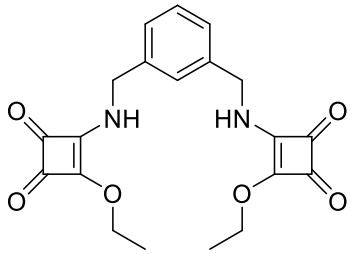

A solution of 1,3-phenylenedimethanamine (0.484 mL, 3.67 mmol, 1 eq) in EtOH (5 mL) was added slowly into the solution of 3,4-diethoxycyclobut-3-ene-1,2-dione (1.87 g; 11.01 mmol, 3 eq) in EtOH (5 mL). Triethylamine (2.56 mL, 18.35 mmol, 5 eq) was then added into the mixture. The reaction was left to stir at room temperature overnight. Solvent was reduced to a small amount and the mixture was added into Et_2O (20 mL) to yield the precipitate. The precipitate was collected by suction filtration and washed with Et_2O to yield the product as a light-yellow solid. (0.169 g, 12%), m.p.: 120-125 °C. **^{1}H NMR** (500 MHz, DMSO-*d_6*) δ 9.29 (s, 1H, NH), 9.07 (s, 1H, NH), 7.38 (t, 1H, *J* = 2.2 Hz, Ar), 7.24 (d, 3H, *J* = 8.3 Hz, Ar), 4.58 (m, 8H, 4 x CH_2), 1.35 (m, 6H, 2 x CH_3); **^{13}C NMR** (125 MHz, DMSO-*d_6*): 189.8, 189.5, 182.9, 182.6, 177.7, 177.2, 173.1, 172.5, 139.3, 139.0, 129.4, 127.1, 126.7, 69.4, 47.6, 17.2, 16.0. **HRMS** (ESI): Calculated for $C_{10}H_5O_2N_2Br$ $[M+Na]^+$, expected: 407.1214, observed: 407.1247, PPM:8.30; **νmax (film)/cm^{-1}:** 3304, 3212 (N-H stretch, secondary amines), 2982, 2948, 1803, 1709, 1693 (C=O stretch, ketones), 1638, 1587, 1509, 1449, 1423, 1408, 1378, 1346, 1335, 1294, 1281, 1239, 1219 (C-O stretch, aliphatic ethers), 1201, 1145, 1113, 1091, 1059, 1012, 988, 955, 904, 886, 866, 812, 783, 744, 703.

(70)3,5,9,11-tetraaza-1,7(1,3)-dibenzena-4,10(1,2)-dicyclobutanacyclododecaphane-4^1,10^1-diene-4^3,4^4,10^3,10^4-tetraone

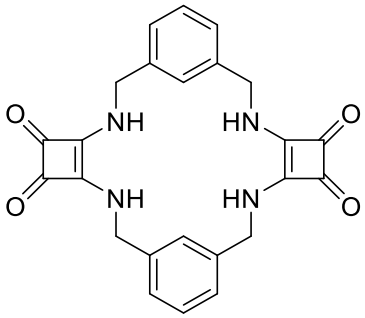

A solution of 1,3-phenylenedimethanamine (0.034 mL, 0.26 mmol, 1 eq) in EtOH (10 mL) was added dropwise into the solution of 4,4'-((1,3-phenylenebis(methylene))bis(azanediyl))bis(3-ethoxycyclobut-3-ene-1,2-dione) (0.1 g, 0.26 mmol, 1 eq) and triethylamine (0.181 mL, 1.3 mmol, 5 eq) in EtOH (150 mL) at the speed of 0.28mL/h using a syringe pump. The reaction was left to stir at 90 ℃ for 72 hours. The precipitate was collected by suction filtration and washed with EtOH and Et_2O to yield the product as a beige solid. (0.074 g, 67%), m.p.≥300 ℃. **^{1}H NMR** (500 MHz, DMSO-d_6) δ 8.51 (s, 1H, NH), 8.0 (s, 3H, 3 x NH), 7.25 (m, 8H, Ar), 4.83 (s, 8H, 4 x CH_2); **^{13}C NMR** (125 MHz, DMSO-d_6): Not found due to the presence of TBA^+ **HRMS** (ESI): Calculated for $C_{10}H_5O_2N_2Br$ $[M+H]^+$, expected: 429.1485, observed: 429.1600, PPM:9.98; **νmax (film)/cm^{-1}:** 3267 (N-H stretch, secondary amines), 1799, 1664 (C=O stretch, ketones), 1593, 1557, 1464, 1452, 1417, 1355, 1342, 1272, 1233, 1152, 1132, 1084, 998, 963, 880, 828, 786, 718, 690.

(101) (5-nitro-1,3-phenylene)dimethanol

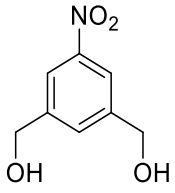

A solution of 5-nitroisophthalic acid (5 g, 23.68 mmol, 1 eq) in anhydrous THF (75 mL) was cooled to 0 ℃ in an ice bath before borane dimethyl sulfide complex (47.4 mL, 94.7 mmol, 4 eq) was added dropwise using glass syringe. The reaction mixture was left to return to room temperature and stirred for 48 hours. MeOH (75 mL) was added slowly into the reaction mixture to dissolve the precipitate. Solvent was removed under reduced

pressure to yield an oily crude product. The crude product was dissolved in Ethyl acetate (100 mL) and washed with saturated $NaHCO_3$ (150 mL) and Brine (150 mL) solution. Solvent was removed under reduced pressure to yield a beige solid. (1.762 g, 41%), m.p.: 85-90 °C. **^{1}H NMR** (500 MHz, DMSO-*d_6*) δ 8.06 (m, 2H, Ar), 7.72 (m, 1H, Ar), 5.3 (t, 2H, *J* = 6.7 Hz, 2 x OH), 4.63 (d, 4H, *J* = 5.7/0.6 Hz, 2 x CH_2); **^{13}C NMR** (125 MHz, DMSO-*d_6*):148.3, 145.3, 130.8, 119.4, 62.3. **HRMS** (ESI): Calculated for $C_8H_9O_4N$ $[M+Na]^+$, expected: 206.0424, observed: 206.0428, PPM:2.00; **νmax (film)/cm^{-1}:** 3186 (O-H stretch, alcohols), 3070, 2912, 1530 (N-O stretch, aromatic nitro), 1455, 1339 (N-O stretch, aromatic nitro), 1311, 1253, 1219, 1147, 1103 (C-O stretch, alcohols), 1062 (C-O stretch, alcohols), 1032, 1000, 985, 929, 908, 874, 772, 745, 676.

(102) 1,3-bis(bromomethyl)-5-nitrobenzene

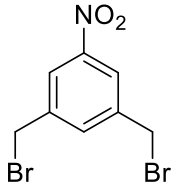

A solution of phosphorus tribromide (2.57 mL, 27.3 mmol, 2.5 eq) in DCM (10 mL) was added dropwise into the solution of (5-nitro-1,3-phenylene)dimethanol (1.6 g, 10.92 mmol, 1 eq) in DCM (20 ml) and stirred for 1 hour at 0 °C . The reaction was then left to stir at room temperature overnight. The reaction mixture was poured over crushed ice (100 g) and extracted by Et_2O (150 mL). The organic layer was washed with saturated $NaHCO_3$ (40 mL) and Brine (40 mL), solvent was removed under reduced pressure to yield an off-white solid. (3.71 g, 78%), m.p.: 95-100 °C. **^{1}H NMR** (500 MHz, DMSO-*d_6*) δ 8.3 (d, 2H, *J* = 1.6 Hz, Ar), 8.01 (t, 1H, *J* = 1.6 Hz, Ar), 4.87 (s, 4H, 2 x CH_2); **^{13}C NMR** (125 MHz, DMSO-*d_6*):148.4, 141.3, 136.8, 124.1, 32.4. **HRMS** (ESI): Not found; **νmax (film)/cm^{-1}:**3067, 3038, 2976, 2287, 1821, 1526 (N-O stretch, aromatic nitro), 1462, 1443, 1357 (N-O stretch, aromatic nitro), 1317, 1274, 1225, 1212, 1175, 1159, 1115, 1096, 1000, 973, 941, 898, 883, 858, 777, 746, 684.

(103) 2,2'-((5-nitro-1,3-phenylene)bis(methylene))bis(isoindoline-1,3-dione)

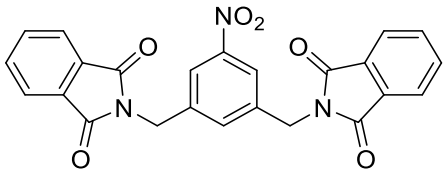

A solution of 1,3-bis(bromomethyl)-5-nitrobenzene (1 g, 3.2 mmol, 1 eq) in EtOH (40 mL) was slowly added into the solution of phthalimide potassium salt (1.3 g, 7.04 mmol, 2.2 eq) in EtOH (20 mL) at 78 ℃. The reaction was left to stir at 78 ℃ for 72 hours. The precipitate was collected by suction filtration and washed with EtOH and Et_2O to yield the product as a white solid. (1.37 g, 97%), m.p.> 300 ℃. **^{1}H NMR** (500 MHz, DMSO-*d_6*) δ 8.09 (d, 2H, *J* = 1.4 Hz, Ar), 7.89 (m, 8H, Ar), 7.74 (s, 1H, Ar), 4.9 (s, 4H, 2 x CH_2); **^{13}C NMR** (125 MHz, DMSO-*d_6*):168.1, 147.6, 139.7, 135.1, 133.3, 132.1, 123.8, 121.8. **HRMS** (ESI): Calculated for $C_{24}H_{15}N_3O_6$ $[M+Na]^+$, expected: 464.0832, observed: 464.0853, PPM: -4.5; **νmax (film)/cm^{-1}:** 3096, 1770, 1714 (C=O stretch, amides), 1612, 1543 (N-O stretch, aromatic nitro), 1469, 1417, 1394, 1368 (N-O stretch, aromatic nitro), 1338, 1327, 1192 (C-N stretch, tertiary amine), 1169, 1117, 1085, 1065, 962, 939, 924, 876, 825, 806, 781, 739, 723, 715, 693, 660.

(104) (5-nitro-1,3-phenylene)dimethanamine

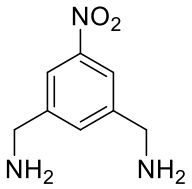

Hydrazine monohydrate (0.84 mL, 11.34 mmol, 5 eq) was added slowly into Asolution of 2,2'-((5-nitro-1,3-phenylene)bis(methylene))bis(isoindoline-1,3-dione) (1 g, 2.27 mmol, 1 eq) in EtOH (20 mL) at 78 ℃. The reaction was left to reflux at 78 ℃ overnight. The precipitate was removed using suction filtration, the solvent of filtrate was removed under reduced pressure to yield the crude product. The crude product was dissolved in water (20 mL) and the pH value of the solution was adjusted to 14 using 1M NaOH solution. The product was extracted by DCM (150 mL), solvent was removed under reduced pressure to yield a brown solid. (0.24 g, 58%), m.p.: Not found. **^{1}H NMR** (500 MHz, DMSO-*d_6*) δ 8.08 (s, 2H, Ar), 7.72 (s, 1H, Ar), 3.83 (s, 4H, 2 x CH_2); **^{13}C NMR**

(125 MHz, DMSO-d_6):148.4, 146.9, 132.9, 119.9, 45.3. **HRMS** (ESI): Not found; **νmax (film)/cm^{-1}:** Not found

(105) 4,4'-(((5-nitro-1,3-phenylene)bis(methylene))bis(azanediyl))bis(3-ethoxycyclobut-3-ene-1,2-dione)

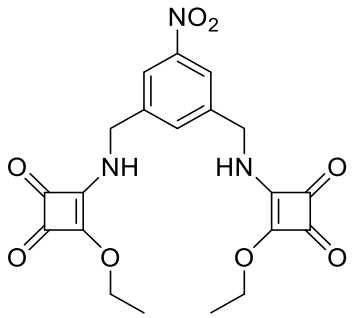

A solution of (5-nitro-1,3-phenylene)dimethanamine (0.1 g, 0.55 mmol, 1 eq) in EtOH (5 mL) was added dropwise into the solution of 3,4-diethoxycyclobut-3-ene-1,2-dione (0.28 g, 1.66 mmol, 3 eq) in EtOH (4 mL). Triethylamine (0.38 mL, 2.75 mmol, 5 eq) was then added into reaction mixture, the reaction was left to stir at room temperature for 2 hours. Solvent was evaporated to a small amount, the precipitate was filtered using suction filtration and washed with EtOH and Et_2O to yield the product as an orange solid. (0.15 g, 63%), m.p.: 205-210 ℃. **^{1}H NMR** (500 MHz, DMSO-d_6) δ 9.33 (s, 1H, NH), 9.13 (s, 1H, NH), 8.13 (s, 2H, Ar), 7.68 (s, 1H, Ar), 4.70 (m, 8H, 4 x CH_2), 1.35 (m, 6H, 2 x CH_3); **^{13}C NMR** (125 MHz, DMSO-d_6):189.8, 189.4, 183.1, 178.0, 177.5, 173.3, 172.5, 148.5, 141.6, 133.3, 121.9, 69.5, 46.9, 46.4, 19.0, 16.0. **HRMS** (ESI): Calculated for $C_{20}H_{19}N_3O_8$ $[M+Na]^+$, expected: 452.1064, observed: 452.1082, PPM: 3.9; **νmax (film)/cm^{-1}:** 3238 (N-H stretch, secondary amines), 1801, 1707 (C=O stretch, ketones), 1597, 1532 (N-O stretch, aromatic nitro), 1494, 1449, 1416, 1381, 1333 (N-O stretch, aromatic nitro), 1287 (C-O stretch, ethers), 1085, 1021, 987, 911, 863, 810, 777, 746, 699

(86) 15-nitro-3,5,9,11-tetraaza-1,7(1,3)-dibenzena-4,10(1,2)-dicyclobutanacyclododecaphane-41,101-diene-43,44,103,104-tetraone

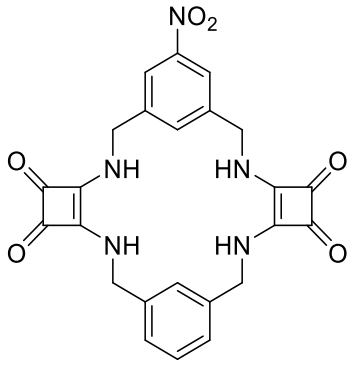

A solution of 1,3-phenylenedimethanamine (0.0097 mL, 0.07 mmol, 1 eq) in EtOH (5 mL) was added dropwise into the solution of 4,4'-(((5-nitro-1,3-phenylene)bis(methylene))bis(azanediyl))bis(3-ethoxycyclobut-3-ene-1,2-dione) (0.03 g, 0.07 mmol, 1 eq) and triethylamine (0.049 mL, 0.35 mmol, 5 eq) in EtOH (50 mL) at the speed of 0.24 mL/h using a syringe pump. The reaction was left to stir at 90 ℃ for 72 hours. The precipitate was collected by suction filtration and washed with EtOH and Et_2O to yield the product as a yellow solid. (0.029 g, 88%), m.p.: >300 ℃. **^{1}H NMR** (500 MHz, DMSO-d_6) δ 9.24 (s, 2H, 2 x NH), 9.18 (s, 2H, 2 x NH), 8.25 (s, 1H, Ar), 8.03 (s, 2H, Ar), 7.72 (s, 1H, Ar), 7.25 (t, 2H, J = 7.3Hz, Ar), 7.11 (d, 1H, J = 7.3Hz, Ar), 4.90 (s, 4H, 2 x CH_2), 4.78 (s, 4H, 2 x CH_2); 13C NMR (125 MHz, DMSO-d6): Not found due to the presence of TBA^+. **HRMS** (ESI): Calculated for $C_{24}H_{19}N_5O_6$ $[M+Na]^+$, expected: 496.1233, observed: 496.1219, PPM: -1.8; **νmax (film)/cm^{-1}:** 3161 (N-H stretch, secondary amines),2937, 1799, 1647 (C=O stretch, ketones), 1563, 1529 (N-O stretch, aromatic nitro), 1423, 1341 (N-O stretch, aromatic nitro), 1281, 1157, 1125, 1097, 959, 908, 883, 831, 775, 745, 689.

(87) 15,75-dinitro-3,5,9,11-tetraaza-1,7(1,3)-dibenzena-4,10(1,2)-dicyclobutana-cyclododecaphane-41,101-diene-43,44,103,104-tetraone

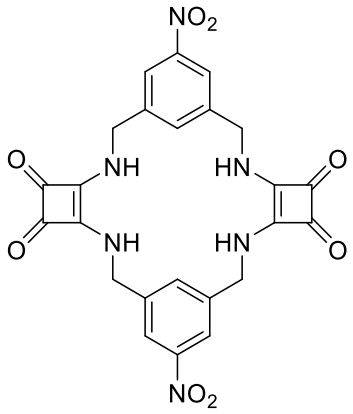

A solution of (5-nitro-1,3-phenylene)dimethanamine (0.042 mL, 0.233 mmol, 1 eq) in EtOH (10 mL) was added dropwise into the solution of 4,4'-(((5-nitro-1,3-phenylene)bis(methylene))bis(azanediyl))bis(3-ethoxycyclobut-3-ene-1,2-dione) (0.1 g, 0.233 mmol, 1 eq) and triethylamine (0.16 mL, 1.165 mmol, 5 eq) in EtOH (150 mL) at the speed of 2.28 mL/h using a syringe pump. The reaction was left to stir at 90 °C for 72 hours. The precipitate was collected by suction filtration and washed with EtOH and Et_2O to yield the product as a yellow solid. (0.086 g, 71%), m.p.: >300 °C. **^{1}H NMR** (500 MHz, DMSO-d_6) δ 9.74 (s, 4H, 4 x NH), 8.41 (s, 2H, Ar), 7.99 (s, 4H, Ar), 4.89 (s, 8H, 4 x CH_2); **^{13}C NMR** (125 MHz, DMSO-d_6): Not found due to the presence of TBA^+. **HRMS** (ESI): Calculated for $C_{24}H_{18}N_6O_8$ $[M+Na]^+$, expected: 541.1083, observed: 541.1081, PPM: 0.5; **νmax (film)/cm^{-1}:** 3156 (N-H stretch, secondary amines), 2938, 1800, 1650 (C=O stretch, ketones), 1564, 1527 (N-O stretch, aromatic nitro), 1428, 1340 (N-O stretch, aromatic nitro), 1286, 1237, 1161, 1126, 1105, 957, 905, 881, 776, 747, 689.

(106) 2,2'-((5-amino-1,3-phenylene)bis(methylene))bis(isoindoline-1,3-dione)

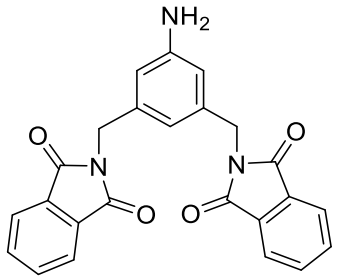

2,2'-((5-nitro-1,3-phenylene)bis(methylene))bis(isoindoline-1,3-dione) (0.1 g, 0.227 mmol, 1 eq) was dissolved in DMF (5 mL) with palladium on carbon (0.01 g). Hydrogen gas was added to the reaction mixture using air balloon. The reaction was left to stir at room temperature overnight. The catalyst was filtered off using suction filtration through a pad of celite. Solvent of filtrate was removed under reduced pressure to yield the product as a beige solid. (0.336 g, 72%), m.p.: 265-270 °C. **^{1}H NMR** (500 MHz, DMSO-d_6) δ 7.88 (m, 8H, Ar), 6.39 (s, 1H, Ar), 6.33 (s, 2H, Ar), 5.15 (s, 2H, 2 x NH), 4.59 (s, 4H, 2 x CH_2); **^{13}C NMR** (125 MHz, DMSO-d_6):168.1, 149.7, 138.0, 135.1, 132.0, 123.7, 113.7, 111.6, 41.3. **HRMS** (ESI): Calculated for $C_{24}H_{17}N_3O_4$ $[M+Na]^+$, expected: 434.1111, observed: 434.1124, PPM: 3.00; **νmax (film)/cm^{-1}:** 3436 (N-H stretch, primary amine), 3358, 1767, 1696 (C=O stretch, amides), 1604, 1466,1428,1393, 1351, 1333, 1272, 1189 (C-N stretch, tertiary amine), 1102, 1086, 1026, 1007, 946, 925, 863, 825, 800, 729, 711, 701.

(108) N-(3,5-bis((1,3-dioxoisoindolin-2-yl)methyl)phenyl)pyrene-1-carboxamide

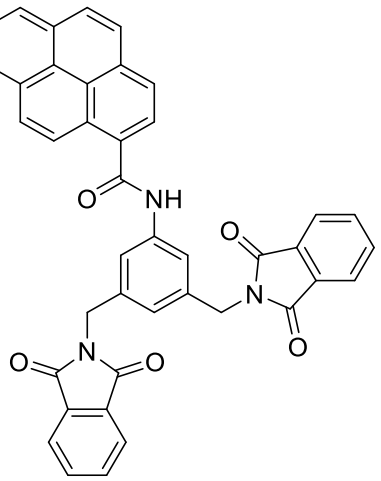

2,2'-((5-nitro-1,3-phenylene)bis(methylene))bis(isoindoline-1,3-dione) (0.05 g, 0.12 mmol, 1 eq) and 1-Pyrenecarboxylic acid (0.295 g, 0.12 mmol, 1 eq) was dissolved in DMF (3 mL) with 4-methylmorpholine (0.026 mL, 0.24 mmol, 2 eq) before PyBOP (0.936 g, 0.18 mmol, 1.5 eq) was added into the mixture. The reaction was left to stir at room temperature for 72 hours. The precipitate was filtered using suction filtrations and washed with small amount of toluene to yield the product as an off-white solid. (0.087 g, 19%), m.p.: > 300 °C. **^{1}H NMR** (500 MHz, DMSO-*d_6*) δ 10.7 (s, 1H, NH), 8.27 (m, 9H, Ar), 7.89 (m, 8H, Ar), 7.74 (s, 2H, Ar), 7.1 (s, 1H, Ar), 4.81 (s, 4H, 2 x CH_2); **^{13}C NMR** (125 MHz, DMSO-*d_6*):168.1, 138.2, 135.1, 132.0, 128.9, 127.7, 123.8, 117.5. **HRMS** (ESI): Calculated for $C_{41}H_{25}N_3O_5$ $[M+Na]^+$, expected: 662.1692, observed: 662.1686, PPM: 16.6; **νmax (film)/cm^{-1}:** 3353 (N-H stretch, amide), 1770, 1704 (C=O stretch, amides), 1661 (C=O stretch, amides), 1602, 1552, 1539, 1466, 1438, 1418, 1389, 1350, 1332, 1300, 1270, 1239, 1210, 1181, 1153, 1116, 1103, 1087, 1022, 1003, 952, 931, 909, 886, 865, 835, 815, 792, 751, 738, 727, 710, 699, 685.

(111) 1-bromo-3,5-bis(bromomethyl)benzene

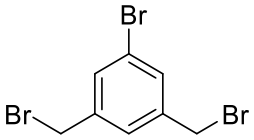

AIBN (6.75 mL, 1.35 mmol, 0.05 eq) was added dropwise into the dolution of 1-Bromo-3,5-dimethylbenzene (5 g, 27mmol, 1 eq) and N-bromosuccinimide (10.1 g, 56.7 mmol, 2.1 eq) in MeCN (30 mL). The reaction was left to reflux at 70 ℃ overnight. Solvent was removed under reduced pressure, CCl_4 (50 mL) was added dissolve the residue. The precipitate was filtered off and washed with CCl_4, the solvent of filtrate was removed under reduced pressure. The resulting residue was purified by column chromatography eluting with petroleum ether to yield the product a white crystal. (0.262 g, 5.4%), m.p.: 88-90 ℃. **^{1}H NMR** (500 MHz, $CDCl_3$) δ 7.47 (d, 2H, *J* = 1.6 Hz, Ar), 7.34 (t, 1H, *J* = 1.6 Hz, Ar), 4.41 (s, 4H, 2 x CH_2); **^{13}C NMR** (125 MHz, DMSO-*d*$_6$):140.3, 132.0, 128.3, 122.7. **HRMS** (ESI): Not found; **νmax (film)/cm^{-1}:** 2970, 1796, 1603, 1571, 1444, 1260, 1210, 1162, 1128, 1114, 1103, 1031, 998, 972, 823, 879, 864, 819, 690.

(112) 2,2'-((5-bromo-1,3-phenylene)bis(methylene))bis(isoindoline-1,3-dione)

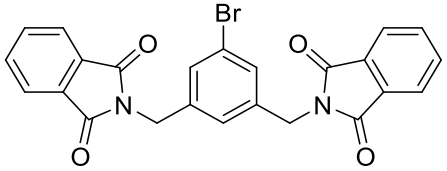

A solution of 1-bromo-3,5-bis(bromomethyl)benzene (0.3 g, 0.87 mmol, 1 eq) in EtOH (5 mL) was added dropwise into the solution of phthalimide potassium salt (0.41 g, 2.19 mmol, 2.5 eq) in EtOH (5 mL) at 78 ℃. The reaction was left to reflux under Ar at 78 ℃ for 48 hours. The precipitate was filtered using suction filtration and washed with EtOH and Et_2O to yield the product as a white solid. (0.38 g, 92%), m.p.: 255-260 ℃. **^{1}H NMR** (500 MHz, DMSO-*d*$_6$) δ 7.87 (m, 8H, Ar), 7.44 (s, 2H, Ar), 7.24 (s, 1H, Ar), 4.75 (s, 4H, 2 x CH_2); **^{13}C NMR** (125 MHz, DMSO-*d*$_6$):168.1, 140.1, 135.0, 132.0, 129.6, 125.7, 123.7, 122.3. **HRMS** (ESI): Calculated for $C_{24}H_{15}N_2O_4Br$ $[M+Na]^+$, expected: 497.0107,

observed: 497.0102, PPM: -1.1;; **νmax (film)/cm^{-1}:** 3460, 3055, 1768, 1703, 1607 (C=O stretch, amides), 1577, 1471, 1425, 1392, 1354, 1339, 1328, 1262, 1192 (C-N stretch, tertiary amine), 1174, 1111, 1101, 1089, 1072, 1033, 990, 955, 932, 897, 875, 861, 831, 811, 791, 724, 709, 694, 686.

(114) 2,2'-((5-(pyren-1-yl)-1,3-phenylene)bis(methylene))bis(isoindoline-1,3-dione)

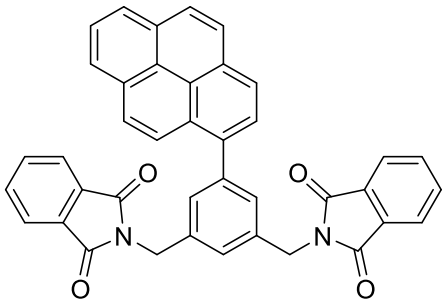

Tetrakis(triphenylphosphine)palladium(0) (0.024 g, 0.021 mmol, 0.05 eq) and sodium carbonate (0.067 g, 0.63 mmol, 1.5 eq) were added to A solution of 2,2'-((5-bromo-1,3-phenylene)bis(methylene))bis(isoindoline-1,3-dione) (0.2 g, 0.42 mmol, 1 eq) and pyrene-1-boronic acid (0.123 g, 0.5 mmol, 1.2 eq) in THF (25 mL)/water (6 mL) mixture. The reaction was left to reflux under N_2 at 80 ℃ overnight. The precipitate was filtered off, the filtrate was extracted with DCM (50 mL) and washed with Brine. Solvent was removed under reduced pressure and the resulting residue was purified using column chromatography eluting with MeOH/DCM (0% to 3%) to yield the product as a brown solid. (0.02 g, 8%), m.p.: Not found. **^{1}H NMR** (500 MHz, DMSO-d_6) δ 8.09 (m, 9H, Ar), 7.86 (m, 8H, Ar), 7.5 (s, 2H, Ar), 7.38 (s, 1H, Ar), 4.92 (s, 4H, 2 x CH_2); **^{13}C NMR** (125 MHz, DMSO-d_6): Not found. **HRMS** (ESI): Not found; **νmax (film)/cm^{-1}:** Not found. Due to the low yield of this compound, fully characterization was not possible.

Chapter 6 References

1. Tang X, Zhu Z, Liu R, Ni L, Qiu Y, Han J, et al. A novel OFF-ON-OFF fluorescence probe based on coumarin for Al3+ and F− detection and bioimaging in living cells. *Spectrochim. Acta. A. Mol. Biomol. Spectrosc.* 2019;211:299-305.

2. Gerlach RF, De Souza AP, Cury JA, Line SRP. Fluoride effect on the activity of enamel matrix proteinases in vitro. *Eur. J. Oral. Sci*. 2000;108(1):48-53.

3. Kumar M, Kumar R, Bhalla V. Thiacalix[4]arene based reconfigurable molecular switches: set-reset memorized sequential device. *Org. Biomol. Chem.* 2011;9(24):8237-45.

4. Osanai T, Fujiwara N, Saitoh M, Sasaki S, Tomita H, Nakamura M, et al. Relationship between Salt Intake, Nitric Oxide and Asymmetric Dimethylarginine and Its Relevance to Patients with End-Stage Renal Disease. *Blood. Purif.* 2002;20(5):466-8.

5. Shao J, Qiao Y-H, Lin H, Lin H-K. A novel switch-on fluorescent receptor for bromide based on an amide group. *J. Incl. Phenom. Macrocycl. Chem*. 2008;62(1):99.

6. Kaur N, Kaur G, Fegade UA, Singh A, Sahoo SK, Kuwar AS, et al. Anion sensing with chemosensors having multiple NH recognition units. *Trends. Analyt. Chem*. 2017;95:86-109.

7. Yang L, Li X, Yang J, Qu Y, Hua J. Colorimetric and Ratiometric Near-Infrared Fluorescent Cyanide Chemodosimeter Based on Phenazine Derivatives. *ACS Appl. Mater. Interfaces*. 2013;5(4):1317-26.

8. Shriver DF, Biallas MJ. Observation of the Chelate Effect with a Bidentate Lewis Acid, F2BCH2CH2BF2. *J. Am. Chem. Soc*. 1967;89(5):1078-81.

9. Park CH, Simmons HE. Macrobicyclic amines. III. Encapsulation of halide ions by in,in-1,(k + 2)-diazabicyclo[k.l.m.]alkane ammonium ions. *J. Am. Chem. Soc*. 1968;90(9):2431-2.

10. Graf E, Lehn JM. Cryptates. XVII. Synthesis and cryptate complexes of a spheroidal macrotricyclic ligand with octahedrotetrahedral coordination. *J. Am. Chem. Soc*. 1975;97(17):5022-4.

11. Gale PA. Anion receptor chemistry. *Chem. Commun*. 2011;47(1):82-6.

12. Busschaert N, Caltagirone C, Van Rossom W, Gale PA. Applications of Supramolecular Anion Recognition. *Chem. Rev*. 2015;115(15):8038-155.

13. Prodi L. Luminescent chemosensors: from molecules to nanoparticles. *New. J. Chem*. 2005;29(1):20-31.

14. Moragues ME, Martínez-Máñez R, Sancenón F. Chromogenic and fluorogenic chemosensors and reagents for anions. A comprehensive review of the year 2009. *Chem. Soc. Rev*. 2011;40(5):2593-643.

15. Beer PD, Gale PA. Anion Recognition and Sensing: The State of the Art and Future Perspectives. *Angew. Chem. Int. Ed*. 2001;40(3):486-516.

16. Gale PA, Busschaert N, Haynes CJE, Karagiannidis LE, Kirby IL. Anion receptor chemistry: highlights from 2011 and 2012. *Chem. Soc. Rev*. 2014;43(1):205-41.

17. Grabowski SJ. What Is the Covalency of Hydrogen Bonding? *Chem. Rev*. 2011;111(4):2597-625.

18. Tomàs S, Prohens R, Vega M, Rotger MC, Deyà PM, Ballester P, et al. Squaramido-Based Receptors: Design, Synthesis, and Application to the Recognition of Tetraalkylammonium Compounds. *J. Org. Chem*. 1996;61(26):9394-401.

19. Tomàs S, Rotger MC, González J, Deyà PM, Ballester P, Costa A. Squaramide-based receptors: Synthesis and application to the recognition of polyalkyl ammonium salts. *Tetrahedron. Lett*. 1995;36(14):2523-6.

20. Gavette JV, Mills NS, Zakharov LN, Johnson II CA, Johnson DW, Haley MM. An Anion-Modulated Three-Way Supramolecular Switch that Selectively Binds Dihydrogen Phosphate, $H_2PO_4^-$. *Angew. Chem. Int. Ed*. 2013;52(39):10270-4.

21. Li Y, Yang G-H, Shen Y-Y, Xue X-S, Li X, Cheng J-P. N-tert-Butyl Sulfinyl Squaramide Receptors for Anion Recognition through Assisted tert-Butyl C–H Hydrogen Bonding. *J. Org. Chem*. 2017;82(16):8662-7.

22. Bondy CR, Loeb SJ. Amide based receptors for anions. *Coord. Chem. Rev*. 2003;240(1):77-99.

23. Deetz MJ, Shang M, Smith BD. A Macrobicyclic Receptor with Versatile Recognition Properties: Simultaneous Binding of an Ion Pair and Selective Complexation of Dimethylsulfoxide. *J. Am. Chem. Soc*. 2000;122(26):6201-7.

24. Mahoney JM, Beatty AM, Smith BD. Selective Recognition of an Alkali Halide Contact Ion-Pair. *J. Am. Chem. Soc*. 2001;123(24):5847-8.

25. Piątek P, Jurczak J. A selective colorimetric anion sensor based on an amide group containing macrocycle. *Chem. Commun*. 2002;(20):2450-1.

26. Jana S, Whiting AL, Hazra A, Sen S, Goswami S, Mehta G, et al. Anion recognition by a family of quinoline-functionalised bis-amide hosts in solid state and in solution. *Supramol. Chem*. 2012;24(6):385-91.

27. Fegade U, Sharma H, Tayade K, Attarde S, Singh N, Kuwar A. An amide based dipodal Zn2+ complex: nano-molar detection of HSO4− in a semi-aqueous system. *Org. Biomol. Chem*. 2013;11(39):6824-8.

28. Saha I, Lee JT, Lee C-H. Recent Advancements in Calix[4]pyrrole-Based Anion-Receptor Chemistry. *Eur. J. Org. Chem*. 2015;2015(18):3859-85.

29. Gale PA, Sessler JL, Král V, Lynch V. Calix[4]pyrroles: Old Yet New Anion-Binding Agents. *J. Am. Chem. Soc*. 1996;118(21):5140-1.

30. Velmathi S, Reena V, Suganya S, Anandan SJJoF. Pyrrole Based Schiff Bases as Colorimetric and Fluorescent Chemosensors for Fluoride and Hydroxide Anions. *J. Fluoresc*. 2012;22(1):155-62.

31. Pushina M, Koutnik P, Nishiyabu R, Minami T, Savechenkov P, Anzenbacher Jr. P. Anion Sensing by Fluorescent Expanded Calixpyrroles. *Chem. Eur. J*. 2018;24(19):4879-84.

32. Taner B, Alici O, Deveci P. Synthesis of a new colorimetric receptor based on calix[4]pyrrole binding oxime for selective recognition of fluoride ions. *Supramol. Chem*. 2014;26(2):119-24.

33. Taner B, Kursunlu AN, Güler E. The example of calix[4]pyrrole derivative containing Bodipy unit: Fluorometric and colorimetric sensor for F− ion. *Spectrochim. Acta. A. Mol. Biomol. Spectrosc*. 2014;118:903-7.

34. Amendola V, Bonizzoni M, Esteban-Gómez D, Fabbrizzi L, Licchelli M, Sancenón F, et al. Some guidelines for the design of anion receptors. *Coord. Chem. Rev*. 2006;250(11):1451-70.

35. Steed JW. Anion-tuned supramolecular gels: a natural evolution from urea supramolecular chemistry. *Chem. Soc. Rev*. 2010;39(10):3686-99.

36. Blažek Bregović V, Basarić N, Mlinarić-Majerski K. Anion binding with urea and thiourea derivatives. *Coord. Chem. Rev*. 2015;295:80-124.

37. Gómez DE, Fabbrizzi L, Licchelli M, Monzani E. Urea vs. thiourea in anion recognition. *Org. Biomol. Chem*. 2005;3(8):1495-500.

38. Boiocchi M, Del Boca L, Gómez DE, Fabbrizzi L, Licchelli M, Monzani E. Nature of Urea−Fluoride Interaction: Incipient and Definitive Proton Transfer. *J. Am. Chem. Soc*. 2004;126(50):16507-14.

39. Matsumoto H, Nishimura Y, Arai T. Fluorescence Sensor with A New ON1–OFF–ON2 Switching Mechanism Using the Excited State Intermolecular Proton Transfer Reaction of An Anthracene-diurea Compound. *Photochem. Photobiol*. 2017;93(5):1187-92.

40. Noroozi-Shad N, Gholizadeh M, Izadyar M. Sensing Activity of a New Generation of Thiourea-based Receptors; A Theoretical Study on the Anion Sensing. *Phys. Chem. Res*. 2016;4(3):427-40.

41. Singh N, Billing BK, Singh J, Agnihotri PK. Thiourea Based Dipodal Receptor Development for Electrochemical Detection of Br^- Ion in an Aqueous Medium. *Electroanal*. 2016;28(4):718-23.

42. Long BM, Pfeffer FM. Norbornene-based anion receptors as D-alanine binders. *Supramol. Chem*. 2015;27(11-12):847-53.

43. Robson RN, Hay BP, Pfeffer FM. Flexible “Arms” and Anion Recognition. *ChemistrySelect*. 2017;2(17):4605-8.

44. Rostami A, Colin A, Li XY, Chudzinski MG, Lough AJ, Taylor MS. N,N′-Diarylsquaramides: General, High-Yielding Synthesis and Applications in Colorimetric Anion Sensing. *J. Org. Chem*. 2010;75(12):3983-92.

45. P. Davis A, M. Draper S, Dunne G, Ashton P. The N-carbamoyl squaramide dimer: a compact, strongly associated H-bonding motif. *Chem. Commun*. 1999;(22):2265-6.

46. Li P, Hu X, Dong X-Q, Zhang X. Recent Advances in Dynamic Kinetic Resolution by Chiral Bifunctional (Thio)urea- and Squaramide-Based Organocatalysts. *Molecules*. 2016;21(10):1327.

47. Quiñonero D, Frontera A, Ballester P, Deyà PM. A theoretical study of aromaticity in squaramide and oxocarbons. *Tetrahedron. Lett*. 2000;41(12):2001-5.

48. Victorio ST, Pablo E, T. TT, M. NWE, K. VI, E. KR. Aromatic Gain in a Supramolecular Polymer. *Angew. Chem. Int. Ed*. 2015;54(36):10502-6.

49. Prohens R, Portell A, Font-Bardia M, Bauzá A, Frontera A. Experimental and Theoretical Study of Aromaticity Effects in the Solid State Architecture on Squaric Acid Derivatives. *Cryst. Growth. Des*. 2014;14(5):2578-87.

50. Prohens R, Tomàs S, Morey J, Deyà PM, Ballester P, Costa A. Squaramido-based receptors: Molecular recognition of carboxylate anions in highly competitive media. *Tetrahedron. Lett*. 1998;39(9):1063-6.

51. Neus Piña M, Carmen Rotger M, Costa A, Ballester P, Deyà PM. Evaluation of anion selectivity in protic media by squaramide–Cresol Red ensembles. *Tetrahedron. Lett*. 2004;45(19):3749-52.

52. Amendola V, Bergamaschi G, Boiocchi M, Fabbrizzi L, Milani M. The Squaramide versus Urea Contest for Anion Recognition. *Chem. Eur. J.* 2010;16(14):4368-80.

53. Załubiniak D, Zakrzewski M, Piątek P. Highly effective ion-pair receptors based on 2,2-bis(aminomethyl)-propionic acid. *Dalton. Trans*. 2016;45(39):15557-64.

54. Zdanowski S, Piątek P, Romański J. An ion pair receptor facilitating the extraction of chloride salt from the aqueous to the organic phase. *New. J. Chem*. 2016;40(8):7190-6.

55. Elmes RBP, Jolliffe KA. Amino acid-based squaramides for anion recognition. *Supramol. Chem*. 2015;27(5-6):321-8.

56. Elmes RBP, K. Y. Yuen K, Jolliffe KA. Sulfate-Selective Recognition by Using Neutral Dipeptide Anion Receptors in Aqueous Solution. *Chem. Eur. J.* 2014;20(24):7373-80.

57. Qin L, Hartley A, Turner P, Elmes RBP, Jolliffe KA. Macrocyclic squaramides: anion receptors with high sulfate binding affinity and selectivity in aqueous media. *Chem. Sci*. 2016;7(7):4563-72.

58. Elmes RBP, Turner P, Jolliffe KA. Colorimetric and Luminescent Sensors for Chloride: Hydrogen Bonding vs Deprotonation. *Org. Lett*. 2013;15(22):5638-41.

59. Quiñonero D, Frontera A, Suñer GA, Morey J, Costa A, Ballester P, et al. Squaramide as a binding unit in molecular recognition. *Chem. Phys. Lett*. 2000;326(3):247-54.

60. Jin C, Zhang M, Wu L, Guan Y, Pan Y, Jiang J, et al. Squaramide-based tripodal receptors for selective recognition of sulfate anion. *Chem. Commun*. 2013;49(20):2025-7.

61. Prohens R, Martorell G, Ballester P, Costa A. A squaramide fluorescent ensemble for monitoring sulfate in water. *Chem. Commun*. 2001;(16):1456-7.

62. Soberats B, Martínez L, Sanna E, Sampedro A, Rotger C, Costa A. Janus-Like Squaramide-Based Hosts: Dual Mode of Binding and Conformational Transitions Driven by Ion-Pair Recognition. *Chem. Eur. J*. 2012;18(24):7533-42.

63. P. Davis A, M. Draper S, Dunne G, Ashton P. The N-carbamoyl squaramide dimer: a compact, strongly associated H-bonding motif. *Chem. Commun*. 1999;(22): 2265-2266.

64. Elmes RBP, Jolliffe KA. Amino acid-based squaramides for anion recognition. *Supramol. Chem*. 2014;27(5-6):321-8.

65. Elmes RBP, Busschaert N, Czech DD, Gale PA, Jolliffe KA. pH switchable anion transport by an oxothiosquaramide. *Chem Commun*. 2015;51(50):10107-10.

66. Elmes RBP, K. Y. Yuen K, Jolliffe KA. Sulfate-Selective Recognition by Using Neutral Dipeptide Anion Receptors in Aqueous Solution. *Chem. Eur. J*. 2014;20(24):7373-80.

67. Busschaert N, Elmes RBP, Czech DD, Wu X, Kirby IL, Peck EM, et al. Thiosquaramides: pH switchable anion transporters. *Chem Sci*. 2014;5(9):3617-26.

68. Cai X-J, Li Z, Chen W-H. Tripodal squaramide conjugates as highly effective transmembrane anion transporters. *Bioorg. Med. Chem. Lett*. 2017;27(9):1999-2002.

69. Edwards SJ, Valkenier H, Busschaert N, Gale PA, Davis AP. High-Affinity Anion Binding by Steroidal Squaramide Receptors. *Angew. Chem. Int. Ed*. 2015;54(15):4592-6.

70. Jacquemin D, Perpète EA, Scuseria GE, Ciofini I, Adamo C. TD-DFT Performance for the Visible Absorption Spectra of Organic Dyes: Conventional versus Long-Range Hybrids. *J. Chem. Theory. Comput*. 2008;4(1):123-35.

71. Thordarson P. Determining association constants from titration experiments in supramolecular chemistry. *Chem. Soc. Rev*. 2011;40(3):1305-23.

72. Supramolecular.org.

73. Niu H, Shu Q, Jin S, Li B, Zhu J, Li L, et al. A simple ratiometric and colorimetric chemosensor for the selective detection of fluoride in DMSO buffered solution. *Spectrochim. Acta. A. Mol. Biomol. Spectrosc*. 2016;153:194-8.

74. Elmes RBP, Gunnlaugsson T. Luminescence anion sensing via modulation of MLCT emission from a naphthalimide-Ru(II)-polypyridyl complex. *Tetrahedron. Lett*. 2010;51(31):4082-7.

75. Pushina M, Koutnik P, Nishiyabu R, Minami T, Savechenkov P, Anzenbacher Jr. P. Anion Sensing by Fluorescent Expanded Calixpyrroles. *Chem. Eur. J*. 2018;24(19):4879-84.

76. Sessler JL, Gross DE, Cho W-S, Lynch VM, Schmidtchen FP, Bates GW, et al. Calix[4]pyrrole as a Chloride Anion Receptor: Solvent and Countercation Effects. *J. Am. Chem. Soc*. 2006;128(37):12281-8.

77. A. Gale P, L. Sessler J, Král V. Calixpyrroles. *Chem. Commun*. 1998;(1):1-8.

78. Shrestha D, Jenei A, Nagy P, Vereb G, Szöllősi J. Understanding FRET as a Research Tool for Cellular Studies. *Int. J. Mol. Sci.* 2015;16(4):6718-56.

79. Yokokawa F, Nilar S, Noble CG, Lim SP, Rao R, Tania S, et al. Discovery of Potent Non-Nucleoside Inhibitors of Dengue Viral RNA-Dependent RNA Polymerase from a Fragment Hit Using Structure-Based Drug Design. *J. Med. Chem*. 2016;59(8):3935-52.

80. Leung ACS, Zhao E, Kwok RTK, Lam JWY, Leung CWT, Deng H, et al. An AIE-based bioprobe for differentiating the early and late stages of apoptosis mediated by H_2O_2. *J. Mater. Chem. B*. 2016;4(33):5510-4.

81. BindFit. Available from: http://app.supramolecular.org/bindfit/.

82. Brynn Hibbert D, Thordarson P. The death of the Job plot, transparency, open science and online tools, uncertainty estimation methods and other developments in supramolecular chemistry data analysis. *Chem. Commun*. 2016;52(87):12792-12805

Appendix

Appendix 2

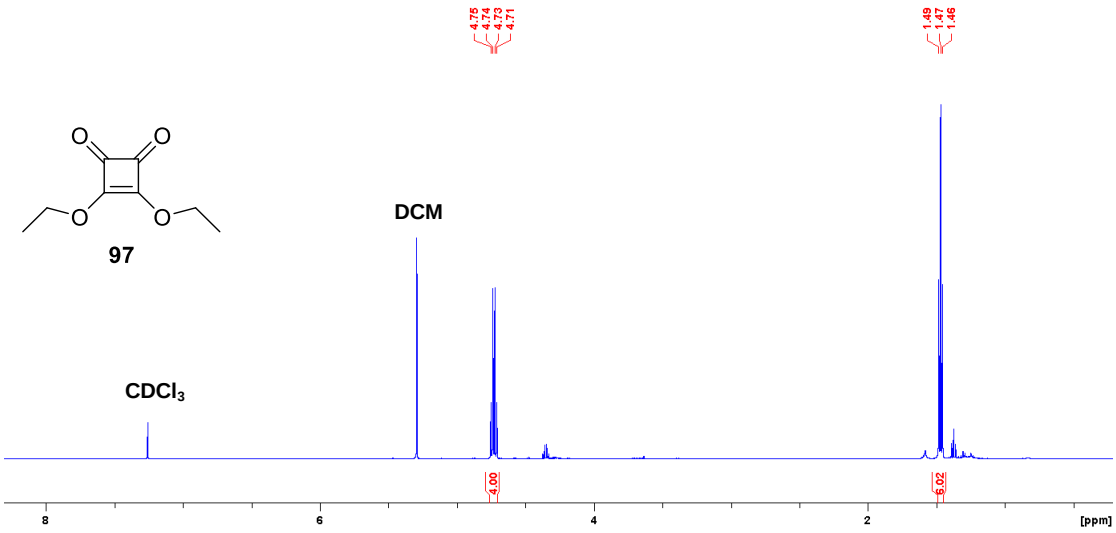

Figure A2.1: The ^{1}H NMR spectrum of compound **97** (500.13 MHz, $CDCl_3$).

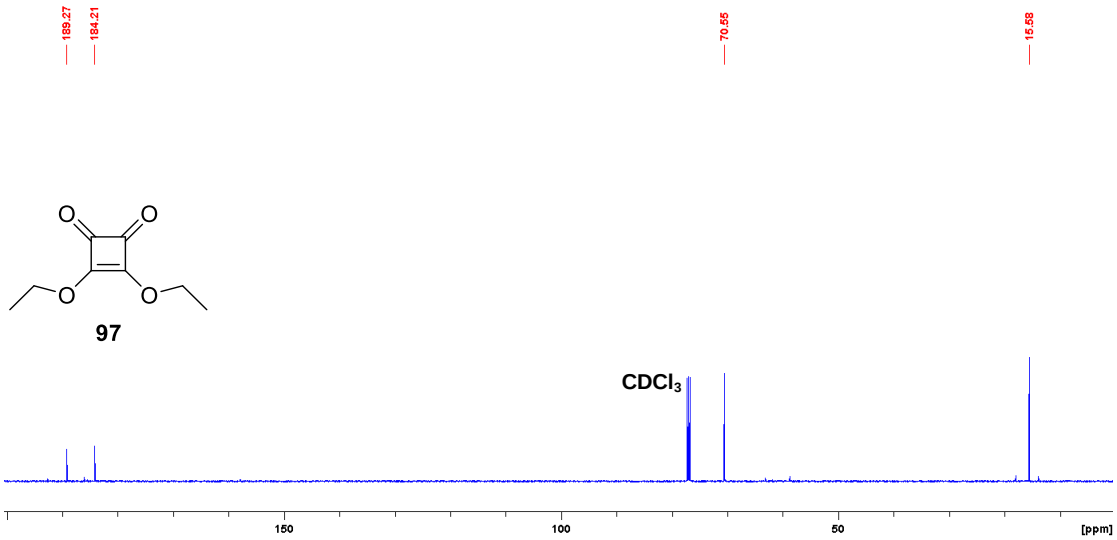

Figure A2.2: The ^{13}C NMR spectrum of compound **97** (500.13 MHz, $CDCl_3$).

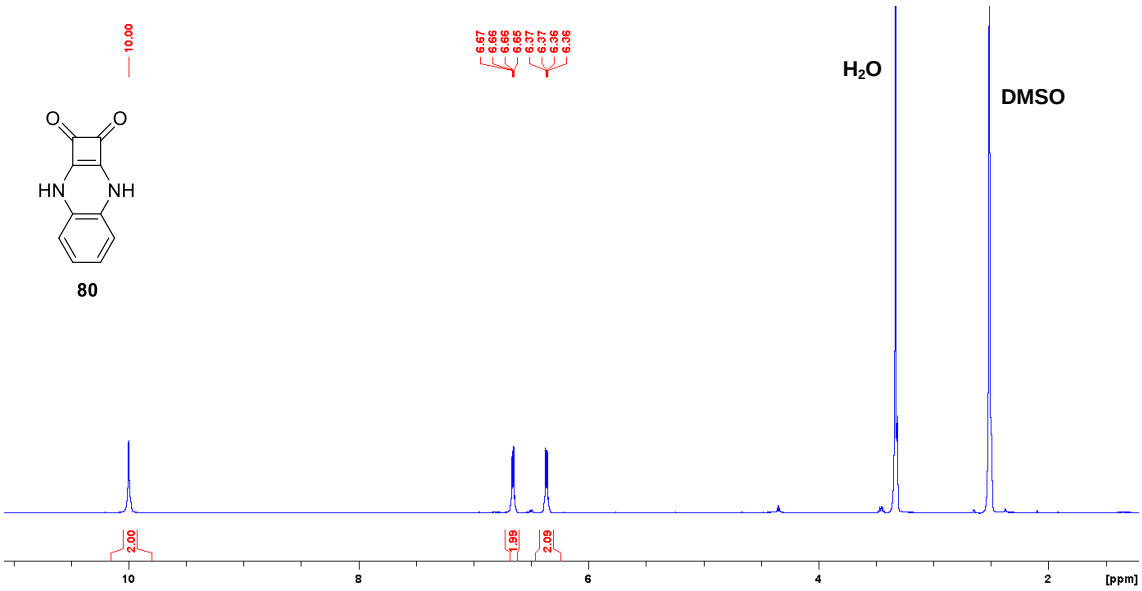

Figure A2.3: The ^{1}H NMR spectrum of compound **80** (500.13 MHz, DMSO-d_6).

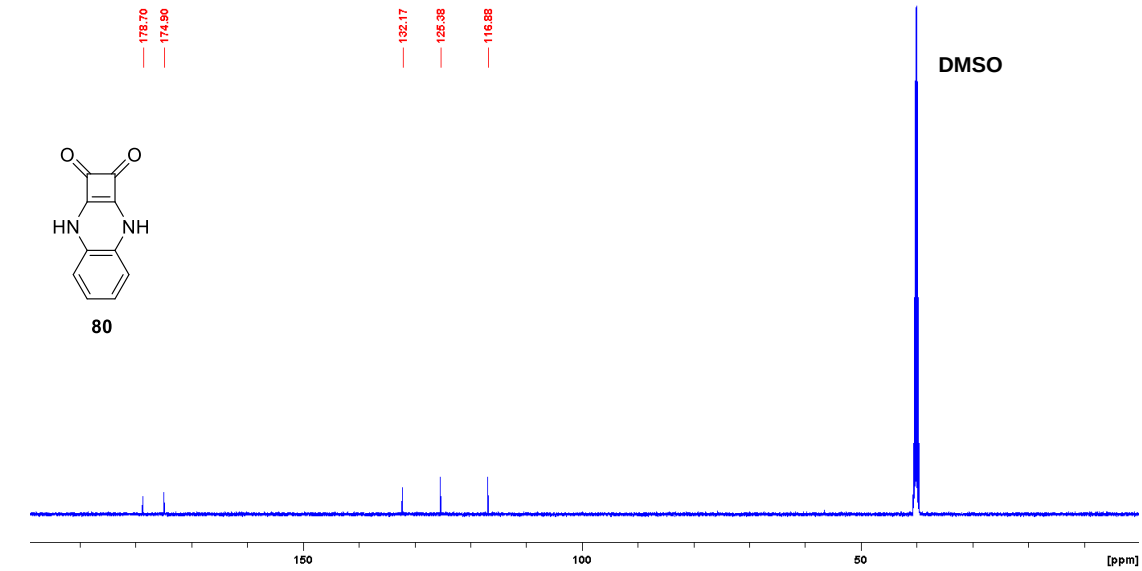

Figure A2.4: The ^{13}C NMR spectrum of compound **80** (500.13 MHz, DMSO-d_6).

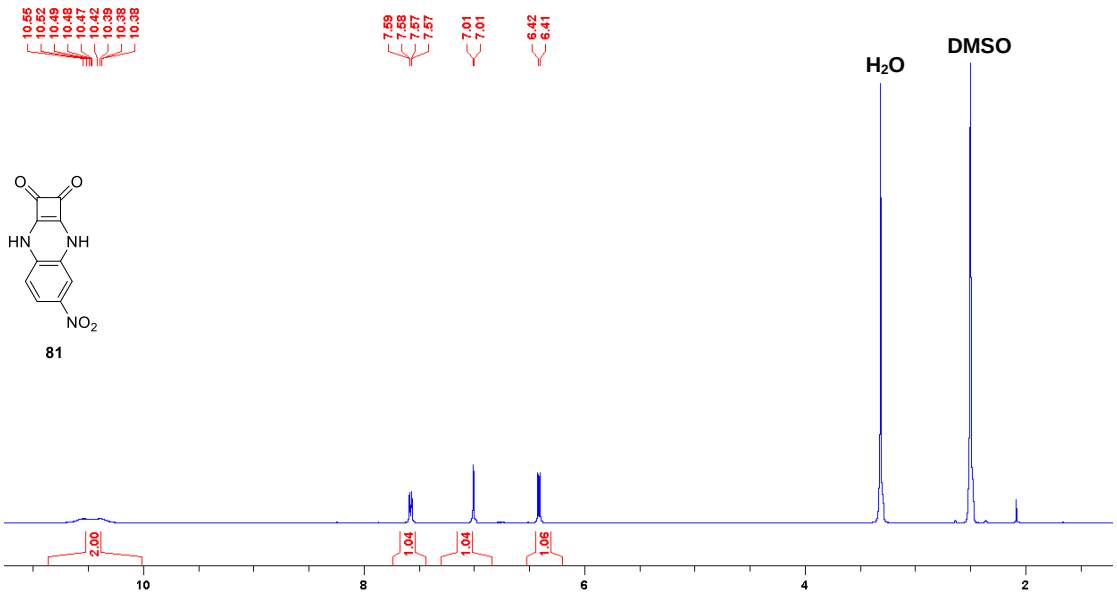

Figure A2.5: The ^{1}H NMR spectrum of compound **81** (500.13 MHz, DMSO-d_6).

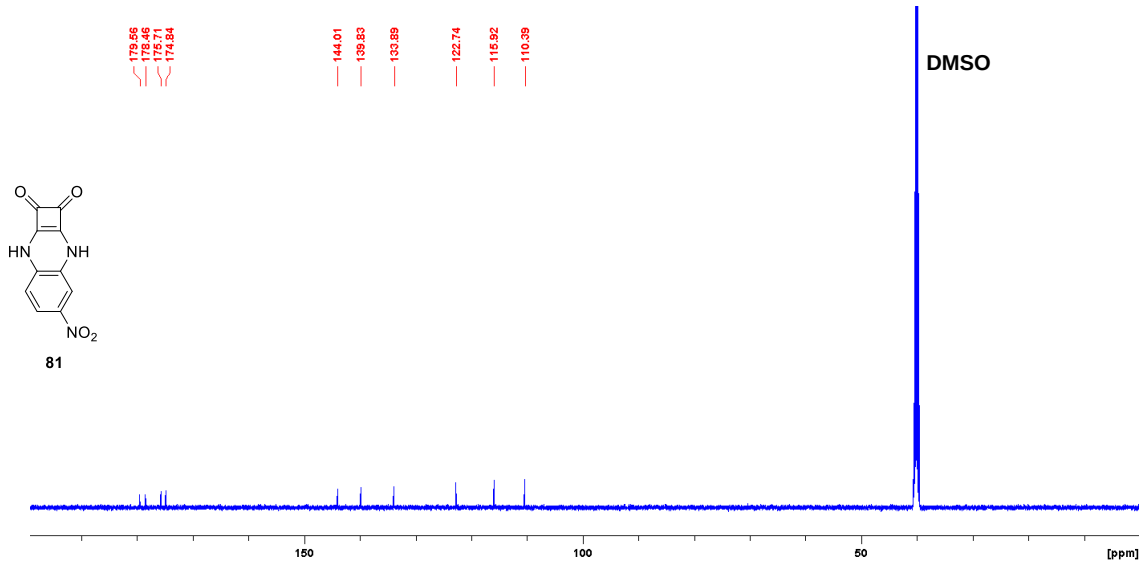

Figure A2.6: The ^{13}C NMR spectrum of compound **81** (500.13 MHz, DMSO-d_6).

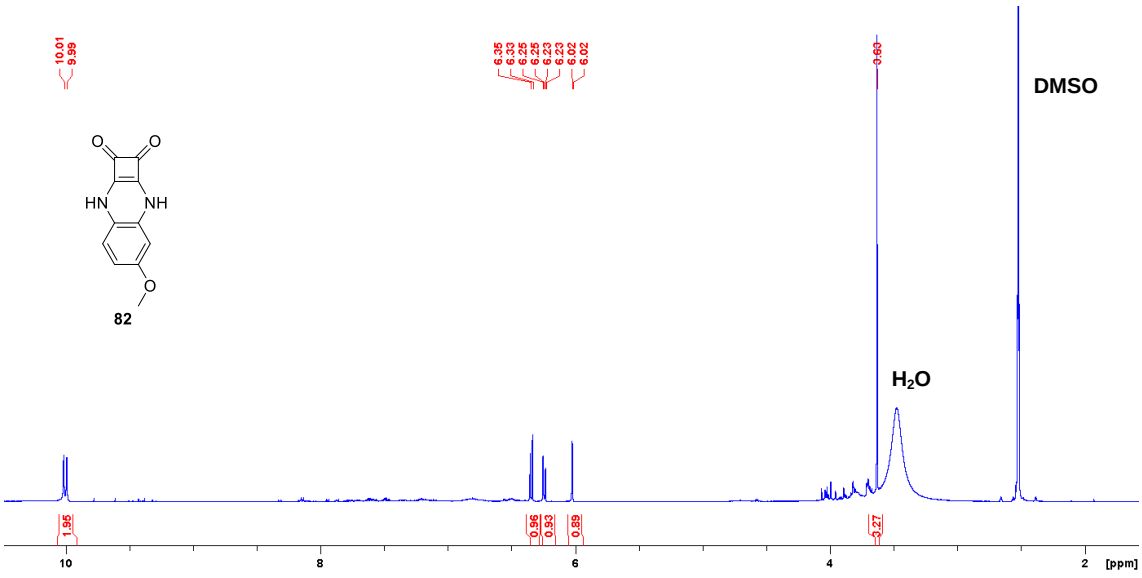

Figure A2.7: The ^{1}H NMR spectrum of compound **82** (500.13 MHz, DMSO-d_6).

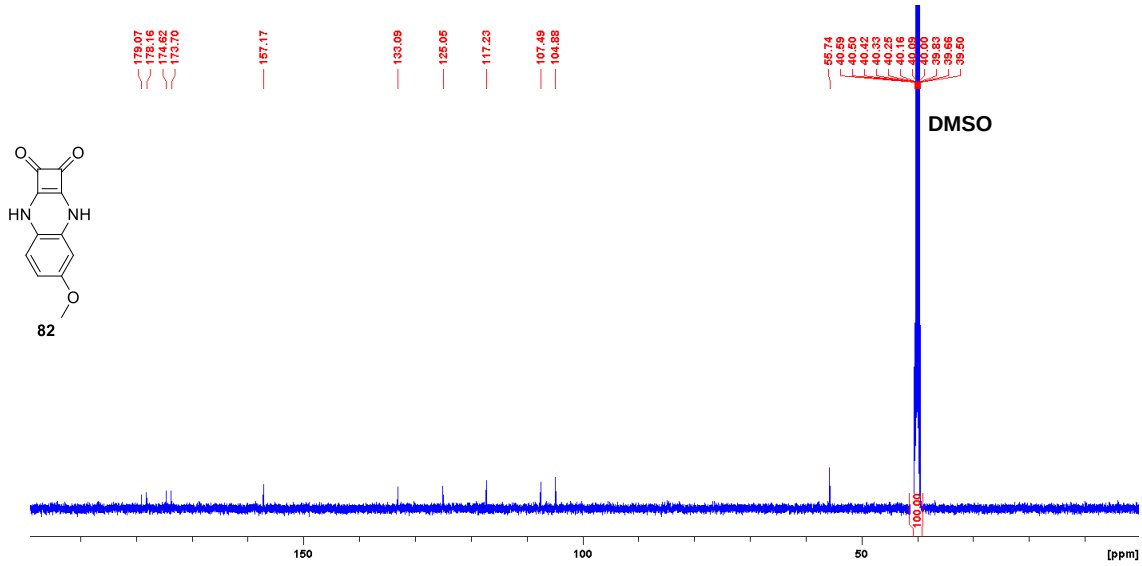

Figure A2.8: The ^{13}C NMR spectrum of compound **82** (500.13 MHz, DMSO-d_6).

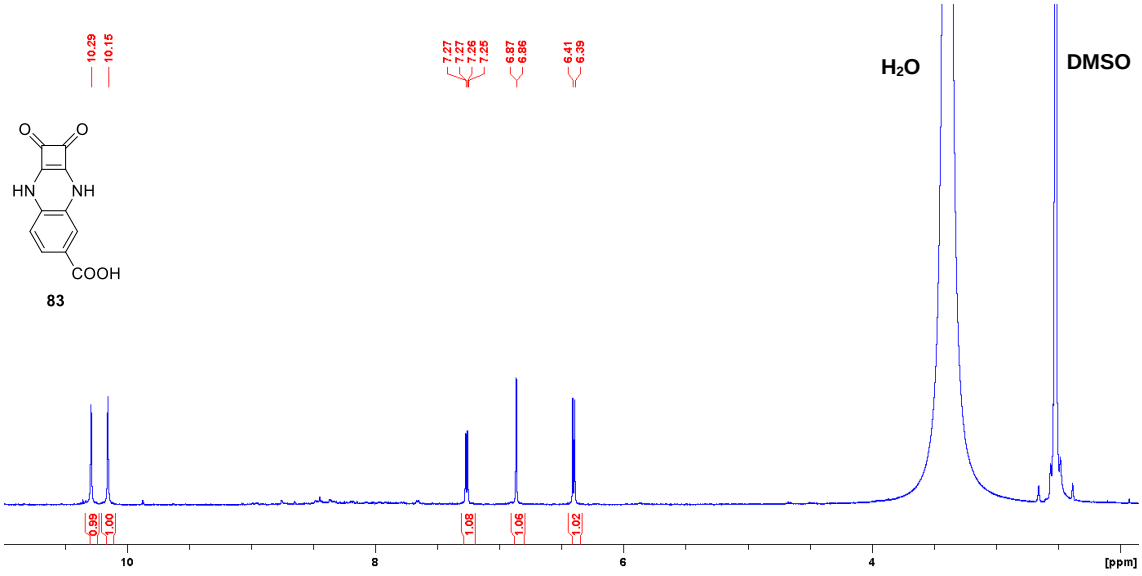

Figure A2.9: The ^{1}H NMR spectrum of compound **83** (500.13 MHz, DMSO-d_6).

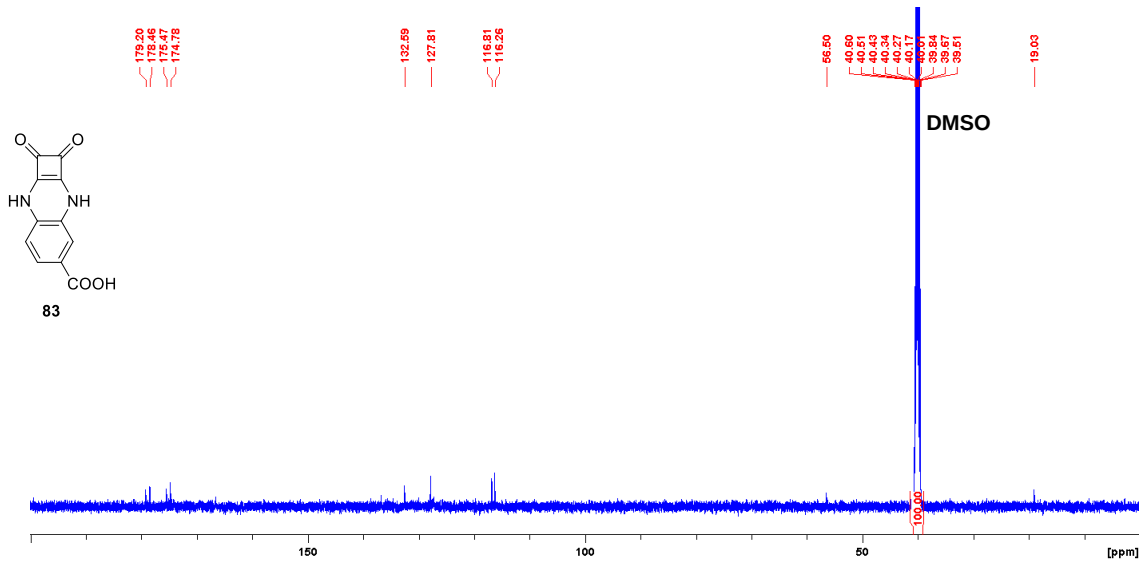

Figure A2.10: The ^{13}C NMR spectrum of compound **83** (500.13 MHz, DMSO-d_6).

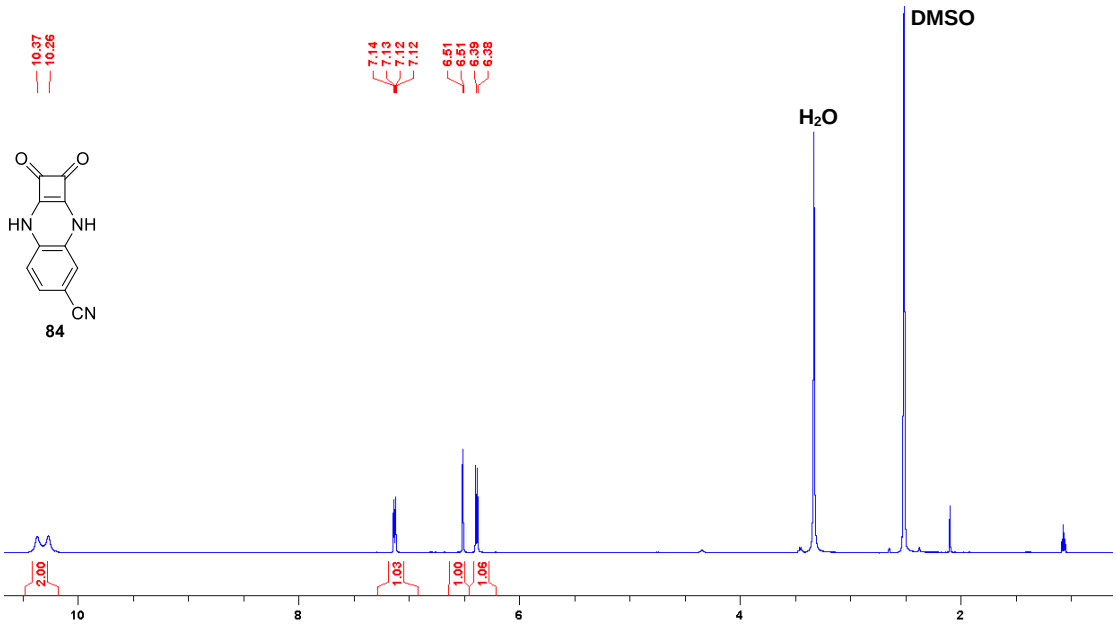

Figure A2.11: The ^{1}H NMR spectrum of compound **84** (500.13 MHz, DMSO-d_6).

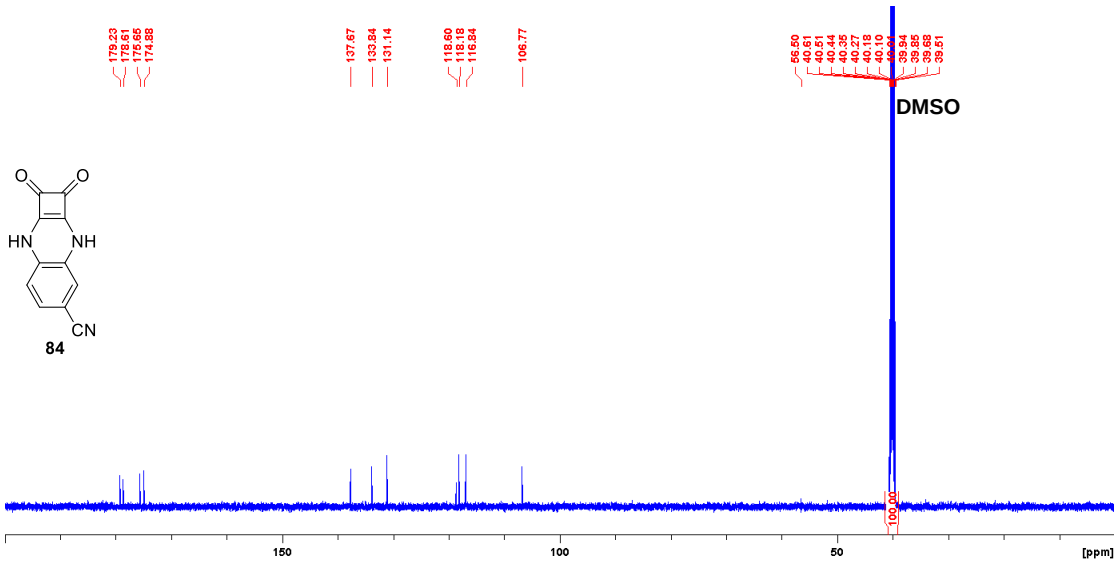

Figure A2.12: The ^{13}C NMR spectrum of compound **84** (500.13 MHz, DMSO-d_6).

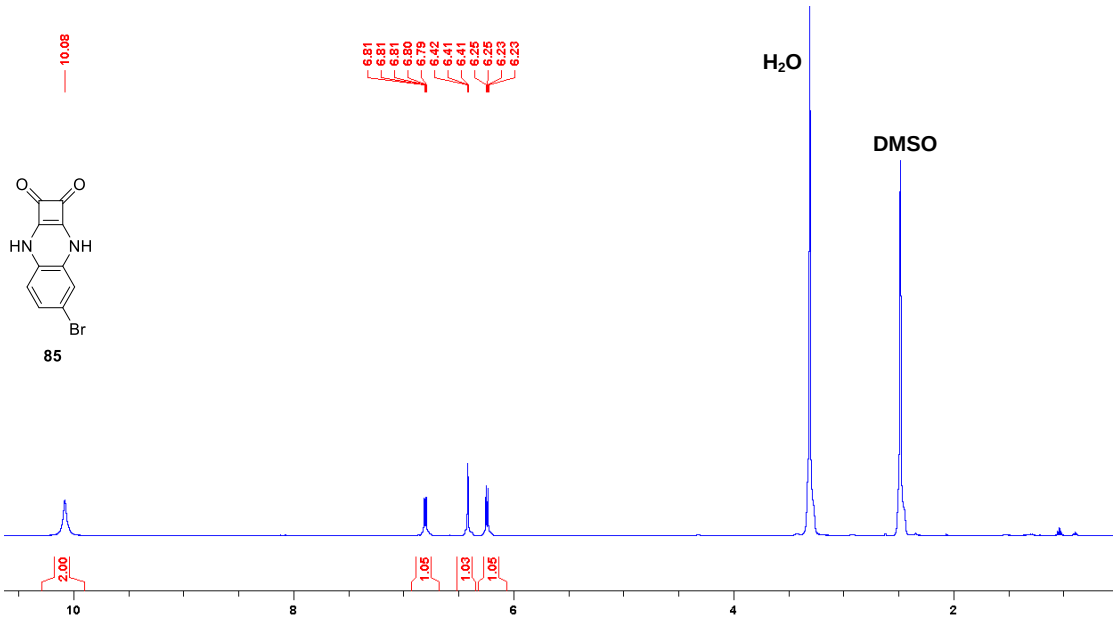

Figure A2.13: The ^{1}H NMR spectrum of compound **85** (500.13 MHz, DMSO-d_6).

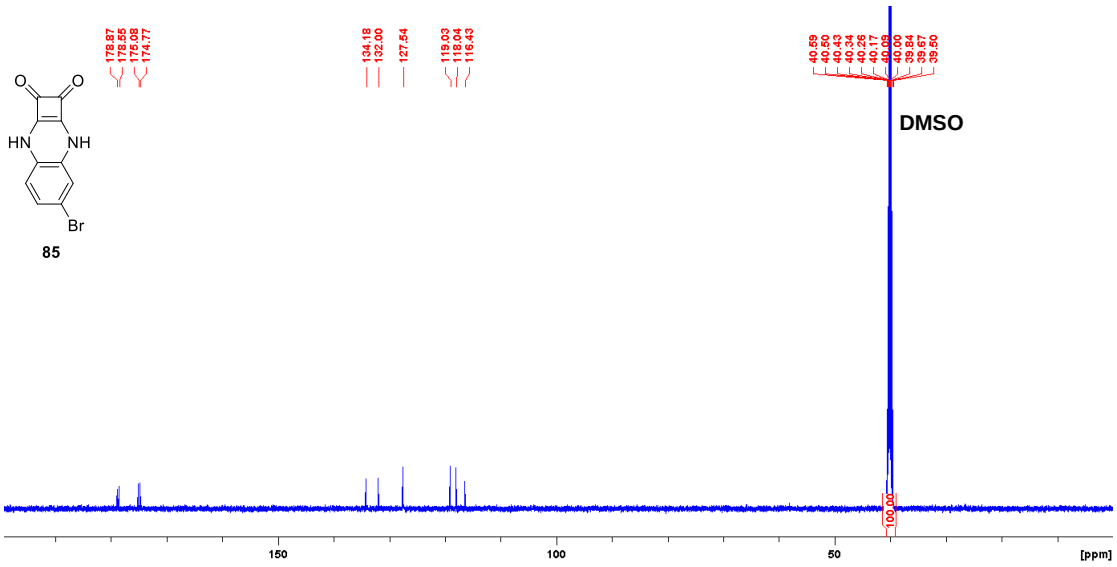

FigureA2.14: The ^{13}C NMR spectrum of compound **85** (500.13 MHz, DMSO-d_6).

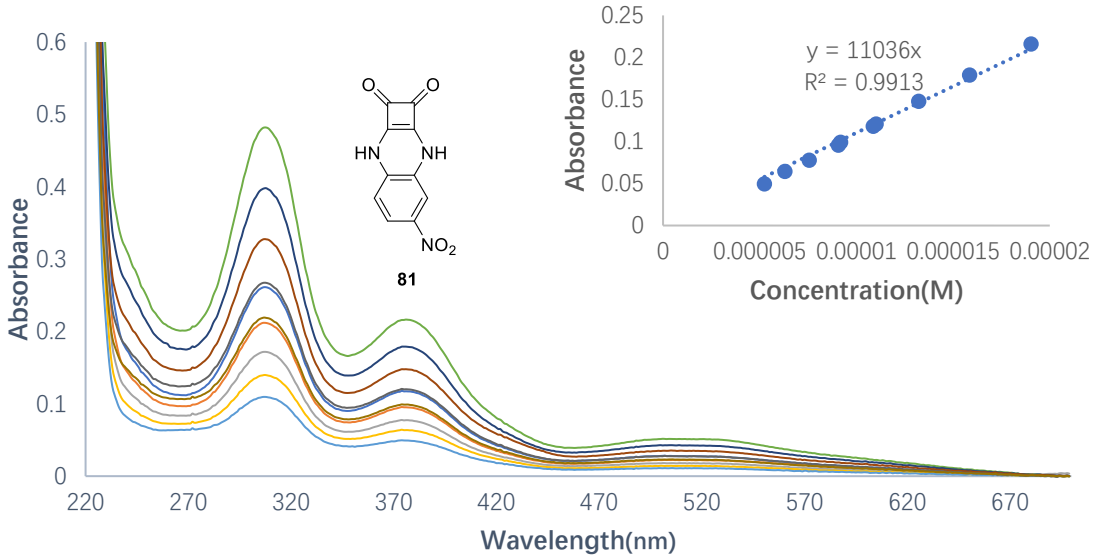

A2.15: Changes in UV/Vis spectrum upon increasing concentration of **81** in PBS buffer solution. Inset: Plots of absorbance at 374 nm as a function of increasing concentration of **81**.

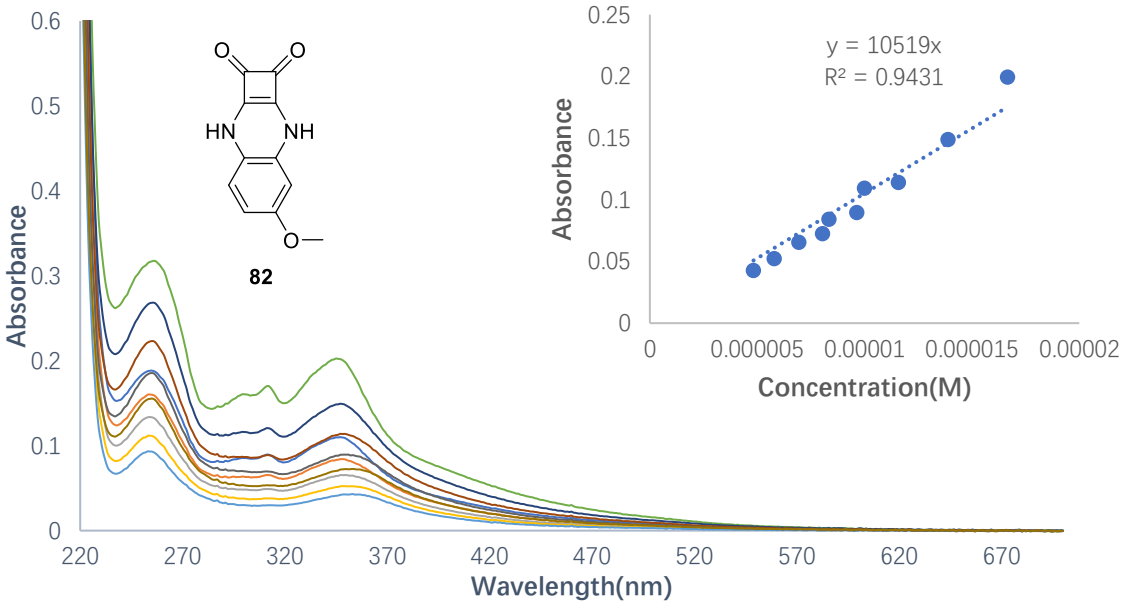

Figure A2.16: Changes in UV/Vis spectrum upon increasing concentration of **82** in PBS buffer solution. Inset: Plots of absorbance at 349 nm as a function of increasing concentration of **82**.

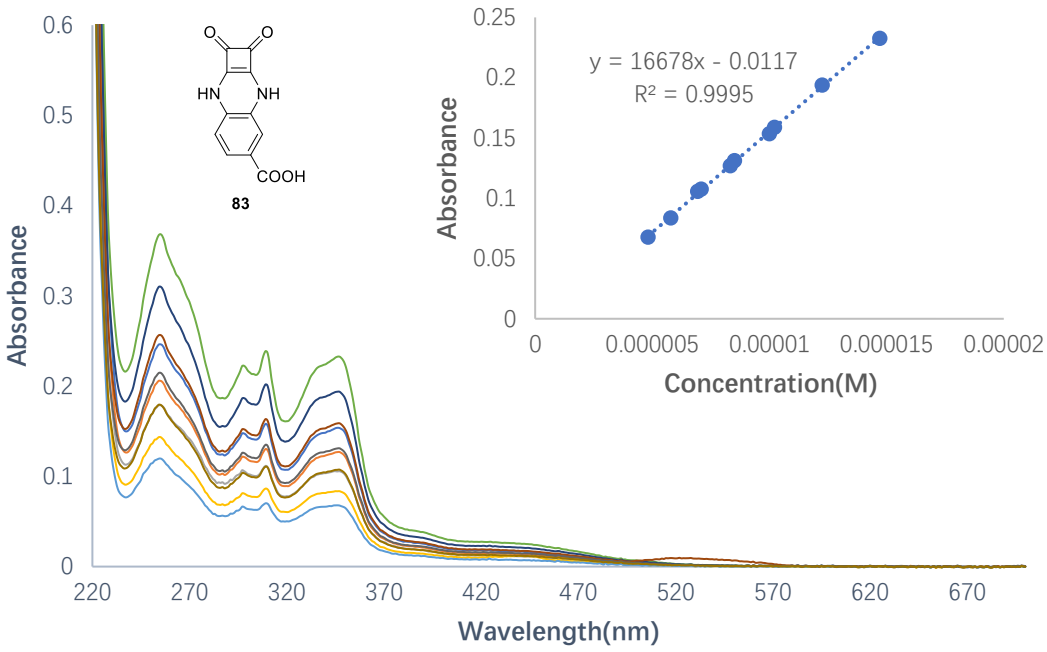

Figure A2.17: Changes in UV/Vis spectrum upon increasing concentration of **83** in PBS buffer solution. Inset: Plots of absorbance at 347 nm as a function of increasing concentration of **83**.

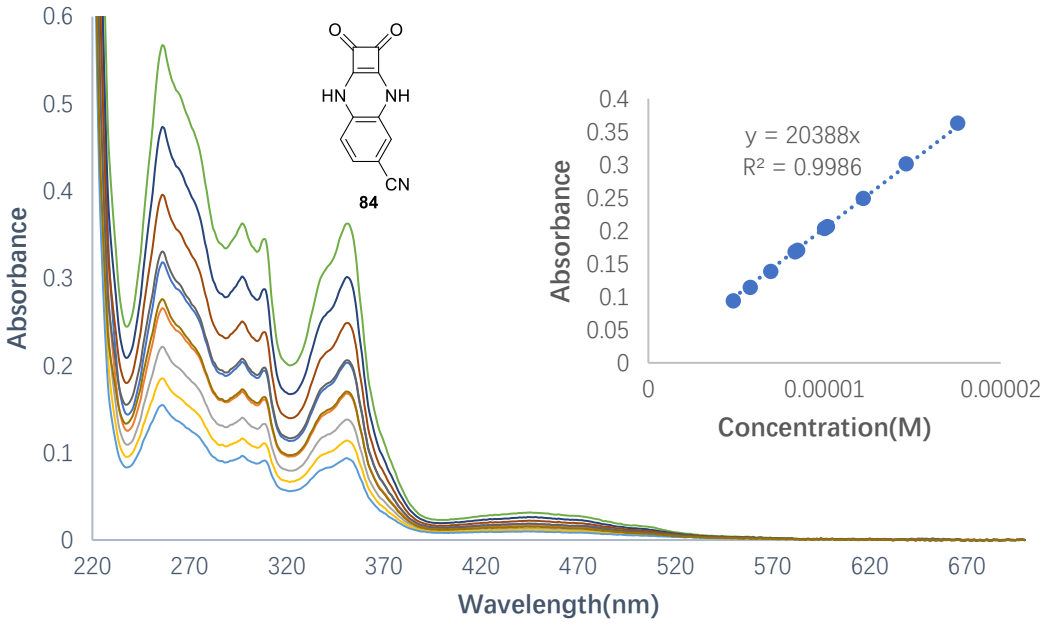

Figure A2.18: Changes in UV/Vis spectrum upon increasing concentration of **84** in PBS buffer solution. Inset: Plots of absorbance at 351 nm as a function of increasing concentration of **84**.

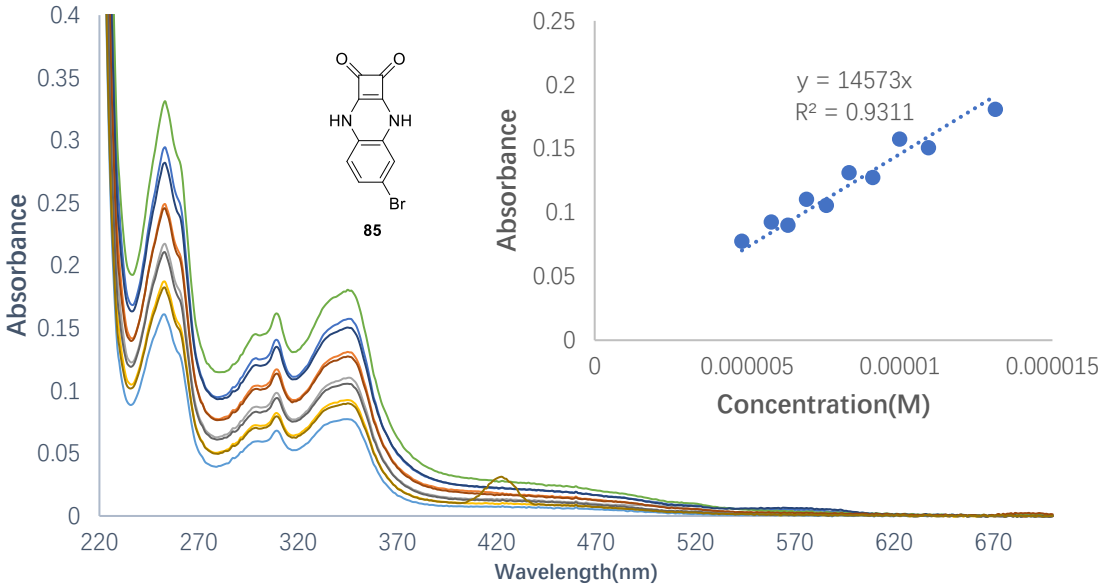

Figure A2.19: Changes in UV/Vis spectrum upon increasing concentration of **85** in PBS buffer solution. Inset: Plots of absorbance at 345 nm as a function of increasing concentration of **85**.

(a)

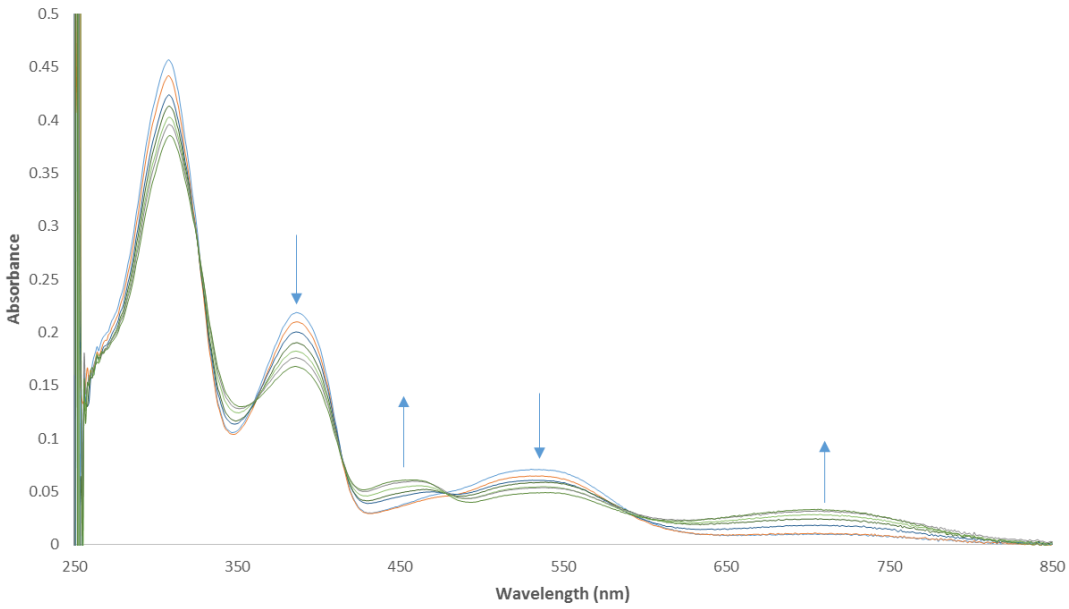

(b)

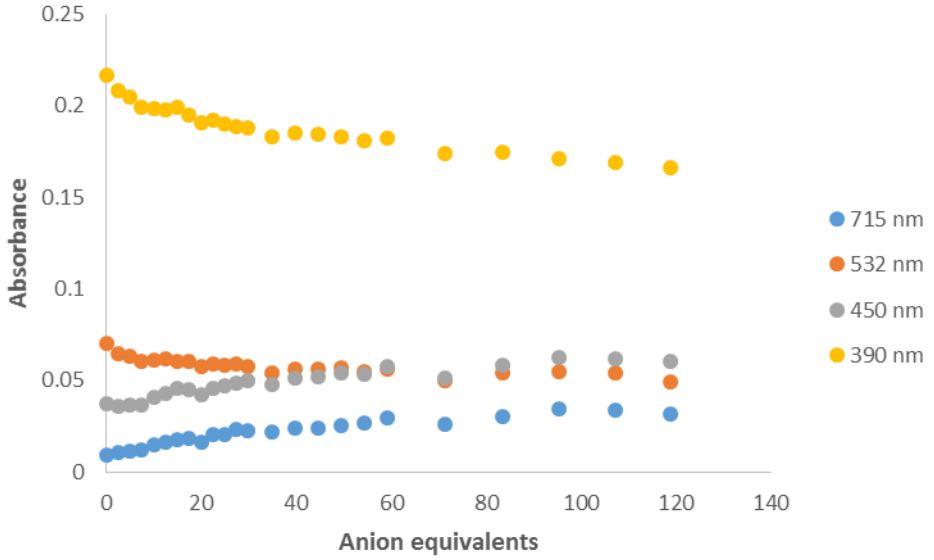

Figure A2.20: (a) Changes observed in the absorption spectrum of **81** (1 x 10^{-5} M) upon addition of TBACl (0 – 1.2 mM) in 0.5% H_2O in DMSO solution. (b) Absorbance changes observed at 715 nm, 532 nm, 450 nm and 390 nm.

(a)

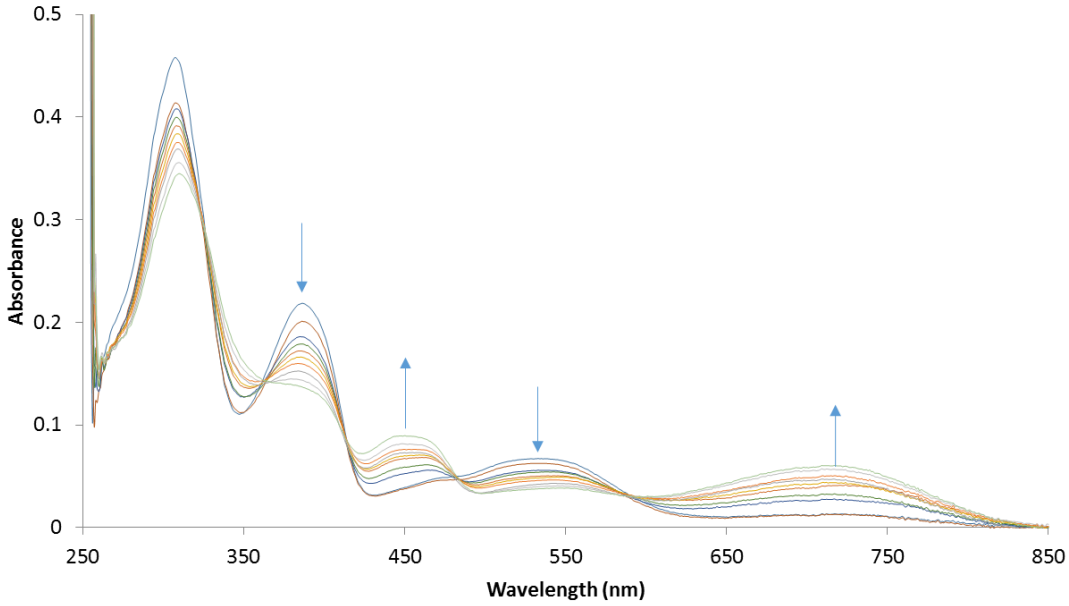

(b)

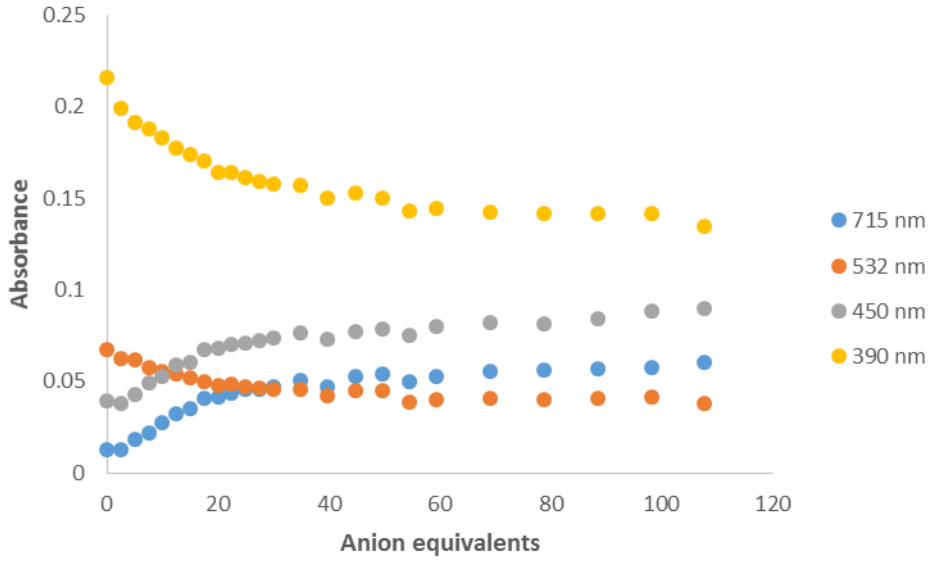

Figure A2.21: (a) Changes observed in the absorption spectrum of **81** (1 x 10^{-5} M) upon addition of TBABr (0 – 1.1 mM) in 0.5% H_2O in DMSO solution. (b) Absorbance changes observed at 715 nm, 532 nm, 450 nm and 390 nm.

(a)

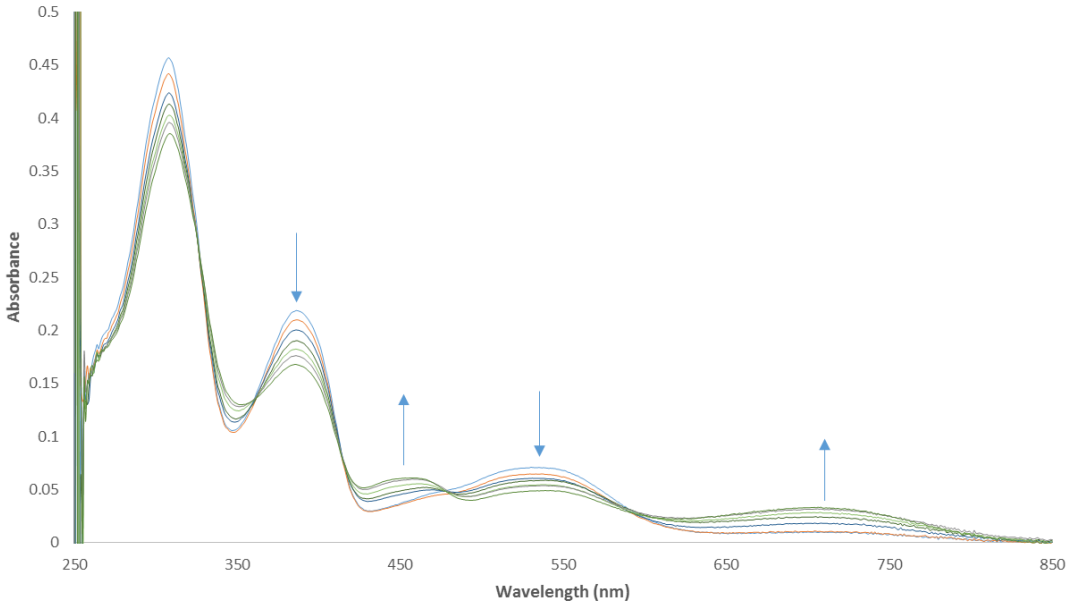

(b)

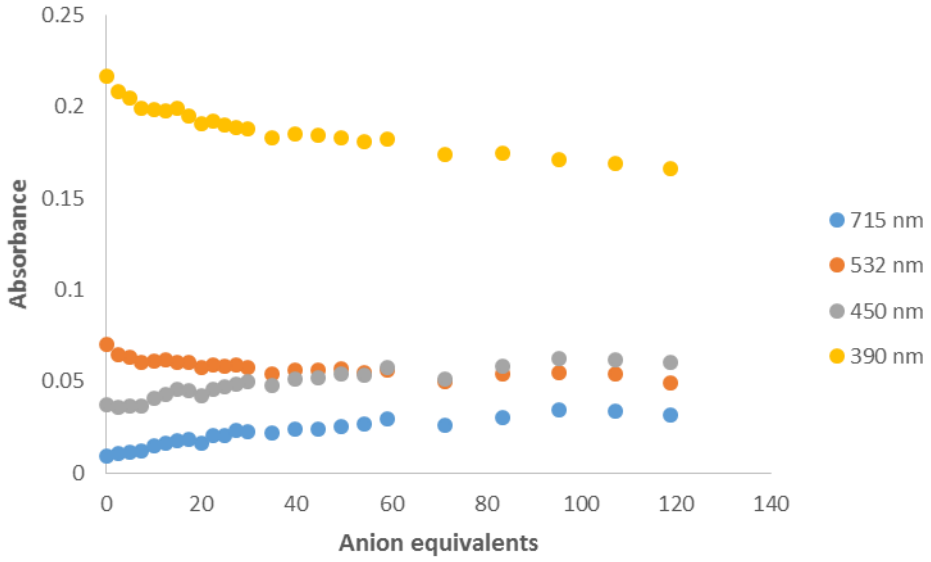

Figure A2.22: (a) Changes observed in the absorption spectrum of **81** (1 x 10^{-5} M) upon addition of TBAI (0 – 1.2 mM) in 0.5% H_2O in DMSO solution. (b) Absorbance changes observed at 715 nm, 532 nm, 450 nm and 390 nm.

(a)

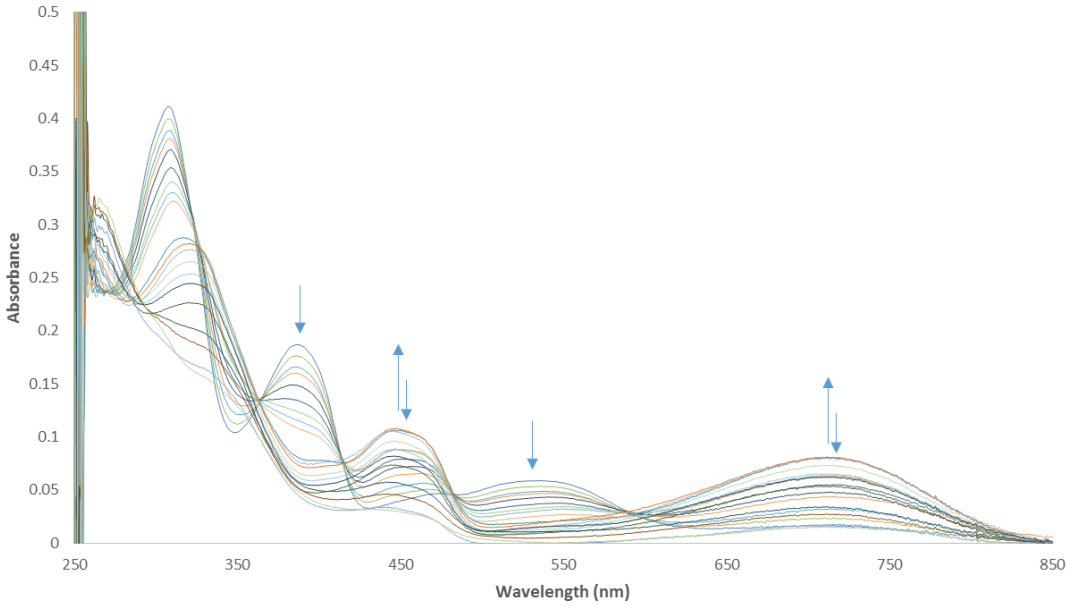

(b)

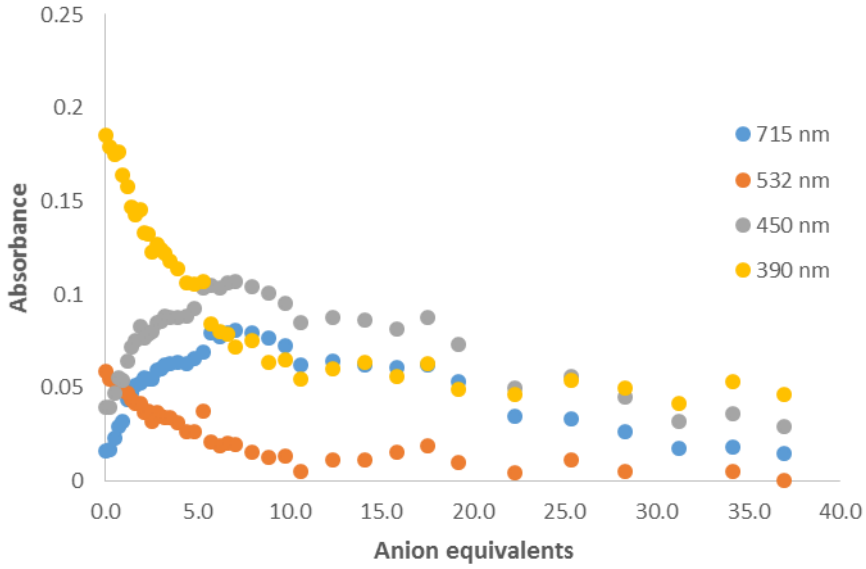

Figure A2.23: (a) Changes observed in the absorption spectrum of **81** (1 x 10^{-5} M) upon addition of TBAF (0 – 0.37 mM) in 0.5% H_2O in DMSO solution. (b) Absorbance changes observed at 715 nm, 532 nm, 450 nm and 390 nm.

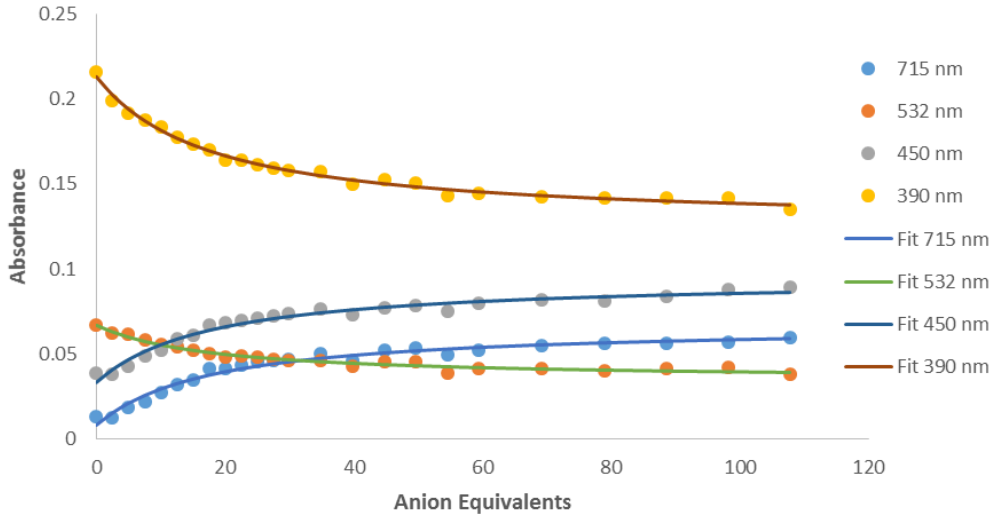

Figure A2.24: Global fitting analysis of **81** (1 x 10^{-5} M) upon addition of TBAF (0 – 0.07 mM) in 0.5% H_2O in DMSO solution according to a 1 : 1 binding model of the absorbance changes observed at 715 nm, 532 nm, 450 nm and 390 nm. K_a = 23262 M^{-1}, Error = 4%, Covariance of the fit = 0.009002

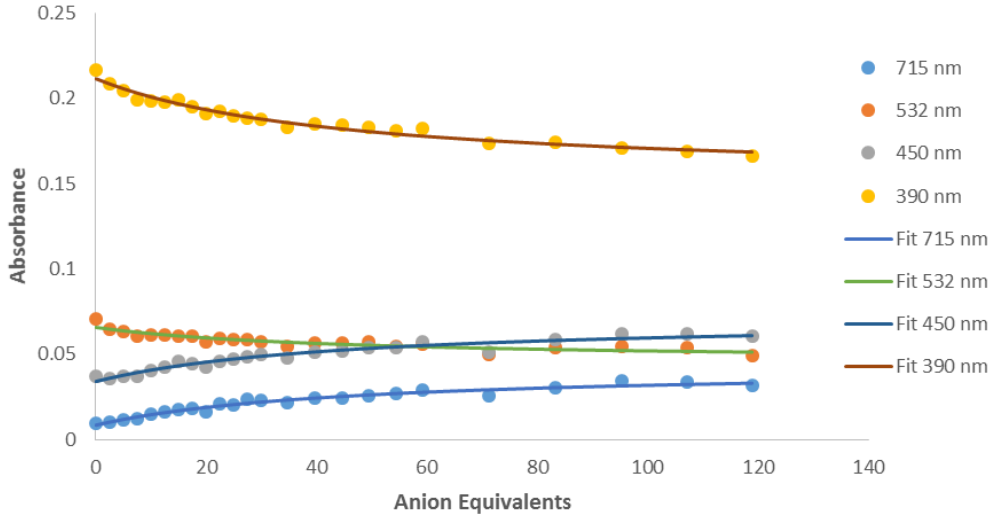

Figure A2.25: Global fitting analysis of **81** (1 x 10^{-5} M) upon addition of TBACl (0 – 0.12 mM) in 0.5% H_2O in DMSO solution according to a 1 : 1 binding model of the absorbance changes observed at 715 nm, 532 nm, 450 nm and 390 nm. K_a = 2257 M^{-1}, Error = 4.86%, Covariance of the fit = 0.009404

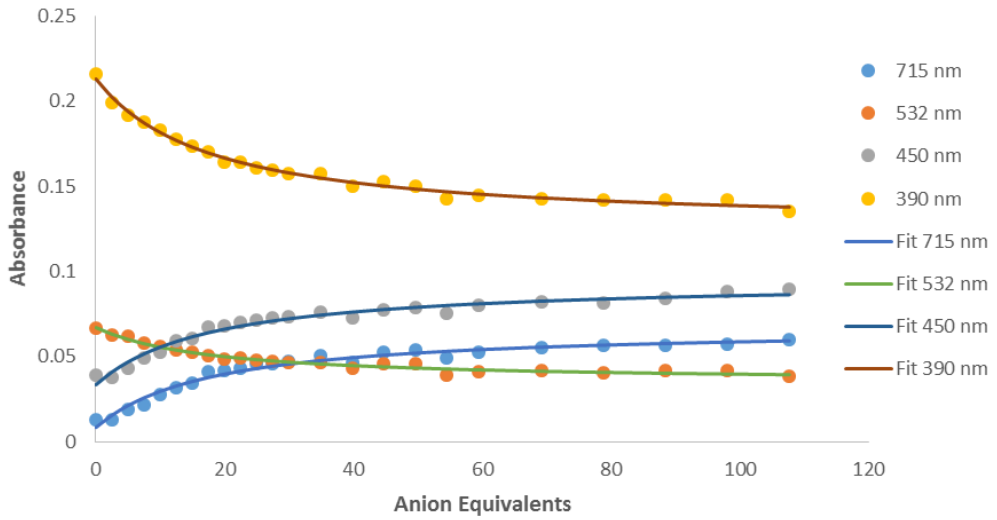

Figure A2.26: Global fitting analysis of **81** (1 x 10^{-5} M) upon addition of TBABr (0 – 0.11 mM) in 0.5% H_2O in DMSO solution according to a 1 : 1 binding model of the absorbance changes observed at 715 nm, 532 nm, 450 nm and 390 nm. K_a = 5835 M^{-1}, Error = 3.67%, Covariance of the fit = 0.0031246

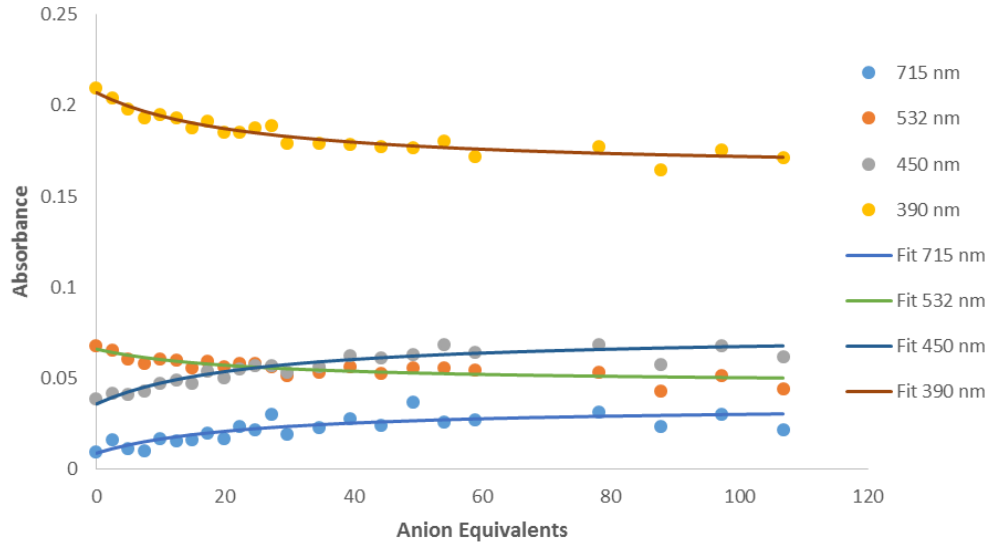

Figure A2.27: Global fitting analysis of **81** (1 x 10^{-5} M) upon addition of TBAI (0 – 0.11 mM) in 0.5% H_2O in DMSO solution according to a 1 : 1 binding model of the absorbance changes observed at 715 nm, 532 nm, 450 nm and 390 nm. K_a = 4323 M^{-1}, Error = 12%, Covariance of the fit = 0.038987

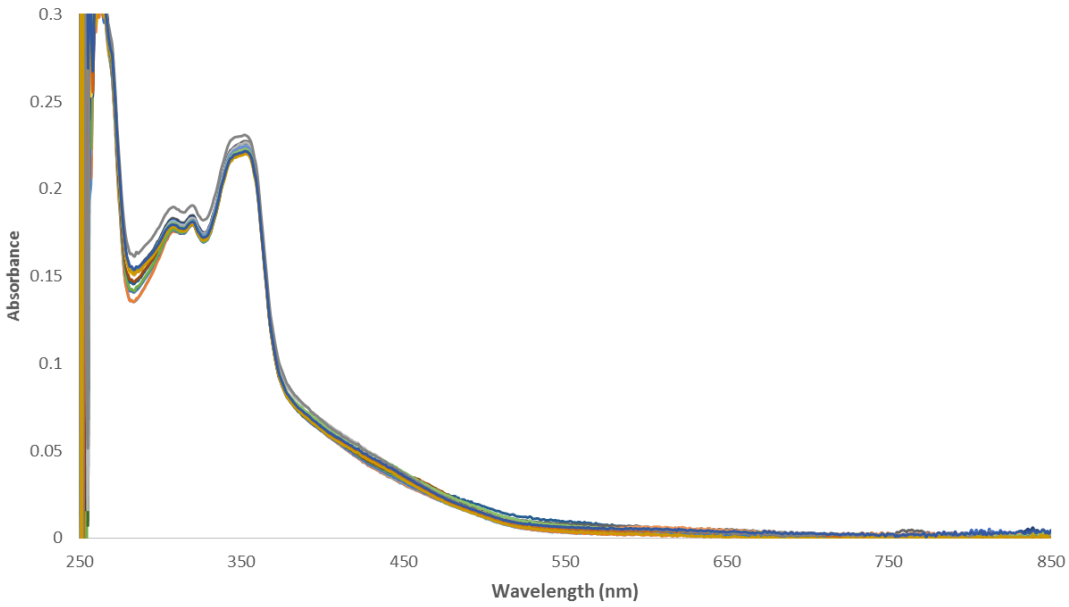

Figure A2.28: Changes observed in the absorption spectrum of **82** (1 x 10^{-5} M) upon addition of TBACl (0 – 1 mM) in 0.5% H_2O in DMSO solution

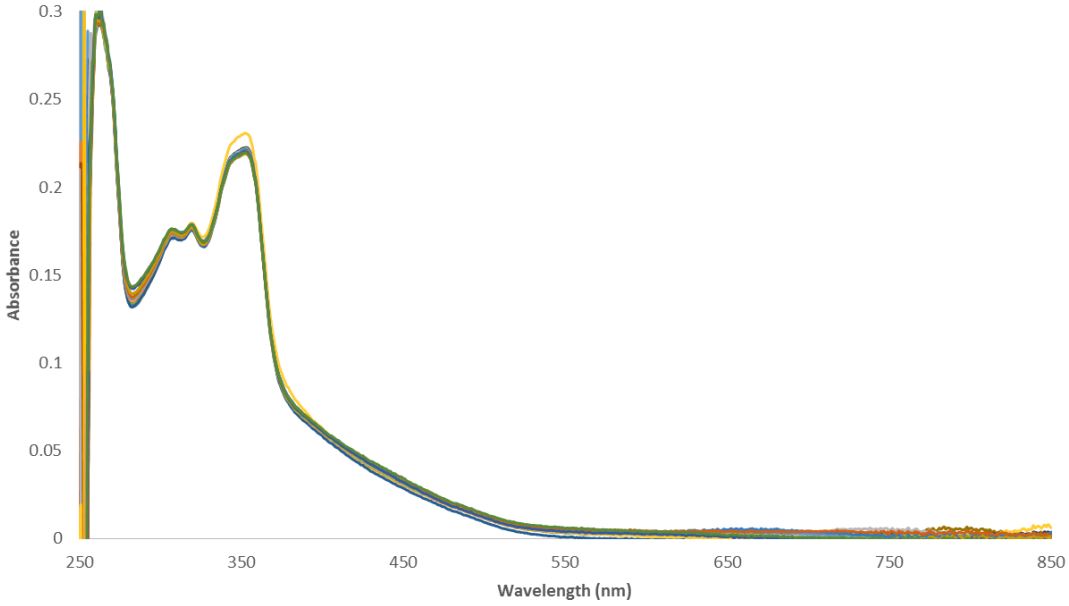

Figure A2.29: Changes observed in the absorption spectrum of **82** (1 x 10^{-5} M) upon addition of TBABr (0 – 1 mM) in 0.5% H_2O in DMSO solution.

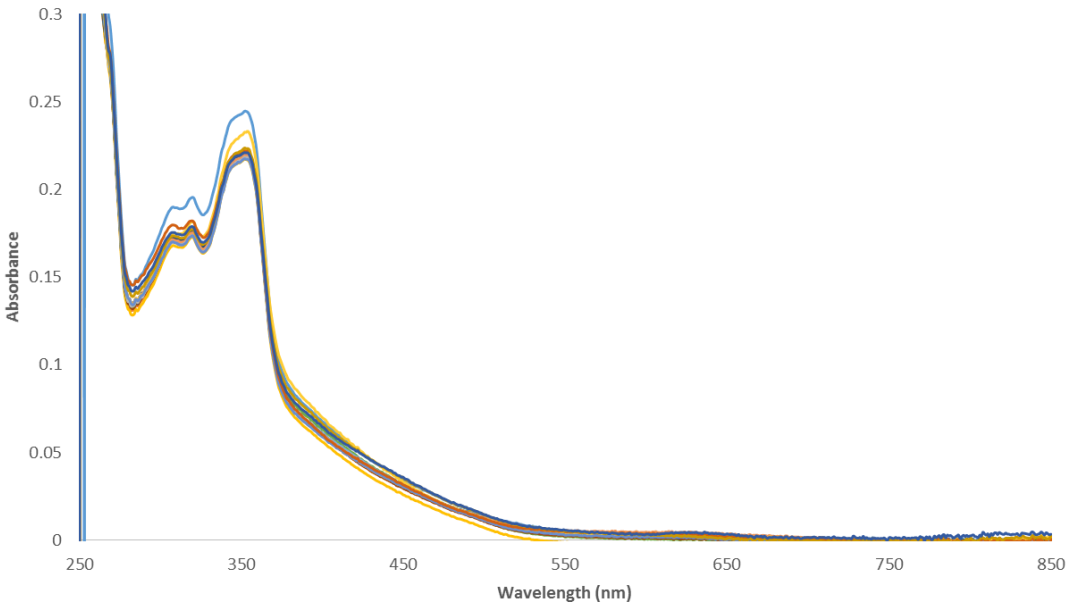

Figure A2.30: Changes observed in the absorption spectrum of **82** (1 x 10^{-5} M) upon addition of TBAI (0 – 1 mM) in 0.5% H_2O in DMSO solution.

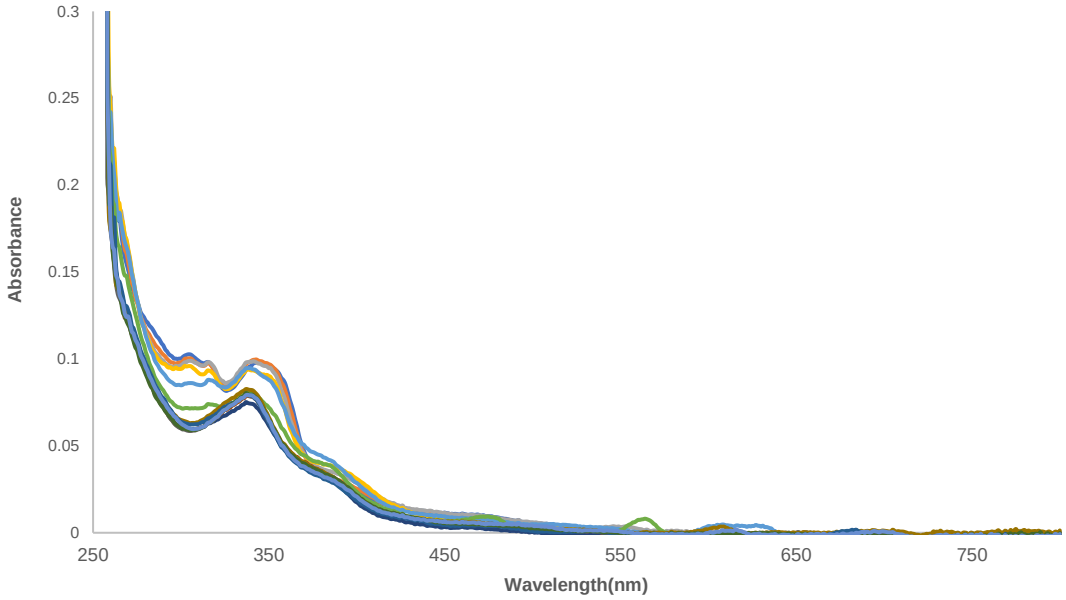

Figure A2.31: Changes observed in the absorption spectrum of **83** (1 x 10^{-5} M) upon addition of TBAF (0 – 1 mM) in 0.5% H_2O in DMSO solution.

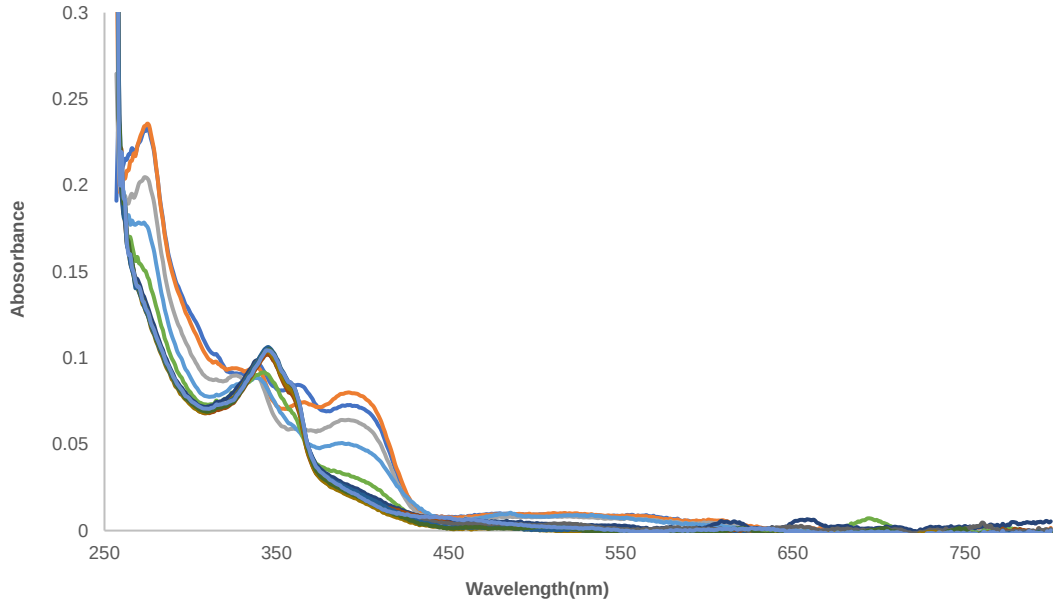

Figure A2.32: Changes observed in the absorption spectrum of **84** (1 x 10^{-5} M) upon addition of TBAF (0 – 1 mM) in 0.5% H_2O in DMSO solution.

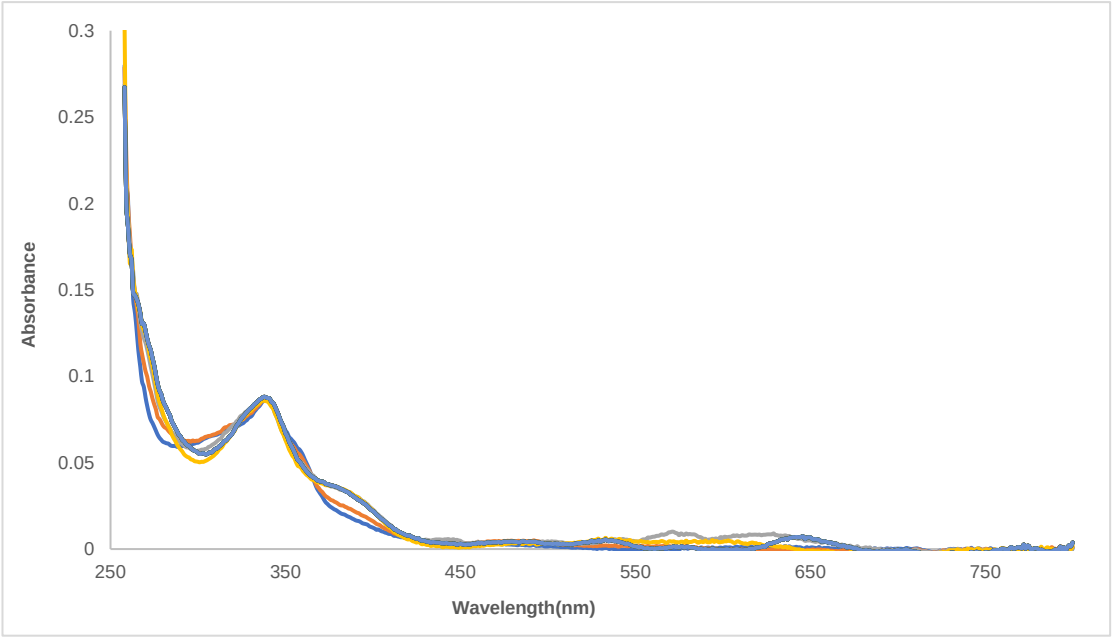

Figure A2.33: Changes observed in the absorption spectrum of **85** (1 x 10^{-5} M) upon addition of TBAF (0 – 1 mM) in 0.5% H_2O in DMSO solution.

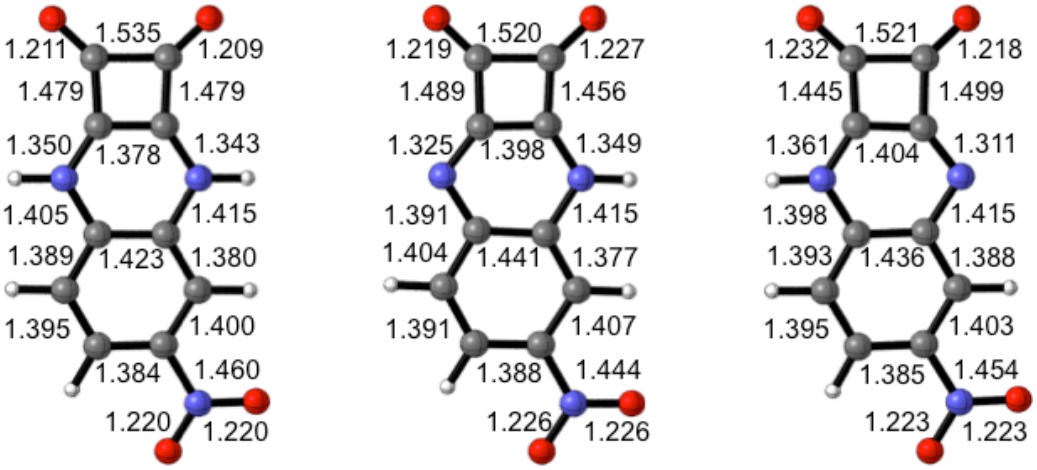

81 **[81-H]⁻ (tautomer N1)** **[81-H]⁻ (tautomer N2)**

Figure A2.34: DFT-optimized geometries of compound **81**, and the tautomers of **[81-H]⁻**. Bond distances are given in Å. [SMD-PCM(DMSO)/M06-2X/aug-cc-pVDZ].

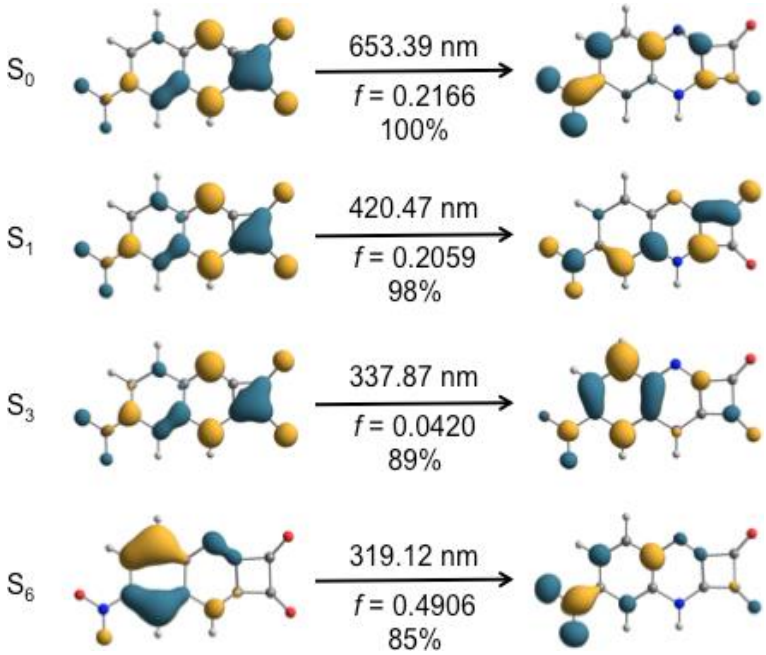

Figure A2.35: NTO plots (isovalue = 0.05) for key electronic transitions in tautomer N1 of **[81-H]⁻**. Excitation energies are given along with oscillator strengths and weight of contributing NTO pair to each transition. [PCM(DMSO)/B3LYP/6-311+G(2d,p)].

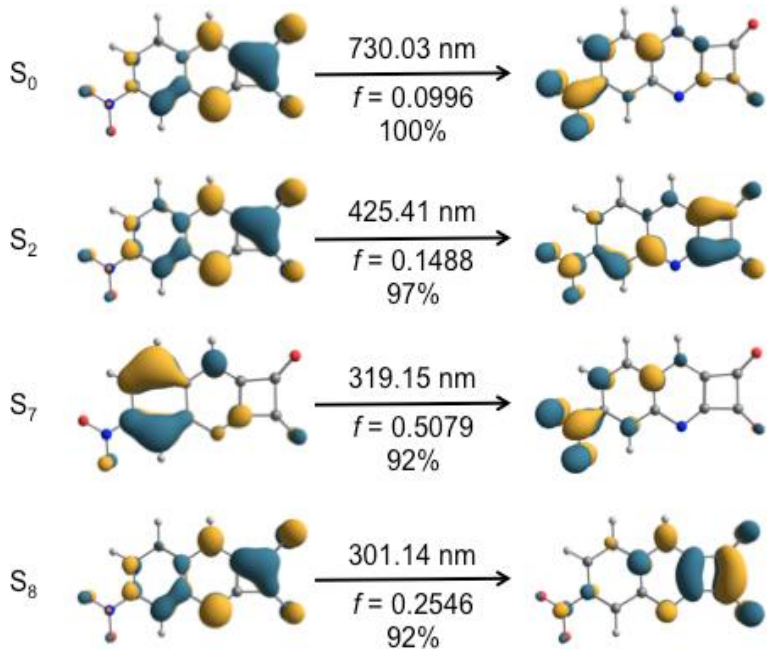

Figure A2.36: NTO plots (isovalue = 0.05) for key electronic transitions in tautomer N2 of **[81-H]**$^-$. Excitation energies are given along with oscillator strengths and weight of contributing NTO pair to each transition. [SMD-PCM(DMSO)/B3LYP/6-311+G(2d,p)].

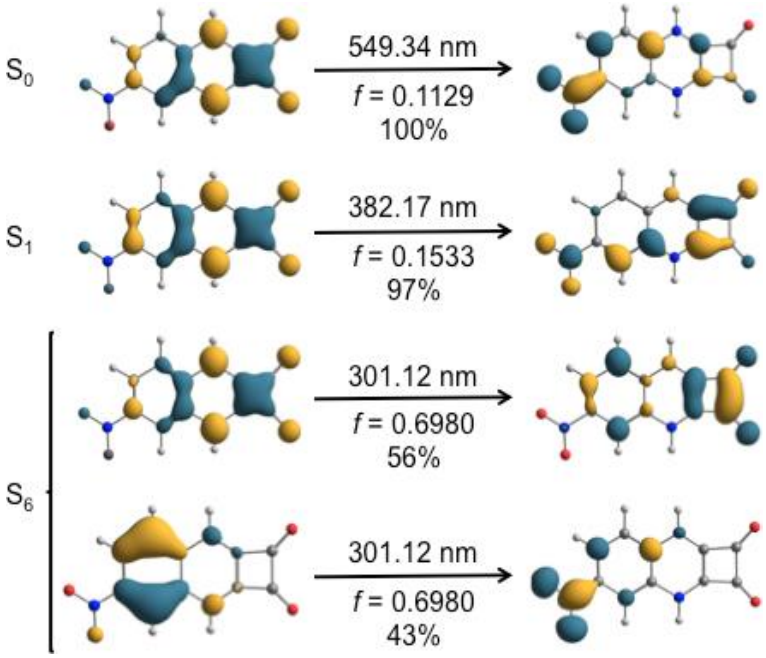

Figure A2.37: NTO plots (isovalue = 0.05) for key electronic transitions in **81**. Excitation energies are given along with oscillator strengths and weight of contributing NTO pair to each transition. [PCM(DMSO)/B3LYP/6-311+G(2d,p)].

	State	Excitation energy (λ_{max})	Oscillator strength	CI coefficient
2	S_0	549.34 nm	*f* = 0.1129	59 → 60 0.69394 59 → 61 0.12507
	S_1	382.17 nm	*f* = 0.1533	57 → 60 –0.11150 59 → 60 –0.11783 59 → 61 0.68207
	S_6	301.12 nm	*f* = 0.6980	57 → 60 –0.45023 59 → 62 –0.51865
[2–H]⁻ (N1)	S_0	653.39 nm	*f* = 0.2166	59 → 60 0.69131 59 → 61 0.14918
	S_1	420.47 nm	*f* = 0.2059	57 → 60 –0.10056 59 → 60 –0.14309 59 → 61 0.67947
	S_3	337.87 nm	*f* = 0.0420	57 → 60 –0.20556 59 → 62 0.60175 59 → 63 0.27915
	S_6	319.12 nm	*f* = 0.4906	57 → 60 0.64438 59 → 62 0.24626
[2–H]⁻ (N2)	S_0	730.03 nm	*f* = 0.0996	59 → 60 0.69670 59 → 61 –0.11807
	S_2	425.41 nm	*f* = 0.1488	57 → 60 0.10548 59 → 60 0.11092 59 → 61 0.68481
	S_7	319.15 nm	*f* = 0.5079	57 → 60 0.66816 59 → 62 0.16912
	S_8	301.14 nm	*f* = 0.2546	56 → 60 0.18108 59 → 62 –0.16284 59 → 63 0.64857

Table A2.1: Calculated excited state energies, oscillator strengths and largest coefficients of the CI expansion (MO contribution to particular state). [SMD-PCM(DMSO)/B3LYP/6-311G+(2d,p).

Appendix 3

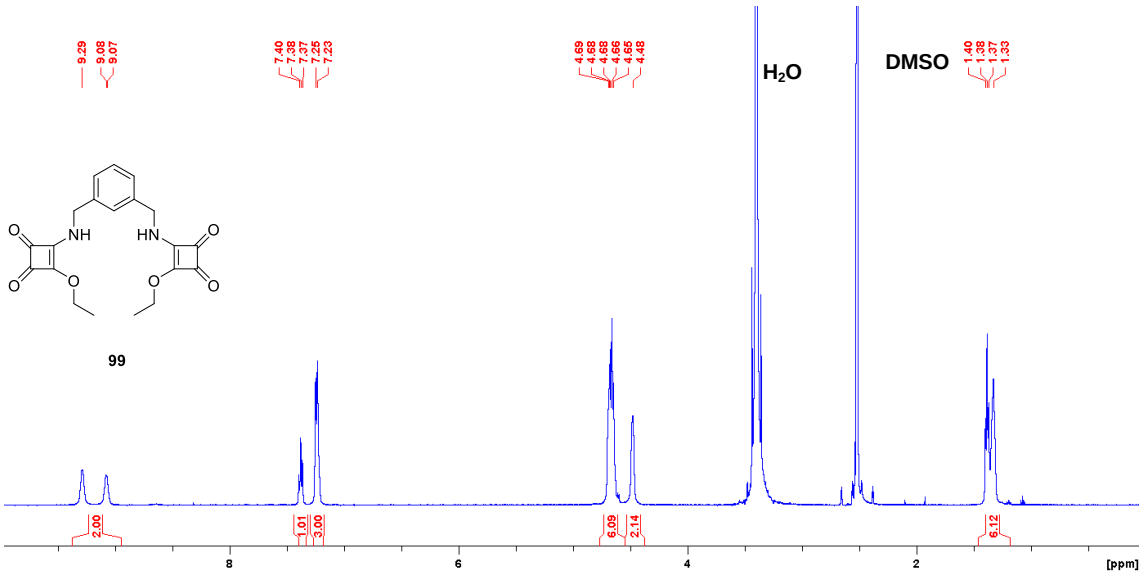

Figure A3.1: The ^{1}H NMR spectrum of compound **99** (500.13 MHz, DMSO-d_6).

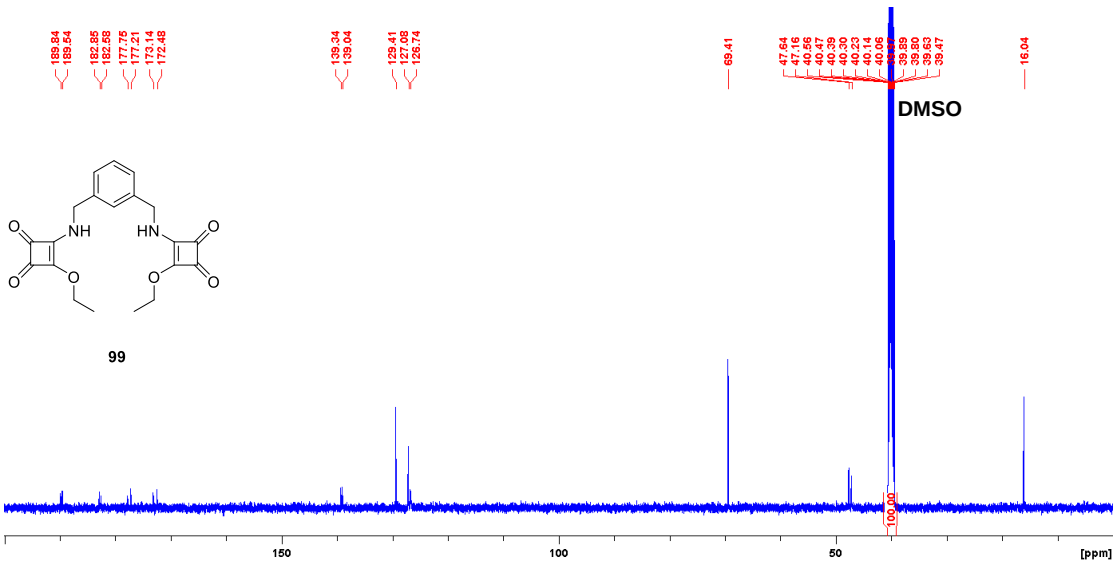

Figure A3.2: The ^{13}C NMR spectrum of compound **99** (500.13 MHz, DMSO-d_6).

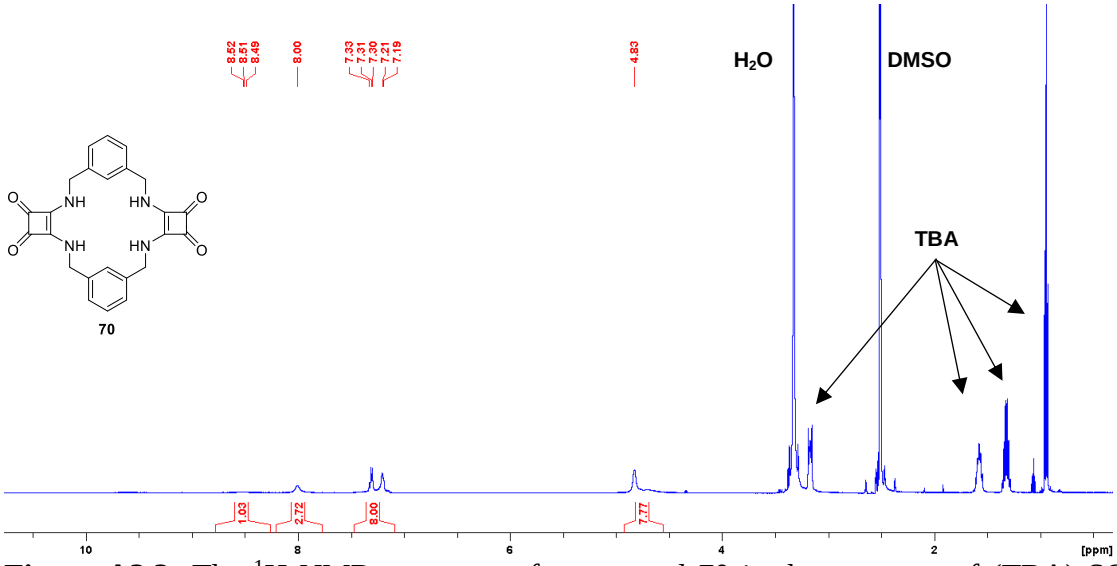

Figure A3.3: The ^{1}H NMR spectrum of compound **70** in the presence of $(TBA)_2SO_4$ (500.13 MHz, DMSO-d_6).

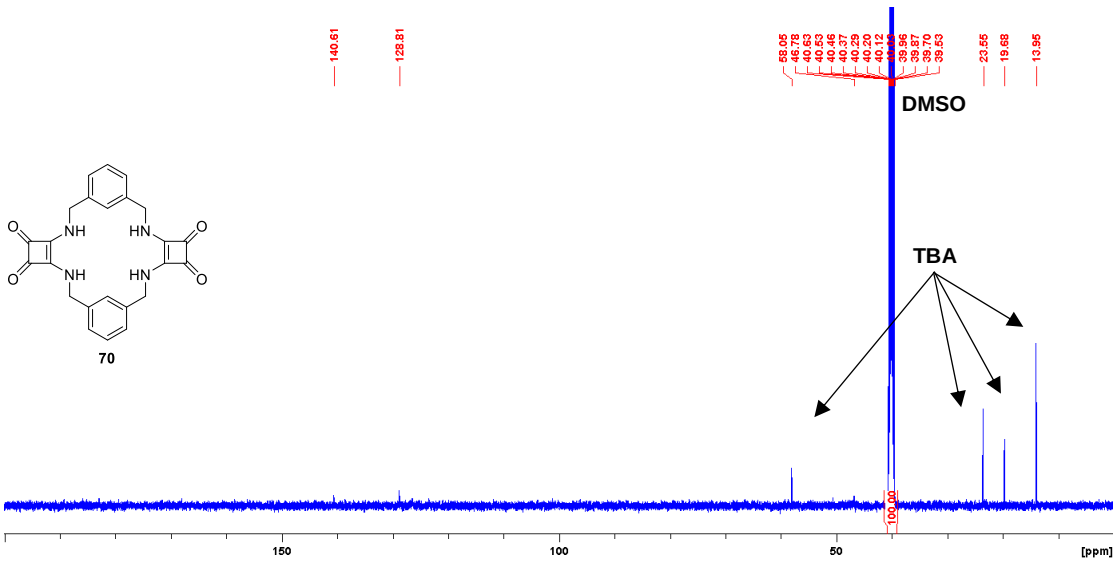

Figure A3.4: The ^{13}C NMR spectrum of compound **70** in the presence of $(TBA)_2SO_4$ (500.13 MHz, DMSO-d_6).

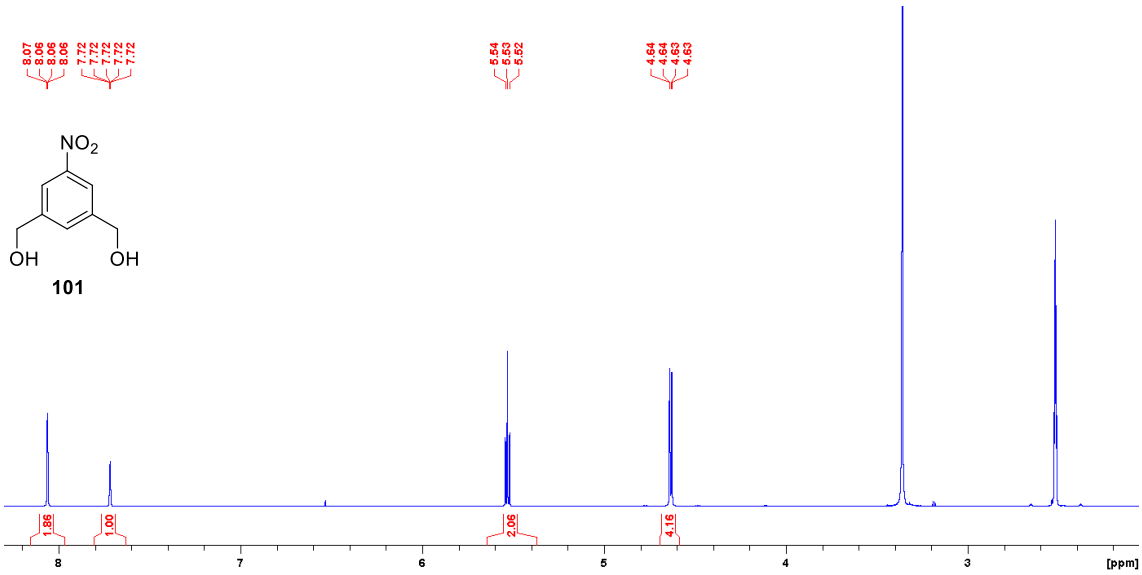

Figure A3.5: The ^{1}H NMR spectrum of compound **101** (500.13 MHz, DMSO-d_6).

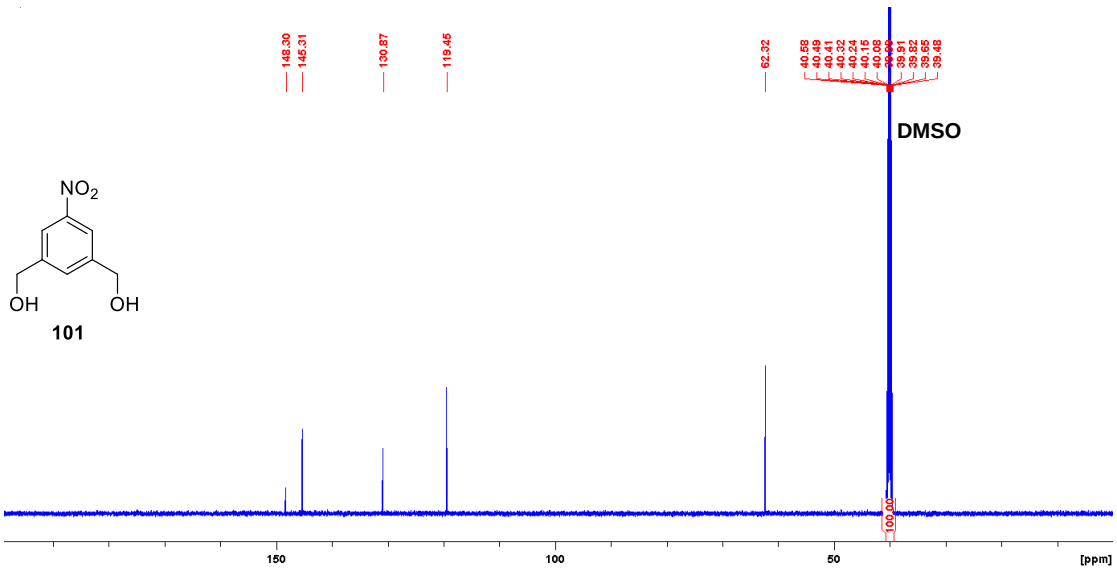

Figure A3.6: The ^{13}C NMR spectrum of compound **101** (500.13 MHz, DMSO-d_6).

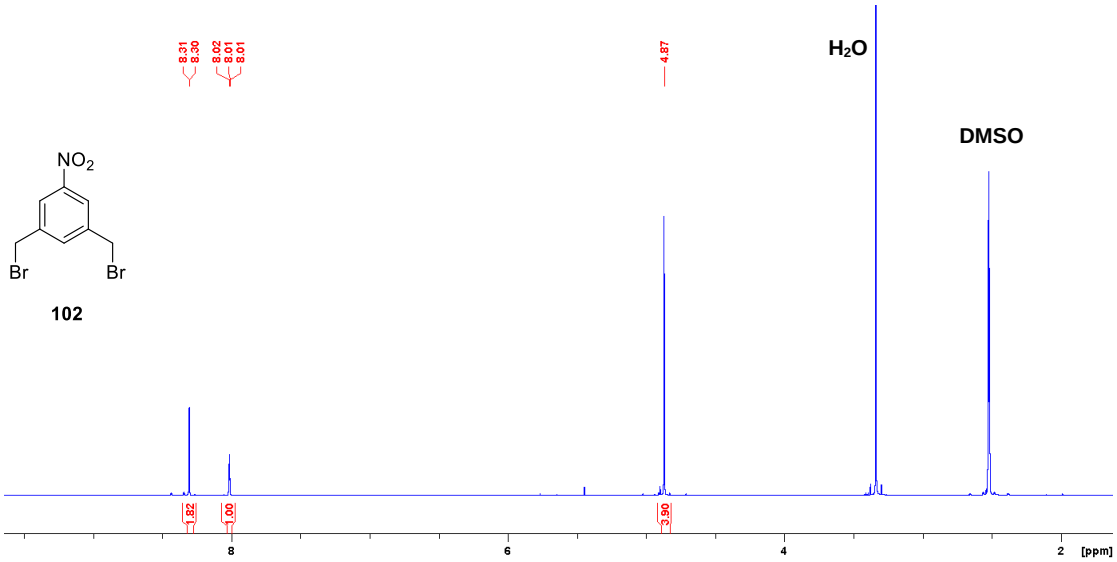

Figure A3.7: The ^{1}H NMR spectrum of compound **102** (500.13 MHz, DMSO-d_6).

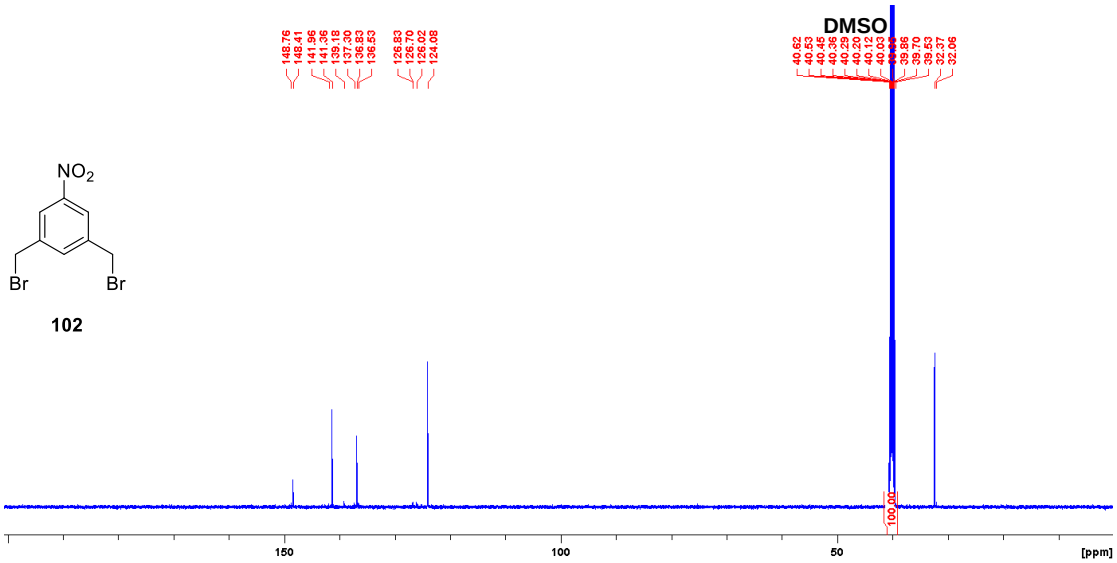

Figure A3.8: The ^{13}C NMR spectrum of compound **102** (500.13 MHz, DMSO-d_6).

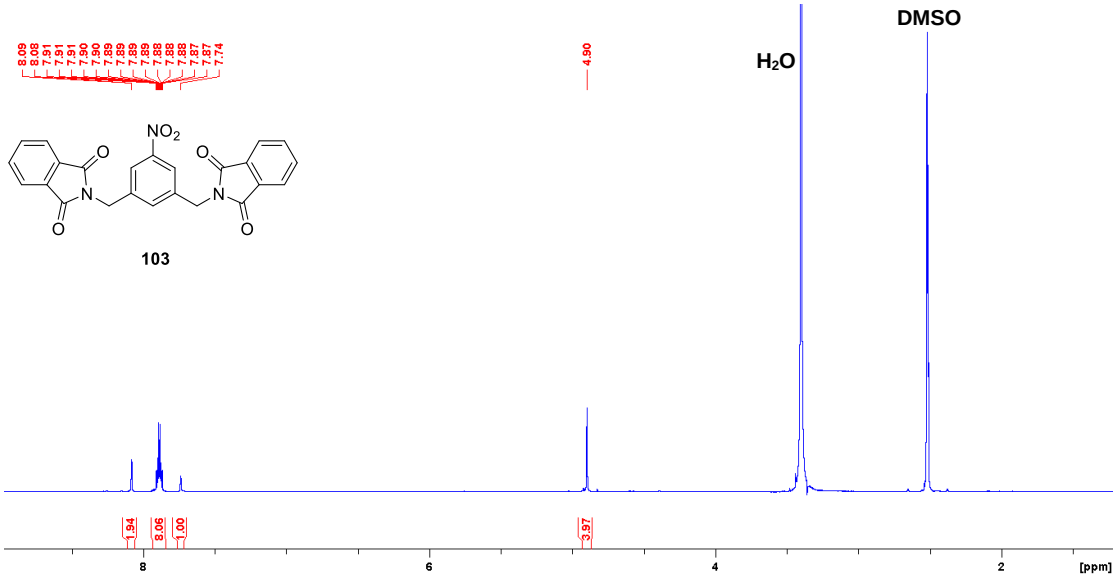

Figure A3.9: The ^{1}H NMR spectrum of compound **103** (500.13 MHz, DMSO-d_6).

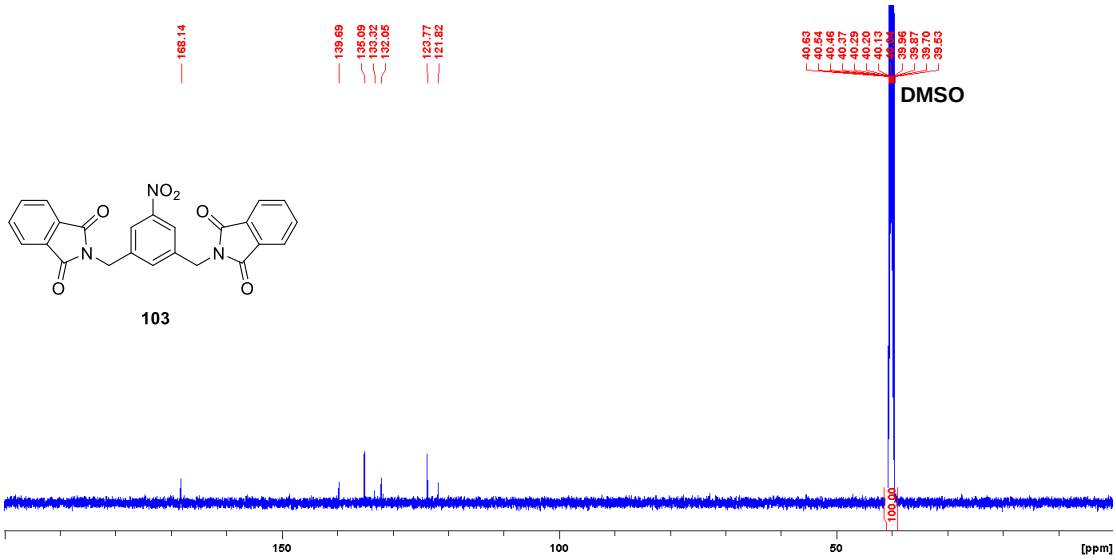

Figure A3.10: The ^{13}C NMR spectrum of compound **103** (500.13 MHz, DMSO-d_6).

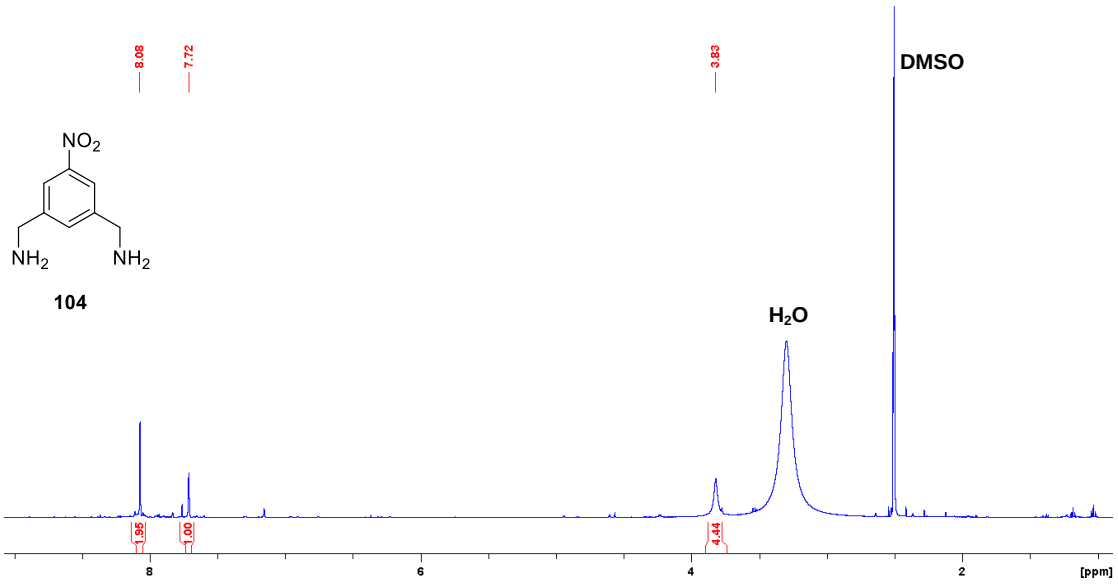

Figure A3.11: The ^{1}H NMR spectrum of compound **104** (500.13 MHz, DMSO-d_6).

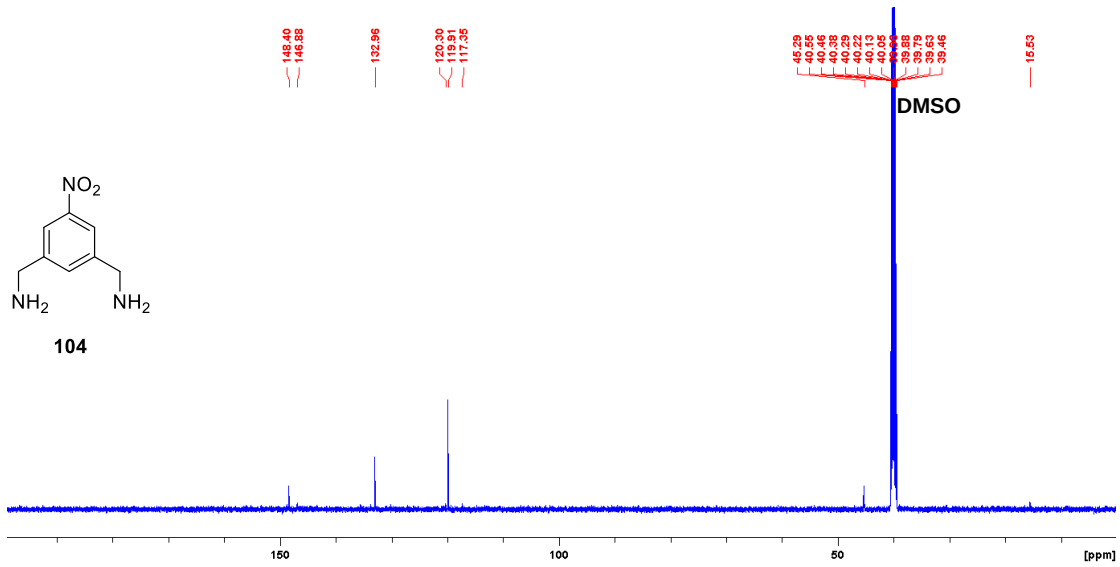

Figure A3.12: The ^{13}C NMR spectrum of compound **104** (500.13 MHz, DMSO-d_6).

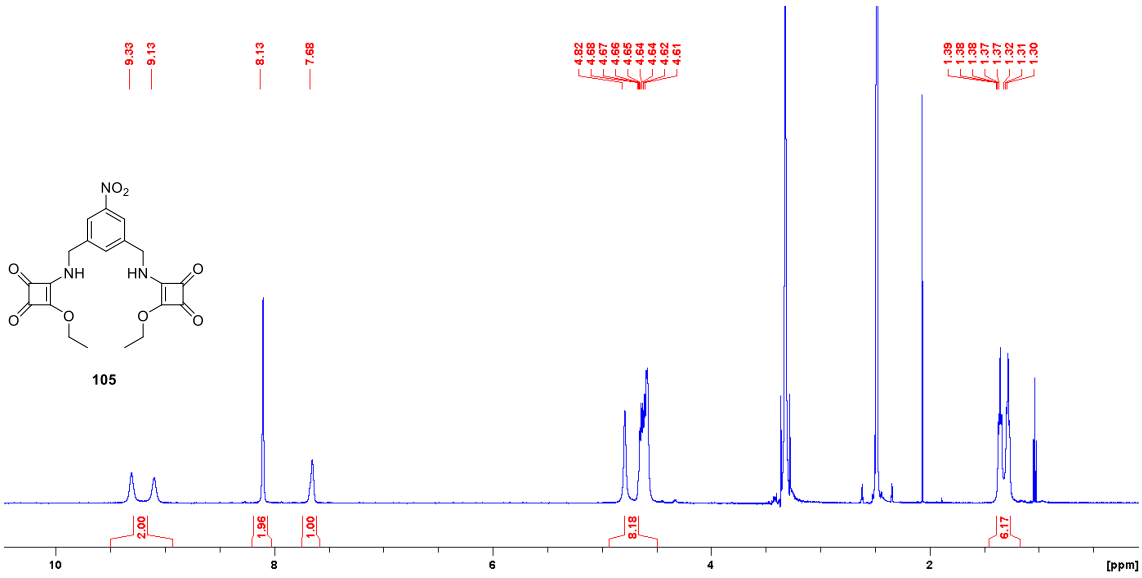

Figure A3.13: The ^{1}H NMR spectrum of compound **105**(500.13 MHz, DMSO-d_6).

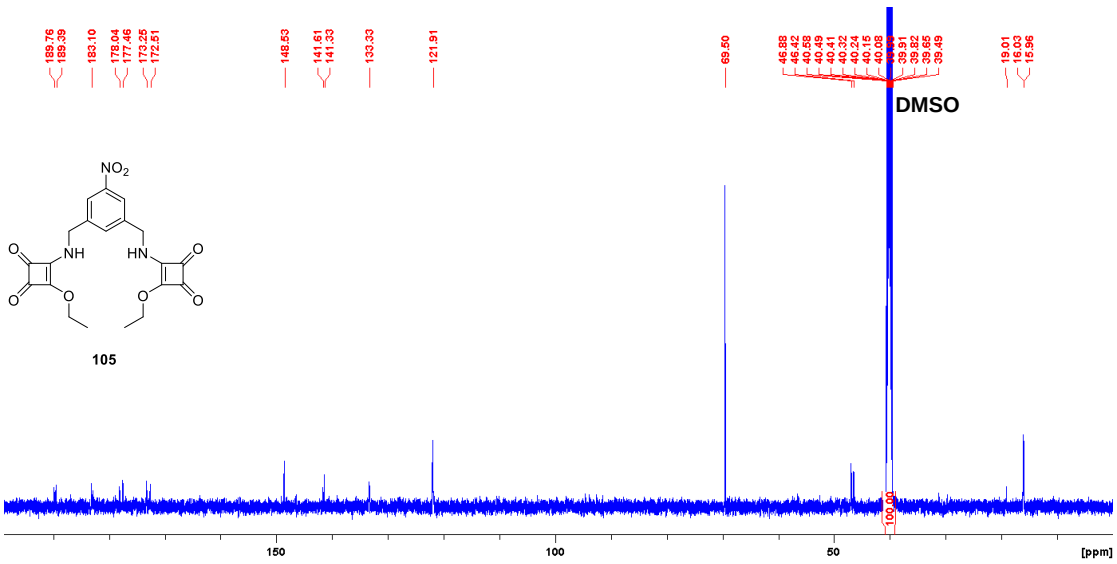

Figure A3.14: The ^{13}C NMR spectrum of compound **105** (500.13 MHz, DMSO-d_6).

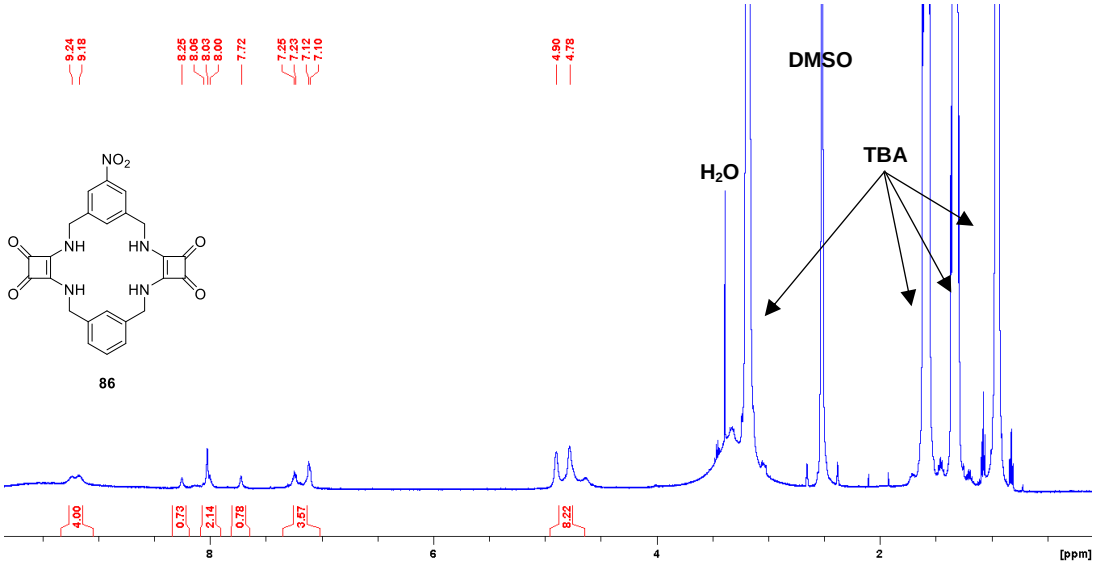

Figure A3.15: The ^{1}H NMR spectrum of compound **86** (500.13 MHz, DMSO-d_6).

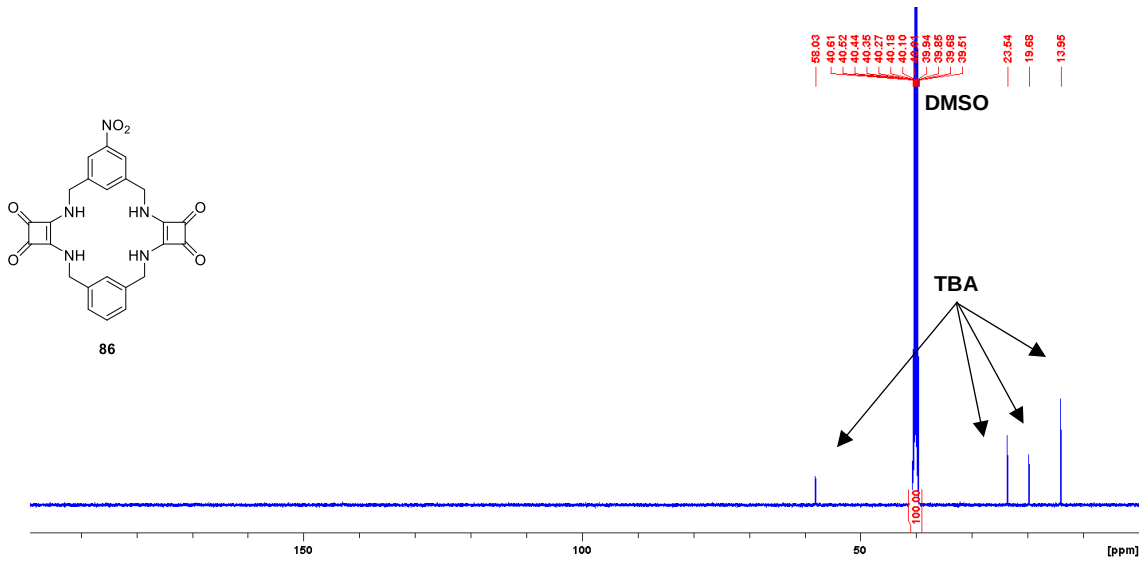

Figure A3.16: The ^{13}C NMR spectrum of compound **86** (500.13 MHz, DMSO-d_6).

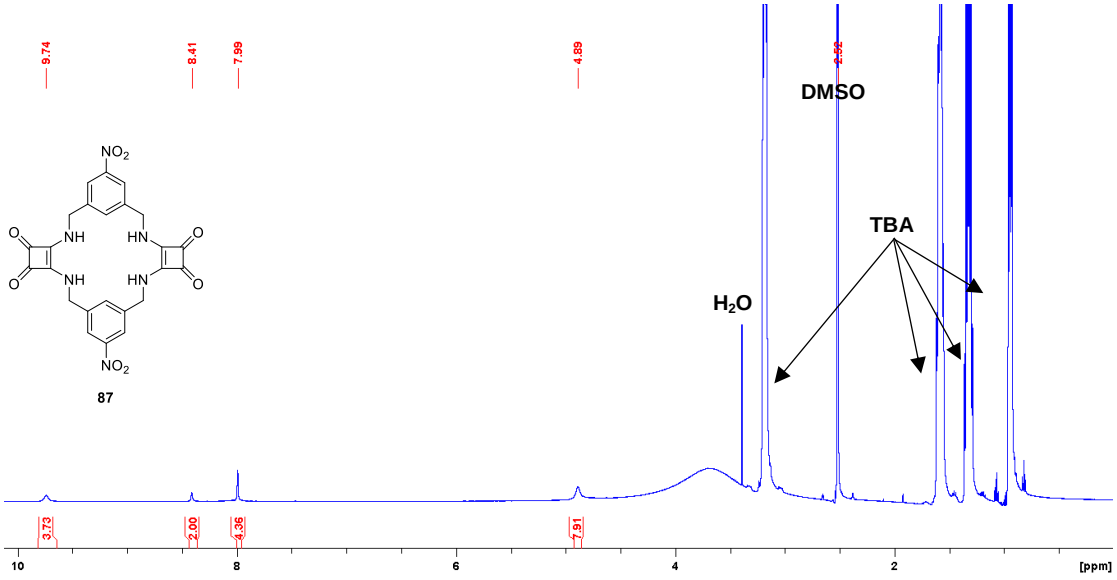

Figure A3.17: The ^{1}H NMR spectrum of compound **87** (500.13 MHz, DMSO-d_6).

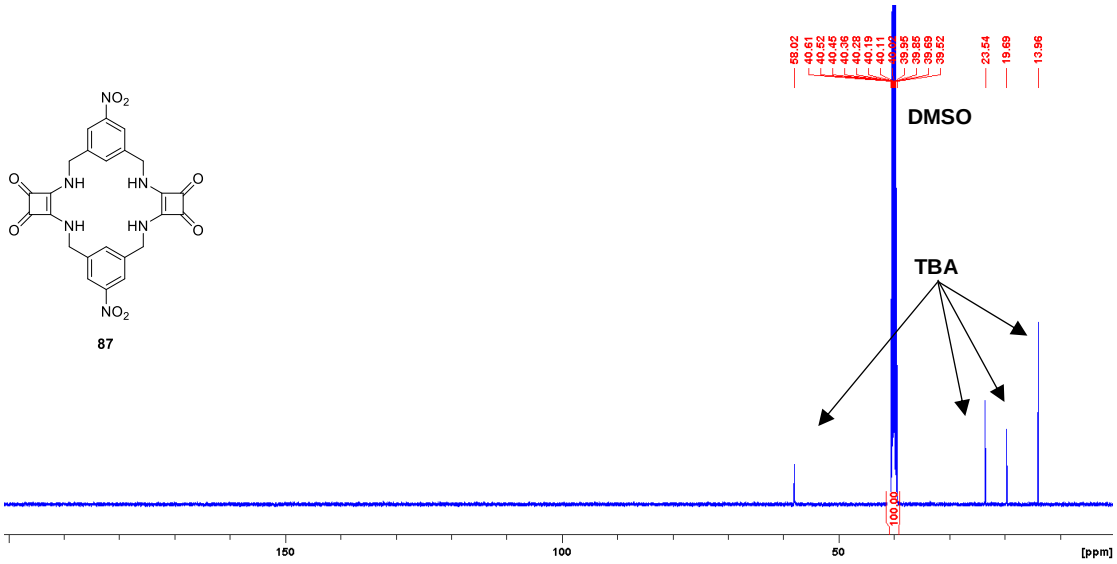

Figure A3.18: The ^{13}C NMR spectrum of compound **87** (500.13 MHz, DMSO-d_6).

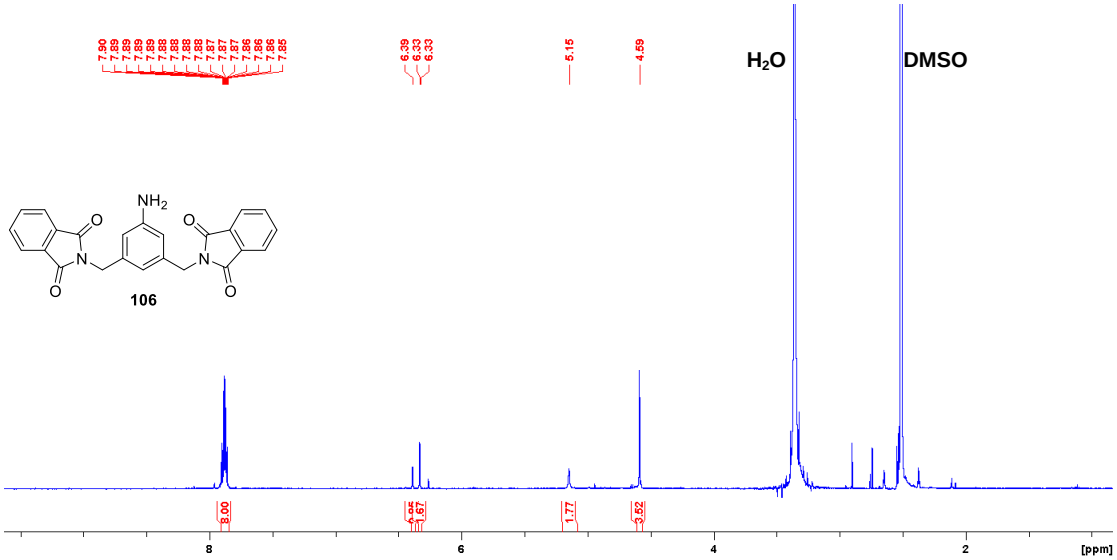

Figure A3.19: The ^{1}H NMR spectrum of compound **106** (500.13 MHz, DMSO-d_6).

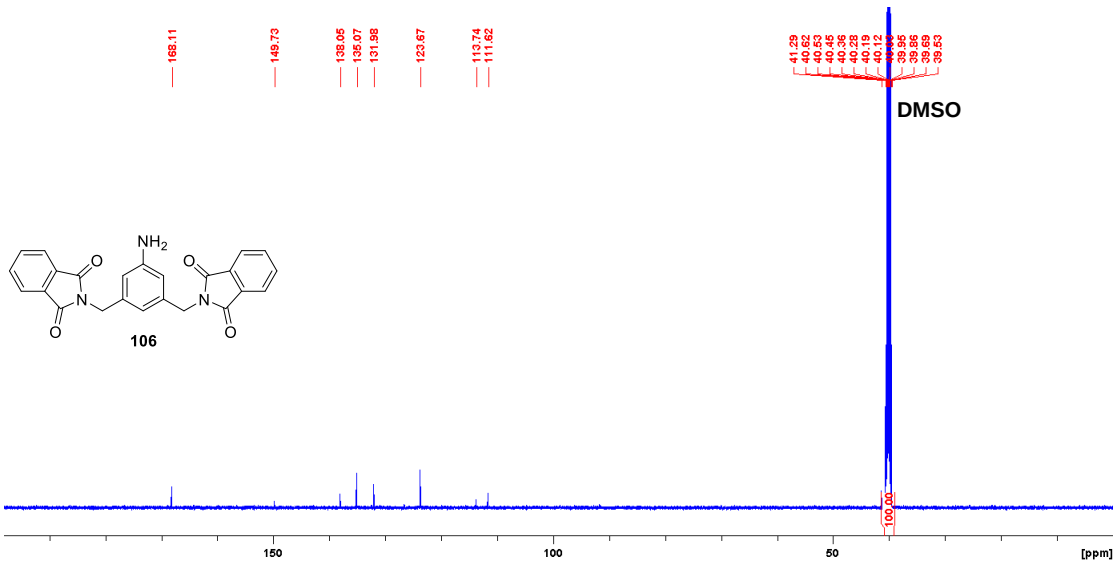

Figure A3.20: The ^{13}C NMR spectrum of compound **106** (500.13 MHz, DMSO-d_6).

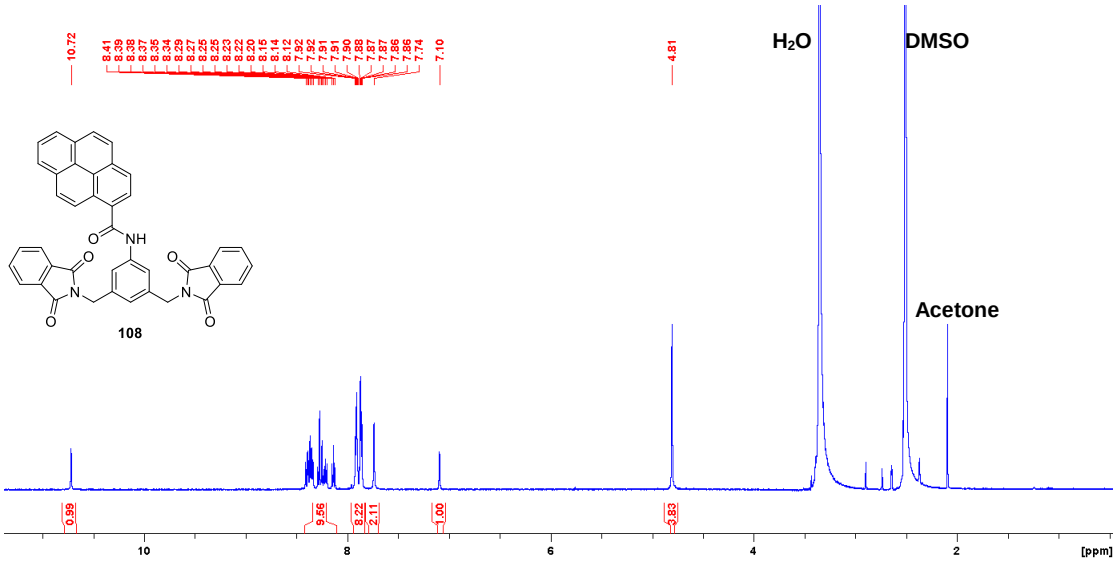

Figure A3.21: The ^{1}H NMR spectrum of compound **108** (500.13 MHz, DMSO-d_6).

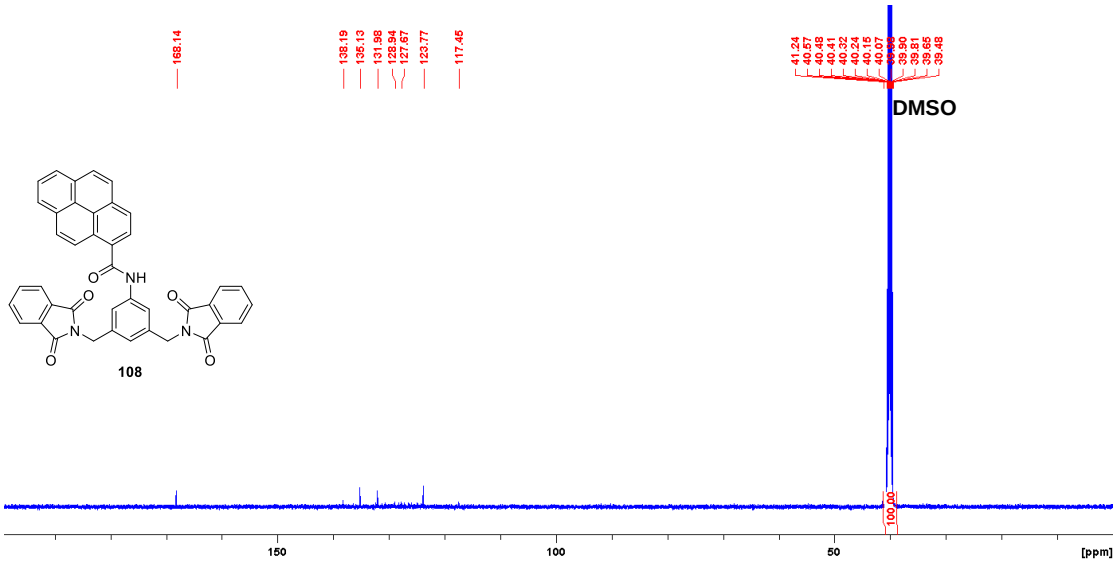

Figure A3.22: The ^{13}C NMR spectrum of compound **108** (500.13 MHz, DMSO-d_6).

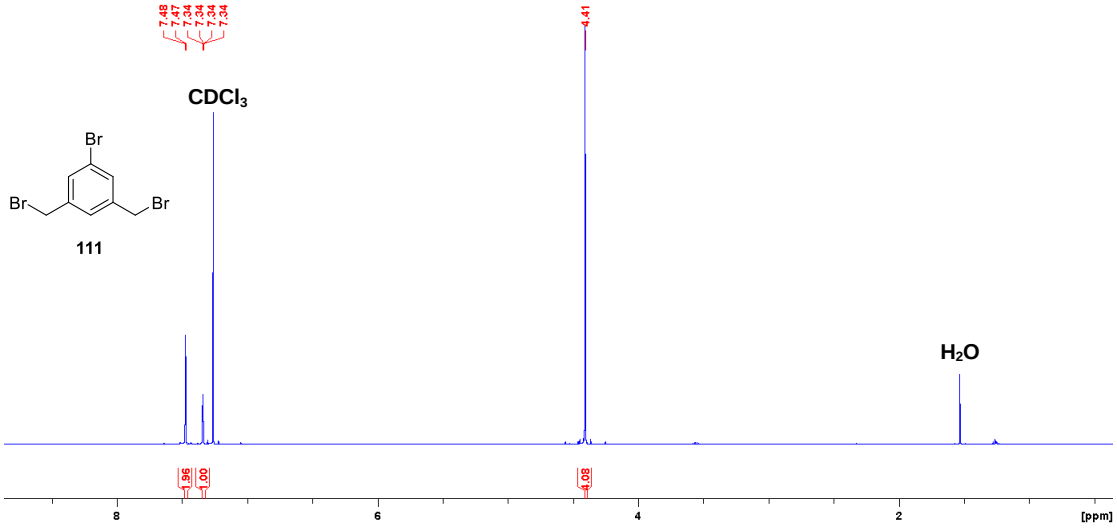

Figure A3.23: The ^{1}H NMR spectrum of compound **111** (500.13 MHz, $CDCl_3$).

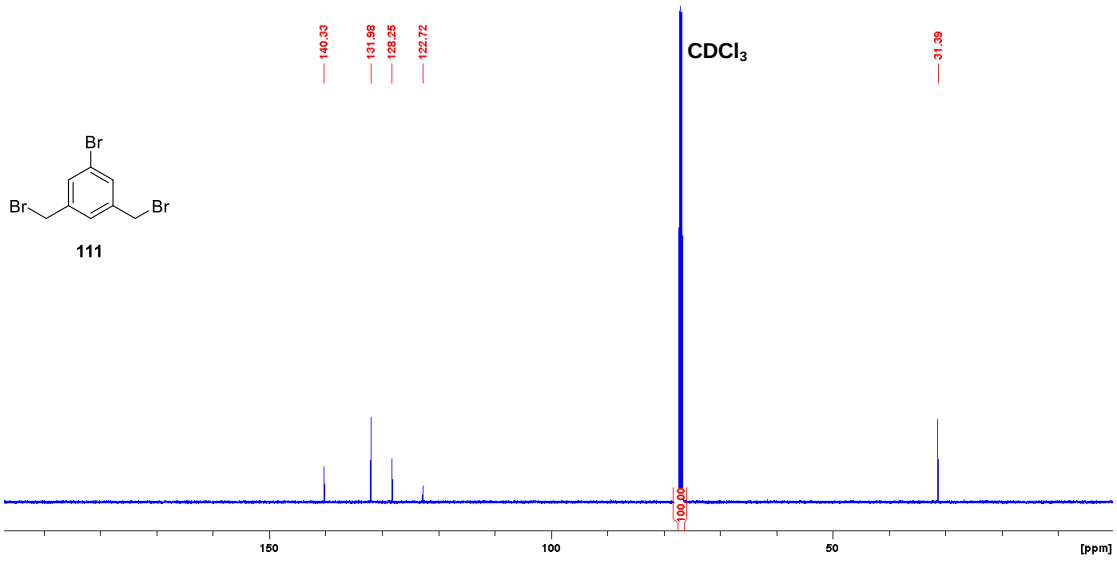

Figure A3.24: The ^{13}C NMR spectrum of compound **111** (500.13 MHz, $CDCl_3$).

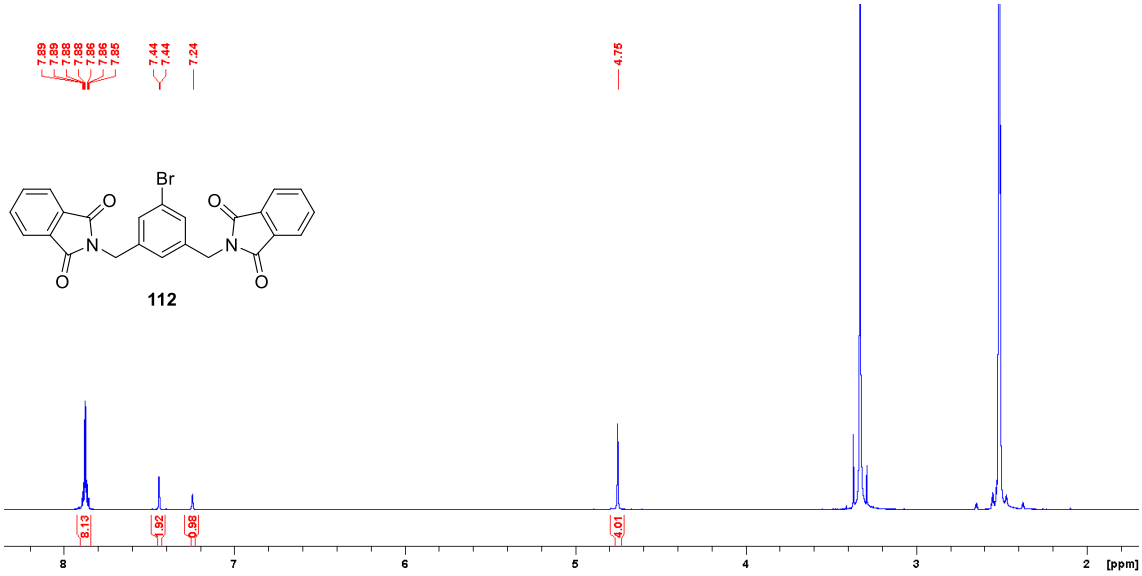

Figure A3.25: The ^{1}H NMR spectrum of compound **112** (500.13 MHz, DMSO-d_6).

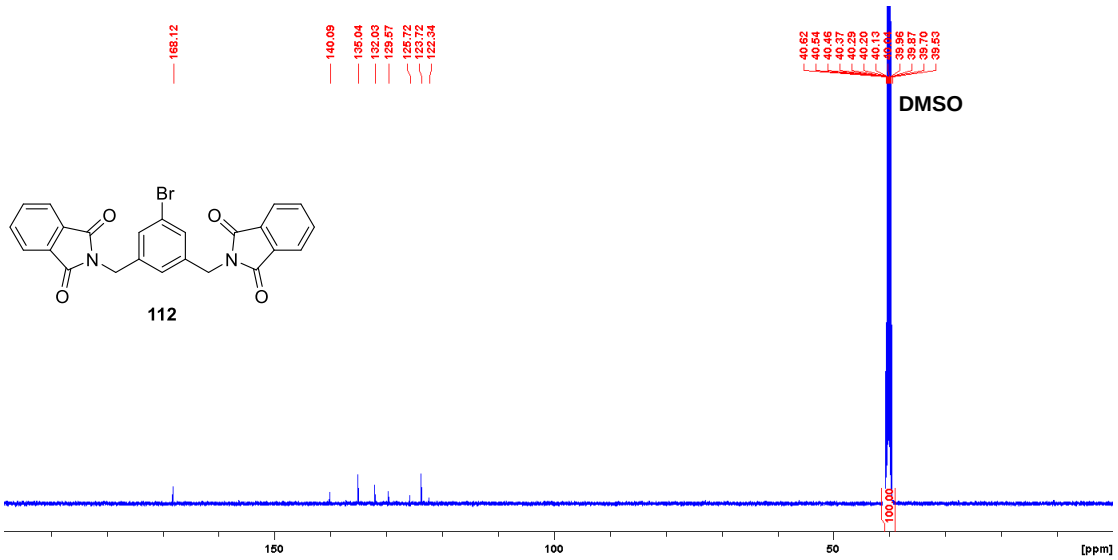

Figure A3.26: The ^{13}C NMR spectrum of compound **112** (500.13 MHz, DMSO-d_6).

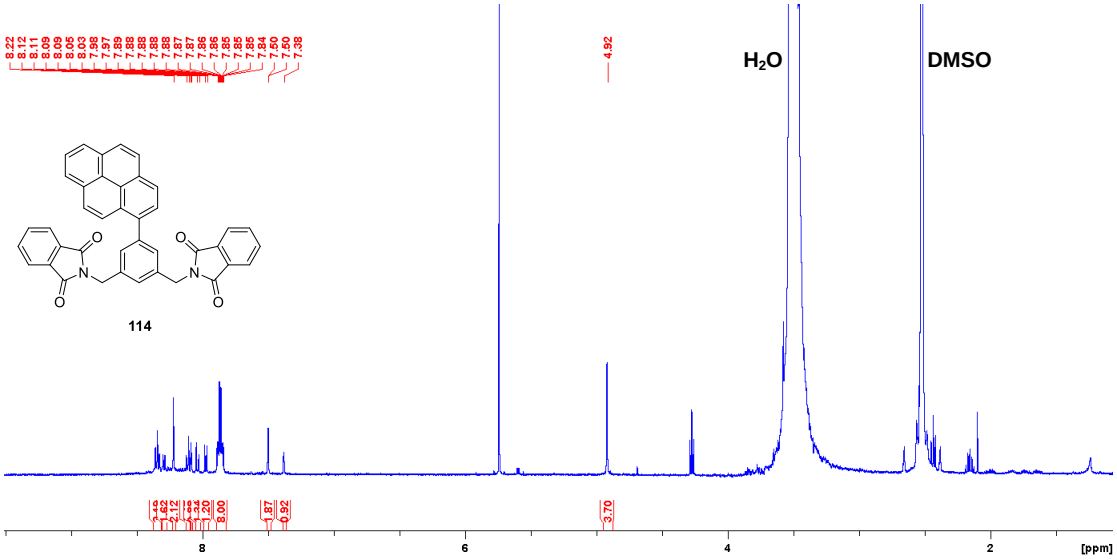

Figure A3.27: The ^{1}H NMR spectrum of compound **114** (500.13 MHz, DMSO-d_6).